Using connectivity to investigate brain (dys)function

Jakub Kopal

THÈSE

En vue de l'obtention du

DOCTORAT DE L'UNIVERSITÉ DE TOULOUSE

Délivré par l'Université Toulouse 3 - Paul Sabatier

Cotutelle internationale : University of Chemistry and Technology in Prague

---

Présentée et soutenue par

Jakub KOPAL

Le 9 avril 2021

Usage de la connectivité pour étudier les (dys)fonctions cérébrales

---

Ecole doctorale : **CLESCO - Comportement, Langage, Education, Socialisation, Cognition**

Spécialité : **Neurosciences**

Unité de recherche :
CERCO - Centre de Recherche Cerveau et Cognition

Thèse dirigée par
Emmanuel BARBEAU et Oldrich VYSATA

Jury

M. Jan KREMLACEK, Rapporteur
M. Maxime BAUD, Rapporteur
M. Demian BATTAGLIA, Examinateur
M. Robert JECH, Examinateur
Mme Isabelle BERRY, Examinatrice
M. Jan MARES, Examinateur
Mme Lenka LHOTSKA, Examinatrice
M. Patrice PERAN, Examinateur

University of Chemistry and Technology, Prague
Faculty of Chemical Engineering
Department of Computing and Control Engineering

Université Toulouse 3 - Paul Sabatier
Centre de Recherche Cerveau et Cognition

Using connectivity to investigate brain (dys)function

DISSERTATION

AUTHOR	**Ing. Jakub Kopal**
SUPERVISOR	**MUDr. Oldřich Vyšata, Ph.D.** **Emmanuel Barbeau, Ph.D.**
STUDY PROGRAMME	Chemical and Process Engineering
FIELD OF STUDY	Technical Cybernetics
YEAR	**2021**

Vysoká škola chemicko-technologická v Praze
Fakulta chemicko-inženýrská
Ústav počítačové a řídicí techniky

Université Toulouse 3 - Paul Sabatier
Centre de Recherche Cerveau et Cognition

Využití konektivity k analýze (dys)funkcí mozku

DISERTAČNÍ PRÁCE

AUTOR | **Ing. Jakub Kopal**

ŠKOLITEL | **MUDr. Oldřich Vyšata, Ph.D.**
Emmanuel Barbeau, Ph.D.

STUDIJNÍ PROGRAM | Chemické a procesní inženýrství (čtyřleté)

STUDIJNÍ OBOR | Technická kybernetika

ROK | **2021**

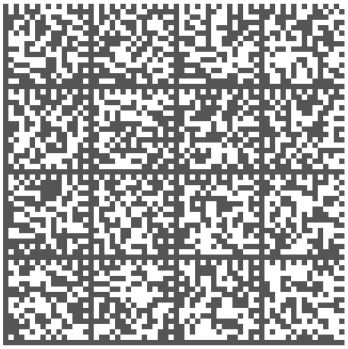

This thesis was created in accordance with agreement Nr. DSP_DV_Jakub Kopal on jointly supervised doctoral thesis at the University of Chemistry and Technology, Prague and the University of Toulouse III - Paul Sabatier in September 2016 —January 2021.

I hereby declare that this thesis is my own work. Where other sources of information have been used, they have been acknowledged and referenced in the list of used literature and other sources. I have been informed that the rights and obligations implied by Act No. 121/2000 Coll. on Copyright, Rights Related to Copyright and on the Amendment of Certain Laws(Copyright Act) apply to my work. In particular, I am aware of the fact that the University of Chemistry and Technology in Prague, or another educational institution where the work was written, has the right to sign a license agreement for use of this work as school work under §60 paragraph 1 of the Copyright Act. Should I in the future grant to a third party a licence for use of this work, the University of Chemistry and Technology in Prague, or another educational institution where the work was written, will be entitled to require from me a reasonable contribution to cover the costs incurred in the creation of the work, even up to the full amount as the case may be.

I agree to the publication of my work in accordance with Act No. 111/1998 Coll. on Higher Education as amended.

In Prague on . . . . . .

Ing. Jakub Kopal

Curriculum Vitae

Jakub Kopal

11.10.1990

Vratičová 277, Prague 5, 15521, Czech Republic

kopalj@cs.cas.cz

Education

- Since 2017: Doctoral studies in **Neuroscience**
  - Doctoral school CLESCO, Toulouse, France
- Since 2016: Doctoral studies in **Technical cybernetics**
  - University of Chemistry and Technology, Prague, Czech Republic
- 2013 – 2016: Master's degree in **Applied engineering informatics**
  - University of Chemistry and Technology, Prague, Czech Republic
- 2010 – 2013: Bachelor's degree in **Process engineering, informatics, management**
  - University of Chemistry and Technology, Prague, Czech Republic
- 2006 – 2010: Gymnasium Arabska, Prague, Czech Republic

Research Experience

- Since 2017: Czech Academy of Sciences, Prague, Czech Republic
  - **Ph.D. student**
  - Institute of Computer Science, Complex Networks and Brain Dynamics group
- Since 2017: Centre de Cerveau et Cognition (CerCo), Toulouse, France
  - Doctoral studies in **Neuroscience**
  - Co-supervisor: Emannuel J. Barbeau, Ph.D.
  - Dissertation: *Using connectivity to investigate brain (dys)function*
- Since 2016: University of Chemistry and Technology, Prague, Czech Republic
  - Doctoral studies in **Technical cybernetics**
  - Teaching: *Applications of Computer Science* (Czech and English language, 400 hours)
  - Co-supervisor: MUDr. Oldřich Vyšata, Ph.D.
- Feb 2016 - Jun 2016: Centre de Cerveau et Cognition (CerCo), Toulouse, France
  - **Internship** at Memory and Learning of Objects and Scenes team
- Jun 2015 - Aug 2015: University of Glasgow, Glasgow, UK
  - **Internship** at Department of Bioengineering
  - Project: Development of a rapid point of care diagnostic device, utilizing surface acoustic waves to manipulate and then sense biological marker

- 2013 – 2016: University of Chemistry and Technology, Prague, Czech Republic
  - Master's student at **Applied informatics**
  - Supervisor: MUDr. Oldřich Vyšata, Ph.D.
  - Diploma thesis: *Memory circuits analysis by deep brain electrodes and complex continuous wavelet analysis*
- Sep 2014 - Dec 2014: University of Oulu, Oulu, Finland
  - Erasmus exchange program, **Bioengineering and computer science**
  - Project: *Dynamic measurements of balance with footwear sensors*
- 2010 – 2013: University of Chemistry and Technology, Prague, Czech Republic
  - Bachelor's student in **Process engineering, informatics, management**
  - Bachelor thesis: *Dynamic Parameters of EEG during Meditation*

Completed courses

- Nov 2015: Universidad Politecnica de Madrid, Madrid, Spain
  - Athens course: **Biosignal processing**
- Apr 2014: Technische Universitat Munich, Munich, Germany
  - Athens course: **Manipulation of time series in time and frequency spectrum**
- Nov 2013: Ecole Nationale Superieure de Techniques Avancees, Paris, France
  - Athens course: **Medical Imaging**
- 2018-2019: Czech Academy of Sciences
  - The Department of Language Studies, **Academic writing**, 3 semesters

Received grants

- 2020: Daily Evolution of Brain Connectivity during the Preictal Period in Intracerebral Recordings of Epileptic Patients
  - Barrande 2020, Czech-French cooperation project
  - Ministry Of Education, Youth And Sports No. 8J20FR037
- 2018: Identification and description of fast memory circuits
  - Internal Grant Agency at University of Chemistry and Technology Prague
- International dual degree PhD – Cotutelle
  - Campus France
- 2017: Functional connectivity changes during walking in patients with multiple sclerosis
  - Internal Grant Agency at University of Chemistry and Technology Prague

Publications

- Bučková,B, Mareš, J., Škoch, A., **Kopal, J.**, Tintěra, J., Dineen, R., Řasová, K. & Hlinka, J. Multimodal neuroimaging correlates of motor disability in multiple sclerosis: towards interpretable machine learning, *In preparation.*
- **Kopal, J.**, Hlinka, J., Despouy, E., Valton, L., Denuelle, M., Sol, J.-C., Curot, J., & Barbeau, E. J. (2020). Dynamic connectivity analyses of intracranial EEG during

recognition memory reveal various large-scale functional networks. *BioRxiv*, 2020.10.30.360529.

- **Kopal, J.**, Pidnebesna, A., Tomeček, D., Tintěra, J., & Hlinka, J. (2020). Typicality of functional connectivity robustly captures motion artifacts in rs-fMRI across datasets, atlases, and preprocessing pipelines. *Human Brain Mapping*, 41(18), 5325–5340.
- Oliver, I., Hlinka, J., **Kopal, J.**, & Davidsen, J. (2019). Quantifying the Variability in Resting-State Networks. *Entropy*, 21(9), 882.
- Besedová, P., Vyšata, O., Mazurová, R., **Kopal, J.**, Ondráková, J., Vališ, M., & Procházka, A. (2019). Classification of brain activities during language and music perception. *Signal, Image and Video Processing*, 13(8), 1559–1567.
- **Kopal, J.**, Vyšata, O., Burian, J., Schätz, M., Procházka, A., & Vališ, M. (2017). EEG Synchronizations Length During Meditation. *Journal of Medical and Biological Engineering*, 37(2), 220–229.
- **Kopal, J.**, Vyšata, O., Burian, J., Schätz, M., Procházka, A., & Vališ, M. (2014). Complex continuous wavelet coherence for EEG microstates detection in insight and calm meditation. *Consciousness and Cognition*, 30, 13–23.
- Vyšata, O., Schätz, M., **Kopal, J.**, Burian, J., Procházka, A., Jiří, K., Hort, J., & Vališ, M. (2014). Non-Linear EEG Measures in Meditation. *Journal of Biomedical Science and Engineering*, 07(09), 731–738.

Posters

- **Kopal, J.**, Hlinka, J., Despouy, E., Curot, J., Denuelle, M., Valton, L., Sol, J.C., Barbeau, E.J., Dynamic causal network analysis of intracranial EEG during a memory task, *Society for Neuroscience*, 2019, Chicago, USA.
- **Kopal, J.**,Tomecek, D., Tintera, J., Hlinka, J., The influence of motion on rs-fMRI functional connectivity depends on atlas size, *Human Brain Mapping*, 2018, Singapore.
- **Kopal, J.**, Despouy, E., Vyšata, O., Valton, L., Curot, J., Denuelle, M., Barbeau, E.J. The dynamics of the functional connectivity underlying visual recognition memory, *Cognitive neuroscience of memory: Recollection, familiarity and novelty detection*, 2017, Liège, Belgium.
- Despouy, E., Deudon, M., **Kopal, J.**, Alloyer, M., Valton, L., Sol, J.L., Lotterie, J.A., Denuelle, M., Barbeau, E.J. The temporal dynamics of rhinal and hippocampus involvement in visual recognition memory, *ICOM 6*, 2016, Budapest, Hungary.
- **Kopal, J.**, Schätz, M., Procházka, A., Burian, J., Vališ, M., Vyšata, O. EEG microstates in Alzheimer's disease computed by continuous wavelet coherence, *World Conference of Neurology*, 2013, Vienna, Austria.
- Schätz, M., Vyšata, O., **Kopal, J.**, Procházka, A., Comparison of complexity, entropy and complex noise parameters in EEG for AD diagnosis, *World Conference of Neurology*, 2013, Vienna, Austria.

Oral communications

- **Kopal, J.**, Hlinka, J., Despouy, E., Curot, J., Denuelle, M., Valton, L., Sol, J.C., Barbeau, E.J. Dynamic causal network analysis of intracranial EEG during a memory task . Workshop on Analysis of Brain Activity 2019, Prague, Czech Republic.
- **Kopal, J.**,Tomecek, D., Tintera, J., Hlinka, J. The influence of motion on resting state functional connectivity depends on atlas size, International Workshop On Functional Magnetic Resonance Imaging In The Neurosciences 2018, Olomouc, Czech Republic.

Other talks and workshops

- Brain Connectivity Workshop 2019, Reykjavik, Iceland
- Doctoral days of the Czech Academy of Sciences 2019
- Conference of post-gradual students 2018, University of Chemistry and Technology
- Summer doctoral days 2017, Czech Technical University

"So I start a revolution from my bed"

John Lennon

Acknowledgements

It is not easy to thank all those who contributed to this thesis as it would not be finished without a great deal of support both in France and the Czech Republic. Whether it was creating new international collaborations or being smuggled across borders during a pandemic, these years I will never forget.

First of all, I would like to express my sincere gratitude to my supervisor Oldřich Vyšata who was instrumental in defining my research path. I am very grateful for his enthusiasm to assist in any way he could throughout my studies. Moreover, I would like to say a special thank you to my second supervisor Emmanuel Barbeau. By responding to one e-mail, he gave rise to a great collaboration. His support, guidance, and comprehensive insights in the neuroscience field have made this an inspiring experience for me. Finally, I would like to thank my co-supervisor, Jaroslav Hlinka, for his invaluable help in all my projects. Only through his guidance and mentorship, I was able to achieve my goals.

This collaborative project would not be possible without the help of all directors and all administrative staff from CerCo, University of Chemistry and Technology, and the Czech Academy of Science. Each of them was always ready to help me with all the bureaucratic obstacles. Furthermore, the Campus France program is truly appreciated. Without their support and funding, this project would not be possible.

No matter where I was, I was lucky enough to always feel at home thanks to my friends. Whether we were having diner with Anna, Annais, Benjamin, Bhavin, Can, Sam, and so many others in Toulouse or if we were playing cards with Anna, Baša, Isa, Jakub, and others in Prague, I was surrounded by the people that I like the most.

Nevertheless, I would not accomplish anything without the endless support of my family. They have always been a stable point in my life, providing me with support and confidence.

Furthermore, the strongest motivation and greatest support was always Palmyre. Not only that she never complained about my weird French accent, but she helped me to go through the numerous goodbyes at the airport, and she was always there for me with a never-ending dose of optimism, empathy, love, and humor.

Finally, I wish to acknowledge the Members of the Committee and all future readers of this thesis for their time and interest.

Summary

We picture the brain as a complex network of structurally connected regions that are functionally coupled. Brain functions arise from the coordinated activity of distant cortical regions. Connectivity is used to represent the cooperation of segregated and functionally specialized brain regions. Whether it is the analysis of anatomical links, statistical dependencies, or causal interactions, connectivity reveals fundamental aspects of brain (dys)function. However, estimating and applying connectivity still faces many challenges; therefore, this work is devoted to tackling them. The first challenge stems from the detrimental effect of systematic noise (such as head movements) on connectivity estimates. We proposed an index that depicts connectivity quality and can reflect various artifacts, processing errors, and brain pathology, allowing extensive use in data quality screening and methodological investigations. Furthermore, connectivity alterations play an invaluable role in understanding brain dysfunction. Investigating the mechanisms of epilepsy, we show that connectivity can track gradual changes of seizure susceptibility and identify driving factors of seizure generation. Identifying critical times of connectivity changes could help in successful seizure prediction. Finally, how the brain adapts to task demands on fast timescales is not well understood. We present a combination of intracranial EEG and state-of-art measures to investigate network dynamics during recognition memory. Understanding how the brain dynamically faces rapid changes in cognitive demands is vital to our comprehension of the neural basis of cognition. In conclusion, the modest goal of this thesis is to at least partially answer some of the many challenges that current neuroscience is facing.

Keywords: neuroimaging, connectivity, network neuroscience, brain function, epilepsy

Souhrn

Mozek si můžeme představit jako komplexní síť strukturně propojených oblastí, které jsou funkčně spojeny. Funkce mozku vznikají koordinovanou činností vzdálených kortikálních oblastí. Konektivita se využívá k reprezentaci spolupráce segregovaných a funkčně specializovaných oblastí mozku. Ať už se jedná o analýzu anatomických vazeb, statistických závislostí nebo kauzálních interakcí, konektivita odhaluje základní aspekty (dys)funkcí mozku. Odhad a aplikace konektivity však stále čelí mnoha výzvám; proto je tato práce věnována jejich překonání. První výzva pramení ze škodlivého účinku systematického hluku (jako jsou pohyby hlavy) na odhady konektivity. Navrhli jsme index, který zobrazuje kvalitu konektivity, tudíž může odrážet různé artefakty, chyby zpracování a patologii mozku. Toto umožňuje rozsáhlé použití při screeningu kvality dat a metodologických vyšetřováních. Navíc změny konektivity hrají neocenitelnou roli v porozumění mozkových dysfunkcí. Zkoumáním mechanismů epilepsie ukazujeme, že konektivita může sledovat postupné změny náchylnosti k záchvatům a odhalit hnací faktory vzniku záchvatů. Identifikace kritických časů změn připojení by mohla pomoci při úspěšné predikci záchvatů. Nakonec stále zůstává nezodpovězeno, jak si mozek dokáže ve velmi krátkém čase poradit s velmi komplexními úkoly. Představujeme kombinaci intrakraniálního EEG a nejmodernějších metod k prozkoumání dynamiky mozkových sítí během experimentu zaměřeného na rozpoznávací paměť. Pochopení toho, jak mozek dynamicky čelí rychlým změnám v kognitivních požadavcích, je zásadní pro naše pochopení vnímání. Skromným cílem této dizertační práce je alespoň částečně odpovědět na některé z mnoha výzev, kterým současná neurověda čelí.

Klíčová slova: neurozobrazování, konektivita, neurověda sítí, funkce mozku, epilepsie

Résumé

Nous nous représentons le cerveau comme un réseau complexe de régions structurellement connectées et fonctionnellement couplées. Les fonctions cognitives découlent de l'activité coordonnée de régions corticales distantes. La connectivité est utilisée pour représenter la coopération de régions cérébrales ségréguées et fonctionnellement spécialisées. Qu'il s'agisse de l'analyse des liens anatomiques, des dépendances statistiques ou des interactions causales, la connectivité révèle des aspects fondamentaux du fonctionnement (dys)cérébral. Cependant, l'estimation et l'application de la connectivité posent encore des problèmes. C'est pourquoi cette thèse est consacrée à surmonter ces défis. Le premier défi provient de l'effet néfaste du bruit systématique (comme les mouvements de la tête) sur les estimations de la connectivité. Nous avons proposé un indice qui décrit la qualité de la connectivité et qui peut refléter différents types d'artefacts, d'erreurs de traitement et de pathologie cérébrale, permettant son utilisation étendue dans le suivi de la qualité des données et les investigations méthodologiques. En outre, les altérations de la connectivité jouent un rôle inestimable dans la compréhension des dysfonctionnements cérébraux. En étudiant certains mécanismes de l'épilepsie, nous montrons que la connectivité peut suivre les changements progressifs de la susceptibilité aux crises et identifier les facteurs déterminants de la génération des crises. L'identification des moments critiques de modification de la connectivité pourrait aider à prédire avec succès les crises. Enfin, on ne comprend pas bien comment le cerveau s'adapte aux exigences des tâches cognitives à une échelle de temps rapide. Nous présentons une combinaison d'EEG intracrâniens et de mesures de pointe épileptiques pour étudier la dynamique des réseaux pendant la mémoire de reconnaissance. Il est essentiel de comprendre comment le cerveau fait face dynamiquement aux changements rapides des demandes cognitives pour comprendre les bases neurales de la cognition. En conclusion, l'objectif modeste de cette thèse est de répondre au moins partiellement à certains des nombreux défis auxquels les neurosciences actuelles sont confrontées.

Mots-clés: neuroimagerie, connectivité, neurosciences de réseau, fonction cérébrale, epilepsie

Using connectivity to investigate brain (dys)function

List of Tables

List of Figures

List of Acronyms

BOLD Blood-oxygen-level-dependent
CT Computed tomography
DTI Diffusion tensor imaging
DTF Directed transfer function
DWI Diffusion-weighted imaging
EC Effective connectivity
ECoG Electrocorticography
EEG Electroencephalography
ERP Event-related potential
FC Functional connectivity
fMRI Functional magnetic resonance imaging
GC Granger causality
HFO High-frequency oscillation
HRF Hemodynamic response function
ICA Independent component analysis
iEEG Intracranial EEG
MDS Multidimensional scaling
MEG Magnetoencephalography
MSC Magnitude-squared coherence
MRI Magnetic resonance imaging
LFP Local field potential
PCA Principal component analysis
PDC Paratial directed coherence
PET Positron Emission Tomography
ROI Region of interest
RSN Resting-state network
SC Structural connectivity
sEEG Stereotactic EEG
SOZ Seizure onset zone
VAR Vector autoregression

Contents

Part I

Preface

The human brain is the most complex system we have ever studied. About 86 billion neurons communicate with each other using trillions of synaptic connections [1]. In early pregnancy, the neurons develop at a rate of 250 000 per minute [2]. The blood vessels that are present in the brain are almost 100,000 miles in length. The average human brain has a size of 1200 cm^3 and it weighs 1400 g. Although it makes up only 2 % of our body weight, it uses up to 20 % of the body's energy. It is our remarkable brain that provides us with complex cognitive abilities. These cognitive abilities involve processes, such as memory, reasoning, planning, or imaging. Although we can be an active source of these actions, it is believed that 95 % of brain operations are autonomous [3]. Indeed, the brain gathers experiences, creates and strengthens our behavioral patterns, and drives our actions.

In our current understanding, we picture the brain as a complex network composed of interconnected brain regions. Segregated regions represent areas of functional specialization. However, successful task performance requires these distant specialized regions to integrate. The integration enables a flexible and efficient flow of information across the whole brain. In other words, brain functions rely on distributed processing, where cognitive processes arise from the coordinated activity of large-scale brain networks consisting of distant cortical regions. Nevertheless, how does the brain dynamically balance segregation and integration? What are the mechanisms for the coordination of activity between different neural networks? Is this knowledge helpful in understanding neurological disorders, and more importantly, can it help treat them? These questions touch upon so many areas that it is inevitable that neuroscience became a multidisciplinary field. It combines knowledge from computer science to biology, from psychology to chemistry, and mathematics to medicine. A collaboration of all these areas is essential if we ever want to fully understand how the brain works. Now more than ever, it is easy to collaborate and share data and knowledge in order to push the limits of our understanding.

Neuroscience itself is a very young field. Just a little more than a hundred years ago, Ramon y Cajal laid the basis of modern neuroscience. Even though his drawings of brain cells are still in use for educational and training purposes, our knowledge about the structure and function of the brain changed immensely in recent years. In 1924 Hans Berger recorded the first human brain electrical activity. We began investigating brain activity, both invasively and non-invasively, using electrodes. The revolution in

structural brain imaging came in the 1970s by introducing computerized tomography to clinical diagnosis in 1973 and the first human scan obtained by magnetic resonance in 1977. Five years later, this technique was used to non-invasively obtain a clinically useful image of patient tissues and identify a primary tumor in the patient's chest. These techniques explained brain structure in unprecedented detail. They were followed by positron emission tomography and single-photon emission computed tomography that allowed mapping brain functions. Another significant advance came in 1990 with the introduction of functional magnetic resonance imaging: brain function imaging technique using the oxygenation status of the blood. This event delineates the start of the modern era of functional neuroimaging. Just 120 years after the famous sketches, we are able to analyze the function and structure of the brain in a way previously unimaginable. Nevertheless, these are only a few examples of the revolutionary imaginary techniques that we have at our disposal nowadays. Moreover, thanks to multi-modal integration, we can explore benefits from all the modalities. Hand in hand with the advances in imaging comes the progress in our understanding. Just between the years 2006 and 2015, the number of neuroscientific studies rose from approximately 27,000 to 38,000, making a total of 340,000 over just ten years [4].

Following the turbulent rise of neuroscience in the 20th century, the field of functional neuroimaging flourished in recent years as noninvasive mapping of brain function became relatively easily available for numerous research groups around the world. As stated in a recent article reflecting on the past 20 years of neuroscience, we strived for functional mapping of brain activity to individual regions. We witnessed the decade of brain cartography. However, several researchers emphasized the shift between localizationist approaches of past decades to more connectivity-based network approaches [5]. This change in perspective is also due to the development of suitable methods, increased computational power, and the acquisition of large datasets. Nowadays, we not only search for the activity of individual regions, but we shifted our focus on investigating relationships between regions; to cite the reflection on past 20 years: *"We moved from mapping countries borders to mapping traffic between them."*. There is a new paradigm that moves beyond the simplistic mapping of cognitive constructs onto individual brain areas and emphasizes instead the conjoint function of brain regions working together as networks [6].

The reasoning for this shift can be illustrated in the recent work of Fox [7]. The authors

pointed out that former studies focused solely on finding correlates of neuropsychiatric symptoms by neuroimaging symptomatic patients. Such an approach identified useful biomarkers; however, it does not tell anything about the causes of the symptoms that would lead to treatment. Therefore, Fox [7] turned their attention to brain lesions as they provide a link between the location and neuropsychiatric symptoms. Interestingly when comparing subjects with similar symptoms (visual hallucinations), the lesions' locations overlapped only minimally. In a meta-analysis, there was no single region associated consistently across various studies with the symptoms. Nevertheless, a breakthrough came when they shifted their attention to networks, specifically when they analyzed to which network all the symptoms map. These networks are based on connectivity, i.e., relationships between regions. In other words, regions linked together (either physically or functionally) belong to the same network. Therefore, they mapped each lesion to a network, and after overlaying these networks, they saw a significant overlap. All in all, it means that the same neuropsychiatric symptoms caused by brain lesions map to a common network. This finding stresses the network etiology of various brain disorders, i.e., that the symptoms are inherent to brain networks or brain circuits rather than a single brain region. This network etiology of brain disorders was further proven for Parkinson's disease [8], migraine [9], or depression [10]. Moreover, it illustrates the shift in our understanding of brain processes. Analyzing brain processes from the perspective of brain networks, their interactions, and underlying connections holds big promises for future discoveries.

In conclusion, to understand complex brain functions, we do not only need to understand how individual brain elements behave in isolation but also how those elements interact with one another. These interactions are described by means of connectivity, whether they are anatomical links, statistical dependencies, or causal interactions. The advent of functional neuroimaging methods enables a comprehensive examination of macroscopic brain activity and an investigation of how segregated regions integrate. First, we must understand the structure and function of brain networks that emerge from brain region integration. The link between structural and functional networks is still fully resolved, even though many advances have been made in recent years [11]. Furthermore, these networks are not static, but rather, they undergo constant changes because neural responses to momentary challenges are not only reflected by a change of neural activity in certain brain regions but also by a global reorganization. This constant reorganization

underpins the continuous information flow. These dynamics are present on various time scales ranging from milliseconds to months and years. Moreover, the brain networks do not only change in their activity or participation in a task but also in their structure. Regions are being recruited and contribute to different brain networks [12].

Nowadays, the availability of a large number of imaging techniques has facilitated the exploration of human brain networks. We developed frameworks for mathematical representation and analysis of high-dimensional datasets. Nevertheless, every technique has its advantages and disadvantages. For example, the functional neuroimaging modalities can be compared in terms of spatial resolution, temporal resolution, cost, invasivity, noisiness, or radioactive dosage. The choice inevitably influences and essentially determines the nature of the analysis. Furthermore, each imaging modality has its specifics when analyzing. Thus, the applied mathematical methods need to be chosen accordingly. However, they face the same variability and complexity. They differ in terms of underlying assumptions, studied relationships, *a priori* knowledge, or data hunger. The plethora of techniques, methods, and results can be confusing when searching for a coherent theory on brain functions. This is why current neuroscientific research is, by definition, multidisciplinary and combines knowledge of medicine, mathematics, or computer science.

As promising as the connectivity studies are, they still face important challenges. Connectivity can be studied on various spatial and temporal scales. From neuronal circuits to brain regions. From static connectivity to dynamic connectivity evolving in the scope of milliseconds, days, and up to years. Moreover, our current brain activity measurements do not represent only true brain activity but also undesirable imaging artifacts. Therefore, this systematic noise has to be treated carefully in order to obtain valuable biomarkers of neurological disorders. Moreover, the remaining challenge is not only to detect but importantly to predict and treat dysfunctions and disorders. These are just a few of the many obstacles we are facing right now. Nevertheless, they are nothing compared to the importance of asked questions. Ultimately, understanding how the brain dynamically adapts to perform various tasks is vital to our understanding of the neural basis of cognition.

OBJECTIVE

The goal of this thesis is to demonstrate how connectivity can contribute to the understanding of brain functions. I review the promises and pitfalls of various connectivity estimation techniques across the most common imaging modalities. Moreover, I illustrate the possible connectivity applications such as analyzing inter-individual differences, investigating brain dynamics, or linking structure and function. Finally, the attractive concept of network neuroscience is portrayed as an elegant follow-up on connectivity analyses. State-of-the-art methods, including dynamic switching between segregation and integration or temporal networks, are introduced as well. Furthermore, I apply this knowledge to three specific research topics. They represent original research, and although they are very different in their nature, i.e., the first one being a methodological investigation of resting-state fMRI, the second one experimental investigation of large-scale dynamics in recognition memory, and the third represent an assessment of long-term connectivity changes in epilepsy, they all bring important advances and are highly relevant to all future connectivity studies. Since all projects were accomplished thanks to a collaborative effort, I generally use the plural form of the first person "we" in the body of the thesis. Furthermore, throughout the thesis, these blue boxes will indicate current challenges, specific questions, or recent advances.

Part II

Theoretical background

Chapter 1

Functional neuroimaging

This chapter aims to give an overview of functional neuroimaging methods available for studying brain connectivity, with a specific focus on those used or referred to in this thesis.

1.1 Different scales of the brain

The brain gathers, processes, classifies and evaluates information from all parts of the human body as well as stimuli from the person's surroundings using the sensory system. It coordinates the human body's functions, from breathing or cardiac frequency to complex processes such as the day-night cycle or self-preservation instinct. Via the hypothalamic-pituitary-adrenal axis, it controls the correct function of the endocrine system. It is the center of learning and memory. Thanks to the brain, we are able to think, speak, imagine, dream, and experience emotions. It creates our personality with all its personality traits.

The human brain can be conceptualized as a complex, hierarchical network in which billions of neurons are precisely organized into circuits, columns, and functional areas. From a microscopic perspective, the brain is primarily composed of neurons, glial cells, neural stem cells, and blood vessels. It is estimated that the number of neurons is almost equal to the number of all other brain cells and is around 86 billion [1]. From the macroscopic point of view, the brain can be separated into four parts: cerebrum, cerebellum, limbic system, and brain stem. The largest of these four parts is the cerebrum. The cerebrum is separated by a large deep groove, known as the longitudinal fissure, into two distinct hemispheres - the left and right hemispheres. The cerebral hemisphere is divided into five lobes associated with higher brain functions, i.e., frontal lobe, parietal

lobe, occipital lobe, temporal lobe, and insula. The outer layer of the cerebrum is called the cerebral cortex. The cerebral cortex is made up of grey matter that is folded to create more surface area forming ridges (gyri) and grooves (sulci). It has six layers, and the thickness of each layer differs significantly across cortical areas.

These different structural levels of organization in the nervous system naturally define the level of our investigation. In functional neuroimaging, the main difference among methods will be the level of analysis. The study of functional brain networks ranges from protein interactions and neuronal circuits to interactions between systems of cortical areas (Fig. 1.1). However, analyzing cognitive architectures involves structures and mechanisms, mainly at the highest level of analysis [13]. Nevertheless, in every analysis, it is important to understand what are the building blocks of the studied network and how these blocks interact and interconnect.

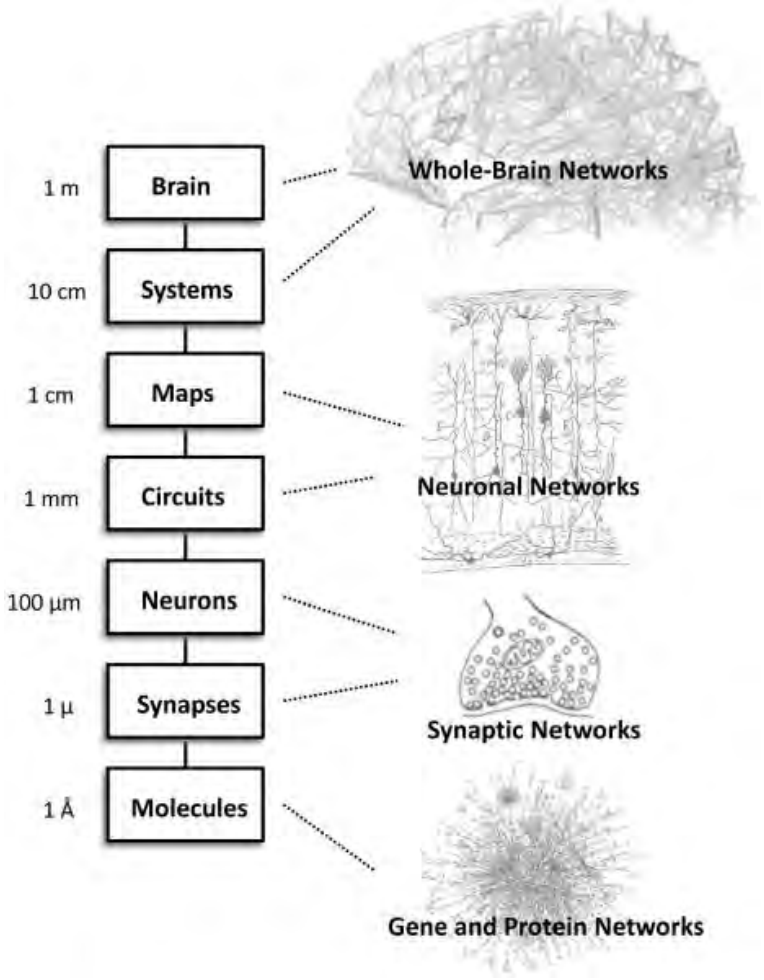

Figure 1.1: Schematic representation of levels of structure within the nervous system. The brain networks can be studied on various levels ranging from synaptic and neuronal networks to whole-brain networks. A current challenge for connectomics is to capture this multi-scale organization by charting network relations among elements across different spatial scales [14]. Adopted from [15].

Brain activity is the basis of every functional neuroimaging method. Neurons are capable of generating electrochemical signals. This electrical signaling represents a fundamental neuronal process. The transmitted information is in the form of an action potential. Suprathreshold neuronal stimulation can cause a momentary reversal of membrane potential leading to massive depolarization of the neuron due to the gradual opening of sodium channels along the axon. The influx of positive ions into the cell creates the electrical signal, which then travels along the axon. When the action potential reaches its peak, sodium channels close and potassium channels open, leading to repolarization and ultimately hyperpolarization. The electrical signal travels down the neuron, and when it reaches the end (the terminal button), it is then chemically transferred to other neurons

via neurotransmitters. Dendrites receive neurotransmitters from axons of other neurons. If the summation of incoming electrical signals reaches a threshold value, a sudden change in membrane potential is triggered, and signaling continues. Therefore, electrical action potential moves like a wave through the brain. The speed of propagation of the wave depends on nerve cell type, but it can reach 120 m/s.

Therefore, neurons have three basic functions:

- Receive signals (or information)
- Integrate incoming signals (to determine whether or not the information should be passed along)
- Communicate signals to target cells (other neurons, muscles, or glands)

At the level of neuronal ensembles, the synchronized activity of large numbers of neurons gives rise to oscillations. This oscillatory neuronal activity is thought to provide a mechanism for dynamic network coordination [16, 17]. The oscillations presumably reflect synchronized rhythmic excitability fluctuations of local neuronal ensembles. Synchronized oscillations facilitate the flow of information between neuronal ensembles [18]. Furthermore, a burst of action potentials occurring during an oscillation may further enhance the reliability of the transmitted information or contribute to establishing long-range synchronization [19]. The brain dynamically coordinates the information flow by changing the strength, pattern, or frequency with which different brain areas engage in oscillatory synchrony [18].

LOCAL FIELD POTENTIALS

An important concept for recordings of brain activity is the Local Field Potential (LFP). LFP represents the electric potential recordable in the extracellular space around neurons. It is generated by synchronized synaptic currents arising on cortical neurons, possibly through the formation of dipoles [20]. LFP sample closely localized populations of neurons. As a result, they differ significantly when recorded from two distinct areas. For example, in the visual cortex, they have been reported to originate within ≈250 µm of the recording [21].

1.2 Mapping brain functions

In the U.S. National Library of Medicine, brain mapping is defined as:

> *"The study of the anatomy and function of the brain and spinal cord through the use of imaging, immunohistochemistry, optogenetics, molecular, stem cell, & cellular biology, engineering, neurophysiology, and nanotechnology [22]".*

The study of mapping function on the structure of the brain is not a new topic. Already at the beginning of the 19th century Franz Joseph Gall started to localize cognitive brain functions. Unfortunately, the focus was on the erroneous concept of phrenology. The idea of phrenology is that each special function or personality trait can be mapped to a spatially distinct region in the brain (Fig. 1.2). The phrenology is considered a pseudoscience as it states that the measurement of bumps on the skull can predict mental traits. More specifically, Gall writes that *"Other things being equal, the relative size of any particular mental organ is indicative of the power or strength of that organ"*. He believed that the brain was made up of 27 individual organs. Even though the methodological rigor was doubtful even for the standards of its time, the model was still an important historical advance toward neuropsychology.

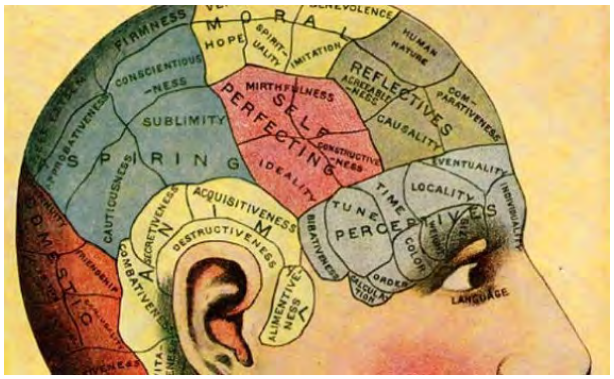

Figure 1.2: Phrenology. Phrenology is a pseudoscience that believes that personality traits can be mapped onto the cortex. Moreover, it states that the size of the area is indicative of the trait power or strength. The theory dates back to the 19th century and Franz Joseph Gall. Source: [23].

Nevertheless, how is it possible that already in the 1950s, a long time before sophisticated neuroimaging methods, we already had very precise maps that localized specific brain functions (Fig. 1.3)? There are two reasons. The first one is the study of subjects with brain lesions caused, for example, by stroke, disease, or traumatic wounds. Since it

provides a clear causal link between brain damage and dysfunctionality, a malfunctioning brain might be the most studied brain in the world. At the end of the 19th century, phrenology was replaced by the clinical–anatomical correlation method, where disorders of the nervous system were explained in terms of either cortical damage or disconnection syndrome. This approach led to the golden age of neuropsychology from 1861 to 1914. Behavioral neurologists and neuropsychiatrists described disorders, such as aphasias (Bastian, Broca, Wernicke), agnosias (Lissauer), apraxias (Liepmann), and alexias (Déjerine).

Until the 1960s, it was believed that memory is part of cognitive functions and that there is no brain area specific for memory. It all changed with patient HM. In 1953 Henry Molaison (1926-2008) had to undergo surgery to remove part of his brain due to severe epileptic seizures. After the surgery, his memory functions were limited [24]. Patient HM suffered from partial memory loss. He could not remember people's names; he forgot daily news; he was severely impaired at recognizing faces. On the other hand, he performed well at recognizing faces of persons that were in the news before his surgery. His childhood memories remained untouched, and his intelligence and intellect did not change at all. His short-term and working memory also did not exhibit any signs of malfunctioning [24]. These groundbreaking observations caused a revolution in understanding the organization of human memory. Moreover, they shaped the development of cognitive neuropsychology, i.e., the study of how the structure and function of the brain are related to specific psychological processes. For the last 50 years, patient HM is the most studied case in the history of neuroscience. His willingness to be studied pushed forward fields such as cognitive neuroscience or neuropsychology. Nevertheless, it was not only HM but many other patients who contributed significantly to our current knowledge. (for an overview, see [25]).

The second source of knowledge was gained through the direct electrical stimulation of the cortex of patients undergoing brain surgery. Originating in the studies of galvanic currents of Alessandro Volta, researchers in the second part of the 20th century began using electrical stimulation of the brain cortex in awake neurosurgical patients to investigate real-time anatomo-functional correlations. Wilder Penfield and his colleagues' work revolutionized our understanding of cortical localization (see the phenomenon of motor and sensory *homunculus*). Not only that the stimulation provides direct evidence about the necessity of brain region or pathway for a given cognitive function, but it also supports

Figure 1.3: Mapping of brain functions. This figure schematically summarises the state of knowledge of localization of the human functional brain in 1957. It is based on data from lesions and studies using direct cortical stimulation during neurosurgery. Source: [25].

causal inferences about the separability of sensory, motor, and cognitive abilities [26].

Even nowadays, direct electrical stimulation is still the only technique that allows direct mapping of white matter tracts *in vivo* in humans. Intraoperative electrical stimulation temporarily inactivates restricted regions during brain surgery and can map cognitive functions in humans with spatiotemporal resolution unmatched by other methods [27]. One successful application is the intraoperative mapping of the subcortical language pathways. In current clinical practices of neurosurgeries, patients are awakened, and they perform several language tasks to assess the functional role of restricted brain regions. In doing so, the surgeon can maximize the resection extent without generating cognitive (especially language) impairments [28]. Furthermore, stimulation also helped investigate other complex systems, such as working memory, attention, executive functions, and consciousness [26].

However, both the stimulation and the study of patients with lesions have a natural limitation as they do not study a healthy brain. For ethical reasons, neither lesions nor direct electrical stimulation of the brain via surgery (for reasons of general risk associated with exposing the brain) may be used in the study of healthy human subjects. Thus, a significant advance came with non-invasive neuroimaging [25].

Nowadays, imaging techniques play a pivotal role in medical research. They are capable of both delineating brain structure and monitoring brain activity. These correspond to two classes of brain imaging - structural and functional. The purpose of structural imaging is to visualize the various brain structures and any physical abnormalities that may affect them (such as tumors, bleeding, blood clots, or birth deformities). The most common structural imaging techniques are Computer Tomography (CT) and Magnetic Resonance Imaging (MRI). On the contrary, functional imaging aims to measure activity in certain parts of the brain while performing certain tasks. This activity can yield many forms, from differences in electrical potential to changes in the level of glucose or blood oxygenation. The functional imaging methods include Positron Emission Tomography (PET), functional Magnetic Resonance Imaging (fMRI), electroencephalography (EEG), and magnetoencephalography (MEG).

Each imaging technique comes with its specifics, and thus they can be categorized based on various aspects. The principle difference is in the underlying physical phenomena of each technique. Further, they differ in invasivity, i.e., the need for direct access to the brain via surgical intervention. All methods differ in their cost, both the cost of the measurement and the instrument itself. Notably, there is an important difference in the temporal and spatial resolution (Fig. 1.4). These two properties often come in the opposite. Frequently techniques with a very good temporal resolution, i.e., the capability to brain activity in terms of milliseconds, do not have the desired spatial resolution. Therefore, they are able to record the activity of only regions or lobes. On the other hand, techniques able to distinguish between smaller neuronal population can only record the activity in the scope of seconds. A method that would combine very high temporal and spatial resolution will inevitably suffer from high-invasivity or high cost.

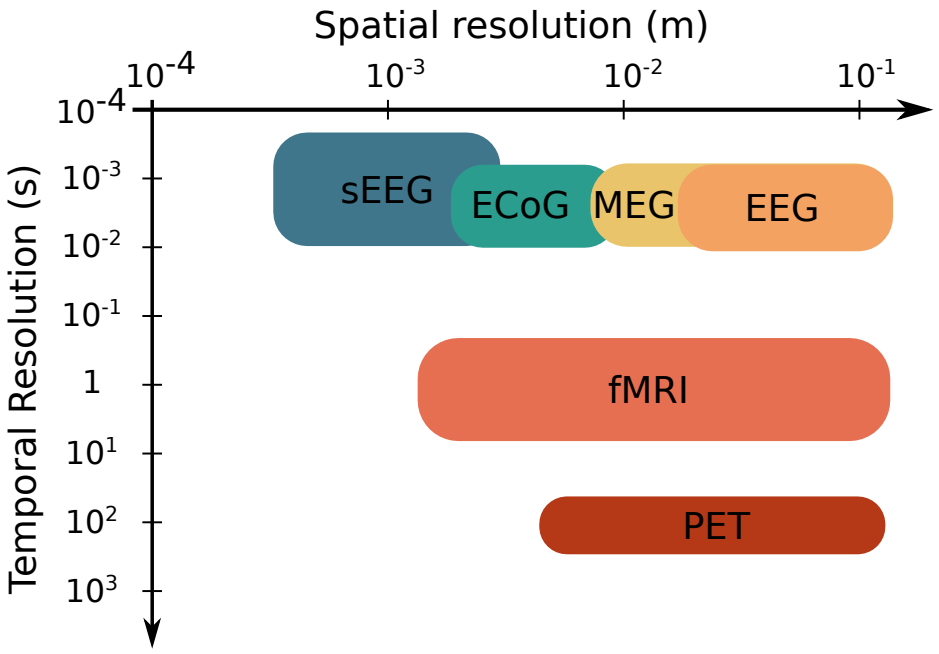

Figure 1.4: Spatial and temporal resolution of neuroimaging modalities. There is a trade-off between the two main characteristics of each functional neuroimaging techniques. Having a good temporal resolution necessarily results in a bad temporal resolution and vice versa. Although iEEG offers high spatial and temporal resolution, it is only due to invasiveness.

1.3 EEG

Electroencephalography (EEG) holds a prominent place among neuroimaging techniques. Its long history and straightforward principles make it the most available method nowadays. EEG is a continuous recording of brain electrical activity. The usual setup includes placing electrodes along the subject's scalp. The electrodes are named and positioned according to the international 10-20 system. The system is based on four principal positions on the head that are easily transferable across subjects: nasion, inion, and two pre-auricular points. Therefore, measurements are comparable across various recording sites. In this setup, 19 electrodes are used (plus ground and system reference). The naming might change in high-density arrays. If the research application demands a high spatial resolution, the high-density array can include up to 256 electrodes. In some systems, each electrode is attached to an individual wire. Other systems use caps or nets into which electrodes are embedded. This is particularly common in high-density arrays, and it greatly simplifies the work and manipulation.

Recorded electrical activity is a measurement of differences in electrical potentials between two points. Therefore, a channel displays a difference in its electrical potential to some other recording site. Nowadays, EEG is typically measured via referential montage. In this montage, each channel represents the difference between an individual electrode and a designated reference electrode. An offline re-referencing could be further applied since any montage can be constructed mathematically from any other. For example, in average reference montage, the summed and averaged outputs of all amplifiers are used as the common reference for each channel. In a bipolar setup, each channel represents the difference between two adjacent electrodes. As a result, bipolar montage is not affected by the influence of a common reference and provides a very precise spatial localization of source origin.

EEG signal usually has an amplitude of 10 µV to 100 µV. It captures postsynaptic potentials or changes in membrane potentials elucidated by neurotransmitters binding to receptors on the postsynaptic membrane [29]. Therefore, each recording channel records the direct activity of millions of neurons in the cerebral cortex. Although it was generally believed that the activity of deep brain structures is not visible from scalp recordings, there has been some direct evidence that scalp EEG indeed can sense subcortical signals [30].

Furthermore, the signal could be contaminated by high-magnitude electrical currents from undesirable artifacts. The artifacts can be generally divided into biological and non-biological. Biological non-neuronal sources include heart and eye movements, muscle and movement artifacts, dental artifacts, transpiration, or artifacts from tongue and other oropharyngeal structures movements. The non-biological artifacts include cable movement, incorrect reference placement, or alternating current electrical and electromagnetic interference.

The goal of a preprocessing pipeline is to detect and remove undesirable artifacts. Although there were attempts on standardized EEG preprocessing, variability across studies remains [31]. Following recommendations of Bigdely-Shamlo *et al.* [32], the most common EEG preprocessing steps include:

- Line Noise Removal - Applying a notch filter at 50 Hz (resp. 60 Hz) power line.
- High-pass Filtering - A high-pass filter with a cutoff frequency of 1 Hz removes long-term trends and drifts. However, the application still raises concerns [33].

- Detection of Noisy Channels - Automatic detection of noisy or outlier channels. Noisy channels could be further interpolated.

The recorded wave-like signal could represent a triggered response to stimuli or spontaneous activity. When the EEG is time-locked to a stimulus to which the participant reacts, it is called an Event-Related Potential (ERP). The time period before the stimulus onset is called a baseline. ERP represents synchronized responses of groups of neurons to afferent excitations. It is a more complex type of response than the unit activity of individual neurons. Each ERP is characterized by its shape, latency of the peaks, amplitude, slope, polarity, and mutual relations of waves.

In addition to ERP, the common analysis focuses on neural oscillations, i.e., the spectral content of EEG. Each wave can be characterized by its amplitude, shape, and frequency. We commonly distinguish six different frequency bands, each corresponding to a different state of mind: from sleepiness and drowsiness to engaged and excited. Historically the classification goes as follows:

- 0.5-4 Hz: Delta-band
- 4-8 Hz: Theta-band
- 8-13 Hz: Alpha-band
- 13-30 Hz: Beta-band
- 30-70 Hz: Gamma-band
- more than 70 Hz: High gamma band

HIGH GAMMA FREQUENCY

The study of high gamma oscillations flourished in recent years. Many studies have shown that high gamma activity with frequencies above 60 Hz is a reliable indicator of population-level cortical activity related to different motor, sensory, or cognitive tasks [34] and inter-regional communication measures [18]. Moreover, the high-frequency range of local field potentials was correlated with fMRI BOLD activity [35]. Finally, findings in epilepsy also drove the interest in frequencies above 70-80 Hz. Since interictal high-frequency oscillations (80–500 Hz) are considered to be strongly bound to the seizure onset zone, they were investigated as electrophysiological biomarkers (more information in [36]). However, their role is far from being resolved. For example, fast ripples (250–500 Hz) seem to be always pathological, but ripples (80–250 Hz) are also involved in physiological processes such as memory consolidation in the hippocampus [37].

Even though we will soon celebrate 100 years from the first recordings, the EEG has gone through a phase of mistrust. After the introduction by Hans Berger in 1924, EEG was first met with skepticism. It took several years before the instrument was generally accepted. The measurements were greatly limited by the available technology, an example being the ink-writing oscillograph used to record measured electrical activity. Since the signal analysis was done manually using visual inspection, it is not surprising that the most obvious 10Hz oscillations were studied first. Although some researchers suggested calling them Berger waver, Berger himself used the term alpha waves. Everything else that did not correspond to alpha waves was called beta waves. It is important to note that even though the Fourier transform was already known at that time, there were no computers to calculate it. Nevertheless, in 1932 Dietsch published a first Fourier analysis of the EEG signal that consisted of a table for a handful of frequencies. Further description of frequency bands came in 1936 with slower frequencies (called delta waves) and frequencies higher than 30 Hz (gamma waves). Especially, the gamma waves were first criticized since the oscillograph was not capable of writing faster than 30 or 50 Hz and fluctuations smaller than five microvolts; both of these characteristics being typical for gamma waves.

Along with describing the frequency content of the signal, researchers also focused

on detecting cognitive responses in the signal. Already Berger observed that the voltages could be influenced by external events stimulating the senses. Even though EEG recorded electrical potentials of the brain, it was difficult to isolate individual neurocognitive processes. A breakthrough came in 1935 when Pauline and Hallowell Davis recorded the first known ERPs on awake humans. A further advance was interrupted by the war, so it was until 1964 when Grey Walter reported the first cognitive ERP component. This year marks the start of the modern era of ERP, where in the next fifteen years, ERP component research became increasingly popular.

From the very beginning, EEG was associated with the analysis of brain diseases. The field of clinical electroencephalography started mainly by the study of epileptic patients. Already in the 1930s, epileptiform spikes, interictal epileptiform discharges, and spike-wave patterns during clinical seizures were described. Furthermore, EEG became an invaluable tool in the study of human sleep. The first description of REM sleep dates back to 1953. Later, the arrival of computers revolutionized the field. Thanks to the ease and insight of EEG recordings, the instrument was increasingly used to study pathology, function, and behavior. Nowadays, when we dispose of large computational power, time-frequency decompositions and pattern recognition algorithms are standard. In the upcoming years, we can expect large-scale multiple-sensor research in the line of open-access big data projects.

The main advantage of EEG is its effectiveness and low cost. It has a very high sampling frequency, i.e., it can record the signal on a millisecond scale. Moreover, it is only a passive recording; thus, it is very safe. On the contrary, it has a very low spatial resolution, i.e., limited ability to accurately record from deep brain structures. Although there are source analysis methods aiming to reconstruct neuronal activities in specific brain areas by solving the so-called EEG inverse problem [38], EEG research has mostly focused on cortical structures due to the non-unique solution to the inverse problem [39]. Nevertheless, EEG can be used simultaneously with fMRI so that high-temporal-resolution data can be recorded simultaneously as high-spatial-resolution data. Moreover, individual anatomical information derived from the MRI is used to improve source imaging. With these advances, EEG continues to be a widely used technology in cognitive science, cognitive psychology, and psychophysiological research, as well as in diagnosing epilepsy or sleep disorders.

1.4 iEEG

Intracranial EEG (iEEG) is an invasive measurement, and so it offers improved spatial resolution compared to scalp EEG. However, it is only feasible for clinical purposes in subjects scheduled for neurosurgery due to the necessary surgical intervention. Intracranial recordings are obtained either using subdural grid electrodes placed on the cerebral cortex after craniotomy or depth electrodes (Fig. 1.5). These two approaches are referred to as electrocorticography (ECoG), resp. stereotactic EEG (sEEG).

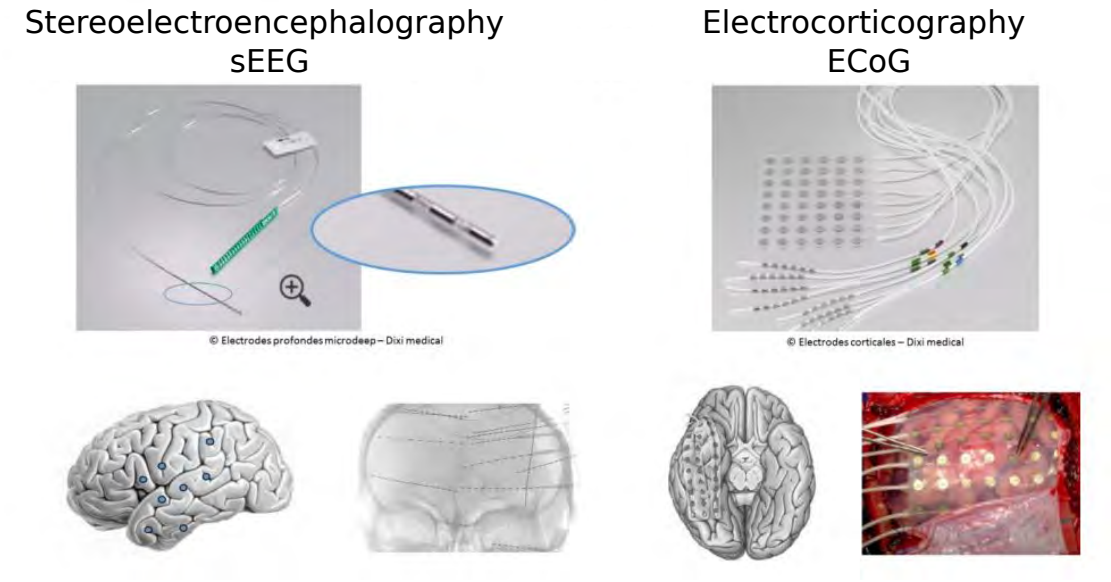

Figure 1.5: Intracranial EEG. Two methods of intracranial EEG: electrocorticography (ECoG) and stereotactic EEG (sEEG). While ECoG grids provide measurements over a large area, they are often implanted only in one hemisphere, and they do not allow monitoring deeper brain structures. In contrast, sEEG can be implanted bilaterally and allows monitoring of superficial and deep cortical structures [40]. About fifteen electrodes can be implanted per patient.

The history of intracranial EEG measurements is tightly linked to the measurements of EEG itself. Driven by the research on epilepsy, the first serial invasive EEG recording over several days using epidural electrodes was performed already in 1939 at the Montreal Neurological Institute. The results proved the usefulness of intracranial EEG in the delineation of the epileptogenic zone. Therefore, ECoG became a standard measurement executed during awake surgeries. The main focus laid on the localization and detection of epileptiform discharges. Moreover, ECoG measurement allowed concurrent direct cortical electrical stimulation for functional mapping of the cortex and identifying critical cortical

structures.

However, in the upcoming years, it became clear that surface measurements are not sufficient as also subcortical and deep brain lesions like the thalamus, basal ganglia, and other regions are involved in the generation of epileptic seizures. Hence, in 1949 the first report about stereotactic implantation of EEG was published. During the same year, Jean Talairach began his revolutionary work on stereotactic procedures. He significantly improved the implantation technique. Moreover, he defined a system of reference lines and structures that allowed an individualized and optimized approach for investigations of deep brain structures and their anatomical localization. Finally, in 1957, he published the first atlas of stereotactically defined brain structures.

Along with Jean Bancaud, they further improved the recording of deep brain structures, and they introduced new clinical features such as the three-dimensional analysis of seizure patterns or seizure patterns distribution, propagation, and correlation. Ultimately, they defined the term epileptogenic network and its constituent components. Until the beginning of the 1980s, sEEG was the gold standard and the main tool for investigations in epilepsy patients. After that, it was accompanied by advanced structure localization using new non-invasive neuroimaging techniques, mainly the CT and MRI scanner (for an extensive overview, see [41]).

Even nowadays, the vast majority of human iEEG studies are conducted in patients with epilepsy [40]. These patients suffer from uncontrollable seizures and are resistant to conventional antiepileptic drug treatment. They are first examined via non-invasive imaging techniques (EEG, MRI, PET) in order to localize their seizure onset zone. If these techniques fail to identify the seizure onset zone, iEEG implantation that includes continuous monitoring, recording spontaneous epileptic seizures, and performing electric stimulation is carried out. The placements of intracranial electrodes can follow standard setups or be tailored to every subject individually based on clinical criteria. The localization of electrodes is commonly confirmed by a fusion of postoperative CT and preoperative MRI scans. Since the activity is recorded directly from/within the brain surface, the signal magnitude could reach hundreds of millivolts. In the current clinical setup, iEEG signals are composed of synchronized postsynaptic potentials (local field potentials), recorded either directly from the exposed surface of the cortex or deep subcortical structures, depending on the chosen technique.

When the activity of deep subcortical structures is to be recorded, each patient is often implanted with 5–15 depth electrodes, unilaterally or bilaterally (each consisting of 10–14 recording contacts). For the implantation, small holes are drilled in the skull. The electrodes often target the limbic structures (medial temporal lobes, cingulate, orbitofrontal, and insular regions), but since they penetrate the brain from its lateral surface, they offer recordings from the lateral sites as well.

ECoG uses subdural grids of electrodes placed directly on the exposed surface of the brain to record electrical activity from the cerebral cortex. ECoG covers a much broader area of surface than sEEG. However, part of the skull needs to be removed for implantation. Moreover, it typically covers the cortical surface of only one hemisphere [40]. Although still considered a golden standard, due to high invasiveness, iEEG is beginning to prevail [42].

After the implantation, subjects typically spend several days in the hospital for further monitoring and recording. During this period, they could undergo a batch of cognitive tests providing neuroscientists with unique and rare data. However, this implies that iEEG recordings are available only from epileptic patients. Thus, epilepsy and tumors could affect brain responses. Therefore, recordings must be inspected carefully for pathological activities.

In summary, iEEG offers a unique view of brain functions with unprecedented spatial and temporal resolution. However, there are inherent disadvantages such as invasivity, low sample sizes, inter-individual variability in neuroanatomy, undersampling of some areas, incomplete coverage of the brain, and limited access to sulci with ECoG.

1.5 MRI

Magnetic Resonance Imaging (MRI) is one of the most common structural imaging techniques. It is capable of high-resolution images of brain structure. Compared to ionizing radiation used in X-rays of Computerized Tomography (CT), it is based solely on magnetic fields and radiofrequency. More specifically, it is based on small magnets in the human body, the hydrogen protons. Up to 60 % of the human body is made of water, and each water molecule consists of two hydrogen atoms. In each hydrogen atom's nuclei, there is a spinning charged particle, i.e., the proton. Its movement produces a magnetic

field called the magnetic moment, and thus hydrogen atom acts as small magnets. In normal conditions, protons are oriented randomly, and there is no overall magnetic field.

MRI scanner consists of a primary magnet, gradient coils, radio-frequency coils, and computer system. The primary magnet produces a unified magnetic field around the patient. Magnets differ in the magnetic field strength, ranging from 1.5 Tesla to 7 Tesla. Upon applying the magnetic field, most hydrogen protons align parallel to the primary magnetic field adopting the so-called low-energy state. A small portion of hydrogen protons would align antiparallel to the primary magnetic field, occupying a high-energy state. This process is called longitudinal magnetization. Moreover, protons are processing, i.e., they spin around the long axis of the primary magnetic field. If they process synchronously, they process in phase. Conversely, when they process separately, they process out of phase. The processing rate is called the Larmor frequency. Larmor frequency changes in proportion to the magnetic field strength.

Gradient coils are three, and they are used to alter the primary magnetic field. Change in their arrangement gives MRI the capacity to image directionally along the x,y, and z-axis. Alteration of the primary magnetic field's strength changes the processing frequency between slices, which is used to slice selection and spatial coding.

A radio-frequency (RF) coil is used to create disturbances in the primary magnetic field. By creating radio waves that resonate with the magnetic field, some low-energy particles flip to a high-energy state, decreasing longitudinal magnetization. Conversely, protons become more synchronized as they process more coherently, increasing transverse magnetization. After switching off the RF pulse, protons release energy and return to the low-energy equilibrium state. This flip back emits an electromagnetic signal recorded by an RF coil. The time for the return to equilibrium (relaxation time) depends on the tissue type. The difference in relaxation time creates the resulting contrast between structures. There are two types of relaxation time constants: T1 and T2. T1 corresponds to increasing longitudinal magnetization as protons return to their original alignment. T2 corresponds to decreased transversal magnetization as protons process more out of phase. However, the T2 time constant is further affected by local inhomogeneities in the magnetic field. Therefore, T2* time constant includes additional effects due to macroscopic and microscopic magnetic field and accounts for the inhomogeneities.

Besides T1 and T2* constants, each imaging sequence is characterized by the repetition

time (TR), defined as the time between two consecutive RF pulses, and the echo time, defined as the time between the RF pulse and the peak of the signal induced in the coil (how soon after excitation the signal is collected). Controlling these characteristics is used to emphasize different tissues.

As there are T1 and T2* relaxation times, resulting images are T1-weighted or T2*-weighted. In the T1-weighted image, new blood and fat appear bright while water appears dark. This image is useful for the diagnosis of blood barrier disruptions or vascular changes. Conversely, in the T2*-weighted image, fat is dark, and water is bright. Therefore, these images provide more anatomical details, especially regarding cerebrospinal fluid (CSF) spaces, and they are used for lesion diagnosis. Their contrast can be further improved using fluid attenuation inversion recovery (FLAIR) procedure where free-flowing water (CSF) appears dark, enabling better delineation of lesions near ventricles and better grey-white matter differentiation.

A special imaging sequence is diffusion-weighted imaging (DWI), measuring the Brownian motion of water molecules. The resulting contrast is generated by the rate of water diffusion at a given location. The diffusion patterns of water molecules can reveal microscopic details about tissue architecture, either in normal or in a diseased state. Every fluid restriction appears bright in the image, and thus, they are useful in detecting ischemia and abscess. Moreover, within cerebral white matter, the diffusion of water molecules is restricted by various obstacles, and thus it is mainly driven by the orientations of axons (so-called anisotropic diffusion). This information is used in diffusion tensor imaging (DTI). DTI, a special kind of DWI, has been extensively used to map white matter tracts in the brain. More on this subject can be found in chapter 2.3. All in all, these techniques revolutionized the field of neuroimaging because they are able to reconstruct white matter pathways and study white matter bundles in living humans [43].

1.6 fMRI

We are now entering into the fourth decade of fMRI measurements. fMRI went from the pioneering experiments demonstrating relatively coarse images of activity in the visual cortex to being the most popular cognitive neuroscience method. Upon framing the fMRI as a valid measurement depicting brain activity, we entered the era of brain-mapping.

The mapping started with basic visual and motor processes and moved to basically all cognitive processes. This "gold rush" of studies attempting to non-invasively localize various cognitive states to specific brain areas went as far as searching for neural correlates of love, politics, and other like topics [44]. The obtained results were alike to those of phrenology. Almost from the very beginning of fMRI, there was another line of research exploring the interactions between different brain areas. Initially, as a second to localizationist but slowly gaining momentum, the connectionist view started to prevail. With the game-changing studies on resting-state networks, we entered the era of brain networks. Nowadays, studies explore the interconnected nature of the brain and how those networks interface in the context of complex human behavior [44].

Functional MRI, as its name suggests, is a functional imagining technique. It is based on the premise that the T2*-weighted image combines the effects of T2 contrast and local inhomogeneities in the magnetic field. These inhomogeneities can be either eliminated or emphasized using a special scanner setup. One of the sources of inhomogeneities is hemoglobin. Hemoglobin exists in two forms in the blood: oxyhemoglobin and deoxyhemoglobin. These two forms correspond to two magnetic states; while the oxy- form is diamagnetic and has no significant effect on the local magnetic field, the deoxy- form is paramagnetic and, in higher concentration, causes a decrease in MR signal. This physical phenomenon is the basis of the blood oxygen level-dependent signal, i.e., the BOLD signal.

The brain highly depends on a tightly regulated blood supply. All neurons need a steady oxygen and nutrients source, defined as resting cerebral blood flow (rCBF). The supply is provided by an extensive network of arteries and capillaries. However, when neurons are active, the steady supply needs to be increased as neurons extract more available oxygen leaving a higher percentage of deoxyhemoglobin. The resulting dip in oxyhemoglobin concentration manifests as decreased MRI signal. After the initial dip, blood vessels increase in their diameter and supply more nutrients and oxygen to meet the demands. Incoming blood to neurons is highly oxygenated, resulting in an increase in MR signal compared to rCBF. Therefore, the BOLD signal reflects these changes in the ratio of oxy- and deoxyhemoglobin. The typical neuronal response called a hemodynamic response function (HRF) manifests as an initial dip in the fMRI signal followed by overcompensation leading to a peak in BOLD 4-6 s following the activation. Therefore, the

BOLD response is typically modeled as the convolution of the stimulus function with the HRF function. Consequently, the BOLD signal is an indirect measurement of neuronal activity that is delayed to the original neuronal activity. The magnitude of MR signal changes to rCBF is 0.1 to 5 percent. However, previous studies proved that the BOLD signal corresponds relatively closely to LFP, reflecting postsynaptic activity [45].

fMRI recording is a sequence of scans where the BOLD signal corresponds to image intensities across the scans. In other words, each image consists of approximately 100,000 cubic volumes (voxels) that span the 3D space of the brain to form approximately 100,000 time-series. Natural limitations arise from the physical phenomena underlying the signal. Mainly, it is the low temporal resolution due to the inherent time delay between neuronal activity and the change in oxyhemoglobin concentration due to the neurochemical mechanisms of regional blood flow. Furthermore, even though the BOLD response is roughly linear, there is evidence of refractory effects or saturation, reducing the BOLD amplitude [46]. Like any other imaging technique, fMRI is also affected by unwanted artifacts. There are many non-neuronal sources of signal variability, such as thermal noise, physiological sources (created by the cardiac and respiratory cycles), scanner and head coil heterogeneities, spiking, chemical shifts, radio-frequency interference, or subject movement [47–50]. They induce undesirable, artificial effects that manifest in complex temporal and spatial patterns from high-frequency spikes to low-frequency drifts. Recent studies pointed out that even small head movements, in the range of 0.5 to 1 mm, can induce systematic biases [51–59].

1.6.1 The art of fMRI preprocessing

As in other imaging modalities, fMRI data preprocessing is used to reduce noise. Preprocessing usually includes image re-alignment, smoothing, filtering, normalization, and other steps [60]. Preprocessed are both fMRI and MRI image sequences. The goal is to minimize the influence of data acquisition and physiological noise. Moreover, it standardizes the locations of brain regions across subjects to achieve validity and sensitivity in group analysis. Here are listed the most common preprocessing steps:

- Removing several first scans to allow signal stabilization.

- Slice time correction - Often multiple slices are sampled during each TR, and typically each slice is sampled at a slightly different time point. Slice time correction ensures that each voxel intensity corresponds to the same time point by applying interpolation techniques.

- Motion correction - Since undesirable small shifts between subsequent images could occur, motion correction ensures that we depict the same brain region at every time point. Rigid body transformation corrects every image to correspond to the first or mean image using three translational parameters x, y, z, and three rotational parameters pitch, yaw, roll.

- Co-registration - fMRI images are registered to the MRI image obtained at the beginning of the sequence. This simplifies the transformation of fMRI to the standard coordinate system and allows overlying intensity images on high-resolution structural images.

- Normalization - Images are adjusted to a standard brain to be comparable across subjects, usable in group analyses, and the results generalizable to the population. Commonly studies use standard brain from the Montreal Neurological Institute. This step is generally accompanied by structural segmentation into two new scans of white matter and cerebrospinal fluid.

- Spatial smoothing - Spatial smoothing of images is applied to increase the signal to noise ratio, validate distributional assumptions, and reduce artifacts. The smoothing kernel size is determined by the fill width at half maximum (FWHM), which measures the width of the kernel at 50% of its peak value.

The preprocessing of scans is followed by a preprocessing of extracted BOLD signals (Fig. 1.6). The denoising steps could include regression of head-motion parameters acquired while performing the correction of head-motion with the addition of their first-order or even second-order temporal derivatives. Further regression of either white-matter and cerebrospinal fluid components identified using principal component analysis or noise components identified using independent component analysis [61] brings further advantages. Other preprocessing steps could include despiking, scrubbing, or outlier detection. Finally, time series are linearly detrended to remove possible signal drift by a band-pass filter. For a detailed comparison of pipelines, see [62].

OPTIMAL PIPELINE

Applying a preprocessing pipeline became an art. There are countless variations and techniques [62]. Critically, there is no consensus on the optimal preprocessing strategy that should be applied to fMRI scans [63]. Recently, Esteban *et al.* [64] proposed a robust, easy-to-use, and transparent preprocessing pipeline called the *fMRIPrep* (Fig. 1.6). Since the preprocessing pipeline can significantly influence derived brain topology measures, a general effective pipeline is of utmost importance. Being able to quantify the performance of each pipeline would greatly help in the search for the optimal one.

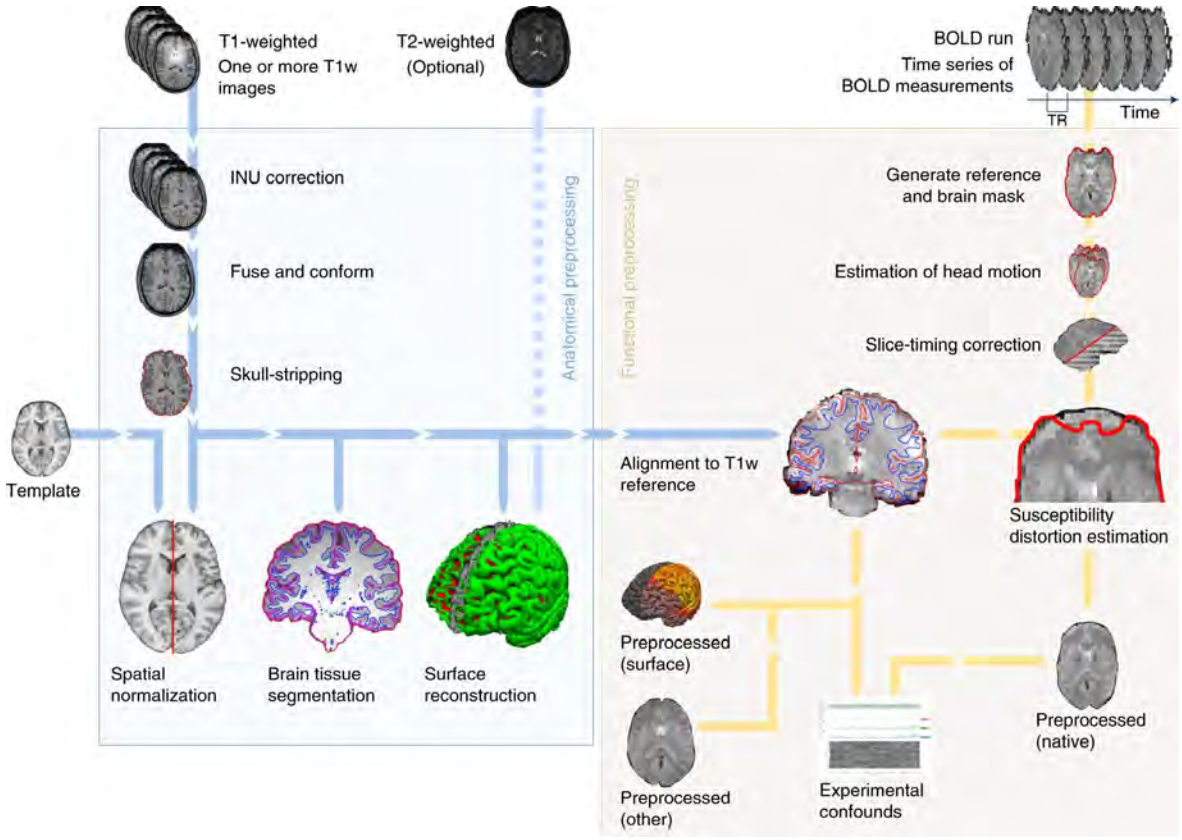

Figure 1.6: Proposed standard for fMRI preprocessing. Currently, there is no consensus on optimal fMRI preprocessing. Each preprocessing consists of several steps applied to T1-weighted and T2-weighted images. Recently, Esteban* et al. *[64] proposed a robust, easy-to-use, and transparent preprocessing pipeline called the fMRIPrep. It performs minimal preprocessing steps, i.e., motion correction, field unwarping, normalization, bias field correction, and brain extraction. Source: [64].*

1.6.2 Brain parcellation

The BOLD signal could be extracted from approximately 100,000 voxels. However, a common approach is to subdivide the brain into units using an atlas-based parcellation method. Brain parcellations divide the brain's spatial domain into a set of non-overlapping regions of interest (ROI) that show some homogeneity with respect to the information provided by one or several image modalities, such as cytoarchitecture, task-based fMRI activations, or anatomic delineations [65, 66]. Indeed, one of the main differences between several parcellations is whether they are based on anatomy or brain functionality. The structural atlases have the advantage of deriving neuro-biologically meaningful brain atlases, but they might fail to fully reflect the brain's intrinsic organization and capture the functional variability inherent to individual brains. Further delineation is based on whether cortical surfaces are subdivided independently for each subject (subject-level methods) or if representative models of a population are built (group-level).

The impossibility of optimal brain MRI parcellation makes the definition of regions of interest arbitrary [67]. Therefore, the number of ROIs ranges from 10 to 10^4 in voxel-based studies (for review, see [68]). Finally, when appropriate parcellation is selected, the final BOLD signal for a given ROI is calculated as either mean intensity across all regions' voxels, or alternatively, as the first component of the principal component analysis of all voxels' time series.

Brain atlases are useful not only in fMRI studies but also while working with iEEG. Typically, iEEG needles target various structures in a non-homogeneous way. Since the sampling of structure differs across subjects, brain atlas offers a way of assignment iEEG contacts to certain brain regions, and thus it increases comparability of implantations across subjects. Moreover, because some regions are either under-sampled or not sample at all, data from all patients could be pooled together, forming a meta-patient with a significantly better-sampled brain.

1.7 Other modalities

There are several other functional neuroimaging modalities, such as positron emission tomography (PET), magnetoencephalography (MEG), functional near-infrared spectroscopy, single-photon emission computed tomography, or functional ultrasound imaging. Here,

we briefly discuss two of them, i.e., MEG and PET, to illustrate why fMRI and EEG are the most common techniques.

Positron emission tomography is based on the same assumption as fMRI, specifically, that the blood flow to an area increases when the area is active. In PET imaging, a radioactive substance called radiotracer is used to visualize and track changes in metabolic processes (e.g., changes in blood flow). Radiotracer consists of radionuclide (positron-emitting isotope) and an organic ligand. The ligands used in PET scanning are compounds normally present in the body, such as glucose, water, ammonium, or molecules that bind to receptors or other sites of drug action. Upon injection, the radiotracer emits positrons, which then emit gamma rays after colliding with brain tissue electrons. The PET scanner detects these gamma rays. Common radiotracers in brain imaging are 18F-FDG and oxygen-15. Using oxygen-15 indirectly measures blood flow to the brain similarly as in fMRI. Using 18F-FDG measures regional glucose use and can be used in neuropathological diagnosis. The limitation of a PET scanner is a low number of scans that can be taken in a session due to the radioactive substance injection. Moreover, the session must be kept short to limit the amount of radiation the subject is exposed to. The typical temporal resolution of approximately 40 s is significantly lower compared to fMRI. Finally, the PET scanner has a high initial cost and ongoing operating costs.

Magnetoencephalography is a direct measurement of brain activity using magnetic fields. Electrical currents generated by neuronal activity create magnetic fields. Even though these fields are faint, they can be measured with highly sensitive magnetometers. The most commonly used magnetometer now is the array of SQUIDs (superconducting quantum interference device). SQUIDs need to be cooled to -270°C, usually using liquid helium. Furthermore, imaging must be performed in a shielded room that blocks other confounding sources of magnetic fields. Although MEG is a similar measurement to EEG, there are important differences. Magnetic fields are less distorted by the skull, and the measurements are reference-free. MEG has a better spatial resolution, but it decays with distance as it detects intracellular currents associated with postsynaptic potentials. Therefore, it is more sensitive to superficial cortical activity. Moreover, MEG is most sensitive to activity originating in sulci in contrast to EEG that detects activity both in the sulci and at the top of the cortical gyri. With very high temporal resolution and no health risks, the main limitation lies in high cost and limited resolution for deep structures.

Chapter 2

Connectivity

In this chapter, we lay the fundaments of connectivity analysis. Key terms and different types of connectivity are introduced here. Moreover, we describe the most common methods of connectivity estimation. As each method is more suitable for a different situation, we try to highlight their strengths and weaknesses. The chapter ends with general recommendations and instructions on optimal method selection.

2.1 Long history

> *"Nothing defines the function of a neuron better than its connections - Understanding these patterns of cortical connectivity is absolutely essential for understanding the relational architecture, and therefore function, of large-scale neurocognitive networks [69]."*

Our current understanding of cognitive abilities is rooted in the coordinated activity of distributed cortical networks, including brain structures remote from each other and connected by long-range association bundles in the cerebral white matter [70]. In this view, connections and connectivity play a key role. Therefore, the field of connectomics [71], the comprehensive study of all aspects of brain connectivity, became one of the major topics of modern neuroscience. However, the history of connectomics, also sometimes labeled as hodology, is very long (for a rich overview, see [23]). The word hodology derives from the Greek *hodos*, meaning "*path*". It is the Greek physician Galen ($\approx$ 200 AD) who concluded that mental actively occurred in the brain rather than the heart. He provided the first anatomical reports based on the dissection of monkeys and pigs. Moreover, he

studied how Gladiators' head injuries impaired thinking and movement. His idea of brain chambers (ventricles) connected by hollow nerves in which a fluid (called *psychic pneuma*) circulates was one of the main theories until the Renaissance.

In the 16th century, a great advance in our understandings came with new methods of brain investigation. The primary method that led to new important anatomical discoveries was the post-mortem dissection. The study of brain anatomy further expanded in the 17th century when researchers recognized that white matter contains fibers whose trajectories could be followed. Detailed anatomical accounts of human brain connectivity were derived. At that time, the concept of connectivity was limited to fibers and tracts. Although a later concept of phrenology offered a way of mapping functions onto the structure, there was another line of thinking, a more holistic view of brain functions. At that time, aphasia was a focus of intellectual speculations. Aphasia is an inability to comprehend or formulate language. Basing their observations on the study of damaged brain and post-mortem inspections, researchers such as Broca and Wernicke identified a region in the left frontal lobe (Broca's area) and in the left posterior superior temporal lobe (Wernicke's area) to play a critical role in speech and language [28]. Therefore, Wernicke and Lichtheim proposed a revolutionary Wernicke-Lichteim model of aphasia (Fig. 2.1). The model is represented as a simple diagram with three language-related centers within the brain and the neural pathways connecting them. However, this model was not only neuroanatomical, i.e., a description of fiber bundle connections, but critically also functional. For the first time, it provides a framework for associating clinical syndromes with specific disruptions of the brain's anatomical connections and thus, classify seven types of aphasia.

In sharp contrast to phrenology, Wernicke and Lichtheim provided the first evidence for the idea of distributed computing in their seminar papers. Based on their observations, complex functions arrive upon coordinated co-activation and integration of several specialized areas. In their view, every area performs a very small task, and large tasks are achieved by integrating smaller local centers. These assumptions align with our idea of distributed processing, where cognitive functions arise from the coordinated activity of large-scale brain networks consisting of distant cortical regions [70].

The Wernicke–Lichtheim model was widely criticized until revived by Norman Geschwind

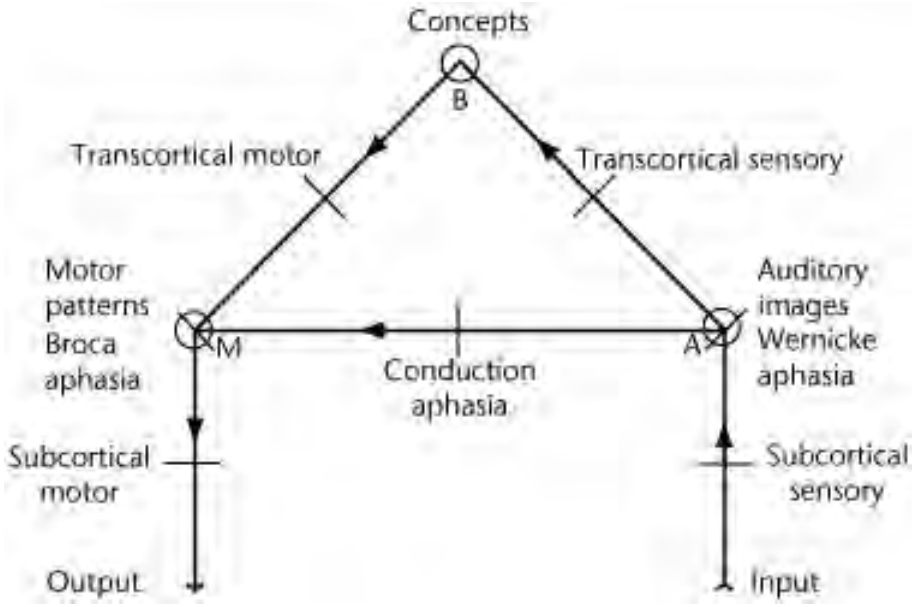

Figure 2.1: Wernicke–Lichtheim Model of Aphasia (based on Lichtheim, 1885). Numbers indicate lesion sites associated with each of the proposed types of aphasia: 1 = Broca's aphasia; 2 = Wernicke's aphasia; 3 = Conduction aphasia; 4 = Transcortical motor aphasia; 5 = Subcortical motor aphasia; 6 = Transcortical sensory aphasia; 7 = Subcortical sensory aphasia. Source: [72].

in the 1960s, who again stresses that language is conceived in associationist terms of centers and pathways. However, it was not only aphasia but also apraxia, agnosia, and various mental disorders that further pushed the connectivity field. In 1885 Theodor Meynert's described how damage to structural connections leads to psychiatric illness. Even though his view acknowledged the central role of fiber systems in functional integration, understanding the nature of the neural activity and the mechanisms by which neural elements exchange and transmit information were still missing [71]. Moreover, assessing brain connectivity still required several steps, such as injection of tracers *in vivo*, sacrifice, brain slicing, time-consuming observations, and skillful but subjective drawings; an example being the detailed anatomical tract-tracing of a parahippocampal-hippocampal network [73]. Most of these steps would be considered unacceptable in human samples.

Therefore, future advances were brought by a complete cellular connection map of the nematode *Caenorhabditis elegans* by Sydney Brenner and extensive studies of visual regions in the macaque cortex by Semir Zeki. His study led to some of the first network diagrams of large-scale cortical systems. This pioneering work stressed the segregation of function into a mosaic of specialized brain regions and their integration in the course of perceptual processing [71]. The first connectivity matrix was then achieved through the

work of Dan Felleman and David Van Essen [74]. Their models of cortico-cortical and cortico-subcortical pathways, including hierarchical and parallel organization, provided solid foundations for future computational approaches to brain function (Fig. 2.2).

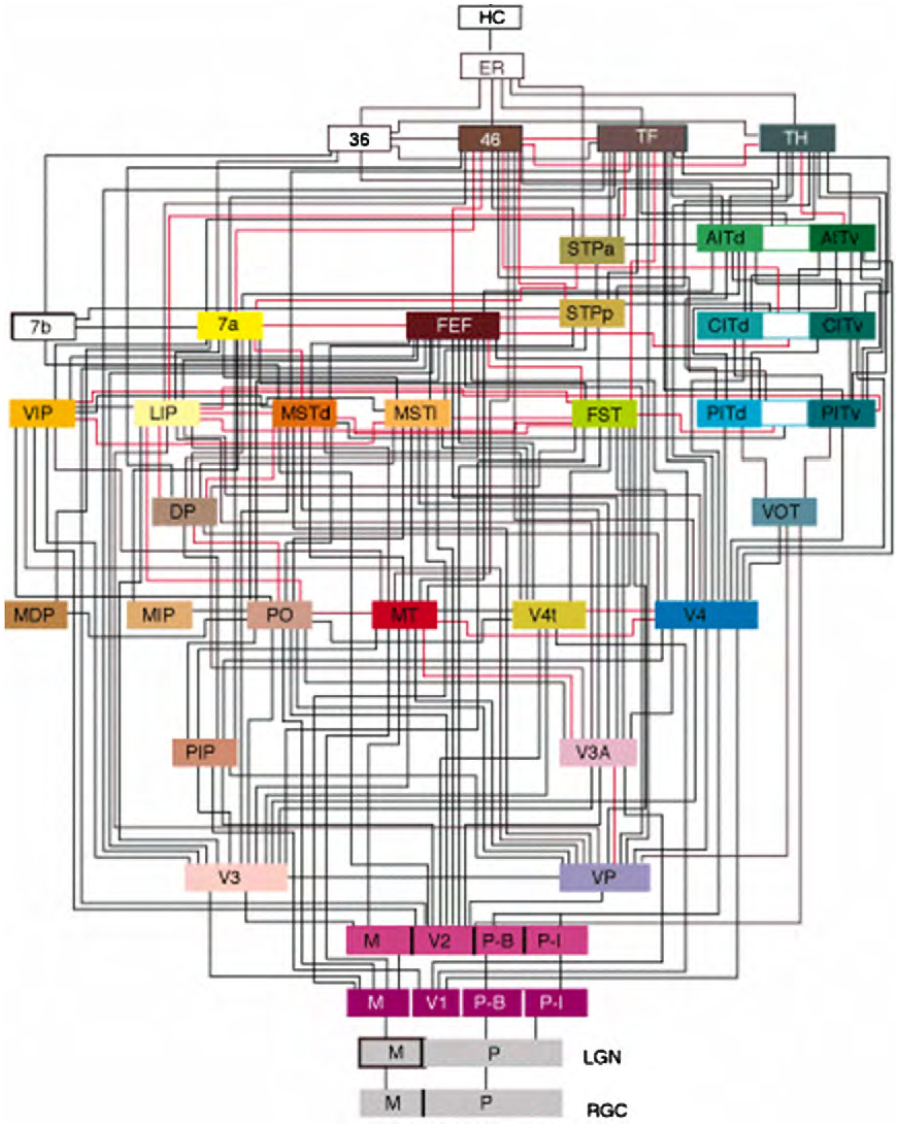

Figure 2.2: Hierarchy of visual areas, The hierarchical model of the visual cortex based on structural connectivity as derived by Felleman & Van Essen [74]. One of the limitations of such a model is the lack of quantification of connectivity strength between different areas meaning that the arrows and lines in the diagrams could represent single axons or large bundles [23].

The revolution came with new neuroimaging techniques, allowing non-invasive, fast, whole-brain, repeatable, and multimodal structure-function measurements in living humans. It was mainly the invention of MRI that allows us to assess multiple modalities, such as structural and functional domains. It helped us frame our current networking

model of cognition, where brain processing results from the integration of parallel (and possibly partially overlapping) subnetworks where connectivity plays the key role [75].

The importance of connectivity was further supported by the studies from computational neuroscience. In the 1980s first computational models were used to combine the knowledge from anatomy (in the form of structural connectivity) and physiology (in the form of differential equations describing the underlying process). In doing so, they generated simulated time series data comparable to recordings obtained from real neuronal systems. Moreover, such a model helps to study the influence of perturbations and alterations. In conclusion, based on the combination of structural and functional mapping techniques, a new term - connectome has emerged, and it can be best characterized as:

> *A comprehensive map of neural connections whose purpose is to illuminate brain function [71].*

2.2 Basic concepts

Historically, neurophysiologists tended to record only from one neuron or neuronal ensemble at a time to determine the recorded unit's functional specialization [76]. A breakthrough came with the macroscopic-level measurement - the EEG. Researchers began investigating functional relationships between the activity of different cortical regions [77]. Furthermore, after the introduction of fMRI, human brain mapping witnessed a sharp increase in popularity. The early studies focused mainly on localizing brain activity by constructing maps indicating brain regions activated by certain tasks. However, several studies also focused on how brain regions interact and how these interactions depend on experimental conditions and behavioral measures. In 1991, the notion of functional synchronization was formally extended to the study of functional and effective connectivity [78]. Over time, the focus shifted from the highly localizationist approaches of early neuroimaging research to a focus on brain networks [5]. Not only brain segregation but also brain integration makes the full picture of brain functioning. Nowadays, the study of connectivity, mainly but not solely with the common macro-scale measurement - fMRI, is a well-established field.

In our current understanding, we picture the brain network as a set of interconnected

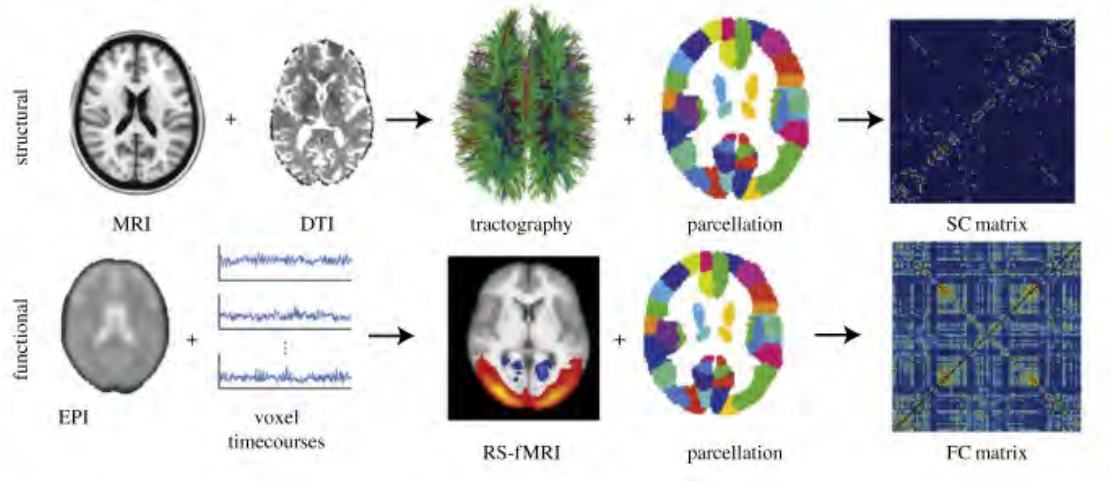

Figure 2.3: Estimating brain connectivity. We distinguish between three fundamental types of connectivity: structural, functional, and effective. Structural connectivity is commonly derived from MRI measurements using tractography. It represents the architecture of the brain and refers to a network of physical connections. On the other hand, functional connectivity is commonly derived from fMRI or EEG. It represents temporal dependencies between time-series of brain activity. Traditionally connectivity between all elements (e.g., parcellated brain regions) is represented by a connectivity matrix. Adopted from: [81].

brain regions with information transfer between different regions. We primarily differentiate between three types of connections: anatomical links, statistical dependencies, and causal interactions [79]. These correspond to three fundamental types of connectivity: structural, functional, and effective (Fig. 2.3). Connectivity is always defined between distinct units within the nervous system, e.g., individual neurons, neuronal populations, or anatomically segregated brain regions. Complex brain networks are thus formed by structurally connected neuronal elements that are functionally coupled. This coupling binds together activities of the distinct neuronal population, and it is thus crucial to elucidating how neurons and neuronal networks process information. Moreover, the interactions among distributed neuronal populations and brain regions are the basis for all cognitive processes [80].

Connectivity can be studied at various levels, such as across time revealing dynamically activated networks, across trials identifying coherent networks of task-related activations, across subjects emphasizing patterns of inter-individual differences, or across studies highlighting tendencies for studies to co-activate within sets of regions [82]. Each branch of connectivity encompasses a large number of methods. The selection of a method depends on underlying assumptions, level of the analysis, imaging modality, and sought

conclusions. The nature of the analyzed data is the main factor for connectivity method selection. As already discussed, data differ in terms of spatial and temporal resolution, or whether they represent neuron activities, neuronal ensemble activities, or regional activities.

Once carefully estimated, the connectome, i.e., the set of all connectivity values, is usually represented by a matrix. This matrix may be a suitable representation of the brain dynamical repertoire, potentially providing behaviorally or clinically relevant markers [60]. Listing all connectivity methods is beyond the scope of this thesis. In 2017 more than 700 neuroscientific articles that included connectivity were published [83]. The most prominent methods for each connectivity type are discussed in the following section.

LEVELS OF CONNECTIVITY

The brain is an emergent system. The complex brain functions emerge from the interactions between its components. Often these architectures are explicitly referred to as networks. Networks are present at different levels, from neurons to neuronal circuits and systems. At each of these levels, it is important to understand how the individual elements work and how they are interconnected into larger systems [15]. Cognitive abilities mostly involve structures and mechanisms at the highest levels. They are described by means of structural and functional connectivity. While anatomical networks provide the skeleton that constrains the passage of neuronal signaling and information, the functional networks represent regions engaged in the same distributed pattern of brain activity.

2.3 Structural connectivity

Structural connectivity represents the architecture of the brain and refers to a network of physical connections. Brain structure can be studied at various levels, from individual synaptic connections linking neurons into neuronal populations to big fiber bundles connecting brain regions. The different levels of cortical connectivity, including the organization of neuronal populations into networks of columns, are depicted in Fig. 1.1. Moreover, structural connectivity is believed to be dynamic. New synaptic connections are formed, or existing ones are eliminated dynamically and depending upon the executed

functions. Although anatomical connections are relatively stable at shorter time scales (seconds to minutes), they are subject to significant morphological change and plasticity at longer time scales (hours to days) [80].

Traditionally structural connectivity was studied using invasive methods [70]. Only recently, with the advance of MRI imaging, new methods have been developed. Currently, DWI-based methods are used to track white matter tracts across the brain [43]. As stated, DWI is based on the diffusion of water molecules. The diffusion is constrained by obstacles in the local environment, such as cell membranes, myelin sheaths, macromolecules, cytoskeleton, and other factors, including temperature, water content, fibrous tissue, or perfusion. Myelinated axons with similar destinations bundle together into fiber tracts and constitute the infrastructure for long-distance communication between spatially disparate brain regions. However, they provide a considerable barrier to water diffusion. The distribution of diffusion directions is aligned in parallel rather than perpendicularly with the direction of these fiber bundles. The degree to which diffusion is restricted to only one direction is described by fractional anisotropy (FA). FA reflects fiber density, axonal diameter, and myelination in white matter. Reduced FA can indicate damage to the axon membrane, reduced axonal myelination, or reduced axonal packing density. Increased FA can indicate supranormal levels of myelination or axonal sprouting [84].

In every voxel, we can represent diffusion displacement in every voxel in x, y, and z directions by a diffusion tensor. By estimating the diffusion tensor at each voxel of the DWI sequence, we obtain tensor imaging maps that provide descriptive brain tissue microstructure measures [43]. The diffusion tensor imaging (DTI) is using this tractography to estimate trajectories of white matter fibers [85]). The DTI is useful in tracking long-range connections and big fiber bundles. However, it is difficult to discover smaller connections due to issues such as the crossing of bundles.

Previous studies have found that the cerebral cortex has a unique modular architecture consisting of densely and reciprocally coupled cortical areas that are globally interconnected [86]. Even though Hagmann *et al.* [87] introduced the whole-brain structural networks mapping already in 2007, there are still discrepancies across studies. While brain regions are commonly defined based on a brain atlas-based parcellation, structural connectivity between two regions is ambiguous. It can be defined as the number, length, volume, or probability of all streamlines between the corresponding regions. Furthermore,

it can also be defined as the mean value of a diffusion metric within the volume along the path of streamlines between the interconnecting regions [88]. Nevertheless, changes in structural connectivity were already found for depression, sclerosis, Parkinson's disease, epilepsy, and other brain disorders (for an overview, see [89]). Moreover, using a connectivity fingerprint method, where the connectivity of each voxel to other regions is analyzed, Osher *et al.* [90] found that anatomical connectivity of individual gray-matter voxels alone can predict fMRI responses to 4 visual categories (faces, objects, scenes, and bodies). These discoveries underpin the relationship between structure and function in the human brain.

2.4 Functional connectivity

Functional connectivity was first measured by cross-correlating spike trains of neurons [91]. However, it can be principally applied to any functional neuroimaging technique. In 1995, Biswal *et al.* [92] recorded a BOLD signal during a finger-tapping task and at rest. When they correlated signals from the left motor cortex with every other voxel, instead of receiving a distribution of random correlations, they found a significant correlation with the right motor cortex (Fig. 2.4). Biswal *et al.* [92] actually successfully identified the motor network. Other research groups further successfully repeated these results [93]. It proved that anatomically distinct regions are capable of generating similar patterns of activity, even at rest. Based on these results, Friston *et al.* [94] formulated the notion of functional connectivity (FC). Functional connectivity is defined as an undirectional statistical association or dependency between two or more anatomically distinct time-series. In other words, regions engaged in the same distributed pattern of brain activity are likely to be doing the same, and thus they are functionally connected.

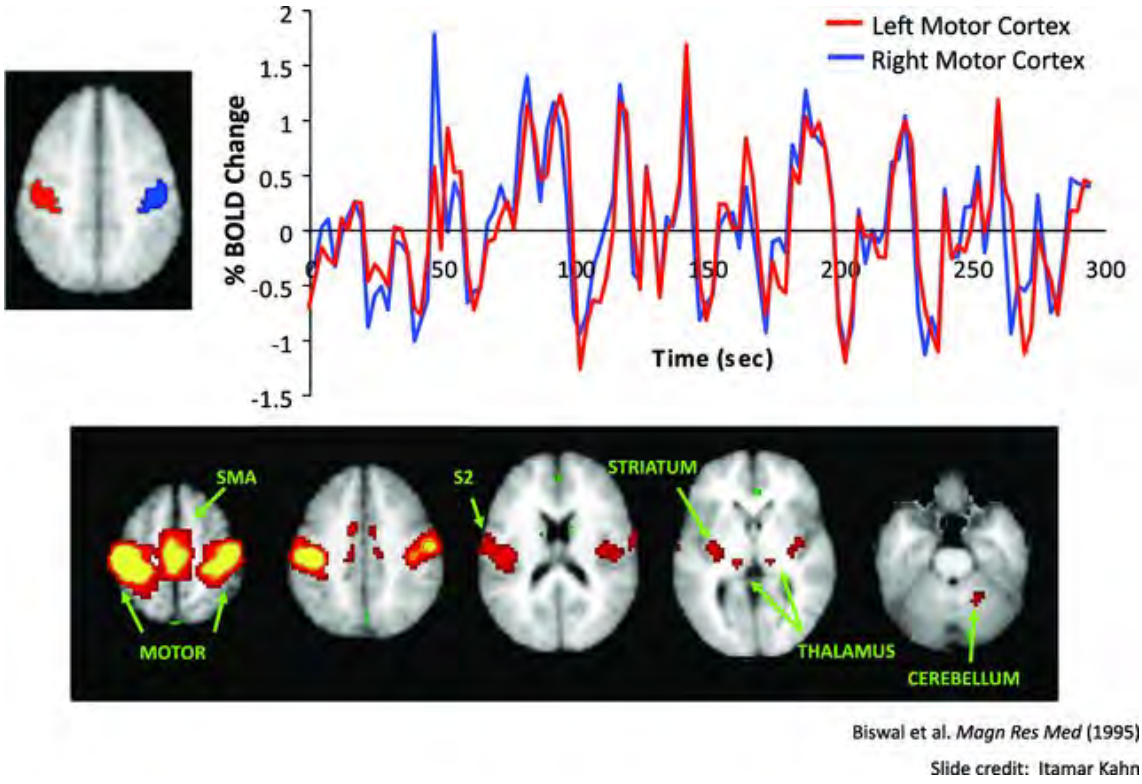

Figure 2.4: First functional connectivity from fMRI measurements. Here is a reproduction of the original result from Biswal et al. *[92]. The resting-state BOLD signal of the left motor cortex is significantly correlated with the signal from the right motor cortex. This finding laid the basis for modern fMRI connectivity analyses. Adopted from [15].*

Functional connectivity captures deviations from statistical independence between distributed and often spatially remote neuronal units. Even though it is solely a statistical concept, it reflects the level of functional communication between regions. FC makes no *a priori* assumptions, such as about underlying biology. Thus, it is a very straightforward approach, and it only relies on the notion that if two events occur simultaneously, they are synchronized (connected). These synchronizations reflecting continuous integration of information across brain regions play a key role in complex cognitive processes [60].

There are many ways on how to classify FC inference methods. We can generally distinguish between two groups: model-based and model-free (Fig. 2.5). In this thesis, we focused primarily on model-based methods that assume linear relationships between interacting elements. These methods are also commonly referred to as seed-based methods. In contrast to these seed-based methods, model-free methods do not require selecting seeds or a specific model. Model-free methods include mutual information, i.e., a measure of the inherent dependence, and machine learning methods. These, among others, include

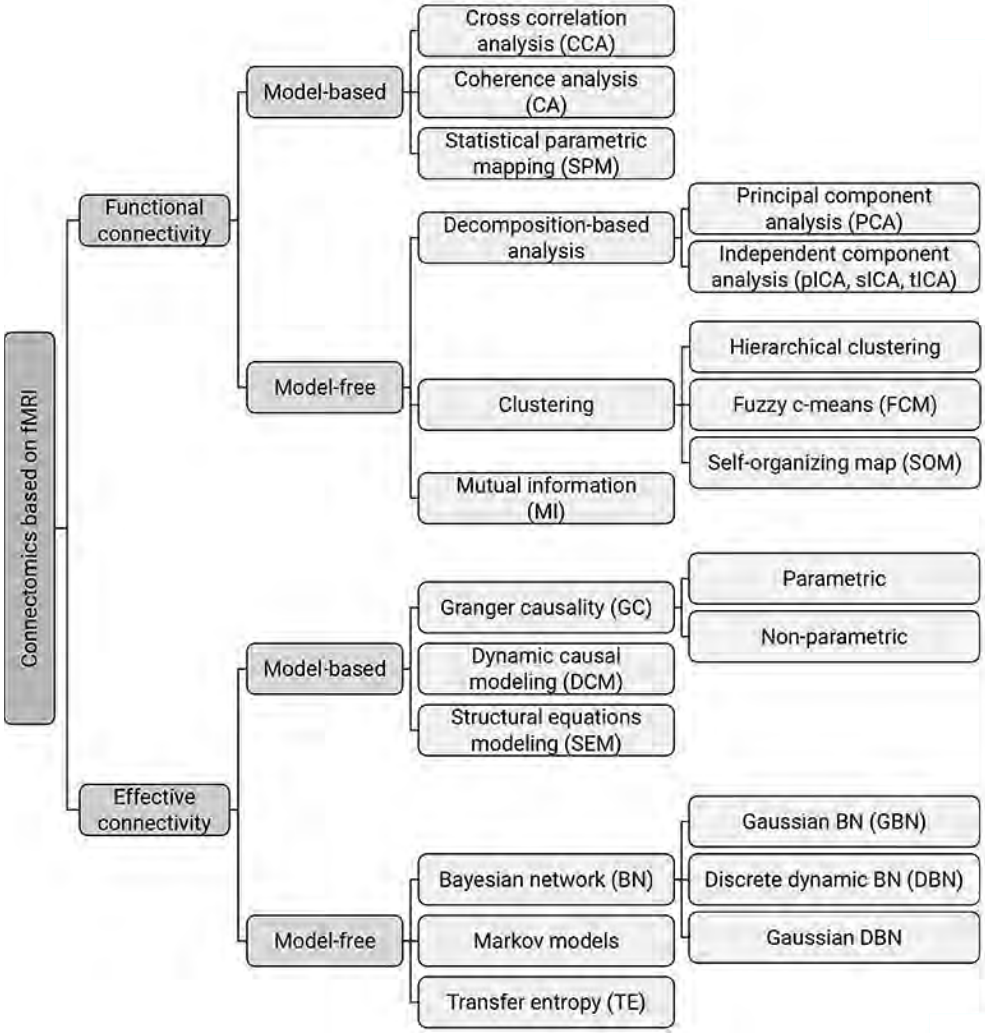

Figure 2.5: Different methods of functional and effective connectivity. There is a large family of both functional and effective connectivity methods that have been applied not only in fMRI but also in other neuroimaging techniques. They can be separated based on various characteristics, one of them being whether they are model-based or model-free. In this thesis, we focus mainly on the model-free methods. Reproduced from [95].

clustering and decomposition algorithms. They are able to capture hidden underlying patterns and quantify non-linear neuronal interactions. By doing so, they "let the data speak for themselves". However, their interpretability is less straightforward compared to seed-based methods.

The first group of model-free methods are decomposition algorithms. Multivariate decomposition methods operate to decompose the original matrix of activity of all regions into separate components. These components represent functionally homogeneous functional units, and they are used to find coherent brain networks. Two main decomposition methods are principal component analysis (PCA) [94] and independent component

analysis (ICA) [96]. PCA transforms a set of correlated variables into a set of orthogonal uncorrelated variables ordered by the amount of variability in the data they explain. These are the patterns that account for most of the variance-covariance structure in the data. On the other hand, ICA decomposes the data into spatially independent component maps with a set of corresponding time courses. These components again represent a mixture of underlying sources that can explain the activity patterns. An advantage is that ICA can isolate the noise to an individual component.

The second group of model-free algorithms form clustering algorithms. The general task of clustering is to group a set of objects so that the objects in the same group (cluster) are more similar to each other than to those in other groups (clusters). These objects might be represented by BOLD time courses of voxels and regions or electrical activity of EEG contacts. Currently, there are over 100 clustering methods that differ in the measure used to quantify similarity. Common algorithms that have been successfully applied in fMRI analyses include hierarchical clustering, k-means, fuzzy clustering, or self-organizing maps [95].

A seed analysis begins with selecting seeds either by *a priory* definition or by choosing from a task-dependent fMRI activation map. The seed is not necessarily a voxel, but it could be a brain region, EEG sensor, performance during a task, or a physiological variable. Further, connectivity between the seed and every other voxel/region is estimated. This can be achieved either by repeating connectivity estimation for every pair in a bivariate scenario or for all regions together using multivariate approaches. The connectivity can yield many forms depending on the analyzed relationships. The distinctions being whether these relationships are linear or non-linear, static or time-varying, frequency-resolved, amplitude-based, or phase-based.

Some seed-based algorithms might not effectively characterize the functional interactions among many together- working brain regions, and they might provide a large number of spurious or insignificant connections. Inverse covariance methods use regularization algorithms (e.g., least absolute shrinkage and selection operator - LASSO) to constrain the inverse of covariance and provide a more sparse representation of the brain network. More about these methods can be found in [97].

Several issues accompany functional and effective connectivity estimation. In LFP or EEG recordings, spurious connectivity can arise from using a common reference channel

where the activity of the reference is present at all channels. A similar effect is caused by volume conduction, where one recording channel picks up the activity of multiple neuronal sources. These issues can be resolved using bipolar montage or using connectivity methods that assume non-zero lag in synchronization. This issue is linked to measuring highly noisy signals (with low signal-to-noise ratio) where spurious differences in connectivity are again a risk [98]. Another interpretational issue is in making inferences about repeated pair-wise measurements. It was already demonstrated that in the case of an interrelated system with more than two channels, bivariate methods supply misleading information [99]. There is a risk that observed interactions are driven by a third source that has not been taken into account. Finally, the small or unequal sample size might also obscure the connectivity estimates as there may be a tendency to overestimate the connectivity in the condition with the smallest sample size [98].

This thesis focuses only on seed-based methods to characterize connectivity between two recorded time courses in a bivariate case or between multiple time courses in a multivariate case. Some of the representatives of these methods are correlation, spectral coherence, Granger causality, or phase locking value. Most of these methods assume temporal stationarity and zero-lag synchrony. To ensure these conditions are met, methods such as dynamic time warping can be used [100]. Moreover, we focus only on measures that assume only linear interactions between two time courses. It was proved that both in EEG [101] and fMRI [102], the interactions are mostly linear and that the linear methods perform well even for non-linear signals. Non-linear measures require long stationary segments and are very sensitive to noise. That makes them prone to errors. Therefore, there needs to be strong reasoning for non-linearity in the data to apply non-linear methods [103]. Moreover, non-linear methods are only bivariate (calculated pair-wise). Finally, the FC is still only a descriptive measure, and it does not provide any direct insight into the causes of observed correlations.

2.4.1 Correlation

A functional connectivity method widely applied in fMRI studies is the Pearson correlation coefficient. It is a statistical measure of linear relationship strength between two variables with values ranging between -1.0 and 1.0. Intrinsically, if two parts of the brain are functionally connected, there should be a correlation between their BOLD time courses.

Pearson's r between signals x and y is defined as:

$$r = \frac{s_{xy}}{s_x s_y} \tag{2.1}$$

where s_x and s_y are the sample standard deviations, and s_{xy} is the sample covariance.

In the general linear modeling framework, the squared correlation coefficient r^2 represents the fraction of the variance of one signal explainable by the other signal and vice versa.

Considering that after correlating all pairs of time series, the connectivity estimates might not be normally distributed, Fisher's r-to-z transformation is used. It transforms Pearson's r to a z-score as follows:

$$z = \frac{1}{2}[ln(1+r) - ln(1-r)] \tag{2.2}$$

The correlation coefficient assumes zero-lag between two signals, and it ignores the temporal structure of the signals. The way to account for a time-lag is to use cross-correlation. The cross-correlation function is computed by shifting (across multiple lags) the two signals with respect to one another before calculating correlation. This function may provide indices about directionality; however, it fails with bidirectional interactions, which is the case for most cortico-cortical connections. In this scenario, the cross-correlation function typically lacks a clear peak and has significant values at both positive and negative lags, indicating complex, bidirectional interactions at multiple delays [98].

The correlation coefficient is a pair-wise measure, and thus it might reflect the indirect influence of a third source inducing concurrent activity in both areas. The experimental setup itself might induce an undesired increase in FC, as Fornito *et al.* [104] describes:

> "*An example of such situation would be the feedforward of stimulus-driven activity in early sensory areas that is forwarded to parietal sensory areas for perceptual analysis and, in parallel, to the premotor cortex for response preparation. Even if both would be implemented in completely segregated streams, this scenario would lead to correlated activity changes in higher sensory areas and motor regions, that is, functional connectivity between them.*"

The way to control for the influence is to use partial correlation. It measures the degree of association between two random variables, with the effect of controlling random

variables removed. Partial correlation is more closely related to effective connectivity than marginal correlation. It was shown to provide relevant insight into the functional relationships between regions of the motor network and, particularly, confirmed the central role of the premotor cortices during simple-hand movements [105]. Moreover, methods calculating partial correlation could involve using matrix inversion and lead to Inverse covariance methods. Finally, a more general approach to the correlation that does not assume linearity is mutual information. Mutual information is a model-free method that detects both linear and non-linear correlations.

2.4.2 Coherence

We already stated that functional connectivity supports long-distance communication in the brain. Moreover, distributed neuronal populations synchronize their activity at specific frequencies [106]. Therefore, a frequency-resolved measure that captures relationships between neuronal ensembles is needed. Coherence is a mathematical method quantifying if two brain regions have similar neuronal oscillatory activity by assessing the frequency content of recorded signals.

First, the coherency measure is defined as:

$$C_{x.y} = \frac{|G_{x,y}|}{\sqrt{G_{x,x}G_{y,y}}} \tag{2.3}$$

where $G_{x,y}$ is a cross-spectral density between signals x and y, $G_{x,x}$ is auto-spectral density of signal x, respectively y.

The coherency is a complex-valued number with a magnitude smaller than or equal to 1 and an angle corresponding to the phase lag between the signals. The modulus of the coherency is known as the coherence or magnitude-squared coherence. It is a real-valued number between 0 and 1 and it is calculated as:

$$Coh_{x.y} = \frac{|G_{x,y}|^2}{G_{x,x}G_{y,y}} \tag{2.4}$$

If coherence is used to estimate the dependence between two EEG sensors, the resulting values can be influenced by volume conduction. The presence of one signal generator in more channels can significantly contribute to higher synchrony, which reflects redundancies in the measurement rather than true brain interaction. However, the coherence

can be represented in the form of real and imaginary values rather than magnitude and phase. It is a different representation of the same quantity. Notably, the imaginary part of the coherence is only affected by the synchronization of two processes time-shifted to each other. Since volume conduction does not result in a time shift, the imaginary part of coherence cannot be affected by volume conduction [107].

COHERENCE AND COMMUNICATION

Imaging methods with a high temporal resolution, such as EEG, iEEG, and MEG, have been investigated in order to understand brain information processing and transfer [108]. Previous studies already identified changes in network coherence in many brain regions and during various behavioral tasks. Such activity modulates functional connectivity among anatomically connected regions. Fries [17] introduced a *communication through coherence* (CTC) paradigm based on the notion that only coherently oscillating neuronal groups can communicate effectively. Therefore, the CTC states that selective communication is achieved through coherence between firing rate oscillation in the sending region and oscillatory gain modulation in the receiving region. While originally CTC focused only on gamma coupling, it was subsequently extended to consider slow (theta or alpha) oscillations as well [109], proving that several rhythms and their interplay render neuronal communication effective, precise, and selective.

Another observed phenomenon called cross-frequency coupling (CFC) proves that oscillations of different frequencies interact [110]. For instance, the phase of the hippocampal theta rhythm modulates the appearance of faster, gamma-frequency oscillations through a process known as phase-amplitude coupling [111, 112]. Recent studies proved that CTC and CFC might be part of the same mechanism for efficient long-range communication [113]. All in all, different co-existing processing modes enable dynamic switching between different modes of attention [114, 115].

The imaginary part of coherency can be derived directly from the complex coherency Eq. 2.3:

$$iCoh = imag(C_{x,y}) \tag{2.5}$$

A disadvantage of this procedure is that the imaginary part is usually very low or

vanishing, leading to missing some of the brain synchronizations. It is the trade-off for the certainty that the non-vanishing parts represent real brain connectivity.

Wavelet coherence

The spectral densities are commonly calculated using Fourier transform, but Wavelet transform could bring further advantages. Wavelet coherence provides a time-frequency resolution. In comparison to the Short-time Fourier transform, it circumvents the need to select a fixed sliding-window size. During the wavelet transform, the signal is continuously convoluted with wavelets of different scales. By adjusting the scale factor, different frequencies are analyzed. A low-scale wavelet is compressed, detecting high frequencies (rapidly changing details of short duration). Conversely, a high-scale wavelet is stretched, detecting low frequencies (slowly changing coarse features that last for a long period). That is why higher frequencies have better resolution in time, and lower frequencies are better localized in frequency. Wavelet coherence was already successfully applied in various scenarios [116–118].

The wavelet coherence of two time series x and y is:

$$WC = \frac{|S(C_x^*(a,b)C_y(a,b))|^2}{S(|C_x(a,b)|^2) \cdot S(|C_x(a,b)|^2)} \tag{2.6}$$

where $C_x(a,b)$ and $C_y(a,b)$ denote the continuous wavelet transforms of x and y at scales a and positions b. The superscript * is the complex conjugate and S is a smoothing operator in time and scale.

2.4.3 Phase locking value

The magnitude-squared coherence depends on both the magnitude and phase of the signals. Therefore, it is difficult to untangle their contributions to the computed coherence value. Since fluctuations in amplitude may contain less information about interactions than the relative phase, phase-based methods are recommended for testing hypotheses where phase and moment-by-moment synchronization changes are considered mechanisms for neuronal communication [17, 98].

The phase locking value (PLV) can be used as a statistic to investigate task-induced changes in long-range synchronization of neuronal activity [119]. This measure computes

the difference between instantaneous phases of brain signals. In functionally connected regions, the difference is constant or close to constant.

First, it is convenient to rewrite the oscillatory activity using Euler's formula. Therefore, the signal x is represented as a continuous process:

$$x(t) = Ae^{i\theta t} \tag{2.7}$$

where A is oscillation magnitude and θ is the phase.

This representation simplifies manipulations with the signal allows examination of the period, phase, and amplitude. Then, the PLV is defined as:

$$PLV = |\frac{1}{N}\sum_{n=0}^{N} e^{i\Delta\theta}| \tag{2.8}$$

where N is the number of trials and $\Delta\theta$ is the difference between the instantaneous phase of the two signals. When averaging across time-points, this measure is referred to as mean phase coherence [111].

The instantaneous phase is defined as the angle between the real and the imaginary parts of the Hilbert analytical signal. For the phase to be physically meaningful, only one oscillator must be present in each signal. This is achieved by employing a narrow-band pass filtering [120]. Other measures that quantify consistency in phase differences are the phase slope index, phase lag index, and pairwise phase consistency.

2.5 Effective connectivity

The next step of a connectivity analysis is instead of measuring indirect connections, to measure directed causal influences between neuronal elements. In contrast to functional connectivity, a purely descriptive measure, effective connectivity (EC) makes more powerful theoretical inferences. However, it is for the cost of strong assumptions. It is defined as the direct influence that one neuronal system exerts over another [94]. Since usually, we are not able to perturb the system to observe caused effects, the EC rests explicitly on models trying to explain system behavior and dependencies. Thus, the EC, representing coupling or directed causal influence, is reduced to a comparison of models. An illustrative example is comparing a model with and without a particular connection to infer the

presence of EC [121]. Aertsen & Preissl [78] proposed that:

> *"The [electrophysiological] notion of effective connectivity should be understood as the experiment and time-dependent, the simplest possible circuit diagram that would replicate the observed timing relationships between the recorded neurons."*

Therefore, in this notion, each model corresponds to an alternative hypothesis explaining how observed data were generated, and thus the EC basically recapitulates the experiment. The link between FC and EC is that the EC corresponds to the parameter of a model that tries to explain FC.

There are fundamentally two groups of effective connectivity analysis: model-free and model-based (Fig. 2.5). The model-based techniques require the specification of the underlying model, for example, using structural connectivity. The EC is then inferred through systematic perturbations of the system. A typical representative of these measures is Dynamic causal modeling (DCM). Another model-based based method is Granger causality (GC). In contrast to DCM, GC is a more data-driven method, and the EC inference is based on time-series analysis. The constraint is thus the detection of only linear relationships.

Effective connectivity can be used to analyze synchronizations, track information flow, and infer causality within a neuronal circuit [122]. The methods of EC are commonly applied both to EEG and fMRI. In fMRI, they were, for example, used to describe the hierarchical organization of the cortical network for face perception [123]. Moreover, using high-density EEG combined with transcranial magnetic stimulation, which allows perturbation of brain networks, has revealed a striking reduction in the extent of effective cortical connectivity during non-REM sleep compared to waking [124].

Here, we describe the two classical EC inference methods: Granger causality (plus its extension to Directed transfer function and Partial directed coherence) and Dynamic causal modeling. Other methods include Structure Equation Modeling, Bayesian network, Transfer entropy, Markov models, or Psychophysiological Interaction.

2.5.1 Granger causality

Granger causality (GC) was originally developed for econometric studies, but nowadays, it is commonly used in various areas. The Granger causality is a statistical hypothesis

test for determining whether a time course is useful in forecasting another. It implements a statistical, predictive notion of causality whereby causes precede and help predict their effect. Following Geweke's estimation of linear dependence, we model each time course using a vector autoregressive (VAR) model of order p [125]. Assuming two jointly distributed time series x and y, then their VAR formulation is:

$$\begin{aligned} x_{1,t} &= \sum_{k=1}^{p} = a_{1,k} x_{t-k} + \epsilon_{1t} \\ y_{1,t} &= \sum_{k=1}^{p} = b_{1,k} y_{t-k} + \sigma_{1t} \end{aligned} \tag{2.9}$$

where a and b are parameters of the autoregressive process, ϵ and σ represent residuals, and p is the model order.

The appropriate model order choice can be problematic because it can vary depending on the subject, experimental task, quality, and complexity of the data and model estimation technique used [126]. Techniques such as Akaike or Bayesian information criterion can be used to estimate the model order.

Under a predictive interpretation, these models quantify the extent to which x and y are predicted by their past. Next, we expand the model to combine how x is predicted by its own past plus the past of y and vice versa:

$$\begin{aligned} x_{2,t} &= \sum_{k=1}^{p} a_{2,k} x_{t-k} + \sum_{k=1}^{p} c_{2,k} y_{t-k} + \epsilon_{2t} \\ y_{2,t} &= \sum_{k=1}^{p} b_{2,k} y_{t-k} + \sum_{k=1}^{p} d_{2,k} x_{t-k} + \sigma_{2t} \end{aligned} \tag{2.10}$$

Finally, Granger causality from y to x (the degree to which the past of y helps predict x, over and above the degree to which x is already predicted by its own past) can be

formally written as the log-likelihood ratio:

$$\begin{aligned} F_{y\to x} &= ln\frac{\Sigma_1}{\Sigma_2} \\ \Sigma_1 &= var(\epsilon_{1t}), \Sigma_2 = var(\epsilon_{2t}) \end{aligned} \tag{2.11}$$

and conversely for Granger causality from x to y. If the inclusion of the cross-autoregressive term significantly improves the model, we say that y Granger-causes x.

Assuming that the generalized variance of a regression model represents a model prediction error, then another interpretation of Granger causality is that it quantifies the prediction error reduction when the past of y is included in the explanatory variables of a process x [127]. The GC is not only a statistical test, but the F-value magnitudes are comparable, and they have a natural interpretation in terms of information-theoretic bits-per-unit-time. It is because, in the Gaussian case, GC is equivalent to Transfer entropy that is often described as a measure of information flow [126].

However, the unconditional causality between x and y might not only reflect direct causes between the two variables, but it can be driven by a third common variable z. This spurious increase especially endangers repeated bivariate analysis. If this z is observed, it can be eliminated by conditioning out. Let us write the reduced and full VAR model for variable x:

$$\begin{aligned} x_{1,t} &= \sum_{k=1}^{p} a_{1,k}x_{t-k} + \sum_{k=1}^{p} c_{1,k}z_{t-k} + \epsilon_{1t} \\ x_{2,t} &= \sum_{k=1}^{p} a_{2,k}x_{t-k} + \sum_{k=1}^{p} b_{2,k}y_{t-k} + \sum_{k=1}^{p} c_{2,k}z_{t-k} + \epsilon_{2t} \end{aligned} \tag{2.12}$$

analogous to Eq. 2.9 and Eq. 2.5.1.

Then the causality Granger causality of y on x conditioned on z is again:

$$\begin{aligned} F_{y\to x|z} &= ln\frac{\Sigma_1}{\Sigma_2} \\ \Sigma_1 &= var(\epsilon_{1t}), \Sigma_2 = var(\epsilon_{2t}) \end{aligned} \tag{2.13}$$

Note that the source, target, and conditioning variables x, y, z may be multivariate,

representing groups of variables. In this scenario, we talk about multivariate GC (MVGC). The fact that MVGC is able to account for group interactions is very important since elements in a multivariate system may function cooperatively, competitively, or interact in a more complex fashion than in traditional bivariate analysis [126, 127].

It is worth mentioning that the GC depends entirely on an appropriate selection of variables. Causal factors that are not incorporated into the regression model cannot be represented in the output. Another feature is that it only represents a directed linear influence between stationary signals. Stationarity is defined as a stochastic process whose unconditional joint probability distribution does not change when shifted in time. To account for directed non-linear forms of interactions, Transfer entropy was implemented.

Although MVGC is a powerful concept commonly used in EEG and fMRI data-driven analyses, it is only a time-domain concept. There are two main functions - Direct transfer function (DTF) and Partial directed coherence (PDC), derived from coefficients of an MVAR model to provide frequency-resolved dependency. As they are very similar with the main difference in applied normalization, we will primarily describe PDC and only mention DTF. However, as connectivity estimation might differ for both methods, there is still ongoing discussion as to which method is preferable. Therefore, for appropriate selection, we refer the reader to [128].

2.5.2 Partial directed coherence

Baccalá & Sameshima [129] introduced a Partial directed coherence (PDC) that is a frequency-domain representation of the concept of GC. It allows discerning the frequency domain characteristics of involved signals, which is especially important in the analysis of EEG and MEG data [129], but PDC was also successfully applied in fMRI [130].

The basis of PDC analysis lies in transforming MVAR coefficients (Eq. 2.11 and Eq. 2.13) to the frequency domain. For a multivariate n-channel process
$X(t) = [X1(t), X2(t), ..., Xn(t)]^T$, the MVAR model is given by:

$$X(t) = \sum_{k=1}^{p} A_k X(t-k) + \sigma(t) \tag{2.14}$$

where A_k contains the MVAR coefficients $a_{ij}(k)$ of order p.

Then their frequency domain representation can be written as:

$$A(f) = \sum_{k=1}^{p} A(k) e^{-i2\pi fk} \tag{2.15}$$

Further, the transfer function can be quantified as $\overline{A_{ij}}(f) = I - A_{ij}(f)$ where the elements of $\overline{A_{ij}}(f)$ are defined as:

$$\overline{A}_{ij}(f) = \begin{cases} 1 - \sum_{k=1}^{p} a_{ij}(k) e^{-2j\pi fk}, & \text{if } i = j \\ - \sum_{k=1}^{p} a_{ij}(k) e^{-2j\pi fk}, & \text{otherwise} \end{cases} \tag{2.16}$$

Finally, the Partial directed coherence from channel j to i at the frequency of f is:

$$\pi_{i \to j}(f) = \frac{\overline{A}_{ij}(f)}{\sqrt{\sum_{k=1}^{n} \overline{A}_{kj}(f) \overline{A}^{*}_{kj}(f)}} \tag{2.17}$$

where $\overline{A}_{ij}(f)$ is an element of $\overline{A}(f)$, n is the number of channels , and $*$ denotes the complex conjugate operation.

PDC reflects the ratio of the power spectrum of X_j at frequency f, which is sent to the spectrum of X_i. Intuitively it can be understood as if the original signal would be filtered to a specific frequency band, and then we would calculate the MVGC.

2.5.3 Directed transfer function

Directed transfer function was introduced by Kaminski & Blinowska [131]. Causal influence of channel j on channel i at frequency f can be written as:

$$DTF^{2}_{j \to i}(f) = \frac{|H_{ij}(f)|^2}{\sum_{m=1}^{k} |H_{im}(f)|^2} \tag{2.18}$$

where $H_{ij}(f)$ is an element of a transfer matrix of MVAR model.

The main difference between DTF and PDC is the matrix inversion and normalization where:

$$H_{ij}(f) = \overline{A}^{-1}_{ij}(f) \tag{2.19}$$

DTF already found multiple applications, for example, in sleep analysis, epilepsy research, or information flow investigation in general[132].

2.5.4 Dynamic causal modeling

Unlike the GC and other data-driven methods, Dynamic causal modeling requires *a priori* definition of a specific model. It relies on comparing different state-space models. Therefore, DCM is not suitable for exploratory analyses, but rather it is used to test concrete hypotheses that generated the data [133]. It is a framework for specifying models, fitting them to data, and comparing their validity. The principle is to model the dynamics of brain region fluctuations that are causing activity in other regions. A set of differential equations describes interactions of neuronal populations that directly or indirectly give rise to functional neuroimaging data. Therefore, we use a forward neuronal model that tries to explain the transformation into the observed response of interacting regions. In the context of fMRI, this forward model relies on the assumptions that changes in neuronal activities cause changes in hemodynamic response, which we can measure using fMRI, and that we can model latent (unobserved) neuronal activations using hemodynamic time series.

As already stated, the EC is based on the parameter comparison of different models. In DCM, the parameters represent the coupling among the latent neuronal activity in various regions. They quantify the directed influences among neuronal populations. Thus, we search for which model (coupling) parameters best account for the observed data. These parameters are estimated from the data using Bayesian statistical methods.

DCM operates with state equations that model the neuronal states and the non-neuronal states. We can write the state-space model as follows:

$$\begin{aligned} \dot{z} &= f(z, U, \Theta^{(n)}) \\ y &= g(z, \theta^{(h)}) + \epsilon \end{aligned} \tag{2.20}$$

where the change in latent neuronal states $\dot{z}$ depends on neuronal function f with parameters $\Theta^{(n)}$, experimental input u, and neuronal activity z. The observed function g of non-neuronal states depend on hemodynamic parameters $\Theta^{(h)}$ and observational noise ϵ.

The neuronal parameters $\Theta^{(n)}$ are of key interest because they represent connection strengths and might be modulated by experimental conditions.

Friston *et al.* [133] defines the change of a neuronal state-vector z as:

$$\dot{z} = (A + \sum_{j=1}^{m} u_j B^j)z + Cu \tag{2.21}$$

where $\dot{z}(t)$ is the latent neuronal activity at time t and $u(t)$ is the known j-th input at time t.

This bi-linear state equation describes how the neuronal activity at time t changes. The matrix **A** represents intrinsic fixed connectivity among regions. It specifies how regions are connected and whether these connections are uni- or bidirectional. The matrix **C** represents the direct driving effects of inputs on the neuronal activations. It specifies how these inputs are connected to different regions. Finally, the matrix **B** represents connectivity modulatory effects. It specifies how the inputs change connections.

Having defined various state-space models, each of which embodies different assumptions about how connectivity is modulated, the Bayesian model comparison method compares the models of how time series data were generated and determines whether data favors one model or another. Originally defined for fMRI [94], the DCM was successfully applied in MEG and EEG studies as well [134].

2.6 Remarks on connectivity estimation

In the previous sections, we touched upon only a very few connectivity estimation algorithms. While some methods differ in their very statistical nature, such as phase locking value and correlation, other metrics can be viewed as derivatives of the basic methods, such as the Granger causality and Partial directed coherence. We focused here only on model-based methods that assume linear relationships. For further reading on functional connectivity methods or modeling of multivariate relationships, we refer the reader to [98], respectively [99].

The choice of an appropriate connectivity measure depends solely on the studying hypothesis and underlying assumptions. Assuming we are studying functional interactions between regions, one would turn to FC and EC methods. If we are interested in directional interactions or have a hypothesis about the underlying model, effective connectivity offers several candidates. Specific hypotheses about structures and dynamics generating observed data can be tested using DCM. On the other hand, a data-driven approach is

applied in methods related to Granger causality. If a specific frequency is of our interest (a common scenario in EEG analysis), one will choose PDC or DTF as Granger causality derivatives. Finally, if we have a strong assumption that non-linear interactions explain a significant portion of variance, Transfer entropy is recommended as a measure operating in the time domain.

When analyzing temporal dependencies and describing observed patterns, FC offers a wide range of methods. Again, we can differ between model-based methods such as correlation or coherence that assume linear dependence or mutual information in case when non-linear interactions account for most of the observed variability. Theoretically, coherence can be viewed as a correlation of signals filtered to a specific frequency band, and thus synchronization on given frequencies can be investigated. Furthermore, if the underlying communication is thought to be based on phase synchronization, the PLV algorithm is preferable to coherence, which also depends on the amplitude. In the case of EEG analysis, investigating the imaginary part of coherency can bring further advantages as it is insensitive to volume conduction. Finally, inferences about repeated pair-wise measurements should be analyzed, preferably via multivariate methods [99].

Chapter 3

Large-scale networks and their properties

Modern neuroscience revolves around networks. Our understanding of brain processes states that complex brain functions arise from interactions between large-scale networks. In this chapter, we begin with the identification of these functional networks. Then, we move to mapping differences between subjects. They could be caused by artificial causes such as noise, but they also reflect real inter-individual differences. How much of these real inter-individual differences are explained by differences in structure still remains an open question. Finally, the fact is even more complicated by the existence of intra-individual variability. Connectivity dynamics and subsequent detection of brain states is a new promising avenue.

3.1 Identification of resting-state networks

Already Biswal *et al.* [92] observed BOLD signal fluctuations during both finger tapping and a resting condition, i.e., in the absence of tasks or stimuli. They consistently identified the same group of functionally related areas in the somatomotor cortex during both conditions. This discovery gave rise to the analysis of resting-state canonical brain networks. The resting-state analysis is rooted in acquiring spontaneous (intrinsic) brain activity data. Task-based analyses can enhance our understanding of dynamic context-dependent interactions, but they often have not contributed to a principled understanding of functional networks [6]. Since the canonical networks are identified at rest, they are

referred to as "resting-state networks" (RSN). They encompass spatially distinct regions with synchronous activity during the rest [135]. One advantage of acquiring data during rest is the possibility to study subjects with neurological disorders who might not be able to perform certain tasks.

Many canonical RSNs have been identified until now (Fig. 3.1), including the default mode network (DMN), the salience network, the dorsal attention system, frontoparietal control system, the somatosensory network including primary and higher-order motor and sensory areas, the visual network spanning much of the occipital cortex, auditory network consisting of the Heschl gyrus, the superior temporal gyrus, and the posterior insula, the medial temporal lobe memory system and the language network including Broca and Wernicke areas (for review, see [135] or [6]). These networks are reliably detected across imaging sessions and different subjects [136, 137]. Moreover, both seed-based and ICA analyses brought consistent results in identifying the networks indicating that these complementary methods extract common signals [135, 138].

Special attention has been brought to the default mode network (DMN) identified by Raichle *et al.* [140]. Regions of this network are consistently active during rest but show extensive deactivation during cognitively demanding tasks [93, 141]. This is the reason why this network was also sometimes labeled as the task-negative network. However, DMN was associated with many active cognitive processes that are internally focused. It is believed that the DMN comprises an integrated system for autobiographical, self-monitoring, and social cognitive functions [142]. Nevertheless, the functions of distinct DFN regions are very different [6]. DMN is primarily composed of the medial prefrontal cortex, posterior cingulate cortex/precuneus, and angular gyrus.

A counterpart to the DMN is the frontoparietal network (FPN), also labeled as the central executive network. It is involved in sustained attention, complex problem-solving, and working memory. The FPN is primarily composed of the rostral lateral and dorsolateral prefrontal cortex and the anterior inferior parietal lobule. The FPN and DMN are two of three networks from the triple-network model [142]. The third network is the salience network that is believed to facilitate switching between FPN and DMN. It comprises the anterior insula, dorsal anterior cingulate cortex, and other subcortical areas, including the amygdala, substantia nigra, ventral tegmental area, and thalamus [135]. Since this network is involved in the orientation of attention, it contributes to various

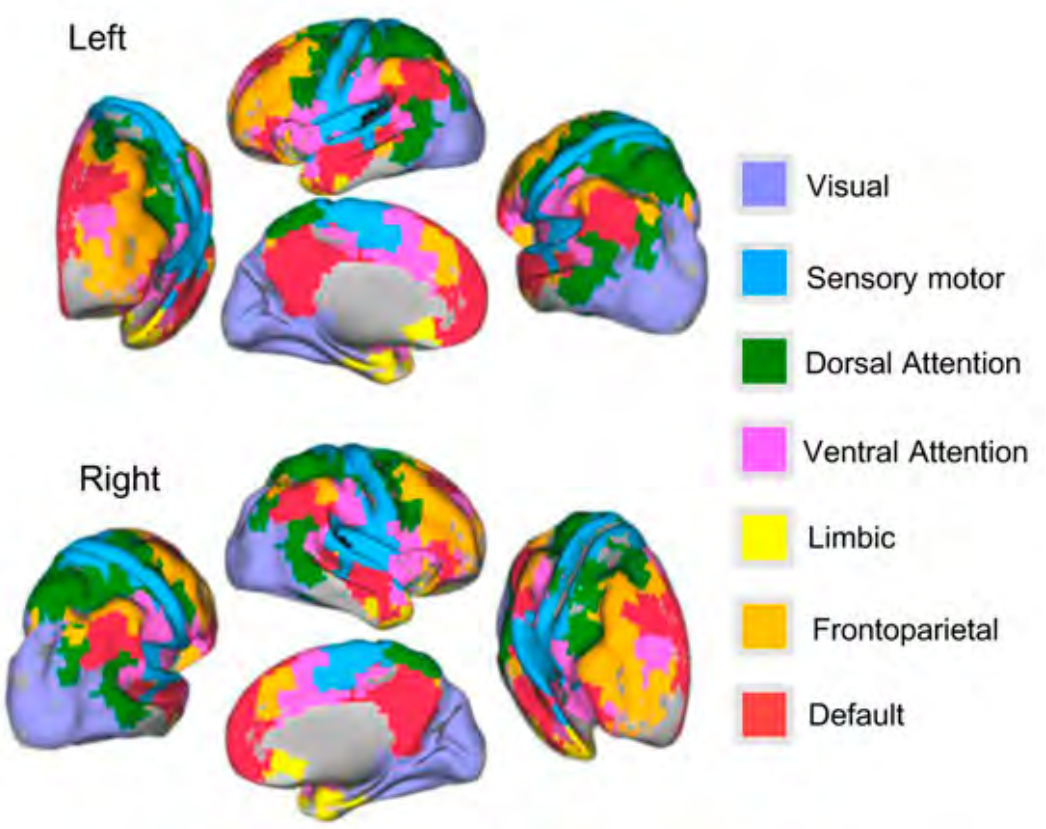

Figure 3.1: Large-scale resting-state brain networks. Visualization of seven large-scale resting-state networks derived from fMRI measurements. The color map indicates colors picturing each of the seven components and their regions on the surfaces. Adopted from [139].

complex functions.

For the description of other networks, we refer the reader to [135]. In general, these canonical networks represent a model of how different sets of brain regions join together as self-organized coalitions and thus provide a coherent framework for understanding cognition. As a result, disruptions in activity in various networks have been implicated in neuropsychiatric disorders. Abnormalities in intrinsic functional connectivity within the DMN and other networks have been observed in Alzheimer's disease, schizophrenia, attention-deficit/hyperactivity disorder, depression, anxiety, epilepsy, autism spectrum disorder, multiple sclerosis, or Parkinson's disease (for review, see [143]). Since these macro-scale canonical networks have largely been based on functional connectivity of fMRI data, further review is based mostly on fMRI as an imaging technique.

3.2 Inter-individual differences

The human brain is characterized by striking inter-individual variability in neuroanatomy and function. If data are averaged across subjects, a notable amount of information about underlying processes can be lost [144]. Although the detection of resting-state networks shows consistency across subjects, imaging modalities, and sessions [138], there is still large inter-individual variability on the level of individual connections. Here, we focus on connectivity variability in the resting-state condition because this variability is reduced during tasks as tasks are associated with increased functional constraints and demands [145]. For further discussion on task variability in FC, see [144]. The functional connectivity variability is at least partly accounted for by ongoing, spontaneous neuronal activity, which been increasingly recognized and studied [145].

There could be several driving factors behind the inter-individual variability in functional connectivity. It could be caused by differences in brain structure or differences in brain functionality. The observed variability is not uniformly distributed throughout the cortex, but significantly higher variability in multimodal association areas and lower variability in unimodal regions were reported [146]. This nonuniformity can have potentially evolutionary roots as it was correlated with the degree of evolutionary cortical expansion, and it was also related to variability in the degree of cortical folding, i.e., the sulcal depth [147]. Further exploration revealed that the regions of high connectivity variability could predict individual differences in cognitive domains [147]. Indeed, the connections with the most variability can predict performance in several cognitive domains [148] and can be used to identify individual subjects [149].

In terms of large-scale networks, the DMN showed low intra-individual variability and intermediate inter-individual variability [147]. The backbone of the DMN and the frontoparietal system does not vary significantly. However, weaker connections do vary, having a particularly pronounced effect on the cross-connections between DMN and the frontoparietal system [150]. Indeed, we observe a general pattern that the strongest correlations are also the most reliable. Furthermore, positive correlations are more reliable than negative correlations [151].

However, it is of high importance to note that some variability can be explained by physiological origins and noise in general [48]. This scenario can be illustrated in the work of Satterthwaite *et al.* [54]. Past studies have reported that neurodevelopment in youth

is associated with increased distant connectivity and reduced local connectivity. It could be, thus, possible that this effect accounts for actual differences in brain functionality. Nonetheless, it is noteworthy that this change in connectivity pattern is the inverse of the effect of in-scanner head motion. Typical motion artifact manifests as increased short-range connectivity and reduced long-range connectivity [52, 53]. This observation suggests that uncontrolled motion might influence estimates of neurodevelopmental trajectories of connectivity. Indeed, subject age was highly related to motion in a group of 456 adolescents [54]. By subsampling the adolescents into groups where age and motion were unrelated, the authors demonstrated that motion had marked effects on all examined measures, i.e., network modularity, dual-regression of independent component analysis, as well as the amplitude and fractional amplitude of low-frequency fluctuation.

VARIABILITY DUE TO HEAD MOTION

Recent results stress the importance of accounting for motion in populations whose in-scanner movement profiles may differ subtly, for instance, when comparing controls to subjects of different ages (e.g., during development or aging) or to individuals experiencing involuntary or repetitive movements (e.g., tics or tremors) [55, 152]. Therefore, inter-individual differences have to be approached carefully and hand in hand with consideration of all possible confounds. An index quantifying the amount of noise present in connectivity estimates promise extensive use in methodological investigations.

3.3 Variability due to disease

Neurological diseases are a significant source of connectivity differences between patients and healthy controls (Fig. 3.2). Connectome-based predictive models built on the connectivity variability across subjects are able to predict symptom scores and behavior [135]. That is why the FC matrix could serve as a behaviorally or clinically relevant marker [60]. Nevertheless, the diseases can be depicted on various levels of connectivity, ranging from strengths of correlation between two regions to differences in connectivity dynamics or derived graph measures. Examining the predictive power of connectivity biomarkers can provide new insights about neurodegenerative diseases [95].

A large number of connectivity analyses systematically examined various diseases (for an extensive overview, see [153] or [154]). Recent findings stress the network etiology of various brain disorders, i.e., that the symptoms are inherent to brain networks or brain circuits rather than a single brain region [7]. Until now, Alzheimer's (AD) and Parkinson's disease (PD) were the focus of most of the research. There is consistent evidence of decreased FC in the DMN across the AD continuum. The decrease is often accompanied by increased connectivity in the attentional frontoparietal and salience networks, likely mirroring compensatory mechanisms [154]. However, the effects in networks other than DMN are very heterogeneous. PD has been associated with alterations of motor and limbic connectivity. Furthermore, disrupted FC in the DMN, frontoparietal, salience, and associative visual networks have been linked to the development of cognitive deficits in PD [154]. Moreover, connectivity changes were proven to be a valuable biomarker in epilepsy [155–157]. Other conditions associated with alteration in the connectivity of networks include schizophrenia, attention-deficit/hyperactivity disorder, depression, anxiety, autism spectrum disorder, multiple sclerosis, Lewy body dementia, or Huntington's disease (for other reviews, see [143], [158]).

In conclusion, most neurodegenerative diseases show distinct altered connectivity patterns or networks. Hence, connectivity seems to be a valuable biomarker. However, there is a great deal of heterogeneity within each disease, which calls for caution in interpreting results. Moreover, the variability in recording conditions and, more importantly, preprocessing pipelines induces another significant deal of variability. The different approaches applied to data makes comparisons across studies extremely difficult [153]. Future studies will greatly benefit from a more homogeneous analytic strategy. They should also move beyond identifying disease to tracking its progression, severity, and, importantly, treatment effects. Despite these caveats, connectivity is on track to be a powerful diagnostic tool.

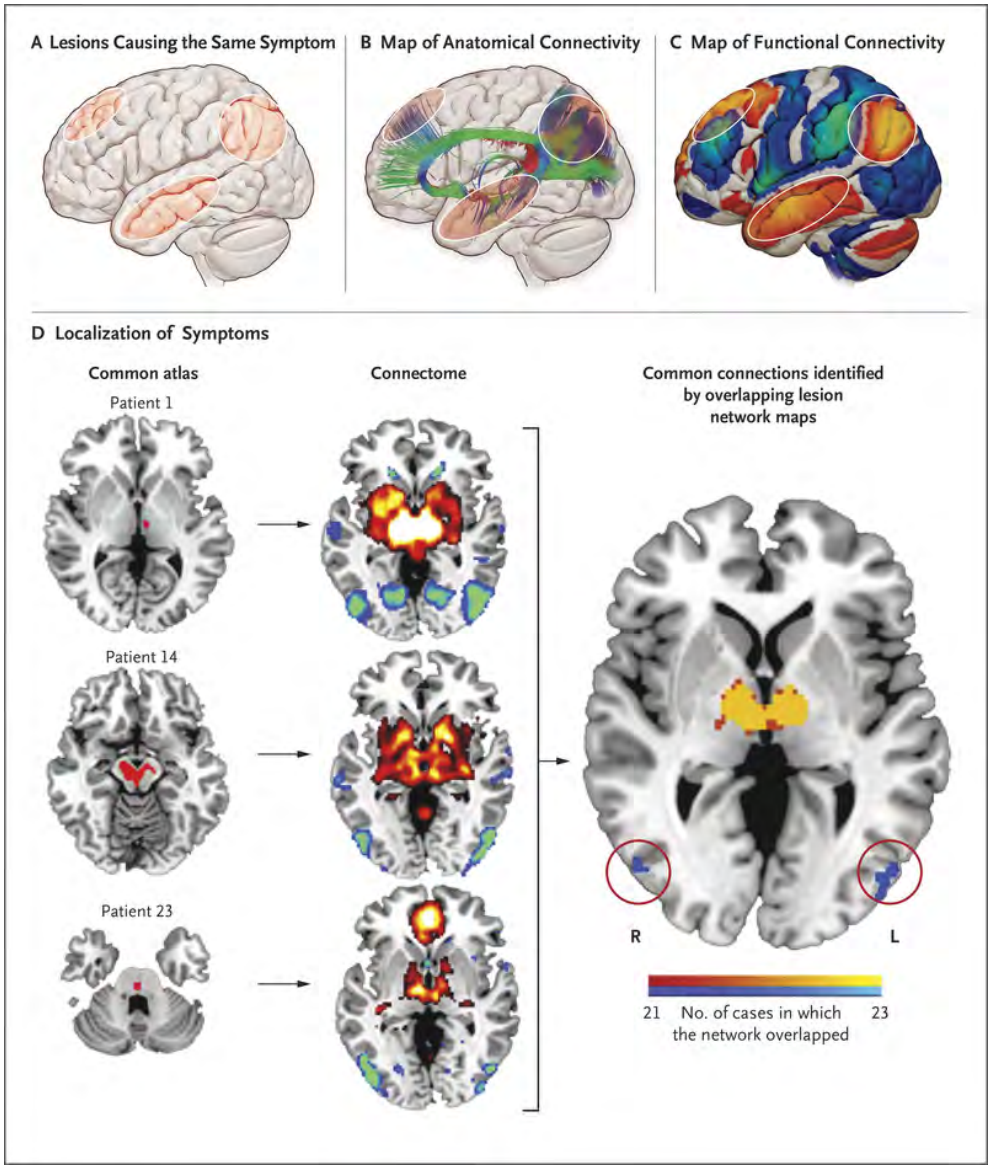

Figure 3.2: Network etiology of brain disorders A) Fox [7] mapped locations of brain lesions causing visual hallucinations. However, the lesions' locations overlap only minimally. In the conducted meta-analysis, there was no single region associated consistently across various studies with the symptoms. Nevertheless, using the means of structural and functional connectivity (B, C), they mapped the symptoms to a common atlas (D). These networks showed significant overlap in 21 out of 22 subjects (E). Therefore, the same neuropsychiatric symptoms caused by brain lesions map to a common network. In this example, lesion locations causing visual hallucinations are functionally connected to a part of the brain involved in visual imagery. Source: [7].

3.4 Linking structure and function

Another factor in differences between functions could be the differences in the underlying structure. There is an ongoing investigation on how the functional networks are

comparable to structural networks. Hypothetically model-based functional and effective connectivity estimators could benefit from the information about the underlying structural connectivity. Indeed, Stephan *et al.* [159] demonstrated that effective connectivity models are improved when the priors on the inter-regional coupling parameters are informed by structural connectivity. The idea that structure influences functional expression has been here since the beginning of EC measurements [133]. Structural connectivity constraints functional connectivity in a way that structurally connected neuronal elements generate communication patterns that aggregated over longer time scales take the shape of functional connectivity. However, there has been disagreement as to whether the boundaries of functional units correspond to the boundaries of structural units [160]. Therefore, is the structure-function relationship straightforward? Is there a one-to-one mapping between SC and FC? Can structural connectivity explain part of the variability in functional connectivity?

The first study relating structural and functional connectivity was done within a single axial slice and demonstrated a strong correspondence between the two phenomena [161]. However, strong FC was also observed between structurally unconnected regions. Future studies tried to replicate these results both on a macroscopic and microscopic scales. Several studies have demonstrated that the presence or strength of a structural connection can predict the strength of the functional connection [11]. Moreover, regions that are central to structural networks have been reported to be central in functional networks as well [151]. However, the link between SC and FC is still imperfect. Until recently, at least 50 % of the variance in functional connection weights remained unexplained by a simple 1:1 correspondence with structure [151]. Including indirect structural connections could account for some unexplained variance in functional connectivity [160], but there are also other factors.

Modeling studies tackle this issue from another perspective. They ask the question of whether neuronal models coupled by parameters derived from SC are able to produce oscillatory activity that would show similar statistical dependencies as observed FC. Several studies successfully proved this hypothesis [11]. However, they also found that the relationship significantly depends on spatial resolution and timescale. The relationship is the strongest if FC is obtained from low-frequency neuronal activity (as in fMRI) aggregated over long time periods (in the order of minutes). One of the reasons is that FC fluctuates

in complex patterns at higher frequencies and within shorter time windows reflecting the rich underlying dynamics [160].

From the observed results, it is apparent that SC has a certain predictive power of the presence and strength of FC. However, the inverse is not true. SC cannot be reliably estimated from FC since strong functional coupling exists between regions that are not directly anatomically linked [160, 161].

Recent approaches shifted their focus from simple one-to-one mapping, but rather they acknowledge the existence of multiple communication strategies. Vázquez-Rodríguez *et al.* [162] built a simple model where FC is estimated by multiplexing different communication strategies represented by Euclidean distance, path length, and communicability. Accounting for different communication strategies significantly improves predictive power. Such results demonstrate the presence of more communication strategies and that different brain regions adopt different strategies. Brain regions with the least structure-function correspondence included medial parietal structures (precuneus, posterior cingulate), lateral parietal and temporal cortices, insular cortex, and anterior cingulate cortex. Conversely, primary sensory regions, including occipital and paracentral cortices, showed relatively high structure-function correspondence [162]. These results show a striking similarity to a unimodal to transmodal hierarchical representation of cortex derived by Margulies *et al.* [163]. While in unimodal brain areas such as the primary sensory area, the relationship between structure and function is very strong, in the transmodal networks such as default mode network or salience network, the relationship is weak (Fig. 3.3).

There are several limitations to our current inferences. While our SC measurements are suited for long-distance connections, resting-state functional connectivity may be more informative about short-range intracortical connectivity. There is a pattern of distance dependence, where coupling decreases with distance [160]. This effect is more prominent in structural connectivity as anatomical wiring is subject to material, spatial, and metabolic constraints. Furthermore, our measurements of functional connectivity are not flawless as well. This dependence could also be driven by non-neuronal sources such as cardiac pulsation and head movements [53]. Moreover, current measures might not capture the dynamic character of functional interactions or the possibility of higher-order interactions, especially in transmodal networks [162]. Finally, other errors could be caused by brain parcellations used to reduce the dimensionality from gray matter voxels to brain regions.

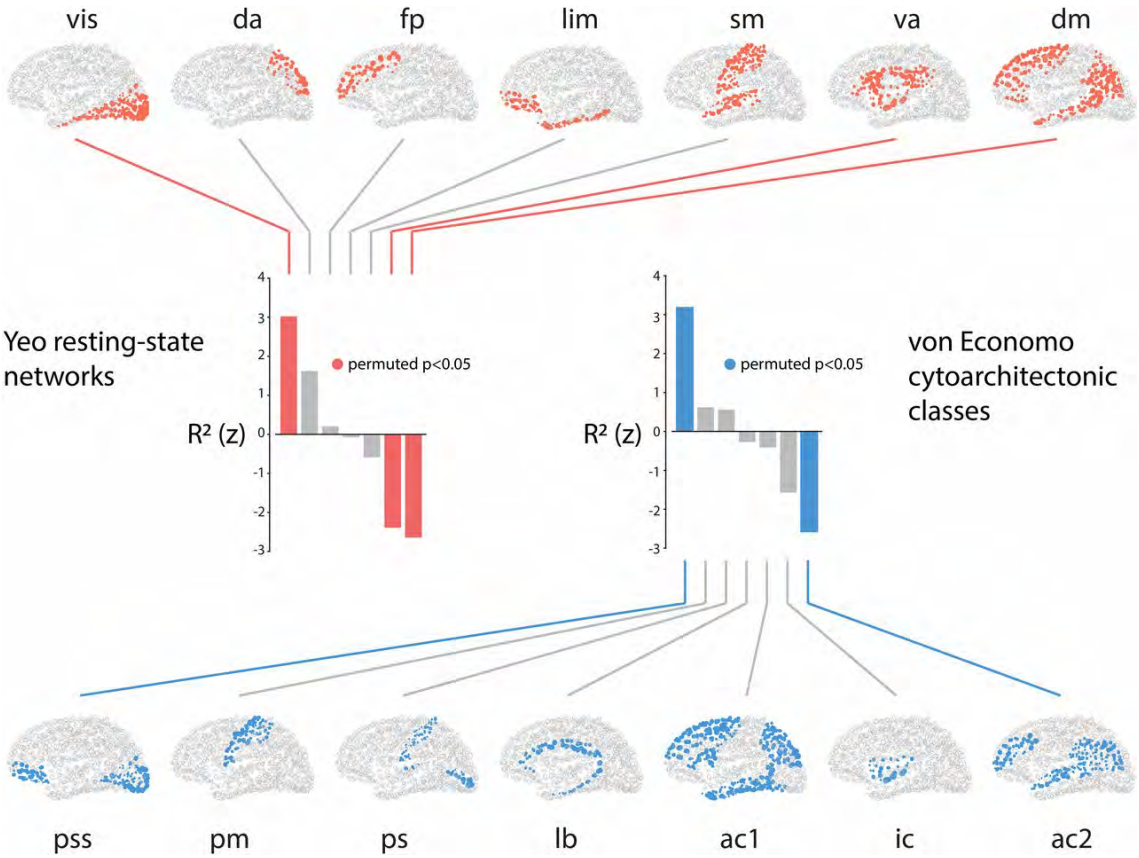

Figure 3.3: Relationship between structural and functional connectivity. According to recent results, the relationship between structural and functional connectivity varies along the unimodal to transmodal representation of the brain. While in unimodal brain areas such as the primary sensory area, the relationship between structure and function is very strong, in the transmodal networks, such as default mode network or salience network, the relationship is weak. Yeo networks: da, dorsal attention; dm, default mode; fp, frontoparietal; lim, limbic; sm, somatomotor; va, ventral attention; vis, visual. von Economo classes: ac1, association cortex; ac2, association cortex; ic, insular cortex; lb, limbic regions; pm, primary motor cortex; ps, primary sensory cortex; pss, primary/secondary sensory. Source: [162].

Unbiased estimation of connectivity quality with respect to various types of noise could bring significant improvements.

MOVING BEYOND GROUP-LEVEL

Notable progress has been made in the mapping functional to structural connectivity. There is an emerging consensus about the relationship between structural and functional networks. Converging evidence supports the idea that structure-function relationships are organized around a hierarchical gradient spanning unimodal to transmodal cortex [164]. Despite promising group-level results, little is known about the correspondence on an individual subject level as we tend to apply uniform brain parcellations assuming that areas can be mapped to identical spatial locations in every participant. Even our group-level estimators might become more powerful if individual estimations are taken into account [11].

3.5 Network dynamics

The presence of inter-individual variability is further accompanied by intra-individual connectivity differences. Previous research already reported rich intra-individual connectivity fluctuations [165]. In high temporal resolution imaging techniques, primarily in EEG, the rich dynamics of both induced and spontaneous synchronizations have long been appreciated. These time-varying changes represent how neuronal signals continuously combine, dissolve, reconfigure, and recombine to form adaptive patterns of activity over a wide range of temporal and spatial scales [166]. Such processes that span various timescales and all canonical frequency bands underlie the flexibility and power of perception, cognition, and behavior to deal effectively with the continually evolving environment. Moreover, there is already extensive work in EEG/MEG microstates (transient, patterned, quasi-stable states of high synchrony) on the scale of milliseconds (e.g., [116, 117]).

However, the macro-scale functional networks have largely been based on functional connectivity maps derived from fMRI data [167]. The first one to observe FC dynamics in fMRI was Chang & Glover [118] using a wavelet coherence analysis on resting-state measurements. The connectivity varied on the scale of seconds to minutes over the duration of a standard resting-state scan, and thus it proved valuable to consider measures

of variability even in slow measurements of fMRI. Future studies confirmed that functional connectivity is not static and that it can exhibit non-stationary and spontaneous relationships. Moreover, these fluctuations are related to underlying neuronal activity, and they are shaped by structural connectivity [168]. Hence, spontaneous fluctuations are currently viewed as the hallmark of recordings of neuronal signals, emergent over time scales spanning milliseconds and tens of minutes (for review, see [169]).

These results question the nature of resting-state measurements. It is known that human subjects engage in a diverse range of mental activities, such as mind-wandering or monitoring of the internal environment, that can alter the brain's functional organization. However, the observed dynamics were proved to be irrespective of conscious and cognitive processing as they were observed in an anesthetized macaque brain as well [168]. The question is then, given the high stability and reproducibility of static FC, why should we expect to see fluctuations in FC? Lurie *et al.* [169] explain this controversy stating that the same pattern of static FC may result from different spatiotemporal patterns of underlying dynamic FC.

The most commonly used strategy of analyzing connectivity dynamics is to use the sliding window approach [165, 168]. In this approach, a time window of fixed length is selected. This window is usually tapered to decrease sensitivity to possible outliers [165]. Data points within that window are used to calculate the metric of interest. The window is then shifted in time by a fixed number of data points (ranging from a single data point to the length of a window) that define the overlap between successive windows. This process results in quantifying the time-varying behavior of the chosen metric throughout the scan [168]. Besides sliding window correlation, sliding window ICA has been used to track the evolution of the obtained spatial components in time [170].

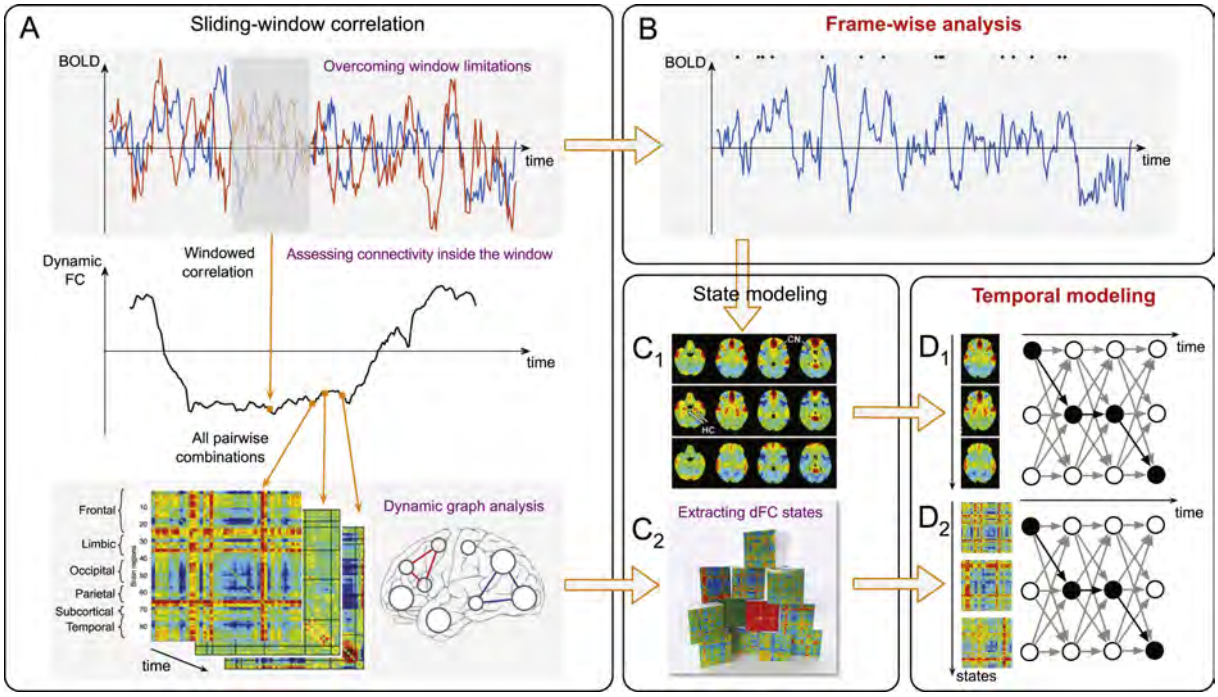

Figure 3.4: Dynamic functional connectivity analysis. (A) The most common way to calculate time-varying estimates of connectivity strength is to use the sliding window approach. Pearson correlation between pairs of BOLD timecourses over a temporal interval spanned by a rectangular window is repeatedly computed while shifting the window by a specific step every time. Performing this procedure for all connections results in a set of connectivity matrices that can be further used to extract brain states using matrix factorization techniques and clustering algorithms (C2). How the brain transition between different states (D2), the actual number of brain states, or how much time it spends in each state are important biomarkers of disease conditions. Alternative approach time the sliding-window approach is the frame-wise analysis (B)(for more information, see [165]). Source: [165].

As a result, time-varying connectivity is represented as a set of matrices. After the estimation, these matrices can be decomposed into a set of connectivity states using matrix factorization techniques and clustering algorithms, such as k-means clustering or PCA [165]. Previous observations suggest that dynamic connectivity can, to some extent, be conceived as a multistable process wherein the connectivity patterns pass through multiple discrete states, rather than varying in a more continuous sense [168, 171]. However, currently, we assume that instead of separate discrete states, a model that considers overlapping states could better represent dynamic connectivity [172]. Nevertheless, by decomposing the matrices and analyzing the number of states, the transition between states, and the dwell time, i.e., time spent in each state, important features serving as biomarkers to disease conditions could be derived [173]. A common predictive feature is

the decreased diversity in visited meta-states reported in schizophrenia, autism, or mild cognitive impairment (for review, see [165]).

Dynamics are not studied only during rest but also during a task. FC changes accompany even the switch between rest and task. The system undergoes fast and spatially distributed functional reconfiguration to accommodate for task demands. Therefore, task-concurrent dynamic-FC metrics have significant behavioral relevance [174]. However, studies have shown that static FC networks observed during task and rest are highly similar, correlating at up to $r = 0.9$ [169], suggesting that even small changes to a largely stable underlying functional network architecture may lead to a wide variety of cognitive and behavioral states. The task-induced dynamics reflect the recruitment of necessary resources, active representation of task goals, optimization of information flow, and focused attention. Although FC has been demonstrated to exhibit changes in various studies [141, 174, 175], there is still high similarity between rest and task (e.g., only 5% increase in energy consumption), and most canonical resting-state networks are still being identified during periods of the task. Typical task-induced changes include higher connectivity among networks recruited by the task, reorganization of highly connected regions, altered relative frequency contributions, increased inter-individual differences, and decreased regional connectivity homogeneity [174].

Despite promising results, several studies pointed out the danger of detecting noise instead of real fluctuations. This caveat was found for both EEG [176] and fMRI studies [177]. Indeed, if the sliding window approach is applied to white noise, rich connectivity dynamics are obtained as well. Therefore, the mere presence of fluctuations in sliding-window is not evidence of true dynamics. Artifactual dynamics might arise due to a low signal-to-noise ratio, changing levels of non-neuronal noise, non-stationarity, or due to the estimation method, for example, when the window length is shorter than the largest wavelength present in both signals (even for deterministic signals with a fixed relationship) [172]. Hindriks *et al.* [177] actually stated that in a typical 10 min resting-state session, it is almost impossible to detect FC dynamics using sliding-window correlations. Nevertheless, they reported that most of the functional connections are, in fact, dynamic, and they can be revealed by session- or subject-averaging of the measures.

It is thus necessary to test the fluctuations against an appropriate null model. One

way to depict fluctuations from those obtained in a static system is to construct confidence intervals, either analytically or using a bootstrapping resampling technique [178]. Moreover, several methods approximate null distributions using surrogate data to test a specific hypothesis. Such data share all statistical properties with the observed data, except that they lack the property one wants to test for [177]. One example is keeping the amplitude spectra of individual time series constant while randomizing the phase, i.e., preserving the temporal auto-correlation and spatial structure [179].

OPTIMAL WINDOW LENGTH

Several parameters can heavily influence the reliability of detected dynamics. The selection of window length limits the current sliding window approaches. The window defines the timescale on which the analysis is performed. Long windows would impede the detection of the temporal variations of interest. On the other hand, a short window increases the risks of introducing spurious fluctuations [165]. A lower limit to safely avoid artifacts is set to the largest wavelength present in the preprocessed fMRI signal [172]. Future methods could be based on adaptive methods, such as Kalman filtering, where the model parameters are continuously estimated, and thus the use of the window is omitted.

If constructed carefully, dynamic connectivity represents a powerful approach that can bring new insights into brain function and dysfunction. Despite fMRI analysis limitations, fMRI functional connectivity fluctuations were found to be correlated with EEG power in different frequency bands (see, for example, [180]). It is believed that multiple neurophysiological processes simultaneously contribute to time-varying BOLD activity [169]. Macro-scale functional networks are currently analyzed using temporal segments, typically 30–60 s long [165]. However, there are various timescales of interest ranging from slow (years) to fast (milliseconds) [167]. Given the rapid changes in brain activity, there is currently a need to study large-scale networks on a fast timescale [181].

Chapter 4

Network neuroscience

Network neuroscience is an elegant extension to connectivity analyses by applying the tools of graph theory [83]. This chapter defines the basic concepts of graphs and how they are actually represented in the brain. We then move to typical metrics used to characterize brain graphs. Specifically, we focus on metrics characterizing network integration and segregation, as these two concepts are fundamental in our current understanding of brain functioning. Furthermore, we describe the new promising field of temporal networks. Finally, we end with a general overview of all steps leading from recording a brain signal to the characterization of network topology.

4.1 Introduction to graph theory

Until now, we used the term network in a very broad sense to label a set of linked brain elements. However, there is a whole mathematical field called graph theory devoted to networks. Its history reaches back to Leonhard Euler and his work called Seven Bridges of Königsberg. This paper, published in 1736, is regarded as the first paper in graph theory history. Nowadays, graph theory is a rigorous, established multidisciplinary field that draws on tools from mathematics, physics, and computer science to describe complex interconnection patterns. In terms of neuroscience, understanding these emerging patterns and, thus, the organization of brain networks will be necessary to understand cognition [182]. The study of networks has been already applied in other biological contexts such as cellular metabolism, gene regulation, or ecology. In recent years, we have

witnessed the advent of *network neuroscience*, leveraging graph theory tools to mathematically characterize brain networks [183]. Graph theory enables an elegant description of network topology only with few parameters. Moreover, it is able to identify critical regions, quantify communication efficacy, or examine motifs on various levels. From the point of graph theory, the brain network is a graph with its constituent components.

4.2 Nodes and edges

A graph is a mathematical structure used to model pairwise relations between objects. Graphs are made up of vertices (also called nodes or points) connected by edges (also called links or lines). In network neuroscience, it is common to talk about nodes and edges [183]; therefore, we will follow this terminology. Their definition highly depends on the used imaging technique, analyzed system, and the scientific question of interest. Different sets of choices can provide complementary information about brain organization and function [184].

Formally, a graph is defined as an ordered pair $G = (V, E)$, where:

- V is a set of vertices (nodes)
- $E \subseteq \{\{x, y\}\} | x, y \in V \text{ and } x \neq y\}$ is a set of edges, represented by unordered pairs of nodes

This object corresponds to a simple directed graph. Note that in this scenario, multiple edges between two nodes are not allowed. Furthermore, such representation can be written in the form of an adjacency matrix. The number of rows and columns of this matrix correspond to the number of nodes. An element between row i and column j corresponds to an edge between node i and j, and in neuroscientific applications, it is commonly represented by a connectivity metric.

Nodes can be represented on various scales, from individual neurons to brain regions. In EEG, a node can correspond to a sensor placed on the scalp or hypothesized neuronal dipoles estimated from source localization techniques. In iEEG, a node can correspond to a single neuron or a recording contact. Finally, in fMRI, nodes often correspond either to individual voxels or brain regions defined upon an appropriate atlas-based parcellation. Therefore, the number of nodes can vary significantly among studies.

Edges are represented by connectivity estimates. As each connectivity has its specifics, each type of edge has to be treated differently. However, the definition of an edge is ambiguous. In structural connectivity, they can correspond to streamline counts (the number of reconstructed streamlines between pairs of parcels), their density, or microstructural properties of streamlines, e.g., their fractional anisotropy. Structural connectivity graphs are generally sparse (most possible structural connections among brain regions do not exist), noisy, and prone to both false positives and negatives [185]. In functional connectivity, the edges typically correspond either to Pearson correlation between parcelled brain regions in fMRI or to phase synchrony/coherence between EEG sensors. Such an adjacency matrix is often very dense. Lastly, a graph based on effective connectivity is similar to a functional connectivity graph. However, there is an important difference. As FC measures are undirected, the corresponding adjacency matrix is symmetrical, while for the directed effective measure, the adjacency matrix can be asymmetrical.

Besides symmetry and asymmetry, there are other important features of adjacency matrices. As already stated, in a directed graph edge (a, b) might not equal to (b, a), unlike in undirected graphs. Further, structural adjacency matrices are commonly binarized. In this post-processing step, a threshold is imposed on observed connections to retain those with the strongest weights or those least likely to represent false positives and thus to reduce measurement noise [184]. However, in sparse matrices, each change in connection has a dramatic impact on the graph measures. The binarization is sometimes applied in FC studies as well. Nevertheless, arbitrary thresholding often leads to a loss of information [186], and derived network measures are unstable across different thresholds [187]. Moreover, graph measures based on a weighted network were better reproducible compared to binarized networks. Applied brain parcellation did not have a significant effect [188]. Therefore, it might be advantageous to retain all connections and work with weighted adjacency matrices.

ANNOTATION OF NODES AND EDGES

Currently, the main limitation of graph theory application is the major simplification that within a given network representation, all nodes and edges are identical and homogeneous [183]. This assumption is inherent in most current applications of graph theory. Future studies can thus turn to the annotation of nodes and edges to address this limitation. Overcoming it will result in the identification of more biologically meaningful network communities.

4.3 Graph metrics

Graphs may be studied and analyzed using a broad range of network analysis approaches that offer insight into the complexity of human brain organization (for review, see [189]). These approaches investigate the network on different scales, from individual nodes and edges on a micro-scale to global properties that characterize the whole network on a macro-scale (Fig. 4.1). All metrics are derived from the analysis of the adjacency matrix.

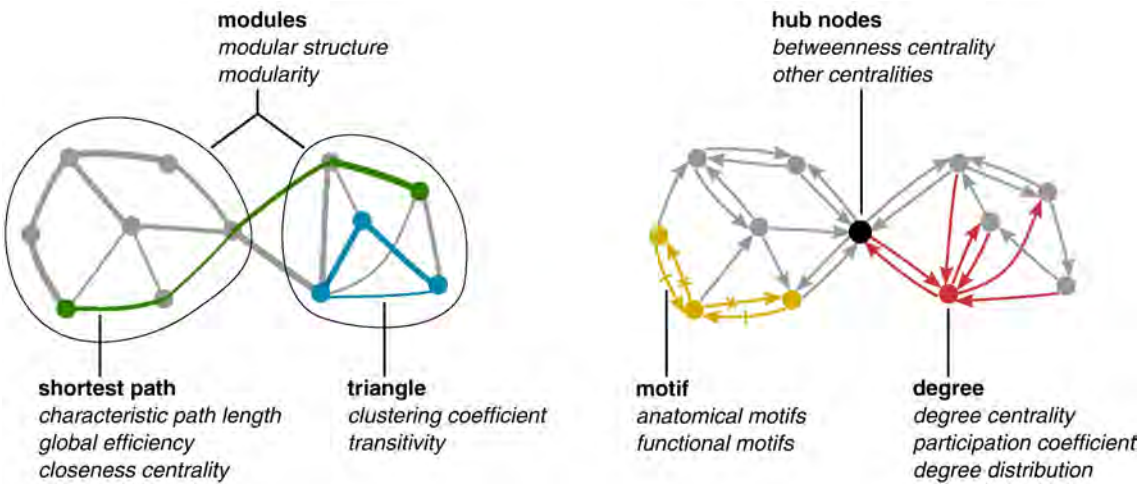

Figure 4.1: Graph metrics. Illustration of various graph metrics calculated based on the adjacency matrix. These metrics represent both micro-scale properties (e.g., degree) and macro-scale properties (e.g., modules and shortest path). The measure (in italics) is typically based on basic properties of network connectivity (in bold type). Source: [189].

It is important to note that all measures need to be tested against an appropriate null hypothesis because derived estimates are greatly influenced by basic network characteristics, such as the number of nodes and links and the degree distribution. The design of a

null model includes the choice of a suitable random graph. There are various types of random models that preserve various subsets of structural parameters. One of the most used null models has a random topology but shares the size, density, and binary degree distribution of the original network. In other words, the models involve edge randomization that preserves nodal degrees [189].

To describe the most common graph metrics, we assume that we have an n-node graph G represented by an $n \times n$ adjacency matrix A, where the element A_{ij} represents the strength of the connection between node i and node j. The set of all nodes in the network is denoted as N. Moreover, we assume only binary and undirected graphs. However, most of the measures can also be extended for directed and weighted graphs [186].

Degree and Strength

We start with a description of local measures characterizing properties of individual nodes and edges. Probably the most fundamental property of a node is its degree. In a binary graph, it is defined as the number of all outgoing and incoming connections. The weighted analog of node degree is node strength, which measures the total weight of all connections incident upon a given node. Nodes with an unusually high degree or strength are referred to as *hubs*. These hubs tend to occupy influential positions within a network.

$$k_i = \sum_{j \in N} A_{ij} \tag{4.1}$$

Clustering

Another measure examining the properties of a single node is the local clustering coefficient. It characterizes the degree to which nodes in a graph tend to cluster together. It is defined as the fraction of a node's neighbors that are also connected one to another. It can be calculated as:

$$C_i = \frac{1}{k_i(k_i - 1)} \sum_{j,k \in N} A_{ij} A_{jk} A_{ki} \tag{4.2}$$

where $k_i = \sum_j A_{ij}$

For a binary network, we define the global clustering coefficient to be the mean local

clustering coefficient values over all N nodes in the graph:

$$C_{glob} = \frac{1}{N} \sum_{i \in N} \frac{1}{C_i} \tag{4.3}$$

where $k_i = \sum_{j \in N} A_{ij}$

Paths and Walks

The measures of path length are commonly used to quantify the topological distance between two nodes. The shortest path length d_{ij} is the minimal number of edges that must be traversed to walk from node i to node j along edges in the graph. This length is only computed in network space, and it does not relate to the actual physical distance between nodes. Moreover, the shortest path can transverse each edge only once, so the path is composed of a unique set of edges. On the other hand, a walk between two nodes can use edges any number of times. Paths and walks are important concepts for the flow of signals and communication [185].

$$L = \frac{1}{N} \sum_{i \in N} \frac{\sum_{j \in N, j \neq i} d_{ij}}{N - 1} \tag{4.4}$$

The signal is less likely to degrade, get transformed, or otherwise attenuate in shorter paths, as they correspond to faster transit times. The average shortest path length in the network, called the characteristic path length, is used to characterize the whole graph. However, since it is an unbounded measure, it is difficult to compare it across networks of different sizes. Moreover, disconnected nodes have a path length equal to ∞. In weighted networks, it is necessary to transform connection weights to a measure of length. This is usually accomplished by negative exponentiation of edge weights, i.e., $L_{ij} = W_{ij}^{-\gamma}$, or by dividing edge weights by their maximum value and taking the negative logarithm, i.e., $L_{ij} = -log(\frac{W_{ij}}{W_{max}})$. These transformations ensure that stronger and bigger weights correspond to smaller lengths.

Efficiency

The characteristic path length is a global average of the shortest path between nodes, and its inverse is called global efficiency. The local efficiency is the global efficiency computed

on the neighborhood of the node and is related to the clustering coefficient.

$$E_{glob} = \frac{1}{N} \sum_{i \in N} \frac{\sum_{j \in N, j \neq i} d_{ij}^{-1}}{N-1} \tag{4.5}$$

Since this formulation uses information regarding the shortest paths through the network, efficiency is often associated with efficient information transmission.

Centrality

Centrality measures identify the most important nodes within a graph. They quantify the nodal importance with respect to the dynamical process taking place on a network. A typical representative, betweenness centrality, is calculated as the total number of shortest paths that pass through a given node. Critical communication hubs have high betweenness centrality as they act as bridging elements between a high number of nodes.

$$C_B(i) = \sum_{k \neq i \neq j} \frac{\sigma_{jk}(i)}{\sigma_{jk}} \tag{4.6}$$

where $j, k \in N$, σ_{jk} is the total number of shortest paths from node j to node k, and $\sigma_{jk}(i)$ is the number of those paths that pass through i.

Modularity

The modularity is a statistic that quantifies the degree to which the network may be subdivided into clearly delineated subnetworks. The subnetworks can go by many names, but in neuroscience, they are commonly referred to as modules (other names include communities or clusters). The modules have dense connections between the nodes within the module but sparse connections with nodes from different modules. Therefore, the optimal community structure is a subdivision of the network into non-overlapping groups of nodes in a way that maximizes the number of within-group edges and minimizes the number of between-group edges. The subdivision is calculated by maximizing the following modularity quality function [190]:

$$Q = \frac{1}{2m} \sum_{i,j \in N} (A_{ij} - \gamma \frac{k_i k_j}{2m}) \delta_{C_i C_j} \tag{4.7}$$

where $m = (1/2m) \sum_{ij} A_{ij}$, γ is a structural resolution parameter influencing the number of obtained modules (higher γ results in higher granularity), $\delta_{C_i C_j} = 1$ if nodes i and j are in the same community, and $\delta_{C_i C_j} = 0$ otherwise.

Maximizing the Q parameter is an NP-complete problem, and therefore heuristic algorithms are used, such as the locally greedy Louvain algorithm. Usually, a maximum of the modularity function across multiple runs is selected as the resulting modularity with its accompanying network partition [191].

As the nodes within a module are highly interconnected, they tend to generate statistically dependent signals, i.e., they exhibit high functional connectivity. Therefore, a module represents a functionally specialized unit. Modular structure supports effective communication [192] as well as functional segregation and specialization [14]. Modularity is ubiquitous in real-world networks, including the brain.

SMALL-WORLD AND RICH CLUB

It is noteworthy that we did not mention calculating popular macro-scale topology characteristics such as small-world or rich club coefficients. Their use is extensively described in the literature [193]. The loss of small-world topology has been linked to various diseases. However, recently there have been calls for caution using these metrics. Specifically, Hlinka *et al.* [194] showed that the functional connectivity approach leads to upwardly biased estimates of small-world characteristics. These findings could be extrapolated to other graph metrics applied to correlation matrices. Therefore, these limitations should be taken into account in order to avoid erroneous interpretations. We refer the reader [193] for more details on these metrics.

The global scale measures express network-wide attributes and are represented by the characteristic path length, efficiency, clustering, or modularity. These metrics are related to two important concepts of network organization. These are segregation and integration. They are the graph counterparts of the long-standing debate in neuroscience about functional specialization versus functional integration in the brain [195]. These two concepts provide essential insight into information processing and transmission. Ultimately they might help explain mechanisms of cognitive processes. Therefore, we describe both concepts in more detail, along with graph metrics used for their characterization.

4.4 Segregation and Integration

Segregation and integration are two key concepts of neuroimaging. The cartographic era focused on the segregated activity of individual regions and, therefore, on mapping brain function to isolated brain regions. We already know that the brain contains large-scale communities that correspond to distinct functional systems of the brain [191]. These communities are fundamental parts of brain networks as they convey functional specialization [196]. The topography of brain networks promotes functional segregation by forming these local network communities that are intrinsically densely connected and strongly coupled. Consequently, the community-based network organization is a fundamental aspect of the functional specialization of each brain system [197].

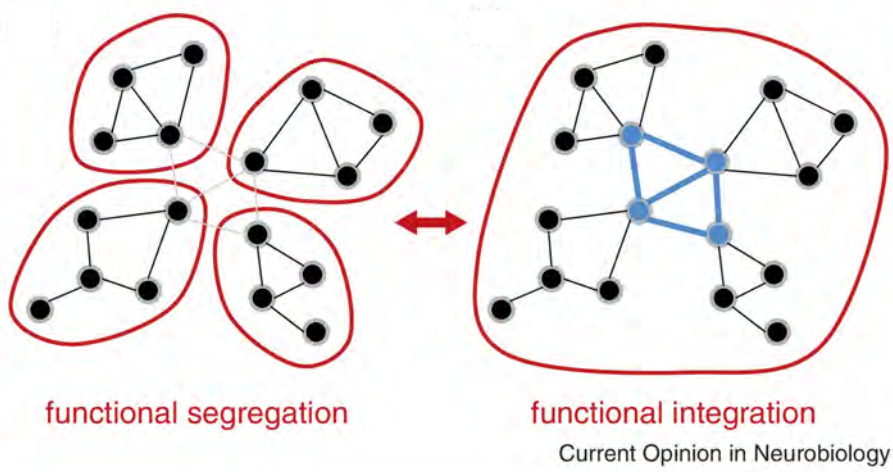

Figure 4.2: Segregation and integration according to graph theory. Schematic diagram showing a set of nodes with a modular architecture. Functional segregation is indicated by strong functional coupling within modules (red) with little or no functional coupling across modules. On the other hand, functional integration is indicated by globally strong functional coupling, including strong information flow across network hubs and their mutual interconnections (blue). Illustration taken from [14].

However, complex brain functions arise from the coordinated activity of distributed regions. Therefore, the local network communities are integrated through network hubs to support global communication. Integration is the extent to which the system is able to bring together distant regions in a coordinated manner. It is secured by the existence of communication hubs with high and diverse patterns of dense inter-connectivity as well as long-rage, cross-modular connections. They enable the efficient routing of information between modules by minimizing both connection distances and wiring costs [198]. These

characteristics are a key feature of small-world networks. In a small-world network, the integration of the segregated information through network hubs links network communities and ensures efficient communication [14]. It is not surprising that this architecture is a hallmark of complex systems as it provides a high rate of information transmission with low energy and wiring costs [199].

The emerging picture suggests that brain networks are designed for effective information processing and synthesis by balancing between segregation and integration. Therefore, healthy brain functioning requires an optimal balance between the two [196]. There is already a body of evidence suggesting that a potential imbalance may directly implicate neuropsychiatric disorders [81]. Thus it is critical to understand both network segregation and network integration and how they relate to different aspects of cognition in order to gain new insights into the mechanisms of neuropsychiatric disorders and complex phenomena of modern neuroscience such as cognition or even consciousness [80, 83, 200].

There are many ways how to quantify these concepts. Typical approaches are based on decomposition or clustering algorithms, such as ICA, seed-based connectivity, or graphs. For example, when measuring the physical distance-dependent connectivity within functional networks, the long-range connections reflect integration, and short-range connections reflect segregation. When clustering or ICA is applied on the FC matrices, a low number of detected FC states could correspond to higher integration and vice versa. However, these approaches do not provide information on the cluster stability, the possible overlap between clusters, or how they are interconnected [14]. Graph theory offers a general language to describe all these properties.

Therefore, we turn to graph theory measures as they can elegantly characterize the segregation into functionally coherent sub-units and quantify the efficiency of information processing between remote units. Moreover, the graph metrics are able to detect important parts of the system (hubs) that are likely to play a key role when switching between different modes of processing. These hubs occupy a position of influence within a brain system, making them fundamental for healthy functioning. Computational models showed that structural damage and disconnection of hub regions cause disruption or loss of functional connectivity [14]. Therefore, damaging the connector hubs may result in pervasive cognitive impairment, while lesions to provincial hubs would be expected to yield specific clinical deficits [81].

Segregation is the extent to which communication occurs primarily within tight-knit communities of regions. These communities comprise anatomically distinct functional circuits that are associated with different cognitive domains [14]. Thus, functional segregation refers to neuronal processing carried out within the communities or modules. Typically, it is measured by modularity, which quantifies the extent to which the network is organized into modules [165]. Modules were already found to map onto known segregated cognitive systems [80]. Interestingly, the modular organization tends to be hierarchical, where smaller modules exist within larger modules [201, 202]. Such architecture enables local computations to be integrated into broader cognitive processes [203].

Integration encompasses the efficiency of global communication and the ability of the network to integrate distributed information. The extent of communication between distinct regions can be modeled by the average length of the shortest communication paths between any two nodes, i.e., the characteristic path length. Commonly, the integration is quantified by its inverse, i.e., the efficiency. The efficiency describes the ease with which a signal can travel from one brain region to another. However, Sporns [14] pointed out that this measure is often maximized in networks with random topology and that direct paths for global communication actually do not provide means for information integration.

The brain continuously searches for a metastable balance between the local segregation of function and the global integration of information. This imposes a dynamic information flow. There is a belief that resting-state community organization represents an optimized state that has minimized the neuronal and metabolic energy demands [204]. The increased segregation results in reduced information flow between networks. Moreover, it is known that the brain shows increased subnetwork segregation during rest/baseline epochs [205]. Therefore, maintaining segregated brain systems at rest allows the brain to rapidly and flexibly adapt a necessary task-related reconfiguration [197]. This reconfiguration is accompanied by integrating distributed systems to efficiently propagate information among different regions leading to effective task performance. Indeed, participants whose brain networks flexibly reconfigured appropriately for a given task performed better on that task [200]. Measures of task-related system reconfiguration have been shown to predict task performance. An increase in cognitive load drives the increase in global integration so that the brain can adopt a more global workspace configuration [206, 207]. Moreover, higher task demands were already associated with decreased modularity [208, 209]. All

in all, these results highlight the highly dynamic brain topology.

DYNAMICS ON A MILLISECOND SCALE

Moments of high modularity/low efficiency are observed when different networks are functionally disconnected, and periods of low modularity/high efficiency, when those distinct networks interact [165, 210]. However, most of the measurements are based on fMRI. Therefore, the dynamic organization of brain networks on a millisecond scale is not yet well understood. There is a need for studies examining how segregation and integration evolve on fast timescales.

4.5 Temporal networks

We already talked about spontaneous and task-induced changes in connectivity patterns present on various timescales from milliseconds (functional) to years (structural). Thus, it is not surprising that graphs representing these connectivity networks are time-varying as well. However, until recently, most of the studies focused on static network descriptions obtained throughout fMRI measurement [80]. Investigating graph dynamics can bring new tools for analyzing dynamic brain reconfiguration [175]. Dynamic network neuroscience views brain networks as evolving and interconnected systems. It was proved that a dynamic, adaptable brain network configuration underlies successful cognition [17]. As a result, dynamic network reconfiguration was introduced as a fundamental neurophysiological process [206, 208, 211].

In the previous section, we touched upon graph dynamics when discussing changes between segregation and integration. We stated that the brain shows increased segregation during rest/baseline epochs [205], which decreases with higher task demands [208, 209]. Commonly these observations are made using the sliding-window approach. As in connectivity estimation, each window is treated as an independent sample represented by a graph. Therefore, for each window, graph metrics are derived, resulting in a time-varying estimate. It turned out that there are strong fluctuations across various graph metrics, such as in coupling strengths or centrality [14], highlighting a continuous functional reorganization of the brain [165]. Therefore, both the topology of the networks and the interactions between them are highly dynamic [168, 173, 209, 210]. The network topology

is tightly linked to information transmission [192]. Moreover, dynamic reconfiguration is directly linked to cognitive performance during various tasks, such as memory [200, 212–214].

However, assuming disjoint individual matrices in each window does not cover all aspects of the contact patterns' temporal structure. There are lines of research aimed to improve this basic approach. Holme & Saramäki [215] reviewed the field of temporal networks and illustrated important advances, drawbacks, and unified some concepts. Firstly, the temporal network comes with many names across various fields, such as temporal graphs, evolving graphs, time-varying graphs, time-aggregated graphs, time-stamped graphs, dynamic networks, or dynamic graphs. From now on, we will stick with the name "temporal network" when referring to a time-dependent analysis of brain networks. The concept of temporal networks is based on a multilayer approach, and it has an important improvement that differs it from simple sliding-window approaches. In the multilayer construct, each layer is represented by an adjacency matrix corresponding to a graph at a single time-point. All layers, also called slices, are mutually coupled and can be analyzed as a single graph construct (Fig. 4.3a). Therefore, the same node exists in all layers and is linked throughout the layers by an edge representing the node's identity. Multiple types of edges can also link nodes within and between layers representing different types of relationships between network elements [184].

The advantage of this approach can be illustrated in the following example. Imagine that at time t_1 nodes A and B are connected and at the following time t_2 nodes B and C are connected. A simple sliding window approach would state that there is no direct or indirect connection between A and C as it only focuses on one adjacency matrix at a time. It stays blinded to all previous and following states. However, the temporal network concept assumes that A and C are indirectly connected and that the information can propagate over time. An important conclusion is that the timings of connections and the time ordering matters [215].

This important shift in perspective necessarily challenges the notion of static graph measures. We assume a set of N vertices V interacting with each other at certain times. The duration of the interactions is negligible. In this case, the system can be represented by a contact sequence — a set of C contacts, triples (i, j, t) where $i, j \in V$ and t denotes time [215]. Each triplet of a contact sequence can never occur twice; thus, we assume

only an undirected graph. For some metrics, the transformation from static to dynamic is straightforward only by aggregation over the chosen period. For example, the nodal degree would become the sum of all edges activated within some time window. On the other hand, the notion of the shortest path in a network is more ambiguous as there could be many paths during the whole time interval. Therefore, this metric needs to be derived with respect to a certain time period, and it is defined as sequences of contacts with non-decreasing times that connect sets of vertices. This path is time-respecting, meaning it begins and ends at certain points in time. Many other metrics, such as temporal path length, reachability, latency, as well as different randomized reference models, have been discussed and reviewed in [215]. A major limitation was the absence of community detection. Not only that there was a lack of universal definition, but another challenge was optimizing multilayer modularity in the construction of appropriate null models for multilayer networks [216]. Since the communities were shown to be the basic building blocks of brain architecture and investigating their changes and stability is of utmost importance.

Mucha *et al.* [217] came with a solution proposing to stitch consequent layers in the sense that node i in a layer r is connected to the same node i in the following layer s and so on. Therefore, each node is always connected to itself from the previous and following layer in a chain-like way (Fig. 4.3b). It is important to note that the node is connected only to itself and not to other nodes in other layers. Formally, A_{ijs} details a direct connection in layer s with interlayer couplings C_{jrs} that connect node j in layer r to itself in layer s. We assume undirected network layers where $A_{ijs} = A_{jis}$ and couplings $C_{jrs} = C_{jsr}$. If the strength of each node individually in each layer is $k_{js} = \sum_i A_{ijs}$ and across layers by $c_{js} = \sum_r C_{jsr}$, then the multilayer strength is $\kappa_{js} = k_{js} + c_{js}$. Finally, the multilayer modularity was defined as:

$$Q_{multiscale} = \frac{1}{2\mu} \sum_{ijsr} [(A_{ijs} - \gamma_s \frac{k_{is}k_{js}}{2m_s})\delta_{sr} + \delta_{ij}C_{jsr}]\delta(g_{is}, g_{jr}) \tag{4.8}$$

where $m_s = \sum_j k_{js}$, $2\mu = \sum_{jr} \kappa_{jr}$, γ_s is the resolution parameter in each layer, and $\delta(g_{is}, g_{jr}) = 1$ if the community assignments g_{ir} of nodes i in layer r and g_{js} of node j in layer s are the same and 0 otherwise.

This new framework makes it possible to study community structure in a much broader class of networks [217]. Moreover, the community assignment makes it possible to directly

compare the nodes' cluster labels across the temporally adjacent layers. Therefore, it is possible to identify flexible nodes that frequently switch their cluster assignments and those that maintain stable assignments across time [185]. Studies reported this flexibility to be sensitive to both intra- and inter-individual variability and, therefore, to be a potential biomarker of cognition and disease [175]. However, there are still important issues that need to be solved. For example, the strengths of connections between layers are chosen arbitrarily. Moreover, it will also be important to incorporate that an individual node could be connected to other nodes in different layers.

So far, we only talked about networks, where each layer represents a different timepoint. However, the multilayer concept offers a great deal of variability. Significant dependencies between networks where each layer corresponds to different subjects, species, diseases, or tasks can be investigated (Fig. 4.3c). Moreover, in other conditions, the individual layer can model other aspects such as brain networks from healthy individuals and patient cohort, structural connectivity, and functional connectivity matrices [184]. As our focus shifted to connectivity dynamics as a fundamental brain functioning mechanism, temporal networks become an exciting avenue for future research. There are still limitations and issues waiting to be resolved; however, pioneering results already showed promising new insights that temporal networks could bring.

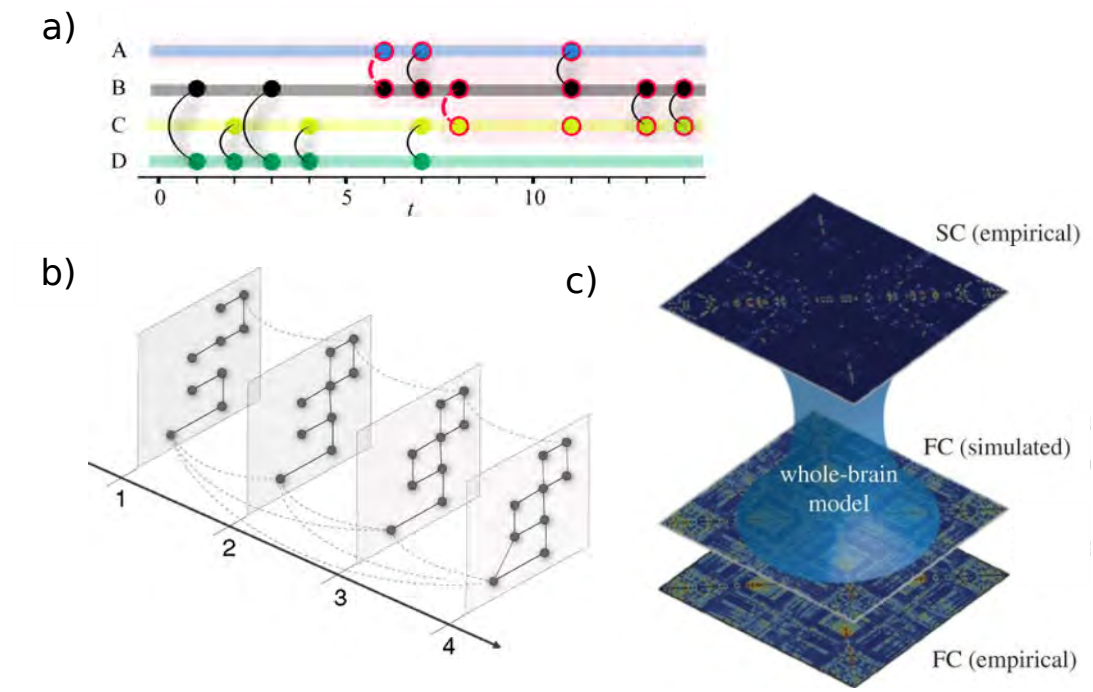

Figure 4.3: Temporal and multislice networks. a) All layers, also called slices, are mutually coupled and can be analyzed as a single graph construct. Here, instead of showing a set of connectivity matrices, the temporal dimension is showed explicitly [215] b) Schematic of a multislice network where each node can also be connected to itself in previous and future slices. In this representation, a node is connected only to itself and not to other nodes in other layers [217] c) In the multilayer construct, each layer might not represent only the temporal dimension. In this visualization, layers correspond to structural, real functional, and simulated functional connectivity. Analyzing this construct could reveal important dependencies and motives among the layers. Adopted from [81].

4.6 Network analysis in fMRI

In this final section, we summarize the individual steps leading from the recording of functional neuroimaging data to inferences about brain network architecture. There are various neuroimaging modalities, each with its advantages and disadvantages. Currently, fMRI is the most commonly used modality as it offers an investigation of macroscopic brain networks. Recorded raw fMRI scans are preprocessed by undergoing several denoising steps (slice timing correction, realignment, image co-registration, normalization based on segmentation, and spatial smoothing). Moreover, the brain parcellation atlas is applied to divide the brain into regions, and the mean signal across all voxels from a given region is extracted. The most common functional connectivity measure in fMRI is the Pearson

correlation. Signals from all regions are cross-correlated to form a connectivity matrix. Such a connectivity matrix corresponds to an adjacency matrix that forms the basis of graph analysis. Using measures of graph analysis operating on the adjacency matrix, a set of topological measures is derived (Fig. 4.4).

In a real-life setting, such an oversimplified scenario is usually not feasible. There is not a general consensus about most of the above-described steps. Therefore, each step comes with an important decision that should be based on available data and investigated hypotheses. Even the first step of preprocessing data is ambiguous as different teams use different strategies. Moreover, the preprocessing pipeline can significantly influence derived brain topology measures, especially when noise is still present even after processing. Optimal brain parcellation is a topic of continuous research. Furthermore, there are two main groups of anatomical and functional atlases. However, even within the groups, the number of regions can vary from dozens to several hundreds of ROIs. Then, the choice of connectivity measure should correspond to asked questions and data. Upon selection, many connectivity measures, such as Granger causality, have tunable parameters that need to be set accordingly. Finally, there is a large group of graph measures, and again the choice should correspond to the investigated hypothesis. Before applying the algorithms, a decision about binarizing the adjacency matrix needs to be made. While there are scenarios, e.g., structural connectivity, where thresholding could lead to noise reduction, there are also studies reporting thresholding to lead to loss of information or being unstable across various thresholds. Ultimately, the obtained measure of brain topology needs to be tested against appropriate null-models.

It is noteworthy that here we only touched upon some issues of static connectivity analysis. Investigating connectivity dynamics brings further questions and decisions about which technique to apply. Moreover, most of the decisions are related to the imaging technique itself. Different modalities pose different challenges. For example, while optimal fMRI preprocessing is still an open question, there seems to be less variability in applied steps in the EEG community. On the other hand, the construction of a network in EEG is less straightforward as one could operate in sensor space or apply the inverse solution and try to map scalp activity to the underlying neuronal source. This approach was not discussed here, as it is beyond the scope of the thesis. However, it should serve as an illustration of all potential tasks that need to be tackled in order to perform robust

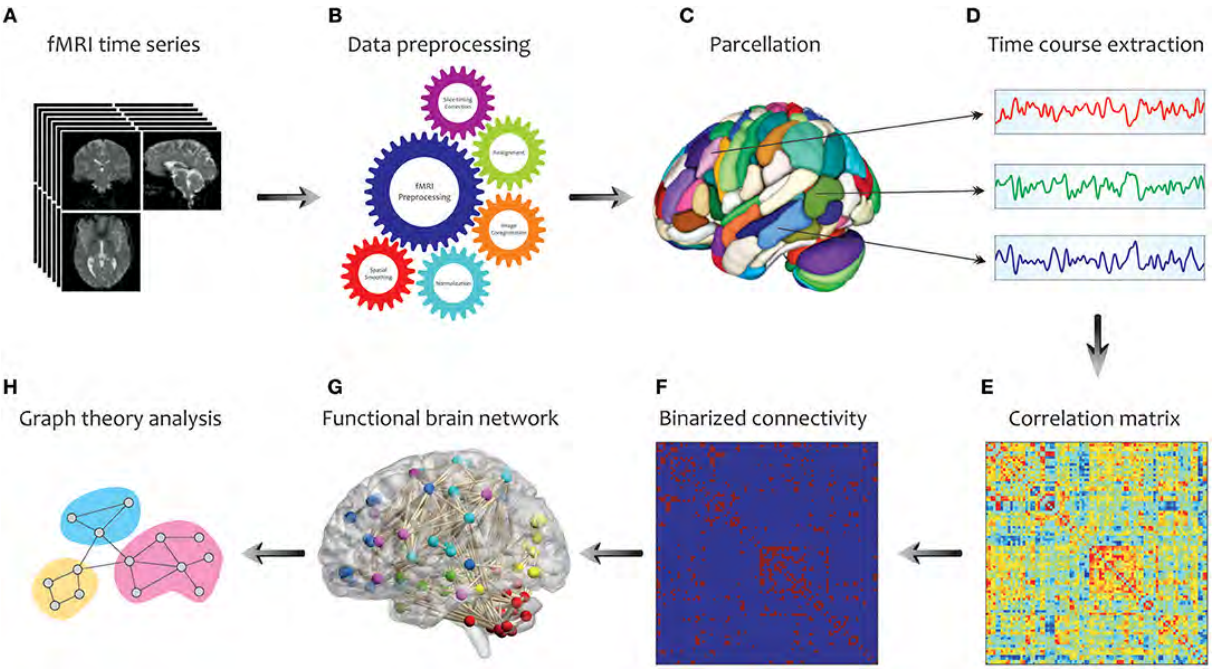

Figure 4.4: Step by step graph analysis in fMRI. The pipeline starts with recording and subsequent preprocessing fMRI time-series. The brain parcellation atlas is commonly applied to divide the brain into parcels, and the BOLD signal is extracted from the respective parcels. Signals from all regions are cross-correlated to form a connectivity matrix. In some analyses, this matrix is further binarized. However, this step is highly debatable. The final connectivity matrix represents an adjacency matrix, i.e., the subject of graph analyses. Reproduced from [95].

network analysis.

Future studies will need to focus on how the slow network dynamics, quantified by graph metrics applied to fMRI measurements, relate to those obtained with much higher temporal resolution (e.g., using EEG, iEEG, or MEG). We know that the brain is able to perform very complex tasks in a very short time (on the scale of hundreds of milliseconds). We assume that during this brief time period, the brain undergoes a massive reorganization that is reflected by changes in graph properties. For these purposes, iEEG recordings offer a very high temporal and spatial resolution. Moreover, recording locations can be mapped to parcellation fMRI atlases to obtain a direct comparison between signals from fMRI and iEEG. Trying to relate network dynamics from different modalities with different timescales could be one of the future lines of research. Nevertheless, iEEG has several limitations, such as the incomplete coverage of the brain, so there are still methodological and technical limitations to be overcome.

Part III

Aim of the thesis

After introducing the concepts of functional and effective connectivity by [78], the study of interactions and synchronization among regions witnessed a remarkable rise in popularity and importance. Building upon the idea of connectivity, the study of large-scale brain networks is currently investigated in various scenarios, from cognitive abilities to mental disorders. That is why this thesis is devoted to connectivity and brain networks. However, it is not driven by a single hypothesis but rather is a methodological demonstration of how connectivity can contribute to the understanding of brain (dys)functions. As the field of connectivity faces several challenges, the presented projects try to contribute to solving some of those.

Large-scale brain networks are typically investigated using functional connectivity and resting-state fMRI. They are characteristic by their intra- and inter-individual variability. This variability has been linked to neurological diseases or differences in structure. Moreover, it has been used for the identification of individual subjects. However, are these changes driven by real differences in structure and function, or do they result from artifacts? It is vital to be able to assess the quality of our estimates. We asked the questions such as whether there is a large inter-individual variability in connectivity quality? If so, what drives this variability? Could it be explained by a particular type of noise, such as head motion?

Currently, most of the network research revolves around fMRI measurements. This technique suffers from a low temporal resolution. However, we already know the brain is able to perform complex tasks on the scale of hundreds of milliseconds. Therefore, there is a need to understand how large-scale networks evolve, integrate, and communicate on these fast timescales. Although segregation and integration have been proposed as mechanisms to accomplish various tasks, our knowledge of their dynamics is limited mostly to fMRI. This thesis presents a novel iEEG study aiming to understand network dynamics during a specific cognitive task focused on recognition memory. There are currently very few whole-brain network studies in the field of iEEG due to many obstacles inherent to iEEG recordings. Their overcoming allowed us to ask questions such as what mechanisms drive recognition memory. Can we observe the reorganization of brain networks on such fast timescales? Not only that it brings novel findings on memory, but it also paves the way for future iEEG studies.

Finally, connectivity has been extensively used to study not only brain functions but

also brain dysfunctions. One such dysfunction that affects the lives of around 50 million people worldwide is epilepsy. Our understanding of epilepsy mechanisms has shifted its focus towards a more dynamic, whole-brain network perspective in the last decades. This perspective makes connectivity an ideal candidate to investigate the mechanisms of its generation. The unpredictability of seizures is one of the main health risks and psychological burdens in epilepsy. Hence, successful seizure prediction can significantly improve the health and quality of life of epilepsy patients. Connectivity has already been successfully applied to the identification of the seizure onset zone. Moreover, its alterations were shown to be a hallmark of upcoming seizures. However, most of the current research focuses on connectivity changes minutes and hours before a seizure. No study in humans so far systematically assessed long-term connectivity changes. Understanding the temporal evolution of connectivity patterns is of fundamental value in uncovering the mechanisms involved in epileptogenesis, as well as in ictogenesis. Nevertheless, can we identify critical times of connectivity changes days prior to a seizure that would help seizure prediction? What drives these changes? Are they localized to a particular region, or do they affect the whole brain?

The questions posed in previous paragraphs illustrate the three research projects carried out within this thesis. Namely:

- Functional connectivity quality in resting-state fMRI
- Large-scale networks dynamics during recognition memory using iEEG
- Long-term connectivity changes in epilepsy

These three projects will be further presented in full detail. Not only that they investigate connectivity in different imaging modalities (fMRI vs. iEEG), but they also explore different time aspects: from stationary to slow timescales (hours and days) and up to very fast time scales (milliseconds).

I believe that my thesis states important fundaments of brain imaging, connectivity estimation, and network analysis. I tried to introduce functional neuroimaging techniques, compare their strengths and weaknesses, illustrate their use, and address the influence of artifacts. Moreover, I tried to portray the wide range of applications for connectivity estimates, whether it is studying the relationship between function and structure, identifying brain diseases, or reflecting dynamic reconfiguration between segregation and integration.

Altogether, these applications could be taken as a guideline and an inspiration for future neuroscientific studies. Furthermore, the investigated research question can hopefully bring a novel understanding of brain processes and thus push the field of neuroscience a little step ahead.

Part IV

Original research

Chapter 5

Typicality of functional connectivity robustly captures motion artifacts in rs-fMRI across datasets, atlases, and preprocessing pipelines

Functional connectivity analysis of resting-state fMRI data has recently become one of the most common approaches to characterizing individual brain function. It has been widely suggested that the functional connectivity matrix is a useful approximate representation of the brain's connectivity, potentially providing behaviorally or clinically relevant markers. However, functional connectivity estimates are known to be detrimentally affected by various artifacts, including those due to in-scanner head motion. Moreover, as individual functional connections generally covary only very weakly with head motion estimates, motion influence is difficult to quantify robustly, and prone to be neglected in practice. Although the use of individual estimates of head motion, or group-level correlation of motion and functional connectivity has been suggested, a sufficiently sensitive measure of individual functional connectivity quality has not yet been established. We propose a new intuitive summary index, Typicality of Functional Connectivity, to capture deviations from standard brain functional connectivity patterns. In a resting-state fMRI dataset of 245 healthy subjects, this measure was significantly correlated with individual head motion metrics. The results were further robustly reproduced across atlas granularity, preprocessing options, and other datasets, including 1081 subjects from the Human

Connectome Project. In principle, Typicality of Functional Connectivity should be sensitive also to other types of artifacts, processing errors, and possibly also brain pathology, allowing extensive use in data quality screening and quantification in functional connectivity studies as well as methodological investigations.

The work presented in this chapter has been published in the Human Brain Mapping journal [218].

5.1 Introduction

Imaging techniques play a pivotal role in medical research nowadays. Functional magnetic resonance imaging (fMRI) is one of the most common methods for research into brain function. Resting-state fMRI (rs-fMRI) is a very prolific and popular subcategory of fMRI measurements. In 1995, Biswal *et al.* [92] found that the correlation of low-frequency fluctuations ($<\approx 0.1$ Hz) in blood oxygen level-dependent (BOLD) signals is a manifestation of the functional connectivity of the brain. Later studies confirmed that fMRI fluctuations are tightly coupled with the underlying neural activity [219, 220]. These spontaneous low-frequency fluctuations in the BOLD signal are therefore used to investigate the functional architecture of the brain [135].

A common approach to the analysis of rs-fMRI data is to assess functional connectivity (FC), defined as temporal dependence of neuronal activity patterns [94], and thus determine which regions are functionally connected. Regions are defined based on a reasonable brain parcellation. Although there is no consensus on optimal parcellation [68, 221], it has been suggested that the matrix of FC among all brain regions may be a suitable representation of the brain connectivity, potentially providing behaviorally or clinically relevant markers [60, 136, 222].

Like any other imaging technique, fMRI is also affected by unwanted artifacts. There are many non-neuronal sources of signal variability such as thermal noise, physiological sources (created by the cardiac and respiratory cycles), scanner and head coil heterogeneities, spiking, chemical shifts, radiofrequency interferences, or subject movement [47–50]. Scanner head motion has long been recognized as a source of artifacts in rs-fMRI [223, 224]. These artifacts originate in changes in head position that can yield many forms

from small involuntary drifts to brief impulsive movements [225]. They induce undesirable, artificial effects that manifest in complex temporal and spatial patterns [51, 92, 223, 224, 226]. Recent studies showed that even small head movements, in the range of 0.5 to 1 mm, can induce systematic biases in correlation strength and thus they can profoundly influence the final estimates of functional connectivity [51–59].

Typical motion artifact manifests as increased short-range connectivity and reduced long-range connectivity, although gross head motion can also increase long-range connectivity [53, 54, 227–229]. These effects influence the correlation values as well as the derived connectivity measures characterizing the network topology [62, 230]). Therefore, they have been both a point of concern and controversy for rs-FC investigations [55, 152, 231–234].

In common practice, fMRI data preprocessing is used to reduce the noise. Preprocessing usually includes image realignment, spatial smoothing, filtering, and confound regression [60]. There is no consensus on the optimal preprocessing strategy that should be applied to rs-fMRI data [63, 235]). Since no preprocessing is completely successful in removing the motion influence [62, 236], it is vital for connectivity studies to be able to quantify the amount of motion artifacts present in FC matrices. However, a reliable measure of FC quality has not yet been established. The absence of robust FC quality measure renders the estimation of the amount of motion artifact in an FC matrix impossible. We propose a new measure - Typicality of Functional Connectivity, that is based on a correlation of a single FC matrix with a typical FC matrix. We analyze it across different datasets, atlases, and preprocessing pipelines.

The individual deviations from a typical FC matrix might not be entirely attributable to artifacts and could be of neural origin. Nevertheless, we suggest that the most prominent deviations are likely to be dominated by non-neuronal related signal changes and thus could identify potentially problematic subjects. Therefore, such measure can be helpful in investigations of individuals and populations whose in-scanner movement profiles may differ subtly, for instance when comparing controls to subjects of different ages (e.g., during development or aging) or to individuals experiencing involuntary or repetitive movements (e.g., tics or tremors)[55, 152]. By definition, it should be sensitive also to other types of artifacts, processing errors, and possibly also brain pathology, allowing extensive use in data quality screening and quantification in functional connectivity studies

as well as methodological investigations, such as the evaluation of preprocessing pipeline performances and the decision on suitable brain parcellation.

5.2 Material and Methods

5.2.1 Data acquisition

Main dataset

For the main study, we took a dataset with 245 healthy subjects (148 right-handed, 132 females, mean age 29.22 / standard deviation 6.99). Participants were informed about the experimental procedures and provided written informed consent. The study design was approved by the local Ethics Committee of the Institute of Clinical and Experimental Medicine and the Psychiatric Center Prague. Each volunteer underwent MRI scanning that included 10 minutes of resting-state functional magnetic resonance imaging acquisitions with eyes closed and acquisition of a T1-weighted and T2-weighted anatomical scan.

Scanning was performed with a 3T MRI scanner (Siemens; Magnetom Trio) located at the Institute of Clinical and Experimental Medicine in Prague, Czech Republic. Functional images were obtained using T2-weighted echo-planar imaging (EPI) with BOLD contrast. GE-EPIs (TR/TE = 2000/30 ms) comprised 35 axial slices - acquired continuously in descending order covering the entire cerebrum (48x64 voxels, voxel size = 3x3x3 mm^3). A three-dimensional high-resolution T1-weighted image (TR/TE/TI = 2300/4.6/900 ms, (170 slices, 162x210 voxels, voxel = 1x1x1 mm^3) covering the entire brain was used for anatomical reference. T2-weighted images were also acquired but not used in the current study.

Alternative dataset

For confirmation and additional analyses, we took a different dataset of 84 healthy subjects (80 right-handed, 48 males, mean age 30.83 / standard deviation 8.48). Each volunteer underwent MRI scanning that included 10 minutes of resting-state functional magnetic resonance imaging acquisitions with eyes closed and acquisition of a T1-weighted and T2-weighted anatomical scan. Scanning was performed with a 3T MRI scanner (Siemens;

Magnetom Trio). Functional images were obtained using T2-weighted echo-planar imaging (EPI) with BOLD contrast. GE-EPIs (TR/TE = 2500/30 ms) comprised 44 axial slices acquired continuously in descending order covering the entire cerebrum (64x64 voxels, voxel size = 2x2x2 mm^3). A three-dimensional high-resolution T1-weighted image (TR/TE/TI = 2300/4.6/900 ms, 169 slices, 176×189 voxels, voxel = 1x1x1 mm^3) covering the entire brain was used for anatomical reference (for more details see [237]).

Human Connectome Project

To be able to repeat and generalize our results, we analyzed preprocessed rs-fMRI of 1081 subjects from the WU-Minn Human Connectome Project (in this paper referred to simply as "HCP"). Data were downloaded from the HCP S1200 Release Resting-State fMRI 1 FIX-Denoised (Extended) package. We used the first 15 minutes of resting-state scans with left-right phase-encoding directions.

Structural dataset acquisitions included high resolution T1-weighted and T2-weighted images (TR/TE/TI = 2400/2.14/1000 ms, voxel = 0.7x0.7xs0.7 mm^3, 256 sagital slices). Resting-state fMRI was acquired at 2 mm isotropic resolution, TR = 720 ms, TE = 33.1 ms, slice thickness of 2.0 mm, 72 slices. (for more details see [238]).

Data were already preprocessed (including spatial distortion correction, motion correction, spatial registration, normalization to MNI coordinates) and denoised using the FIX ICA-based automated method. Artifacts, such as head motion or cardiac pulsation, are regressed out from high-pass filtered data, along with 12 head-motion-related confound regressors (more details in [239, 240]).

5.2.2 Preprocessing

Stringent

Initial data preprocessing was performed using a combination of the SPM12 software package (Wellcome Department of Cognitive Neurology, London, UK) and CONN toolbox (McGovern Institute for Brain Research, MIT, USA) running under MATLAB (The Mathworks). CONNs default preprocessing pipeline (*defaultMNI*) comprises of the following steps: (1) functional realignment and unwrapping, (2) slice-timing correction, (3) structural segmentation into white matter and cerebrospinal fluid & structural normalization to the MNI space, (4) functional normalization to the MNI space, (5) outlier

detection, and (6) smoothing with 8mm kernel size.

The default denoising steps in the CONN toolbox included a component-based noise correction method (CompCor) performing regression of six head-motion parameters (acquired during the correction of head-motion) with their first order temporal derivatives and five principal components of white-matter and cerebrospinal fluid. This default preprocessing might be suboptimal due to not suppressing the motion artifacts sufficiently (potential remedy could be including 24 instead of 12 motion parameters, although adding quadratic expansions showed similar preprocessing efficacy, see [241]), or due to removing some part of the neural-induced signals (for discussion on the use of components in preprocessing see [242]). Time series from defined regions of interest were additionally linearly detrended to remove possible signal drift and finally filtered by a band-pass filter with cutoff frequencies 0.009 - 0.08 Hz. This preprocessing pipeline is labeled as *stringent* further in the manuscript.

To form functional connectivity matrices, we cross-correlated the ROI-based average BOLD time series. In line with the most common practice, we use the Pearson correlation coefficient to quantify functional connectivity and form FC matrices. Note that although other non-linear approaches for functional connectivity assessment have been proposed, the linear Pearson correlation coefficient was shown to be sufficient under standard conditions [102, 243]. Fisher's r-to-z transformation was applied to each correlation coefficient to increase the normality of the distribution of correlation values [244].

Moderate

We additionally used two more lenient processing setups in our analyses. In comparison with the *stringent* pipeline, the *moderate* denoising steps only included regression of six head-motion parameters and one principal component of white-matter and cerebrospinal fluid. A band-pass filter with broader cutoff frequencies of 0.004 - 0.1 Hz was applied.

Mild

The *mild* preprocessing consists of only CONNs default preprocessing pipeline - *default-MNI*. No further filtering or regression was done.

5.2.3 Atlas choice

We chose a parcellation based on Craddock atlas because it offers an option to select the number of ROIs that represent spatially coherent regions with homogeneous connectivity. For each subject, we calculated 23 FC matrices that differ in the number of ROIs: ranging from 10 to 840 ROIs. With the increasing number of ROIs, the size of each ROI decreases (Fig. 5.1). If not stated otherwise, the default parcellation is into 200 regions (on average comprising 91.9 ± 18.8 voxels). The regions in Craddock atlas are created using a spectral clustering algorithm with various similarity metrics and group-level clustering schemes (for details see [245]).

Moreover, to assess generalization to other types of atlases, we also used AAL atlas (90 ROIs) - the most common anatomical atlas [246].

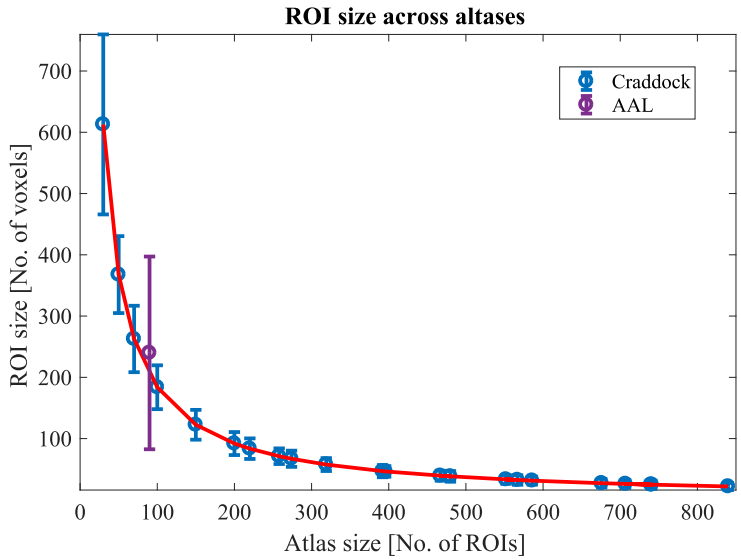

Figure 5.1: ROI sizes decreases with the number of ROIs. ROI sizes for 23 atlases based on Craddock spectral clustering method and for anatomical AAL atlas (in purple). The ROI size decreases with the increasing number of ROIs. The mean size (number of voxels) with ± standard deviation is plotted.

5.2.4 Quantifying motion

Reporting motion statistics should be fundamental for any fMRI study, but Waheed *et al.* [247] analyzed 100 most recent fMRI studies, and only 10 % provided a table of motion metrics. Two of the most used motion metrics are framewise displacement (FD) and the derivative of root mean square variance over voxels (DVARS). We used mean FD and

mean DVARS to quantify the amount of motion during a given scanning session. Fig. 5.2 depicts the distribution of each metric.

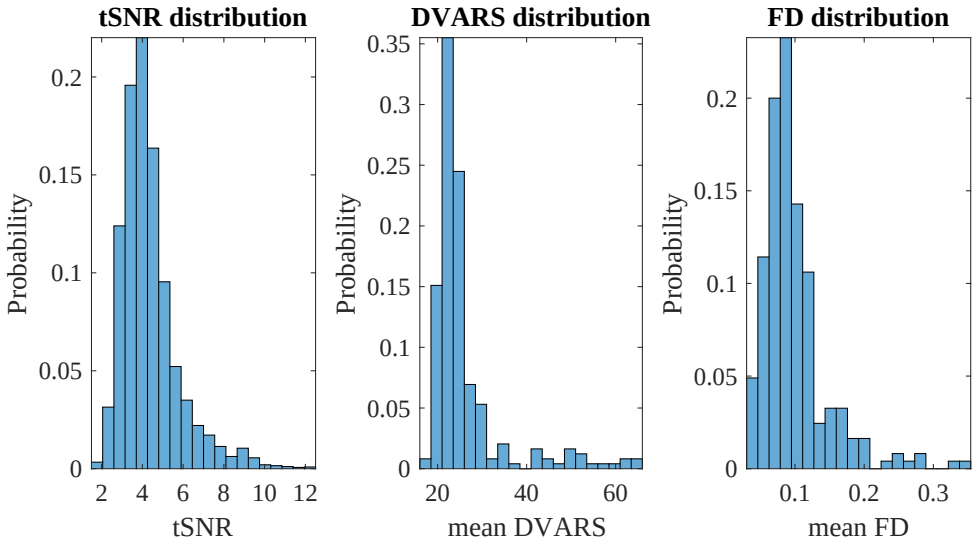

Figure 5.2: Motion metric distributions. Mean of DVARS and FD are metrics commonly used to describe the gross head movement of a given subject. Based on the motion metrics, all subjects would meet the inclusion criteria for analysis in most MRI laboratories. The distributions of tSNR and motion metrics (represented by mean FD and mean DVARS) for the 245 subjects used in this study are plotted.

Framewise displacement (FD)

The fMRI data allow the estimation of six head realignment parameters for each volume. Thus, head position is described at each time point by six parameters (translational displacements along X, Y, and Z axes and rotational displacements of the pitch, yaw, and roll). Framewise displacement represents a summarizing parameter of head motion from one volume to the next. It is an average of the rotation and translation parameters differences (Eq.5.1). Since it is based on realignment parameters, it is therefore unaffected by subsequent preprocessing steps [53].

$$FD_i = |\Delta d_{ix}| + |\Delta d_{iy}| + |\Delta d_{iz}| + |\Delta \alpha_i| + |\Delta \beta_i| + |\Delta \gamma_i| \tag{5.1}$$

where displacement of i-th brain volume in x-direction is $\Delta d_{ix} = d_{(i-1)x} - d_{ix}$ and similarly for the other rigid body parameters. Rotational displacements were converted from degrees to millimeters by calculating displacement on the surface of a sphere of

radius 50 mm.

FD is the most popular metric among motion statistics. It was reported in 24 % of recent fMRI studies compared to similar root mean square (RMS) metric which was reported only in 10 % of recent fMRI studies [247].

Derivative of root mean square variance over voxels (DVARS)

The derivative of root mean square variance over voxels quantifies changes of intensities between two images and it is calculated as the root mean square value of the differentiated BOLD time series within a spatial mask at every time-point (Eq.5.2)[248]. DVARS is not derived from realignment parameters, and thus it could reflect any kind of bias. Nevertheless, the head motion has been proven to be a significant contributor to fluctuations in DVARS [233]. The quantity is calculated after functional connectivity processing and it is defined as:

$$DVARS(\Delta I)_i = \sqrt{\langle [\Delta I_i(\overrightarrow{x})]^2 \rangle} = \sqrt{\langle [I_i(\overrightarrow{x}) - I_{i-1}(\overrightarrow{x})]^2 \rangle} \tag{5.2}$$

where $I_i(\overrightarrow{x})$ is image intensity at locus $\overrightarrow{x}$ on frame i and angle brackets denote the spatial average over the whole brain.

Since it is based on BOLD signal intensity, DVARS differs greatly across datasets and processing strategies [227]. It can be influenced by blurring kernel size, frequency filter characteristics, sequence characteristics, etc. DVARS was reported only in 8 % of the recent fMRI studies [247].

5.2.5 Measuring FC quality

Estimating connectivity quality and assessing its relationship with motion is vital for all connectivity studies. Currently, there is no measure used in literature that allows quantifying it per subject. Here we present our new metric along metrics proposed by other groups.

Typicality of Functional Connectivity (TFC)

We propose the Typicality of Functional Connectivity as a new measure for how to estimate FC quality. It is based on a correlation between an individual subjects FC matrix

and a typical FC matrix of a given cohort (Eq. 5.3). To exclude the influence of diagonal values, we vectorized the upper triangular form of all FC matrices (ignoring the diagonal elements).

$$TFC_i = \frac{(1 + r_P(FC_i, \overline{FC}))}{2} \tag{5.3}$$

where i is the subject's index, r_P is a Pearson correlation coefficient and $\overline{FC}$ is the typical FC matrix. Throughout the manuscript Spearman correlation is denoted as r_S and Pearson correlation as r_P.

TFC ranges between 0 and 1, where 0 is a complete anti-correlation, 0.5 is a correlation of 0, and 1 is a maximal correlation with the typical FC matrix.

As the template, we use the mean FC matrix of 10 % subjects with the lowest motion (lowest mean FD). Taking mean FC across the whole dataset instead of 10 % of subjects gives similar results. Subjects are taken from the *Alternative* dataset (see Methods section). Thus, no subjects need to be eliminated from further analyses. If an alternative dataset with similar preprocessing is not at disposal, low-movement subjects from the same dataset can be used. We assume that by averaging FC matrices of low-movement subjects, we obtain a useful estimate of awake human brain functional connectivity. While minor or moderate deviations may represent effects of interest corresponding to inter-individual variation in brain function, larger anomalies are likely to arise due to artifactual sources of signal variation and should be subject to screening.

Euclidean L^2 distance

Instead of using correlation as a similarity measure with the typical matrix, we also used distance. More specifically, the Euclidean L^2 distance defined as the mean distance between FC values from an upper triangular form of a single FC matrix (without diagonal) and corresponding typical FC values, resulting in a non-negative value characterizing matrix typicality (Eq. 5.4).

$$d_i = \frac{1}{N} \sum_{j=1}^{N} (FC_i^j - \overline{FC^j})^2 \tag{5.4}$$

where i is a subject's index, j is an FC value index, $\overline{FC}$ is the typical FC matrix, and N is the number of FC values.

Geodesic distance

Introduced by Venkatesh *et al.* [249], the reasoning behind this distance metric is that the correlation matrices lie on a non-linear space. Geodesic distance between two points on the positive semidefinite cone (e.g., two FC matrices) is the shortest path between them along the manifold. Since it is not guaranteed that the typical FC matrix would lie on the manifold, we define this quality measure as the mean geodesic distance between a full FC matrix and all other FC matrices (Eq. 5.5).

$$d_i = \frac{1}{N}\sum_{j=1}^{N}\sqrt{trace(log^2(FC_i^{\frac{1}{2}}FC_jFC_i^{\frac{1}{2}}))} \tag{5.5}$$

where i, j are subject's indices.

Quality control-functional connectivity (QC-FC)

In literature, the most used way to evaluate the presence of a motion artifact are quality control - functional connectivity (QC-FC) values [54, 62, 227, 241]. This group measure examines how motion affects FC values for each pair of regions across subjects. Each FC value is directly correlated with a summary motion statistic (either mean FD or mean DVARS) across subjects. The median of these values shows if motion tends to increase or decrease connectivity and a correlation of QC-FC with distance reveals the presence of spurious distance dependence.

5.2.6 tSNR

The temporal signal to noise ratio is a useful measure of data quality [250]. Van Dijk *et al.* [52] have found that low values of tSNR identify subjects with high head motion or other causes of data instability. For each ROI, the mean signal is divided by the standard deviation over the BOLD run, and tSNR is calculated as the mean tSNR value across all ROIs in the brain (Eq. 5.6). An alternative is using a voxel-based tSNR, where the signal

from each gray matter voxel with signal values > 150 is used instead of ROIs.

$$
\begin{aligned}
tSNR_r &= \frac{\frac{\sum_{t=1}^{T} S(r,t)}{T}}{\sqrt{\frac{\sum_{t=1}^{T}(S(r,t)-\overline{S(r)})^2}{T}}} \\
tSNR &= \frac{1}{R}\sum_{r=1}^{R} tSNR_r
\end{aligned}
\tag{5.6}
$$

where $S(r,t)$ is the signal magnitude at the ROI r in the time t. $\overline{S(r)}$ is a temporal mean. T is the number of all brain volumes, and R is number of all ROIs.

5.3 Results

We used TFC to estimate per subject quality and we analyzed it with respect to motion, atlas size, and preprocessing. We used FC matrices with *stringent* preprocessing parcellated into 200 ROIs using Craddock atlas as a default setup. The TFC metric was based on a comparison with the mean FC matrix of 10 % subjects with the lowest mean FD from the *Alternative* dataset. Using the Spearman correlation, we found that it is significantly correlated with motion metrics ($r_S^{DVARS} = -0.37, p < 10^{-8}, r_S^F D = -0.20, p = 0.002$)(Tab. 5.1), meaning that an FC matrix of a subject with high mean head movement is less similar to the typical FC matrix compared to low-movement subjects (Fig. 5.3a). A correlation coefficient between a motion metric and TFC demonstrates a dependence between FC quality and gross head motion. The effect is more prominent in a high-moving subgroup of subjects. Both FD and DVARS are significantly related to FC quality but mean DVARS shows a generally higher absolute correlation than mean FD.

Instead of TFC, we also tried a method based on Euclidean L^2 distance from the typical FC matrix and mean geodesic distance from the cohort. Unlike TFC measure, which shows significant both Spearman and Pearson quality-motion correlations, the correlations of L^2 distance with motion were significant only using Pearson correlation and FD ($r_P^{FD} = 0.13, p = 0.05$) because this relationship was driven mainly by outliers. Correlations with geodesic distance also did not show consistent significances and yielded only two significant results ($r_P^{DVARS} = 0.39, p < 10^{-9}, r_S^{FD} = -0.13, p = 0.04$) (Tab. 5.1).

	DVARS		FD	
	Spearman	**Pearson**	**Spearman**	**Pearson**
TFC	-0.37 ($2*10^{-9}$)	-0.38 ($7.3*10^{-10}$)	-0.20 (0.002)	-0.23 ($2.8*10^{-4}$)
L^2-distance	0.01 (0.87)	-0.09 (0.18)	-0.02 (0.81)	0.13 (0.05)
Geodesic distance	-0.10 (0.11)	-0.39 ($2*10^{-10}$)	-0.13 (0.04)	-0.08 (0.20)

Table 5.1: Correlation of different measures of FC quality with motion metrics. Only TFC shows significant correlations for both motion metrics and both Pearson and Spearman correlations. The corresponding p-values are in brackets.

Since motion parameters may contain outliers and Spearman correlation is less sensitive to outliers compared to Pearson correlation (see [251]), we prefer to use it throughout the manuscript when assessing the relationship with motion.

We further analyzed only TFC as a quality measure. We evaluated it for every subject across Craddock atlases with varying number and size of ROIs, from 10 to 840 regions, and for AAL atlas with 90 ROIs. From Fig. 5.3b, it is evident that FC quality decreases as the atlas size increases. Therefore, more detailed FC matrices are of worse quality. We investigated whether this gradual decrease is driven by the increased effect of motion on signals in small regions. We calculated correlations between motion and TFC across variously detailed atlases and found that, except for atlases with less than 100 regions, the relationship is stable ($r_S^{DVARS} \approx -0.38, p < 10^{-9}, r_S^{FD} \approx -0.23, p \approx 0.001$)(Fig. 5.4a). AAL atlas shows similar results to Craddock atlas of corresponding size ($r_S^{DVARS} = -0.33, p < 10^{-7}, r_S^{FD} = -0.24, p < 10^{-4}$).

By default, the typical FC matrix is based on connectivity estimates of subjects from a different dataset (identical preprocessing pipeline). The correlation with motion would be only slightly stronger if based on low-movement subjects from the same dataset (for the price of losing 10 % subjects). If we use all subjects from the current dataset for the calculation of the typical FC matrix, the observed relationships are weaker (Fig. 5.4b), possibly due to the presence of various types of noises. Even using a different dataset with different preprocessing, such as HCP, still gives significant results (only for DVARS).

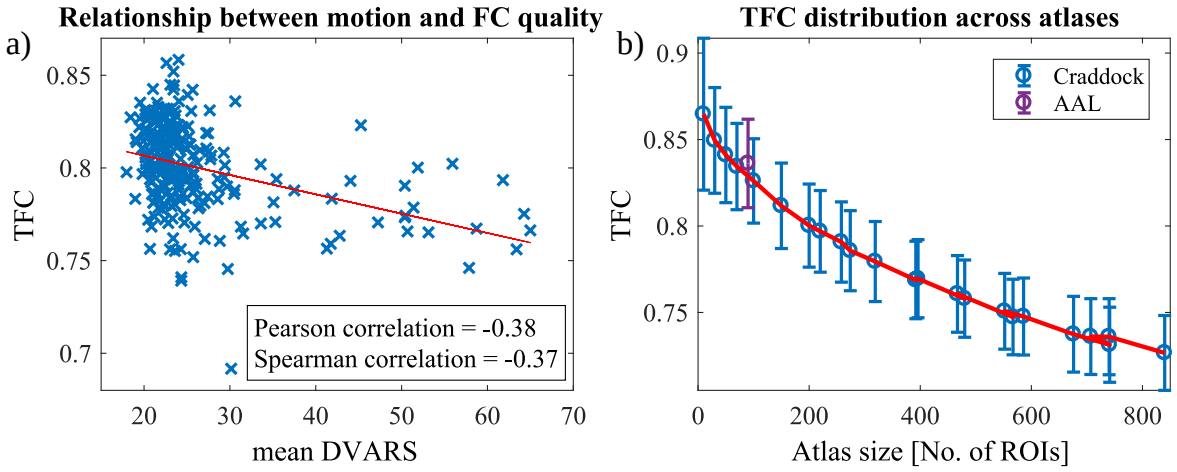

Figure 5.3: Introduction of new FC quality metric - TFC. a) The significant relationship between mean DVARS and TFC proves that subjects with worse FC quality (lower correlation coefficient between a single FC matrix and the typical FC matrix) exhibit higher levels of motion. Calculated for Craddock atlas with 200 ROIs. b) The quality of functional connectivity is decreasing as the number of ROIs increases. Mean ± standard deviation of TFC across atlases is plotted. Purple mark indicates AAL atlas.

Censoring volumes acquired during periods of high-motion is a widespread preprocessing step in rs-FC studies. We varied the threshold for volume exclusion from FD>0.2 to FD>0.5 in order to analyze the effect of volume censoring on TFC (Fig. 5.4d). Censoring was performed only after preprocessing was complete and only for the motion corrupted volume (although we obtained similar results if two volumes before and one after were discarded as well). Only a few FC matrices seemed to degrade in quality. We did not observe a substantial change of TFC even under the strictest conditions, where more than 15 % of volumes were excluded on average.

Besides the influence of ROI size and censoring on FC quality, we also analyzed the influence of data preprocessing on FC quality. We compared FC quality for three different preprocessing pipelines based on their strictness - *stringent*, *moderate*, and *mild*. In Fig. 5.4d we see that with the increasing strictness the individual FC matrices more resemble the typical FC matrix: mean($TFC_{stringent}$)=0.80, mean($TFC_{moderate}$)=0.77, mean(TFC_{mild})=0.71. These TFC distributions are statistically different based on paired t-test between every pair of preprocessing pipelines (all p-values $< 10^{-16}$). For all these cases, we used the typical FC matrix of a dataset with *stringent* preprocessing, but results were similar if each preprocessing stream used its own FC matrix as a golden standard.

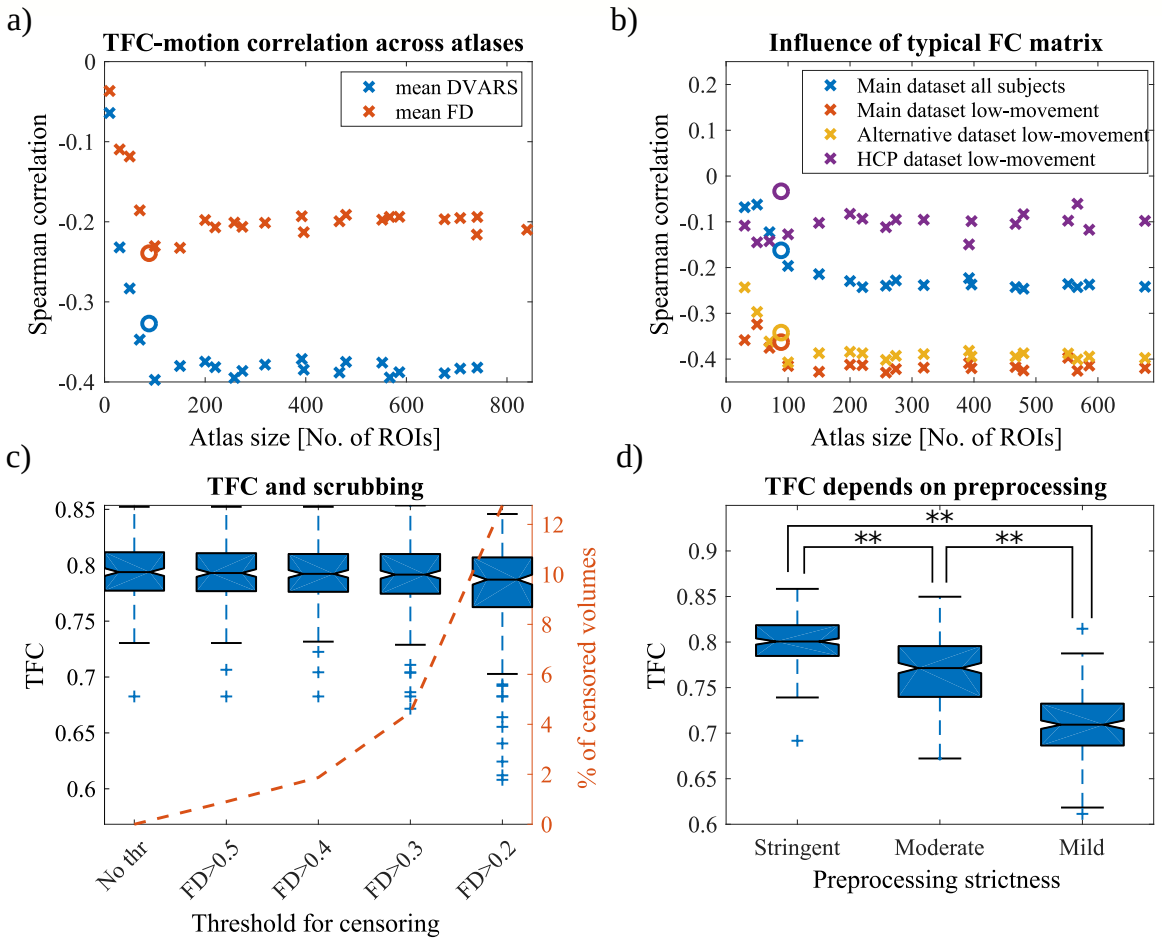

Figure 5.4: Analysis of TFC. a) Spearman correlations between TFC and two summarizing motion metrics for atlases with different number of ROIs. Except for the very small atlases, the relationship between FC quality and motion is constant. A circle mark indicates AAL atlas. b) The highest absolute correlation of the TFC-DVARS dependence is obtained if low-movement subjects of the same dataset are used for the calculation of the typical FC matrix. Although, it is comparable to using low-motion subjects of a different dataset. because the typical matrix of the Main dataset is comparable to a typical matrix of the Alternative dataset ($r_P = 0.86, p < 10^{-16}$) and similar to the typical matrix of HCP dataset ($r_P = 0.68, p < 10^{-16}$). Using all subjects from the same dataset yields lower correlations. c) High movement volumes were censored based on an increasingly strict threshold. No substantial changes in TFC distributions are observable. d) Comparison of quality of FC matrices of all subjects for three different preprocessing pipelines with different levels of strictness; stringent being the strictest and mild the most lenient. FC matrices with more strict preprocessing are significantly more similar to the typical FC matrix (paired t-tests).

To compare TFC with other quality measures, we calculated QC-FC values. We obtained a positive median of QC-FC and significant negative correlation between QC-FC and distance for both quality control metrics ($r_S^{FD} = -0.13, p < 10^{-9}, r_S^{DVARS} =$

$-0.02, p = 0.02$)(Fig. 5.5a,b). Nevertheless, only 21 % of DVARS-FC values (resp. 13 % for FD) were significant (Fig. 5.5c). The relationship between QC-FC and distance is constant across atlases of various sizes (Fig. 5.5d).

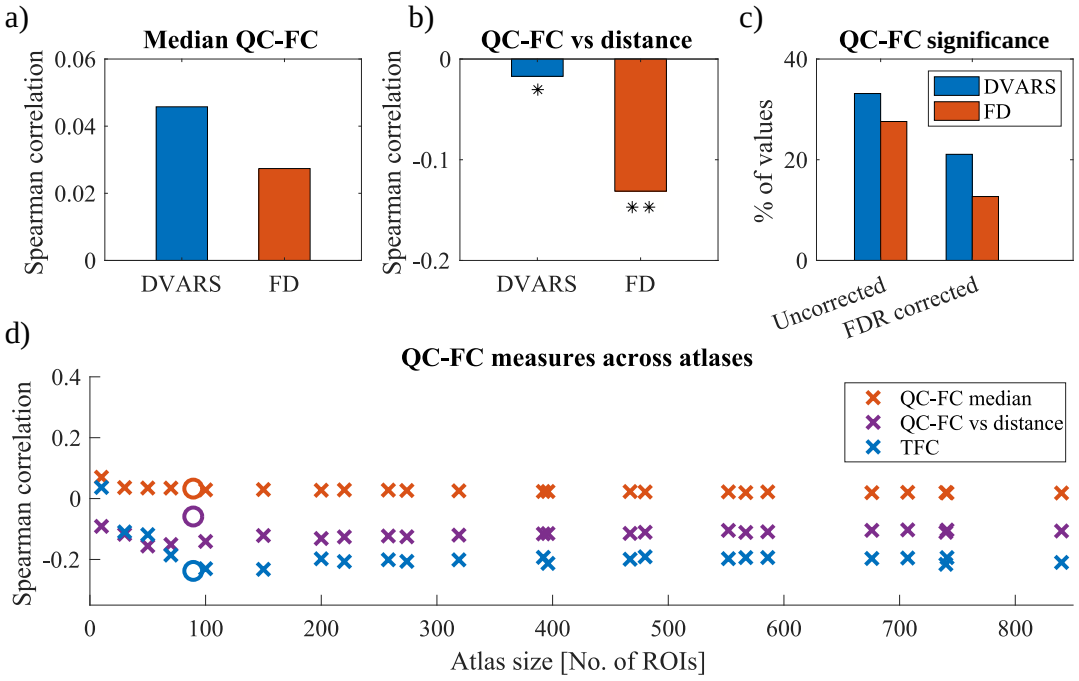

*Figure 5.5: Comparison of TFC with QC-FC metric. a) The QC-FC correlations quantify the association between inter-individual variance in functional connectivity and gross head motion. A positive median of QC-FC values signifies that head motion increases connectivity (for both FD and DVARS). b) This effect is more prominent for short-links and it is more specifically related to motion as correlations are stronger when FD models quality controls. * signifies $p< 0.05$, ** $p< 0.001$ c) On the other hand, the amount of edges that are significantly affected by movements is more easily detectable with DVARS. d) Above mentioned effects are stable across atlases with different number of ROIs. Magnitudes of TFC correlations are higher than the median of DVARS-FC, proving its viability as an estimator. Plotted only for mean DVARS but results with FD are similar. A circle mark indicates AAL atlas.*

So far, we focused only on the quality of connectivity matrices, but the noisiness of the underlying BOLD time series can also be estimated in the form of tSNR. It is apparent that tSNR measures different data aspects compared to TFC as they correlate only weakly ($meanr_S = 0.26$, all p-values $< 10^{-6}$)(Fig. 5.6a). We obtained similar results for both voxel-wise and ROI-wise tSNR. To test whether there is a change in tSNR-motion relationship across parcellations, we correlated it with FD and DVARS across differently sized atlases (Fig. 5.6b). DVARS displays a progressive increase of absolute

correlation with tSNR, unlike FD (changes of correlations between smallest and highest atlas: $\Delta r_S^{DVARS} = 0.13, \Delta r_S^{FD} = 0$, all p-values $< 10^{-11}$).

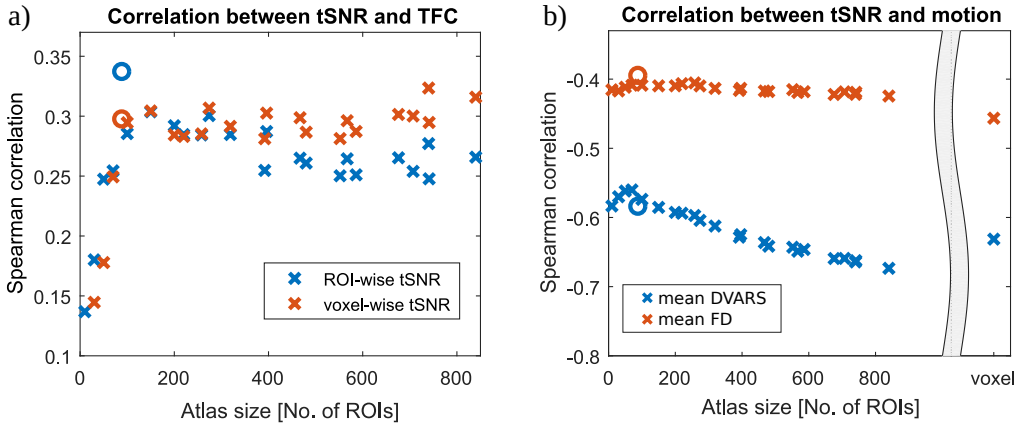

Figure 5.6: Comparison of TFC with tSNR. a) tSNR measures different data aspects than TFC as the correlation is weak. Nevertheless, it is significant and positive. b) With decreasing size of ROIs, the relationship between tSNR and mean DVARS gets stronger. This trend is not present for FD, suggesting that the phenomenon is potentially caused by other types of noise than a head movement.

To demonstrate the robustness of our methods, we applied the same analysis to the HCP dataset. Even though it is a dataset with a different preprocessing pipeline, we observed only slightly higher magnitudes of TFC compared to the main dataset (Fig. 5.7a). Similarly, TFC magnitudes were decreasing with increasing atlas size. Again, TFC significantly correlated with both motion metrics ($r_S^{DVARS} = -0.13, p < 10^{-5}, r_S^{FD} = -0.23, p < 10^{-12}$). Using AAL parcellation yielded FC matrices of higher quality with a lower amount of motion (weaker TFC-motion correlation, especially for FD, $r_S^{FD} = -0.11, p < 10^{-4}$). We confirm that the TFC-motion relationship is stable across various atlases (except for the smallest ones). In general, mean FD showed stronger absolute correlations with TFC (Fig. 5.7b). When analyzing QC-FC values, only the median FD-FC values showed a spurious increase in connectivity (Fig. 5.8a). Moreover, we did not obtain a significant correlation between QC-FC values and distance (p>0.05 for both FD and DVARS), proving successful mitigation of distance dependence and other motion-related impurities for the HCP preprocessing pipeline. On the contrary, a relatively high amount of FC values was correlated with head movements (> 50 % for FD). Based both on QC-FC and TFC, the head motion effect on connectivity seems to be constant and independent of ROI size (Fig. 5.8b).

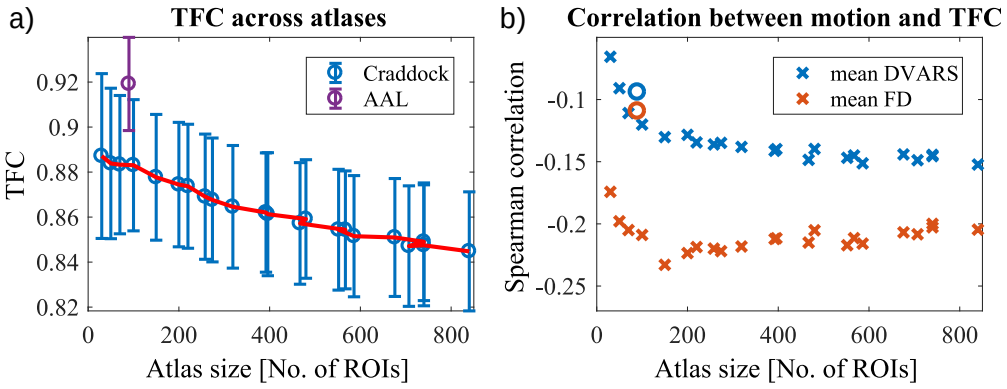

Figure 5.7: HCP dataset quality assessment. a) The HCP dataset shows higher magnitudes of TFC compared to the Main dataset. Similarly, TFC is decreasing with decreasing atlas size. A purple mark indicates AAL atlas. b) Again, the TFC-motion relationship is stable across various atlases (except for the smallest ones). Mean FD shows a stronger absolute correlation with TFC. A circle mark indicates AAL atlas.

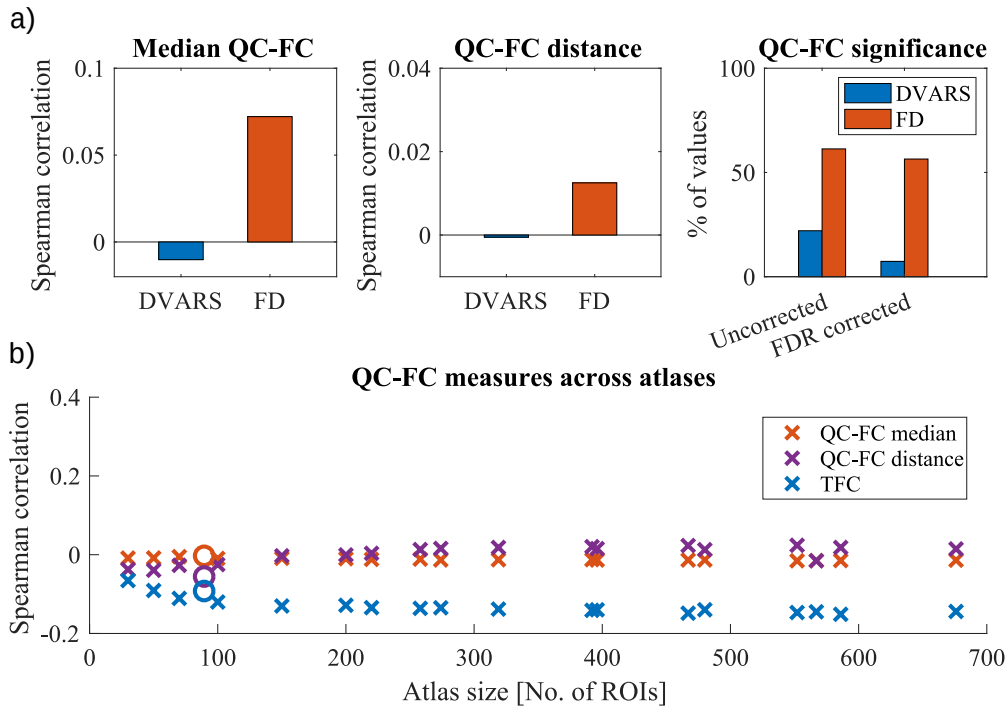

Figure 5.8: TFC and QC-FC in the HCP dataset. a) In the analysis of QC-FC values, only the median FD-FC values shows a spurious increase in connectivity. Moreover, the correlation between QC-FC values and distance was not significant, proving successful mitigation of distance dependence for the HCP preprocessing pipeline. Nevertheless, a relatively high amount of FC values is correlated with head movements (> 50 % for FD). b) Even in the HCP dataset, TFC is significantly correlated with the motion (mean FD). Based both on FD-FC and TFC, the head motion effect on connectivity seems to be constant and independent of ROI size.

Several times, when comparing results across differently sized atlases, we observed an effect of atlas size when up to 100 ROIs were used. This effect might be driven by two factors: by the number of regions or by the size of regions. To test the first hypothesis, we randomly selected 50,100,150,...,700 ROIs out of an atlas with 950 ROIs. We calculated both TFC and ROI-based tSNR and analyzed their relationship with head movement 1000 times. In this scenario, the number of voxels in a region is fixed (21.9 $\pm$ 0.3) and only the number of regions varies. Neither based tSNR nor TFC depends on the number of regions. We only observed a small gradual increase in the TFC-motion relationship when only a few regions were selected (Fig. 5.9a).

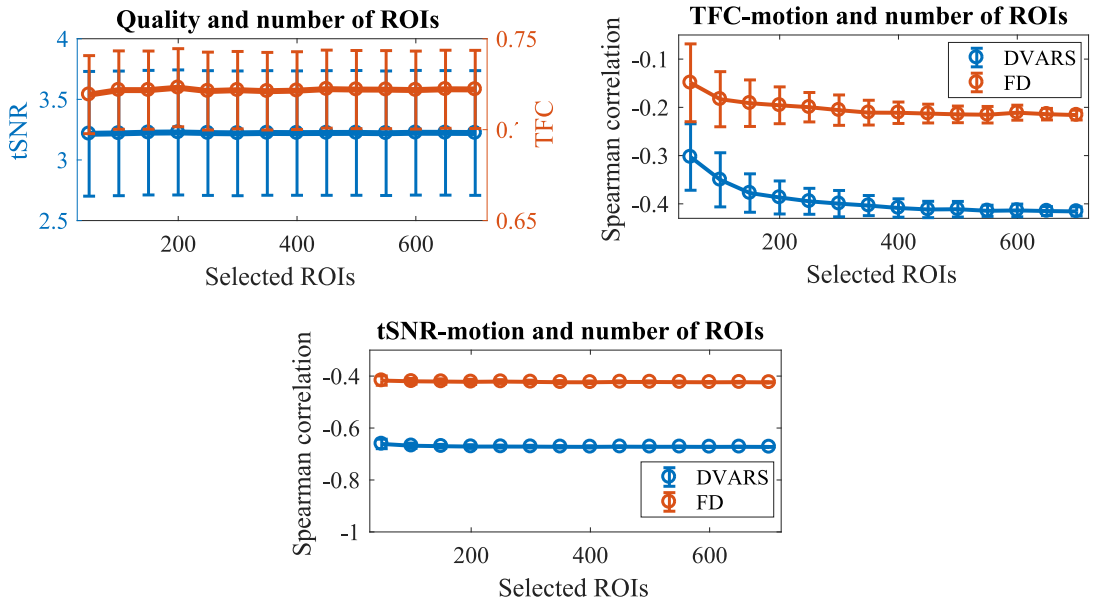

Figure 5.9: Are atlas size effects driven by the number of regions? a) In an atlas with 950 ROIs, we randomly selected 50,100,150,...,700 ROIs to get quality estimates depending only on the number of regions but independent of the number of voxels. Neither ROI-based tSNR nor TFC changes with the number of regions. Only the relationship between TFC and motion is slightly weaker for smaller numbers of regions.

To test the second hypothesis, we took an atlas with 100 ROIs (183.8 $\pm$ 35.8 voxels per region) and we created different geometrical shapes around the central voxel that varied in the number of voxels (Fig. 5.9a). Un-smoothed data were analyzed to avoid the effect of smoothing kernel size. We used FSL routines (FMRIB Software Library v5.0, Analysis Group, FMRIB, Oxford, UK) to create our parcellation schemes. Both tSNR and TFC increase with the increasing number of voxels. On the contrary, TFC-motion dependence is weaker for the low number of voxels (Fig. 5.10b). These results suggest that regions

with few voxels produced noisier data and FC matrices. Additionally, when choosing only a few regions (<100), it is more difficult to estimate a significant relationship between quality and movement

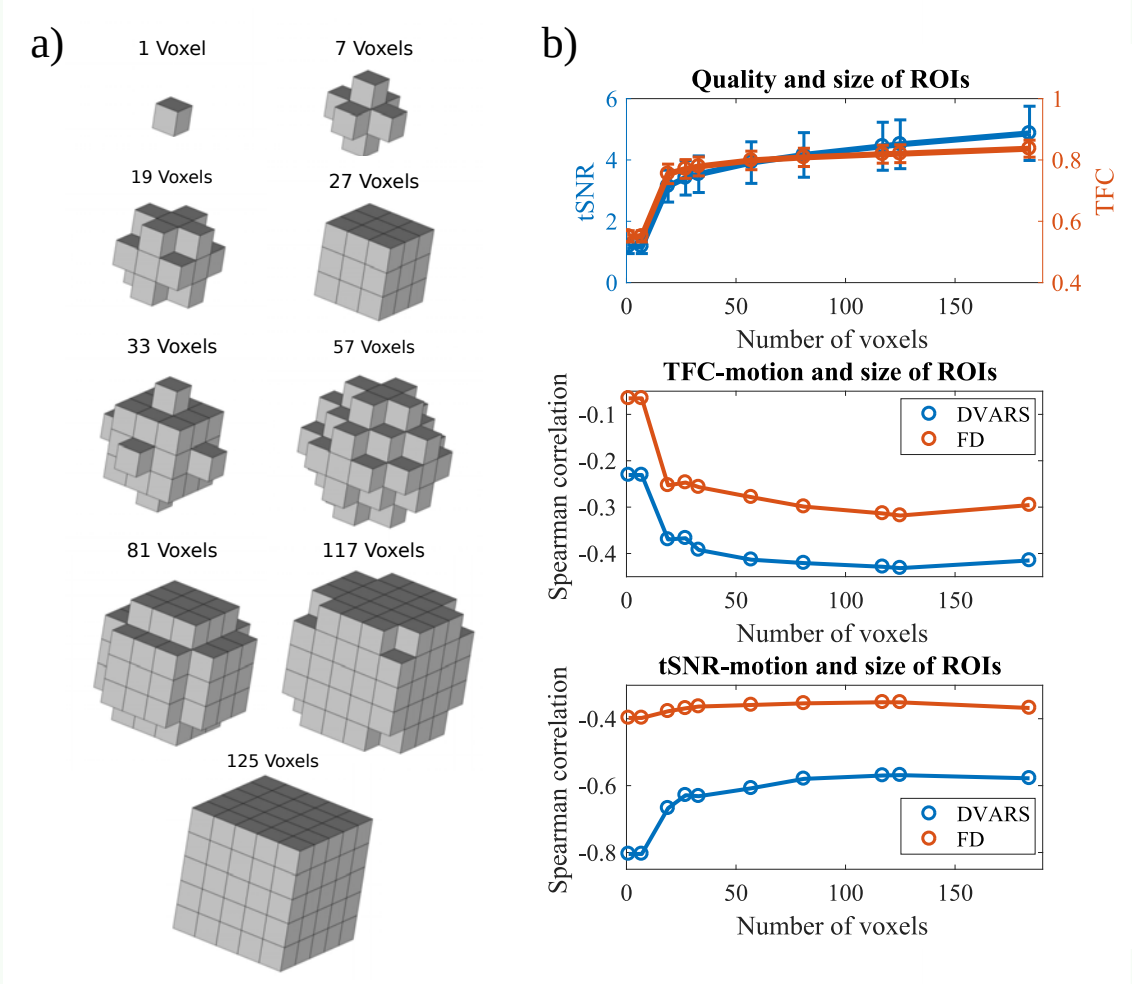

Figure 5.10: Are atlas size effects driven by the number of voxels? a) To create a brain parcellation with a fixed number of regions but a varying number of voxels, we built different geometrical shapes around a central voxel of a region. b) Within an atlas of 100 ROIs, we varied the number of voxels that formed a region. Both voxel-based tSNR and TFC depend on the number of voxels. Moreover, while the tSNR-DVARS relationship is stronger for the smaller number of voxels, the opposite is present for the TFC-motion relationships.

5.4 Discussion

5.4.1 Estimation of FC quality

The lack of a gold standard for FC quality estimation has hampered direct comparison among different groups (neurodevelopmental, aging, neuropsychiatric), preprocessing

pipelines, and brain parcellations. We introduced a new measure (TFC) to describe the quality of a functional connectivity per subject. This measure is based on a correlation of a single FC matrix with the low-motion group-average connectivity matrix. As we showed, it provides a reliable estimate of FC quality with respect to motion and possibly other types of noise. Low-movement subject's FC matrices are strongly correlated with the typical FC matrix compared to high-movement subjects, despite the fact that even our high-movement subjects were healthy controls and would meet inclusion criteria for analyses in most MRI laboratories. Moreover, by visual inspection, it is apparent that subjects with low TFC either lost the modular structure present at the typical FC matrix or show a general artifactual increase in connectivity. An alternative measure to TFC could be Euclidean L^2 distance from the typical FC matrix or mean geodesic distance from the cohort, but our results suggest that these measures are less specifically related to motion. One of the reasons could be that they are more sensitive to other global artifacts.

Currently, many studies propose QC-FC values as a measure of motion impact [62, 228, 252]. QC-FC values are correlations between vectors of summary quality (motion) control values (e.g., mean FD, mean DVARS) with vectors of outcome measures (FC values) across subjects. A limitation of this measure is that it is used only on a group level and it does not allow single subject descriptions. We confirmed that head movements generally increase connectivity (median QC-FC similar to the one reported in [62] and [241] for corresponding preprocessing pipeline) and that it affects distance dependency - increased short-range connectivity and decreased long-range connectivity [53, 228, 229]. This spatial pattern is specifically related to motion as we found stronger dependence for FD. As reported in [62], the number of links related to motion varies significantly (in our results less than 25 % QC-FC values significant). Power *et al.* [228] warned about the possible difficulty of establishing reliable QC-FC correlation if there is little variability in the QC measure. Moreover, QC-FC values are sensitive to outlying values and a few scans with marked abnormalities can obscure relationships present across most other datasets [253]. Finally, they were criticized that they lie on a flawed assumption that "artifact-free" rs-FC is unrelated to motion QC measures [254]. That is why QC-FC should be complemented with other assessments.

Several other metrics have also been adopted in prior studies, including FD-DVARS

correlations [152]. DVARS was used as a predictor of data quality rather than an estimate of the amount of motion. Before the preprocessing, DVARS strongly correlates with FD, and this similarity diminishes with processing [227]. That is why DVARS could serve as a marker of nuisances in an FC matrix [53, 227, 255]. Nevertheless, DVARS changes during processing steps, even when the motion artifact is not filtered out [226]. Therefore, it is not recommended to use the FD-DVARS relationship as an FC quality estimate, but rather it is advised to use DVARS as a motion metric. Another metric sometimes used to assess the presence of motion and the success of denoising strategies are FD-BOLD signal correlations. It has been suggested that the positive FD-BOLD correlations (especially in primary and supplementary motor areas) may reflect motion-related neural activity [59, 230]). However, according to Power *et al.* [228], these correlations are probably not related to neural activity. Finally, Saad *et al.* [256] proposed a global correlation (i.e., mean across all FC values) as a quality estimator, but the reported correlation with motion was not statistically significant.

Other methods entail identification and exclusion of time points for which head movement exceeds a certain threshold [225, 227]. Such threshold becomes increasingly stringent as the effects of motion have received greater recognition [257]. Recently, overly aggressive censoring of volumes was reported due to motion estimates that were artifactually inflated by respiratory artifacts (Gratton et al., 2020). We did not investigate such measures (e.g., Δr reported in several articles [53, 227, 258, 259] or MAC-RSFC [254]) because they require data scrubbing and our goal was to avoid discarding any frames/time points. Nevertheless, we investigated the influence of censoring on TFC. We did not observe substantial changes in the results of the analysis, even under the strict threshold (censoring volumes where FD>0.2). Moreover, according to Muschelli *et al.* [152], censoring seems to be unnecessary or even be detrimental when CompCor approaches are used for denoising resting-state data.

Corrections of group-level statistics are commonly implemented by regressing a summary motion metric for each subject [52, 54, 59, 227]. However, we propose that adding TFC measure could bring further advantages, especially in investigations of potentially problematic individuals, populations in which head-movement profiles differ subtly (e.g., children or elderly cohorts) or individuals experiencing involuntary or repetitive movements (e.g., tics or tremors). TFC offers extensive use in data quality screening and

quantification in functional connectivity studies as well as methodological investigations.

5.4.2 Effect of ROI size

After introducing the TFC measure, our secondary goal was to analyze it under different conditions such as different preprocessing pipelines, varying atlas sizes, or across censoring thresholds. While the censoring did not have a substantial effect, as already discussed, the increasing strictness of the preprocessing pipeline did generally increase TFC values.

For the first time, we now discuss the interesting but unexplored topic of the influence atlas size on FC quality. The impossibility of optimal brain MRI parcellation makes the definition of regions of interest arbitrary. The number of ROIs ranges from 10 to 104 in voxel-based studies (for review see [66, 67]). However, how ROI size affects FC is unclear. Therefore, we examined the quality of FC matrices of varying sizes with respect to motion; the size of FC matrices varied from 10 to 840 ROIs, according to Craddock atlas.

We found an effect of ROI size on the FC quality, meaning a finer parcellation yielded noisier FC matrices. According to QC-FC values, this effect is not related to head movements as medians QC-FC and QC-FC correlations with distance were constant across atlases. Using TFC confirmed that the decrease in quality is specifically related to other types of noise, only large ROIs (atlas with < 100 ROIs) showed increasing absolute correlation between TFC and DVARS/FD with decreasing ROI size. However, large ROIs carry the risk that the mean time course may not represent any of the constituent time courses if different functional areas are included [66]. Moreover, if analyzing too few regions, it is more difficult to establish a reliable relationship with gross head motion.

Using tSNR, we analyzed if the ROI size also affects BOLD signal quality. tSNR is a well-established estimator of data quality, considering all types of noise. Unfortunately, the tSNR value is highly dependent on recording parameters, and thus it is difficult to compare it across studies. Nevertheless, similarly to Van Dijk *et al.* [52], who reported strong Pearson correlation between voxel-based tSNR and RMS ($r_P^{RMS} = -0.57, p < 0.001$), we also report significant Spearman correlation between voxel-based tSNR and both mean FD ($r_S^{FD} = -0.46, p < 10^{-16}$) and mean DVARS ($r_S^{DVARS} = -0.63, p < 10^{-16}$). According to Fig. 5.5f, there is a gradual decrease in correlation between tSNR and DVARS with increasing atlas granularity. Such results suggest that there is an increasing effect of noise on the BOLD signal. Nevertheless, it might be more specifically related to

other types of noise than a head movement. We conjecture that this observation could be potentially linked to the fact that DVARS is by definition sensitive to temporal signal variations beyond those reflected in (apparent) head motion, and might thus reflect more strongly other sources of artifactual signal variation such as cardiac pulsation [50] or respiratory rate variability [260]. Although the motion is believed to have a dominant effect on frame-to-frame signal intensity changes [51, 233, 248].

In conclusion, both time-series and FC matrices based on smaller ROIs are noisier. It is the size of regions (number of voxels) and not the number of regions that plays a critical role here. Moreover, we argue that motion is not the main driving effect behind this quality decrease. In all fMRI studies, it is advised that applied atlas parcellation should be chosen carefully with respect to the application and expected outcomes. Our finding that the less detailed FC matrices are of better quality is useful for all functional connectivity studies when a detailed FC matrix is not necessary, so finer brain parcellation can be sacrificed for more robust estimates of connectivity. Our recommendation here is in line with the one of Zalesky *et al.* [67] that if possible, less detailed atlases will produce more robust results because they are less susceptible to noise. Nevertheless, large ROIs must be created carefully, and we do not recommend using Craddock atlas with less than 100 ROIs

5.4.3 Limitations and future directions

To ensure the robustness of our findings, we have replicated the analysis on the HCP dataset. We replicated all our obtained results and proved TFC to be a reliable FC quality estimator. The HCP dataset was preprocessed using a severe preprocessing pipeline (including censoring time points). Therefore, it is generally of better FC quality (higher TFC) compared to our dataset. That is why the obtained correlations with head movements were generally lower, i.e., the head motion is less present in the dataset. That could also be the reason why the QC-FC correlation diminished, as reported in Ciric *et al.* [62], where ICA-AROMA was the only method to show virtually no QC-FC distance-dependence. Again, we did not find a significant change in the TFC-motion relationship except for the very small atlases. The question arises as to which motion metric is optimal. Currently, the most used motion parameters across studies are DVARS and FD [247]. As Power *et al.* [53] pointed out, it is difficult to quantify the effect of motion with

only one parameter. Nevertheless, according to our dataset mean DVARS showed the strongest correlation with FC quality (r_S up to -0.4). Contrarily, the HCP dataset exhibited the strongest correlations between FD and TFC (r_S up to -0.25). Other summarizing parameters, such as maximum DVARS or DVARS variance, could be used as well because they capture other features of motion (big spike-like movements, constant small drift). However, Van Dijk *et al.* [52] showed that they are all highly correlated (the mean motion was strongly correlated with both max motion and a number of movements). Therefore, we reported only mean FD and mean DVARS.

Every quality metric employing FD or DVARS is limited by the precision of the measure itself [228]. Since motion takes the form of regionally heterogeneous effects on functional connectivity estimates, better measurements of motion can yield better predictions of FC quality. For example, using slice-derived motion metrics rather than volume-derived estimates could be beneficial because they are only a simplification of movement over the acquisition of all slices [261]. Nevertheless, Satterthwaite *et al.* [57] and Yan *et al.* [59] found that motion correction with voxel-wise motion metrics offered insufficient advantages over the more easily computed general models.

Another possible improvement is using a shorter TR. The rapid subTR displacements were thought to play a significant role in regional motion artifact interactions [226]. Nevertheless, previous studies found that sub-TR FD traces are noisier and less useful in identifying outlying time points [227]. While it is true that the large movements are divided into several smaller movements, they get lost amidst the constant respiratory-related motion.

Recently, Power *et al.* [262] found out that there are multiple respiration-related effects present in realignment parameters, some of them manifesting as high-frequency fluctuations. Therefore, realignment parameters, typically considered as a direct indicator of head motion, may as well reflect other modulations such as respiratory motion effects on the magnetic field that have no association with actual head motion [260]. Although these effects are routinely filtered out from the gray matter signal, hence do not affect resulting FC values, they can negatively affect methods for motion correction (scrubbing, spike regression) or degrade the FC-motion relationship [254]. Indeed, we observed lower correlations of TFC with motion metrics in the HCP dataset with a sub-second sampling rate. Future studies could use dips in DVARS that still seem to reflect the true head

movements or FD values that are notch filtered and a 4-TR differential is calculated as recommended in [263] and [262].

Moreover, the respiration-related high-frequency fluctuations in motion in fast-TR fMRI datasets are also reported (in an aliased form) in standard single band TR datasets. Suggested low-pass filtering of motion metrics can increase their link with fMRI signal quality, especially in studies of older subjects or cohorts with increased body mass index [263]. Thanks to the shorter TRs of multiband data, it is now possible to identify respiration-related content and so the future studies could focus on its relationship with FC quality.

Unfortunately, we are not able to provide a single value that would separate bad and good FC matrices due to the complexity of all contributing factors, such as the lack of ground truth of FC. Therefore, the decision on which scanning session should be discarded is still based only on a summary motion statistic reaching some threshold (for example RMS movement over half a voxels width [258] or more than 20 volumes with RMS greater than 0.25 mm [62]). We only propose adding the TFC measure for group-level corrections. Other directions for mitigating the motion artifact include using multi-echo imaging [264] or using head molds [259].

A possible objection is that the typical connectivity matrix is not an appropriate golden standard. While a perfect estimate of clean FC without any effect of artifacts is not achievable, we assume that by averaging FC matrices of low-movement subjects, we obtain a useful estimate of typical awake human brain functional connectivity. Obtained results prove that the observed individual differences significantly reflect artifacts, in particular those resulting from head motion. Thus, using TFC is a useful measure identifying potentially problematic subjects. Moreover, we found that the group-average FC matrices from different groups were very similar (correlation of the typical matrix from the Main dataset with similarly preprocessed typical FC of the *Alternative* dataset is $r_P = 0.86, p < 10^{-16}$, resp. $r_P = 0.68, p < 10^{-16}$ between *Main* and HCP dataset). Therefore, we obtained similar results regardless of the applied typical FC matrix. Moreover, using the typical FC matrix from a different dataset has the advantage that no degrees of freedom are lost, i.e., subjects used for the computation of the typical FC matrix do not have to be discarded from subsequent analyses.

While deviation of individual functional connectivity from the typical FC might happen not only due to artifacts but also due to meaningful interindividual variability in "true neuronal" FC, in practice, the FC deviations from the typical FC arise due to a mix of artifacts/noise and the presence of specific individual FC patterns. Our rationale here is thus not that any deviation from typical FC is only and fully due to artifacts, but instead that the most significant deviations from the typical FC are likely to be substantially affected by artifacts.

5.5 Conclusion

In current resting-state fMRI studies, there is a need for a sufficiently sensitive measure of individual functional connectivity quality. In this paper, we presented a new method of functional connectivity quality evaluation for rs-fMRI data. The Typicality of Functional Connectivity captures deviation from the standard brain connectivity patterns. We found that this metric is significantly correlated with motion metrics across different datasets, parcellations, and preprocessing pipelines. Furthermore, we used it to demonstrate that there is a gradual decrease in the connectivity quality and the data quality in more detailed brain parcellations with ROIs composed of fewer voxels. This quality decrease is not related to head motion, but to other types of noise as the motion-quality relationship remained constant across parcellations. In conclusion, TFC allows extensive use in screening data quality, comparing high-movement groups or denoising strategies, and choosing optimal brain parcellation. Our findings should be considered when a robust estimate of connectivity is more important than fine brain parcellation.

Chapter 6

Large-scale networks dynamics during recognition memory using iEEG

Recognition memory is the ability to recognize previously encountered events, objects, or people. It is characterized by its robustness and rapidness. Even this relatively simple ability requires the coordinated activity of a surprisingly large number of brain regions. The current research focused on the analysis of a limited number of *a priori* defined regions. Consequently, the organization and dynamics of the large-scale networks underlying recognition memory remain unknown. We recorded intracranial EEG, which affords high temporal and spatial resolution, while epileptic subjects performed a visual recognition memory task. We analyzed dynamic functional and effective connectivity as well as network properties while recognition memory unfolded. Various networks were identified, each with its specific characteristics regarding information flow, dynamics, topology, and stability. The first network mainly involved the right visual ventral stream and bilateral frontal regions. It was characterized by early predominant feedforward activity, modular topology, and high stability. It was followed by the involvement of a second network, mainly in the left hemisphere, but notably also involving the right hippocampus, characterized by later feedback activity, integrated topology, and lower stability. The transition between networks was associated with a change in the network topology. Overall, these results confirm that several large-scale brain networks, each with specific properties and temporal manifestation, are involved even during simple tasks. Understanding how the

brain dynamically faces rapid changes in cognitive demand is vital to our comprehension of the neural basis of cognition.

The work presented in this chapter is currently in a revision process [265].

6.1 Introduction

Visual recognition memory has been studied since the 1960s [266] with a tremendous number of findings that have helped to reveal how massively accurate [267], fast [268], and long-lasting [269] it can be. The remarkable efficiency and robustness of this system imply that it has a strong ecological value. These studies have also pinpointed the medial temporal lobes as critical for this type of memory [270, 271]. In a broader sense, it has consistently been shown that visual recognition memory relies on the "what" system, i.e., the visual ventral stream, which involves many temporo-basal brain regions such as the lingual, fusiform, and parahippocampal gyri. The participation of the ventral stream is asymmetric in the sense that visual recognition memory relies more on the right than on the left hemisphere [272–275]. In addition, visual recognition memory also involves parietal and frontal lobe regions, probably for processes concerned with confidence and decision-making (for a review and a model, see [276]).

Even a relatively simple task, such as deciding whether an object has already been seen or not, thus requires the involvement of a surprisingly large number of brain regions. The temporal dynamics of recognition are now better understood as the first behavioral responses occur in approximately 360 ms [268], the first neural differences between targets and distractors are identified at approximately 200 ms [275, 277, 278] and many different brain regions are involved up to 600 ms or more. Even though the activity of participating brain regions appears to be partly sequential, it is mostly overlapping [279], and what specific interactions take place between regions is unknown.

Brain regions do not operate in isolation but are interconnected in large-scale networks [16, 280–282]. The basis of every network is connectivity, defined as either anatomical links (structural connectivity), statistical dependencies (functional connectivity), or causal interactions (effective connectivity) [79]. Substantial evidence supports the hypothesis that the architecture of brain networks is non-random and is optimized to support cognitive

abilities. Interesting properties underpin this efficient architecture, such as high modularity [83]. The modular architecture is characterized by small subsystems (communities), composed of different brain regions with a vast number of local connections and few distant connections. This hierarchically modular structure supports effective communication [192] as well as functional segregation and specialization [14].

Given the continually evolving environment, and depending on the system's demands, there are continuously changing patterns of interactions between brain regions [14, 175]. Therefore, both the topology of the networks and the interactions between them are highly dynamic [168, 173, 209, 210]. As a result, it has been suggested that dynamic network reconfiguration is a fundamental neurophysiological process [206, 208, 211]. Emerging findings suggest that networks are non-stationary [168], although robust characterization of this non-stationarity remains a methodological challenge [176, 283]. It is generally assumed that their reconfigurations are driven by higher-order cognitive control systems, involving mainly the frontal cortex [211, 284]. Moreover, dynamic reconfiguration is directly linked to cognitive performance during memory [200, 212–214].

Although it is clear that recognition memory requires the participation of different networks, little is known about their dynamical organization. This is due to the fact that current studies of large-scale network dynamics are based either on fMRI or EEG. Temporal networks based on fMRI are usually analyzed using multiple, possibly overlapping, very long temporal segments, typically 30-60 seconds long [168, 173]. In contrast, surface EEG studies suffer from low spatial resolution and might not capture the contributions of medial temporal brain structures.

Because visual recognition memory is so fast, the modifications of large-scale functional networks that support such ability need to be examined on a millisecond-by-millisecond timescale and with high spatial resolution. Therefore, we analyzed intracranial EEG, an approach that meets these needs. We calculated functional and effective connectivity, as well as underlying graph properties. Considering that the contribution to visual recognition memory of each hemisphere differs significantly, we assumed that it would be reflected in the connectivity patterns. We ran the first set of analyses based on this hypothesis. We then examined whole-brain network topology and investigated fluctuations in network properties, i.e., changes in integration and segregation as memory processes unfold [200, 208]. Ultimately, understanding how brains dynamically adapt to perform very fast tasks

is vital to our understanding of the neural basis of memory.

6.2 Material and Methods

6.2.1 Patients

Intracranial EEG (iEEG) was recorded for eighteen patients with drug-refractory epilepsy (8 women, age: 37.61 ± 11.37 years old). They were admitted to the Epilepsy Monitoring Unit at Toulouse University Hospital for the identification and possible subsequent resection of the epileptogenic zone. In each patient, 8 – 13 depth electrodes were stereotaxically implanted. The depth electrodes were 0.8 mm in diameter and contained 8 to 18 platinum/iridium contacts, each 2 mm long (Microdeep depth electrode, DIXI medical, France). Each implantation was individually tailored to the seizure onset zone, and the placement of each depth electrode was based exclusively on clinical criteria independently of this study.

The preoperative MRI and postoperative CT images were fused and normalized to the Montreal Neurological Institute (MNI) brain atlas for precise contact localization (for more information, see [279]).

Intracranial EEG activity was recorded using two synchronized 64-channel acquisition systems (SystemPlus Evolution, SD LTM 64 EXPRESS, Micromed, France) with a sampling frequency of 256 Hz for two patients and either 1,024 or 2,048 Hz for the others (high pass-filter: 0.15 Hz). None of the patients had a seizure within 6 hours before the recordings.

This study was approved by the local University Hospital Ethics Committee (CER No. 47–0913). Informed consent forms were signed for the implantation and the use of iEEG data for research purposes.

6.2.2 Visual recognition memory test

Each subject performed a visual recognition memory task, namely the Speed and Accuracy Boosting procedure (SAB)(Fig. 6.1), while the intracranial EEG was being recorded [268]. Each block began with an encoding phase during which 30 trial-specific stimuli (targets) were presented individually for at least 3 s (self-paced) in the center of a gray screen. The

stimuli were taken from an extensive database of high-quality cropped photos of everyday objects. Participants were explicitly instructed to remember all stimuli. A distracting phase followed during which the subjects watched a colored cartoon video with sound on for 3 minutes. Finally, the subjects underwent the recognition memory phase when the 30 targets and 30 distractors were shown. Subjects were required to respond to the targets only by raising their finger as quickly as possible from an infrared pad. A 600ms response time limit with audio feedback forced subjects to answer as quickly and accurately as possible. Responses were based on a go/no-go design. If a go response was given before the response time limit, positive audio feedback was played if the stimulus was a target (Hit). Negative feedback was played if it was a distractor (False alarm). If a no-go response was given, positive audio feedback was played if the stimulus was a distractor (Correct rejection). Negative feedback was played if the stimulus was a target (Miss). Since subjects performed well in the task, we analyzed only the Hits and Correct rejections (CR) in this study as they represented most of the recorded trials. The SAB test is demanding and requires one or two training sessions, which were not included in subsequent analyses. Patients participated in 7–10 SAB blocks depending on their willingness.

We evaluated each subject's performance using two discrimination indices, i.e., d-prime and minimal reaction time (minRT). The minRT is defined as the minimal processing time required to recognize targets, and it was computed by determining the latency at which correct go responses (Hits) started to significantly outnumber incorrect go responses (false alarms) [268]. As in previous studies [279], we used 20ms time bins and a Fisher's exact test ($p < 0.05$), followed by at least two significant consecutive bins to compute the minRT. For more information about performance, recordings, and SAB test, we refer the reader to Despouy *et al.* [279].

6.2.3 Recordings

We used a bipolar montage between adjacent contacts to remove artifact contaminations, identify local activations, and provide a reference-free representation of the phenomena under observation [285]. A single bipolar montage (i.e., TB 1-2) is referred to as a "channel" throughout this study. Preliminary visual inspection of the iEEG recording and manual artifact rejection procedures excluded an average of 14 % of all trials (range:

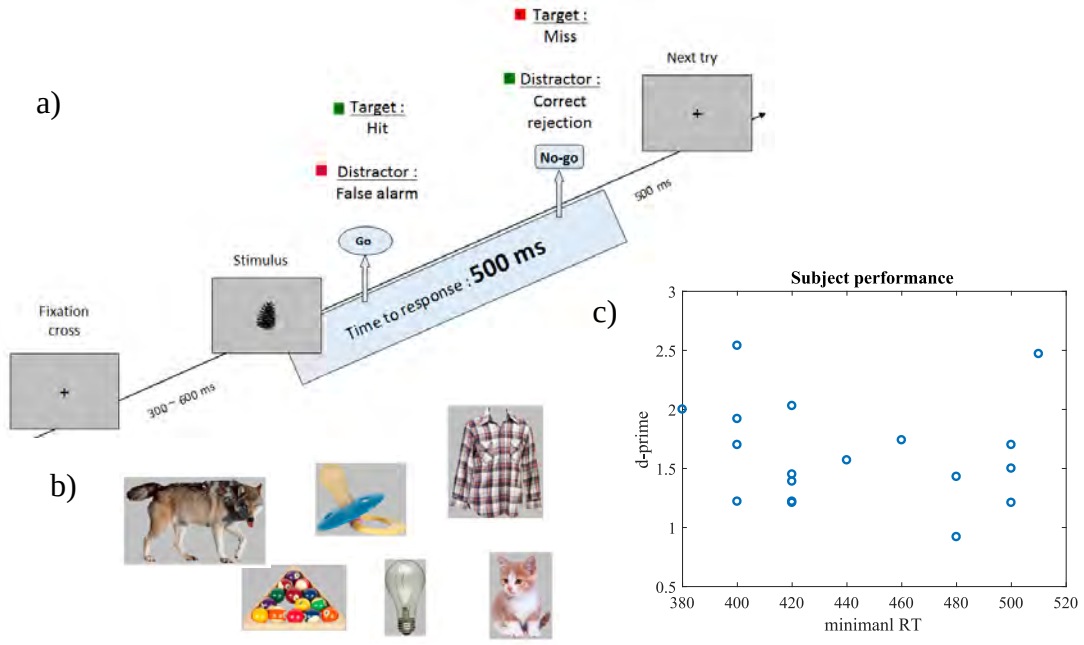

Figure 6.1: SAB test and performance a) Illustration of the SAB procedure with a response deadline at 600 ms. b) Example of stimuli used during the encoding phase. c) The performance of each participant is characterized by d-prime and minimal reaction time.

8–22 %) with interictal activity across participants. This procedure decreased the risk of including trials modified by epileptic activity.

6.2.4 Channels and trials selection

Magnitudes of subsequent causality estimates depend on the number of channels and trials. Therefore, we had to ensure an equal number of trials and channels for each patient. We only included channels that do not share a common contact to avoid spurious increases in connectivity. There was a maximum of 30 channels that obeyed this rule for one patient. Reducing the channel numbers to 30 in all other patients required a further selection process. We manually selected channels localized in grey matter (based on MRI images) and visually recognizable neural responses to the stimuli. Furthermore, we included only the first 64 trials of Hits and CR for each patient (minimal number of successful trials for the worst-performing subject). Therefore, with an *a priori* selection, we analyzed 18 subjects with 30 channels per subject, i.e., a total of 540 channels (Fig. 6.2a), 308 of which were in the left hemisphere and 232 in the right hemisphere.

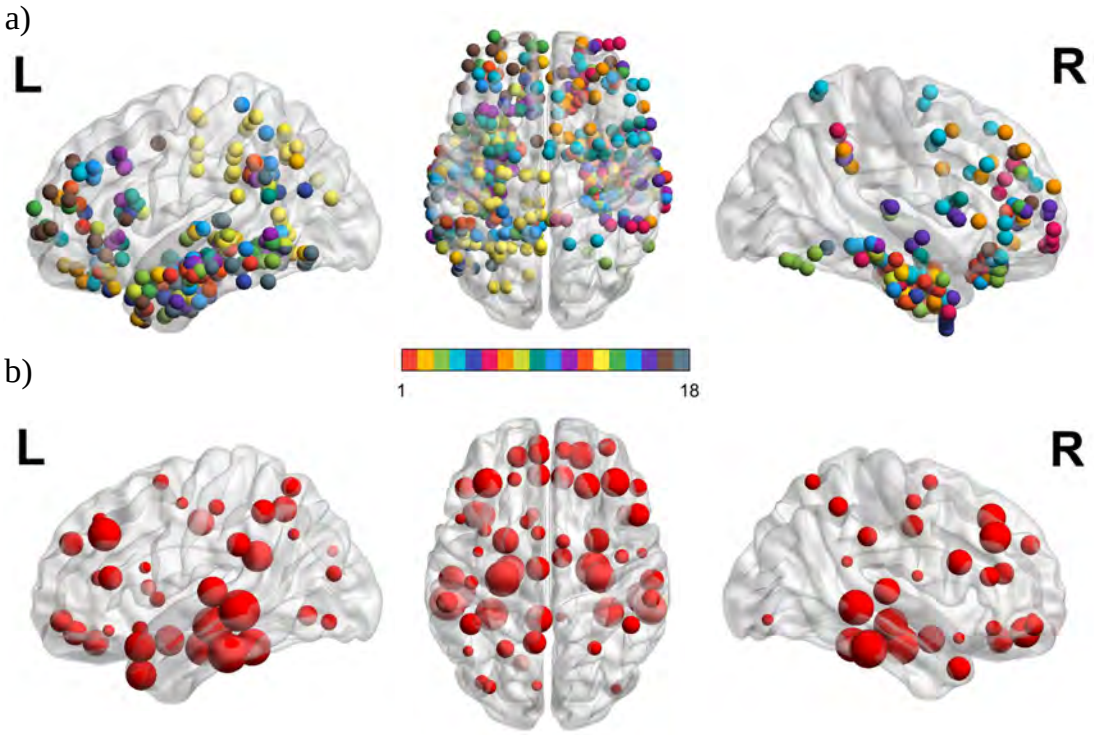

Figure 6.2: iEEG recordings. a) Overview of all recording locations across subjects. We recorded the brain activity of 18 epileptic subjects using multiple intracranial depth electrodes that targeted different brain regions. For each subject, we analyzed 30 bipolar channels, resulting in a total of 540 channels. The different colors corresponded to different subjects. b) We mapped these channels to the AAL atlas based on their MNI coordinates, covering 68 out of 90 possible regions with different channel densities. The size of each sphere corresponds to the sampling density of the region.

6.2.5 iEEG preprocessing

iEEG preprocessing consisted of downsampling each channel to 256 Hz (original sampling frequency for two subjects) and subtracting the ensemble mean across trials to ensure stationarity [126]. We analyzed the 200 ms pre-stimulus baseline and 800 ms after the stimulus onset. To perform sliding-window connectivity analyses, we segmented each trial into windows of 64 samples (250 ms). We used a shift of 4 samples between two consecutive windows (similar results were obtained with a window of 32 samples). Each sliding-window was multiplied by a Hanning window to suppress spurious connectivity and reduce sensitivity to outliers [165]. All data were processed with MATLAB [286]

6.2.6 Connectivity analyses

We investigated functional (FC) and effective (EC) connectivity in sliding windows. We estimated dynamic FC and EC for each of the 18 subjects. To compare global levels of connectivity, we calculated the mean connectivity for each subject. Conversely, we pooled all connectivity estimates across subjects to analyze lateralization or directionality because the implantation varied significantly.

Functional connectivity

We estimated FC between two channels as the mean Pearson's correlation coefficient across all trials (Fig. 6.3a).

Effective connectivity

We used dynamic multivariate Granger causality (MVGC) to estimate the EC between channels. It implements a statistical, predictive notion of causality whereby causes precede and help to predict their effects. Classical Granger causality from Y to X (the degree to which the past of Y helps predict X, over and above the degree to which X is predicted by its past) can be formally written as the log-likelihood ratio:

$$\begin{aligned} F_{Y\to X} &= ln\frac{\Sigma_1}{\Sigma_2} \\ \Sigma_1 &= var(\epsilon_{1t}), \Sigma_2 = var(\epsilon_{2t}) \\ X_{1,t} &= \sum_{j=1}^{M} = a_{1j}X_{t-j} + \epsilon_{1t} \\ X_{2,t} &= \sum_{j=1}^{M} = a_{2j}X_{t-j} + b_{2j}Y_{t-j} + \epsilon_{2t} \end{aligned} \tag{6.1}$$

where X and Y represent recorded time series from two channels, a and b are parameters of the autoregressive process, ϵ represents residuals, and M is the model order (we used a constant order of 10, but similar results were observed using orders of 5 or 15).

We used the freely available toolbox from [126] to calculate MVGC in overlapping sliding windows between all channels, separately for each patient. With the multivariate extension, it is possible to control for common causal influences [127]. Because our

testing paradigm was time-constrained, and we used very short time windows, estimating the multivariate autoregressive (MVAR) model parameters might have been difficult. Nevertheless, we overcame this difficulty through the "vertical regression" implemented in the toolbox to address short time windows when multiple trials were available. This method is based on the assumption that each trial is an independent realization of the same underlying stochastic generative process. Therefore, we ended up with only one estimated MVAR model for all trials (Fig. 6.3b).

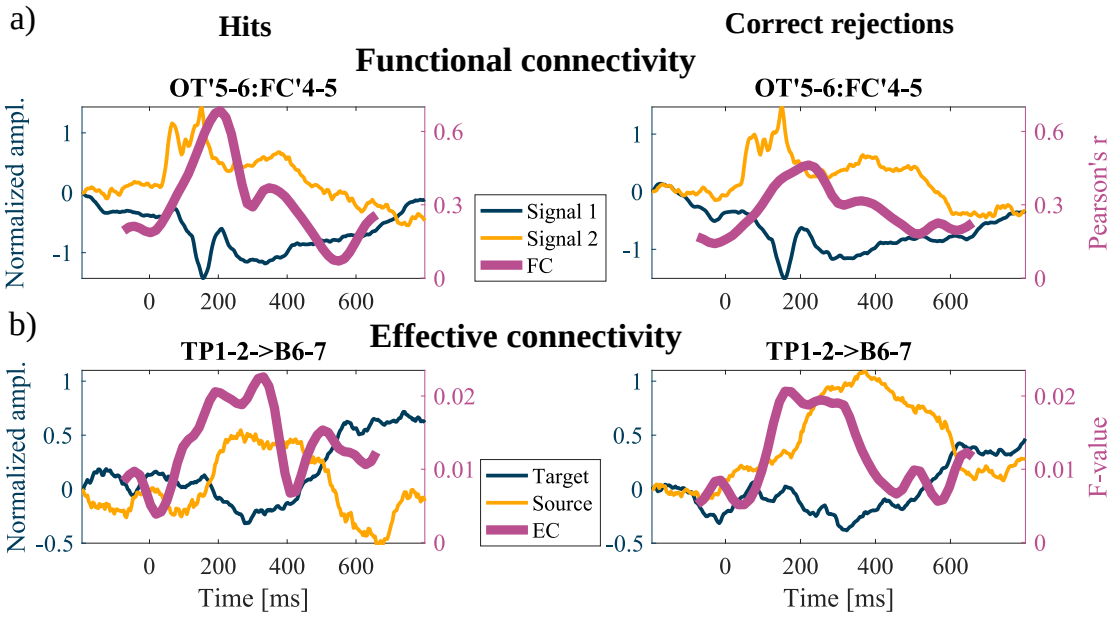

Figure 6.3: Connectivity examples. a) Examples of dynamic correlation (i.e., functional connectivity) for a given channel pair (OT'5-6 and FC'4-5) for both Hits and Correct rejections. Note that a correlation is an undirected measure. b) Examples of dynamic Granger causality (i.e., effective connectivity) for a given channel pair (TP1-2 and B6-7) for both Hits and Correct rejections. According to the definition of Granger causality, the source influences the target.

We used the definition given by [287] of feedforward direction as the causal influence of posterior channels onto the more anterior channel. If their y coordinates were identical, feedforward was defined as the causal influence of the lower onto the higher channel based on the z coordinates (this occurred in 3 % of the cases).

Statistical testing

It is important to stress that in this study, we were limited by several factors such as the low number of subjects, short time windows, and tailored implantations, all of which are

inherent to iEEG recordings. Moreover, the connectivity estimates followed a non-normal distribution. Therefore, for statistical testing, we used bootstrapping as a resampling technique, whereby random sampling with replacement from the distribution of interest is used to estimate the sampling distribution of almost any statistic [178]. To be more specific, we used the bias-corrected implantation that corrects bias and skewness in the distribution of bootstrap estimates. For a detailed description, see [288].

We calculated confidence intervals of dynamic connectivity (e.g., Fig. 6.4b,c) by creating a bias-corrected bootstrap distribution of mean connectivity values at each time-point. We used the hybrid method where a 90% confidence interval from 10,000 repetitions is plotted around a mean value of the original distribution.

We tested whether there was a difference in mean value between Hits and CR across subjects using a two-tailed paired sample bootstrap test with 10,000 repetitions (Fig. 6.4a, 6.5a). If the test is performed across time (Fig. 6.4b,6.5b), the resulting p-values were corrected for multiple comparisons in the time domain with the FDR algorithm.

The original bootstrap method is designed for independent, identically distributed data. A standard bootstrap is not appropriate when data samples are dependent (such as time series). Therefore, we used a stationary bootstrap - a block technique that attempts to preserve the underlying autocorrelation [289]. This technique is based on a circular wrap of data (end-to-start wrap around the data around a circle) and a random window length that removes the edge effect of uneven weighting at the beginning and the end [290]. To test whether there was a significant difference in mean feedforward connectivity between the left and right hemispheres (Fig. 6.6b), we compared the two corresponding stationary bootstrap distributions and calculated a p-value, as mentioned above.

Finally, to test whether there was a significant increase in a time course (Fig. 6.4c, 6.6c), we created a bias-corrected bootstrap distribution of mean connectivity in each time window by randomly sampling subjects with repetitions 10,000 times. Then, we compared each bootstrap distribution to the baseline bootstrap distribution (from a time window centered at -75 ms) to obtain the resulting p-values.

6.2.7 Graph analyses

Two key concepts in graph theory are nodes and edges. In our analyses, nodes represent brain regions. We used the AAL atlas [246] that parcellates the brain into 90 regions

(including subcortical regions) to obtain identical parcellation for each subject. Each recording channel was assigned an area in the atlas based on its MNI coordinates using the SPM12 software package (Wellcome Department of Cognitive Neurology, London, UK) and the Anatomy toolbox [291]. Channels that did not belong to any region were not used in the mapping. Regions with no recorded signal were discarded, which resulted in the coverage of 68 out of the 90 AAL atlas regions (Fig. 6.2b). Note that in the AAL atlas, the perirhinal, parahippocampal, and entorhinal cortices are collectively referred to as the parahippocampal region.

The second constituent component of a graph are the edges. We defined an edge between two regions as the mean MVGC of all corresponding channels. Since every graph can be represented as an adjacency matrix, and since we used a sliding window technique, our dynamic brain networks formed a set of adjacency matrices. Each adjacency matrix was based on data from all patients and represented an incomplete weighted directed graph. Traditionally, these matrices are thresholded and binarized to reduce measurement noise [184], but arbitrary thresholding often leads to a loss of information [186], and network measures are unstable across different thresholds [187]. Consequently, we opted to work with weighted directed graphs.

Two important concepts of network organization that might explain human cognitive abilities are segregation and integration. They provide essential insight into information processing and transmission. Segregation is the extent to which communication occurs primarily within tight-knit communities of regions. On the other hand, integration is the extent of communication between distinct regions. It is the ability of the network to integrate distributed information [14, 203]. Both segregation and integration can be modeled with various measures [182]. We analyzed our dynamic memory networks in terms of efficiency and modularity [148]. All analyses were performed using The Brain Connectivity Toolbox designed for MATLAB [189].

Modularity

Modularity quantifies the degree to which the network may be subdivided into densely interconnected communities that maximize the number of within-group edges and minimize the number of between-group edges [190]. We applied the iterative Louvain algorithm to the adjacency matrix with a resolution parameter of $\gamma = 1$ and random initial conditions

for each time window of dynamic connectivity. A maximum of the modularity function across 10,000 runs was the resulting modularity with its accompanying network partition [191].

As we dynamically assign modularity index to each node, we define the instability index. It is the relative number of node allegiance changes over the whole time course.

Efficiency

Global efficiency is defined as the average inverse shortest path between any two nodes [292]. Considering that it is linearly dependent on connectivity strength between nodes, we normalized it by dividing it by the mean connectivity across all non-zero edges.

Null model

The use and choice of a null model are crucial in graph analyses [176, 177]. To create a stationary system with an identical covariance structure, we used an amplitude-adjusted multivariate extension of Fourier surrogates (MVFS) that matched the amplitude spectrum and amplitude distributions (see [293]). We compared the magnitudes to the null models, i.e., we divided the obtained metric by a mean metric obtained in 1,000 surrogate networks [294] and analyzed their dynamics. It is of note that Fourier surrogates could not be used to test the significance of global causality. Moreover, we could not use the Erdos-Renyi null model due to incomplete brain coverage and the non-existence of certain links.

6.3 Results

Firstly, we compared global FC, approximated by Pearson's correlation, for Hits and Correct rejections across all subjects and the entire brain. We observed a higher level of correlation for Hits across time (Fig. 6.4a, bootstrap $p < 10^{-16}$). Unwrapping this analysis in terms of time showed that although the patterns were quite similar (Pearson's $r = 0.98$, $p < 10^{-16}$), there were significant differences between the two conditions starting at approximately 290 ms (bootstrap $p < 0.05$, FDR-corrected) (Fig. 6.4b). Because visual recognition memory relies more on the right than on the left hemisphere, we performed the same FC analyses focusing on each hemisphere. The patterns of left and right

hemisphere FC were almost identical (Pearson's $r = 0.98$, $p < 10^{-16}$). The significant increase (bootstrap $p < 0.05$, FDR-corrected) in FC occurred slightly earlier in the right hemisphere (150 ms) than in the left (170 ms) (Fig. 6.4c).

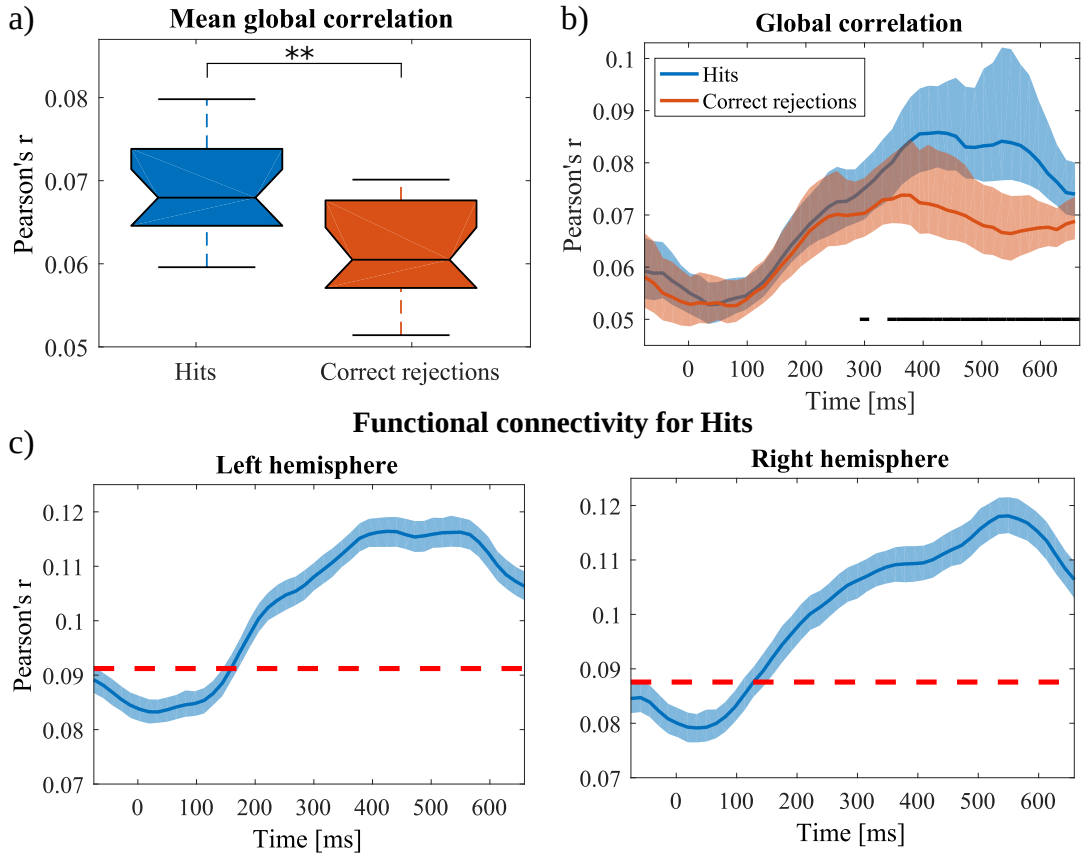

Figure 6.4: Connectivity analyses. a) We observed a higher level of global correlation for Hits than Correct rejections ($p < 10^{-16}$). b) Resolved in time, there is a significant difference in correlation between the two conditions starting from 290 ms. The 90% bootstrap confidence interval is plotted in shaded colors. The black horizontal lines indicate significant time intervals. c) If we focus on the FC within each hemisphere, very similar temporal patterns can be observed (Pearson's $r = 0.98$, $p < 10^{-16}$). Compared to the baseline, we see a significant increase in both right hemisphere (starting from 150 ms) and left hemisphere correlations (starting from 170 ms). The red dotted lines represent the threshold for a significant change from the baseline.

Since directionality cannot be tested by correlations, we further analyzed effective connectivity by Granger causality. We calculated MVGC using vertical regression in short sliding windows, thereby providing a dynamic estimate of causality strength. Averaged in time, MVGC for Hits and Correct rejections across subjects and the entire brain were not significantly different (bootstrap $p = 0.28$) (Fig. 6.5a). Although, the conditions showed different dynamics (Pearson's $r = 0.22$, $p = 0.13$) no significant difference was noted in

terms of time (bootstrap $p > 0.05$, FDR-corrected) (Fig. 6.5b).

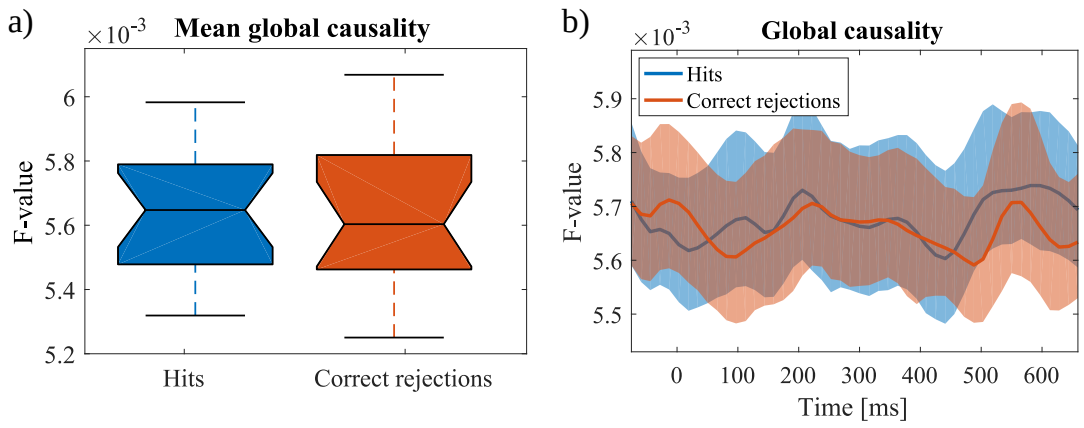

Figure 6.5: Causality analyses. a) Unlike for correlation, the mean global causality for Hits was not statistically higher than for Correct rejection ($p = 0.28$). b) Moreover, the time courses of mean causalities were not significantly correlated (Pearson's $r = 0.22$, $p = 0.13$), and there were no statistical differences in time ($p > 0.05$, FDR-corrected).

Following these preliminary analyses, we analyzed dynamic causality in more detail by focusing on feedforward and feedback directionality within each hemisphere. We calculated partial Pearson's correlations (controlling for global causality) between the time courses of these conditions. We found significant similarities between feedforward and right hemisphere causality time courses ($r = 0.61$, $p < 10^{-5}$) (Fig. 6.6a). On the other hand, the feedback causality time course was closely connected with the left hemisphere ($r = 0.70$, $p < 10^{-7}$) and across both hemispheres time course ($r = 0.48$, $p < 10^{-3}$). It is importance to note that such significant correlations were not found for Correct rejection, neither were they randomly obtainable. This was confirmed by shuffling the labels of the links.

Further analyses of Hits showed that the causality of feedforward connections was higher than that of feedback connections in the right hemisphere (bootstrap $p = 0.005$), while the reverse was true in the left hemisphere (bootstrap $p = 0.001$) (Fig. 6.6b). Furthermore, the significant increase in the right hemispheric feedforward causality occurred much earlier (170 ms, bootstrap $p < 0.05$) than the left hemisphere feedback causality (270 ms, bootstrap $p < 0.05$) (Fig. 6.6c).

To further improve our understanding of the networks supporting visual recognition

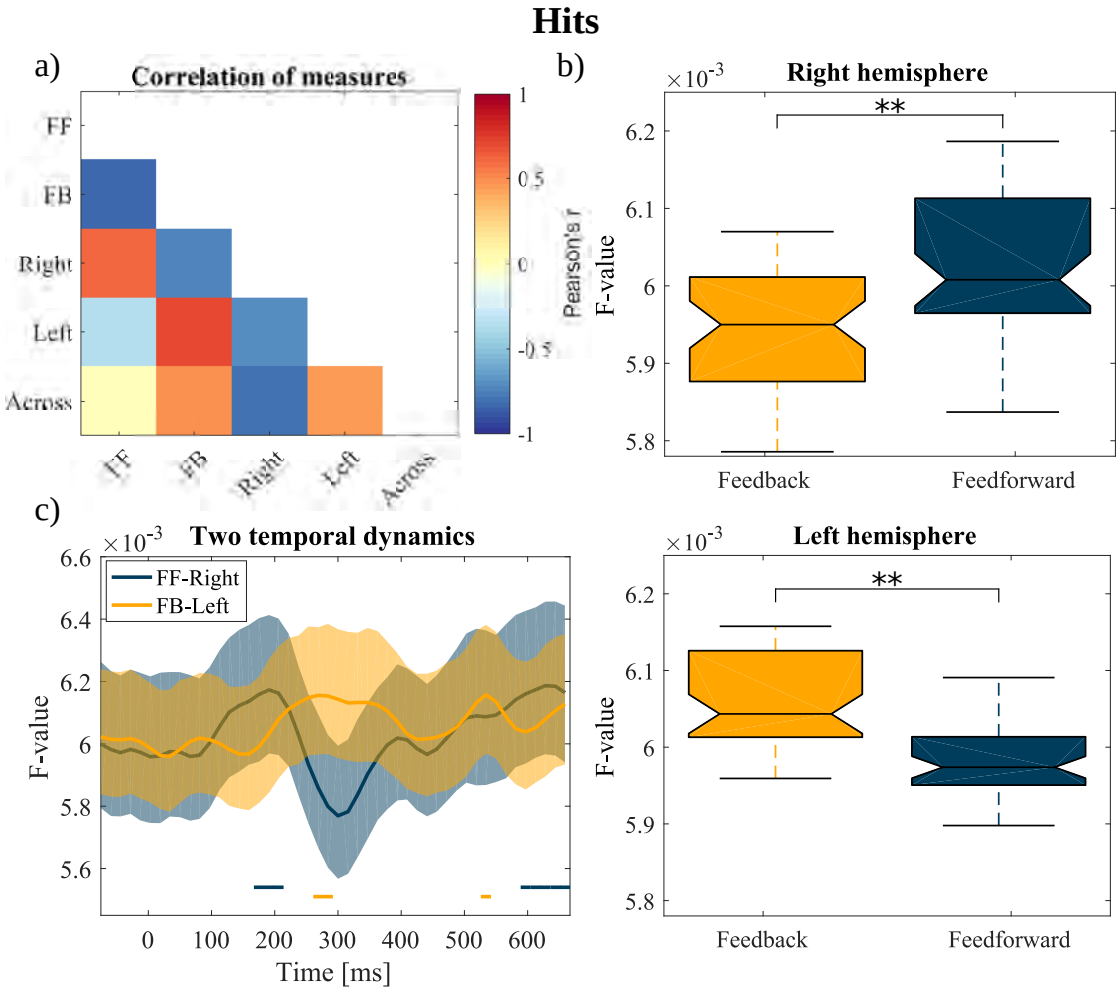

Figure 6.6: Effective connectivity analyses for Hits. a) We investigated the temporal evolution of causality based on directionality and lateralization. We found striking similarities for some of the patterns: right hemisphere and feedforward causality were highly correlated, as well as left hemisphere (or across-hemisphere) and feedback causality. These two modes were highly anti-correlated. Non-significant correlations (FDR-corrected) were set at 0. b) When time is averaged, we observe more feedforward causality in the right hemisphere ($p = 0.005$) and more feedback causality in the left hemisphere ($p = 0.001$). c) The right feedforward causality significantly increased as of approximately 170 ms and then decreased at 300 ms. This decrease was associated with a significant increase in left feedback causality. The 90% bootstrap confidence interval is plotted in shaded colors. Horizontal lines indicate periods of significant increase.

memory, we switched to data-driven analyses (i.e., whole-brain rather than by hemisphere). Therefore, we focused on two metrics that describe network topology: modularity (a measure of segregation) and efficiency (a measure of integration). Network topology changed over time (Fig. 6.7a). We observed a highly segregated (modular) topology from

110 ms after stimulus onset. It then transitioned into a more integrated (efficient) topology at approximately 220 ms. Moreover, the significant increase in modularity (MVFS $p < 0.05$, FDR-corrected) occurred just before the increase in right hemisphere feedforward causality (Fig. 6.7b). Similarly, the increase in efficiency occurred just before the increase in left hemisphere feedback causality (Fig. 6.7c). These results suggest that changes in network topology could precede (and maybe drive) changes in information flow. We observed similar modularity and efficiency patterns even with a different brain parcellation, namely the Harvard-Oxford atlas (Pearson's r between dynamic modularity from AAL and Harvard-Oxford atlas $r = 0.51$, $p < 10^{-3}$, resp. efficiency $r = 0.47$, $p < 10^{-3}$).

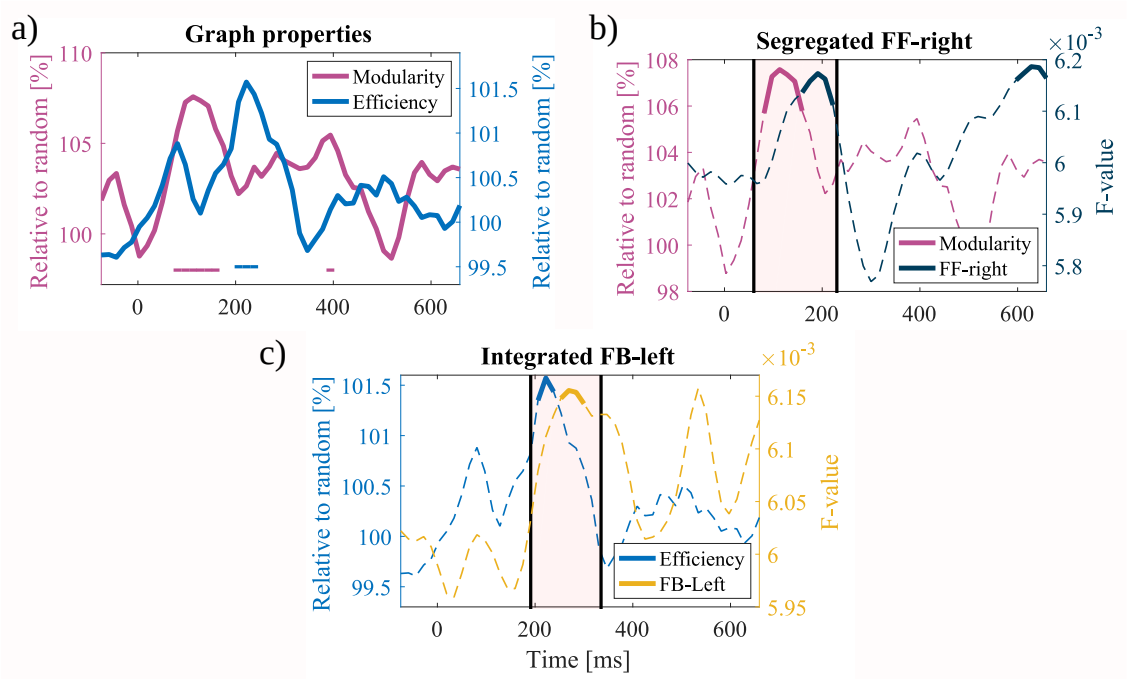

Figure 6.7: Changes in the network topology across time. a) At approximately 110 ms, the network shows a more modular topology. This segregated state is followed by a more integrated structure characterized by higher efficiency at 220 ms. Horizontal lines represent periods of significant increase/decrease. b) After the first peak of modularity at 110 ms, a significant increase in right hemisphere feedforward causality at approximately 150 ms can be observed. c) In addition, the first peak of efficiency at 220 ms precedes a significant increase in left hemisphere feedback causality at 250 ms. Solid lines indicate significant values. The rectangles highlight the time intervals of interest.

In addition, we used the Louvain algorithm to detect community structures in networks. We consistently identified three main communities at each time window, i.e., three highly interconnected sub-graphs (Fig. 6.8a). Based on the most frequent allegiance of

each node, the first community comprised regions of the right temporal lobe as well as many frontal regions bilaterally. The second community comprised regions in the left hemisphere, mostly from the temporal lobe and other parietal and frontal lobes. Interestingly, both the left and the right hippocampi were more linked to this second community. The third community comprised the left parahippocampal and inferior frontal gyri as well as the left amygdala.

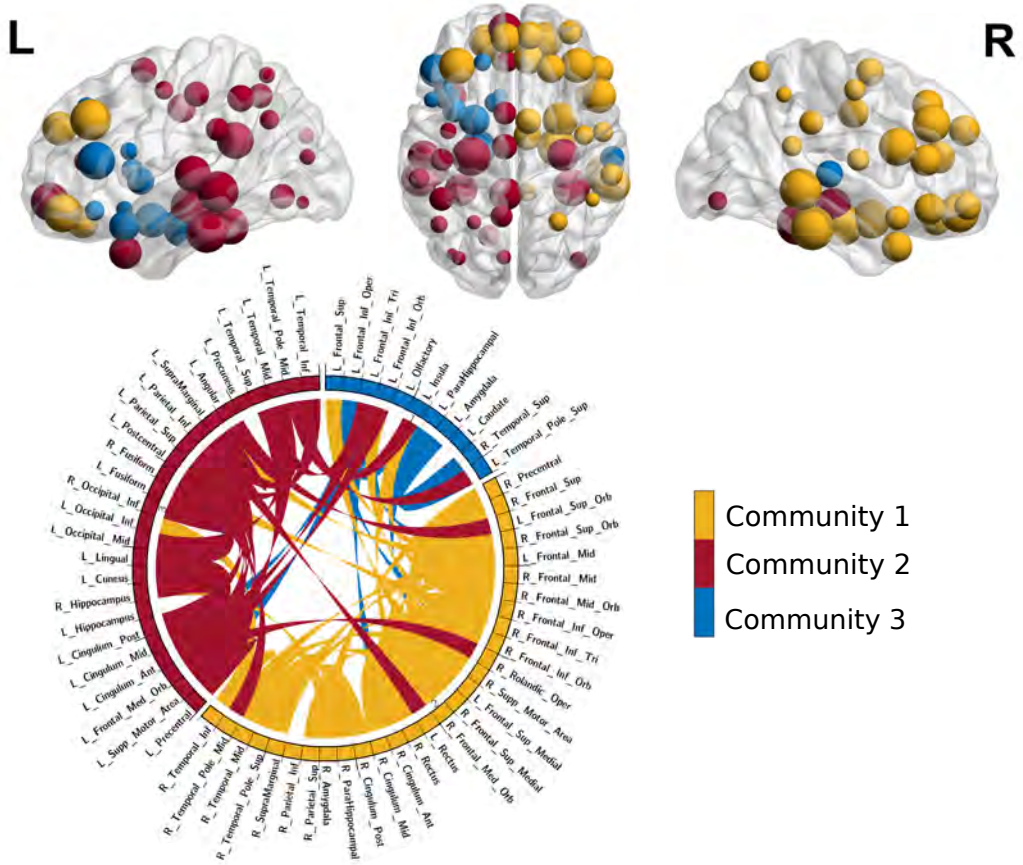

Figure 6.8: Network communities. The Louvain algorithm for community detection consistently identified three main communities. The first community comprises regions of the right visual stream and medial temporal lobe structures as well as frontal regions in both hemispheres. The second community comprises regions in the left MTL and the right hippocampus. The third community comprises the left parahippocampal gyrus, left amygdala, and left inferior frontal gyrus. The size of the spheres in the brain graph corresponds to the nodal strength. For representation purposes, the circular form [295] shows only the 3 % consisting of the strongest links.

Some nodes changed their allegiance throughout the time course, but the core of each community remained stable. The communities differed in their stability (one-way ANOVA, $p < 10^{-3}$), with the first community being the most stable, i.e., having the

lowest instability index (Fig. 6.9a). Therefore, if a node changed allegiance, it was mostly between the second and third community.

The first community showed the earliest increase in causality compared to baseline, at a similar timing as the increase of feedforward causality in the right hemisphere (Fig. 6.9b). Furthermore, the first community feedforward causality correlated significantly with that of the right hemisphere identified in the first set of analyses ($r = 0.76$, $p < 10^{-9}$). Likewise, the causality increase in the second community occurred later, in approximately 230 ms (Fig. 6.9b). The feedback causality correlated significantly with the feedback causality in the left hemisphere ($r = 0.41$, $p = 0.004$). The causality of the third community remained comparable to the baseline. Moreover, in the analysis of the directionality of influence, defined as the ratio between feedforward and feedback causality, the communities differed significantly (one-way ANOVA, $p < 10^{-16}$). The first community exhibited a significant prevalence of feedforward interactions (bootstrap $p < 0.05$, FDR-corrected), while the second showed a prevalence of feedback interactions (Fig. 6.9c).

All in all, the two functional systems identified on the basis of a hypothesis regarding the hemispheric lateralization of visual recognition memory are also identifiable with a data-driven community analysis. However, the community analysis offered a more detailed delineation of participating structures than a simple dichotomy between the right and left hemispheres.

Finally, we associated the observed connectivity patterns with the subjects' performances. We assumed that a higher performance level was associated with neural activity that resembles typical activity. Moreover, we expected the feedforward causality to drive fast response, unlike the feedback. Therefore, we calculated a one-sided Pearson correlation between the typicality of neural response (correlation between subjects' causality time course and the template of right feedforward and left feedback causality - from Fig. 6.6c) and the minimal reaction time and d-prime (Tab. 6.1). The descriptive analysis showed that the right hemisphere feedforward causality were negatively correlated with minimal reaction times (the more typical the neural response, the faster the minimal reaction times; $r = -0.32$, $p = 0.13$) while the left hemisphere feedback causality showed a positive correlation ($r = 0.59$, $p = 0.006$). In terms of d-prime, we tested for positive correlation and did not find consistent results across measures. We obtained identical p-values using permutation testing with 10,000 repetitions.

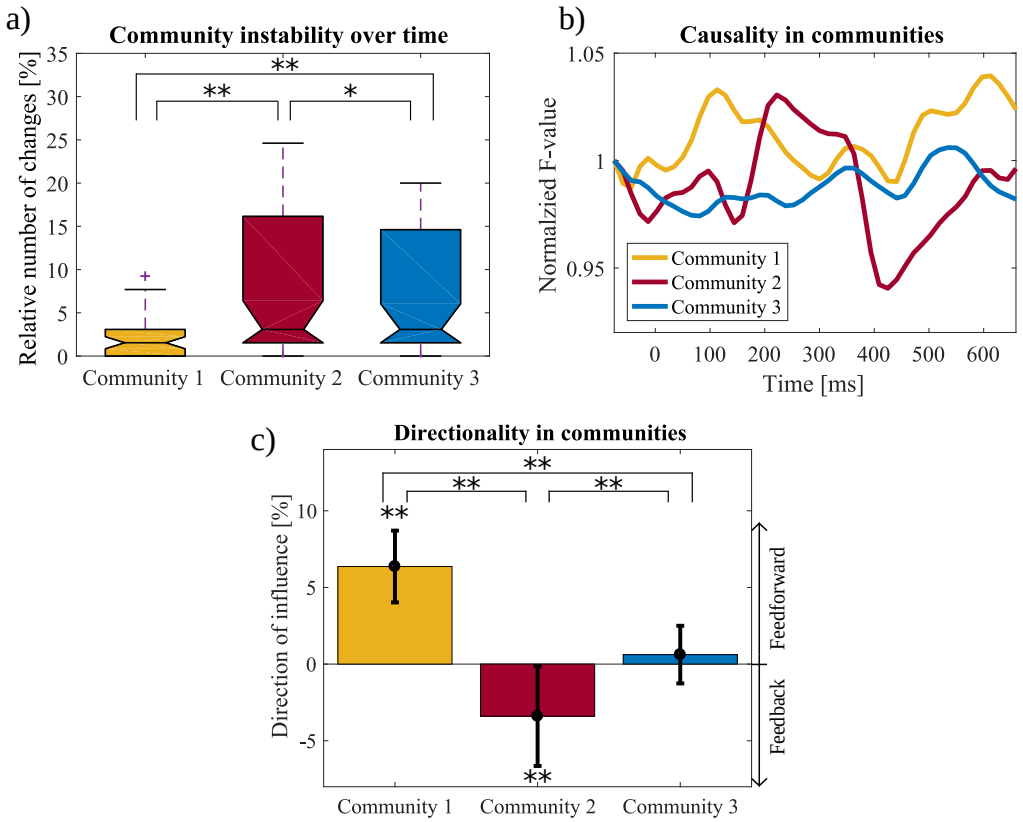

Figure 6.9: Community analyses. a) Even though the core of each community remained stable across the time course, some nodes changed allegiance. The first network shows the highest stability, i.e., the lowest instability. b) The first community showed the earliest increase in causality (110 ms). The second community followed at approximately 220 ms. c) Temporal average ± standard deviation of the direction of influence is significantly different between communities. Moreover, the first community exhibits a significant prevalence of feedforward causality. Conversely, the second community displays a significant prevalence of feedback causality ($p < 0.05$, ** $p < 0.001$, FDR-corrected).*

	Minimal Reaction Time **Pearson's r** (p-value)	**d-prime** **Pearson's r** (p-value)
FF-Right typicality	-0.32 (0.13)	0.15 (0.16)
FB-Left typicality	0.59 (0.006)	0.06 (0.43)

Table 6.1: The relation between connectivity and performance. We correlated the typicality of the subjects' right feedforward and left feedback connectivity with their performance on recognition memory tasks as assessed by minimal reaction time (an index of the speed to perform the task) and d-prime (an index of task performance). Left hemisphere feedback causality showed significant positive correlations with minRT. We obtained identical p-values using permutation testing with 10,000 repetitions.

6.4 Discussion

A typical characteristic of visual recognition memory is its rapidness. Subjects in this study were able to respond correctly in less than 600 ms, with the fastest correct responses being approximately 370 ms, consistent with previous results [268]. Although the perirhinal cortex and hippocampus have been identified as the core brain regions that support recognition memory, studies have consistently reported many other brain regions, mainly in the temporal lobe, but also in the frontal and parietal lobes [279, 296–298]. Nevertheless, little is known about the relationships between these brain regions and how they evolve over time. The amount of functional networks that are activated during recognition memory is also unknown. Therefore, there is a need to understand the large-scale functional brain networks' dynamical organization that underlie recognition memory on a millisecond-by-millisecond scale [80, 181].

Because this endeavor requires a high spatial and temporal resolution, we analyzed functional and effective connectivity of intracranial EEG in short sliding time windows to track connectivity changes and information flow during a visual recognition memory task. We identified large-scale brain networks involved in successful recognition. The first network mainly involved the right visual ventral stream and the bilateral frontal regions. It was characterized by predominant feedforward activity, starting rapidly in approximately 110 ms post-stimulus and peaking at 190 ms, modular topology, and high stability. It was followed by the involvement of a second network, predominantly in the left hemisphere, but notably also involving the right hippocampus, characterized by predominant feedback activity, which peaked at 270 ms, integrated topology, and lower stability. It is important to note that the patterns of right hemisphere-feedforward and left hemisphere-feedback connectivity were found only for Hits but not for Correct rejections. Interestingly, the peaks in modularity and efficiency (the transitions from less segregated to more segregated and from less integrated to more integrated topology) preceded the peaks in right-feedforward and left-feedback connectivity, which suggests a link between changes in network topology and modes of information processing. Overall, these results confirm that several large-scale brain networks, each with specific properties and dynamics, rapidly unfold (i.e., in less than 300 milliseconds) during recognition memory. These networks involve many brain regions bilaterally, even for such a basic cognitive capacity.

6.4.1 Different networks unfold rapidly in time

We performed two types of analyses to identify the networks that support recognition memory. The first one was driven by the hypothesis that there would be a high level of asymmetry between both hemispheres. The second was data-driven (it involved all recorded brain regions with no *a priori* selection of brain regions or hemispheres) and was based on the identification of brain region communities (by maximizing the number of within-group edges and minimizing the number of between-group edges [190]). Both analyses were carried out dynamically over the entire time period. It is important to note that both were convergent, demonstrating robust findings, although the data-driven analysis provided complementary information.

The hemispheric analyses revealed a robust functional difference between the right and left hemisphere. The right was mainly characterized by a feedforward information flow, while the left mainly by the feedback information flow. The difference between the amount of feedforward and feedback connections was significant within each hemisphere (Fig. 6.6b). Interestingly, the dynamics of the two hemispheres were different since the peak of the feedforward information flow in the right hemisphere occurred in approximately 170 ms. In contrast, the peak of the feedback information flow in the left hemisphere occurred later, in approximately 270 ms, at a moment when the feedforward information flow in the right hemisphere sharply decreased (Fig. 6.6c).

The data-driven analysis identified three networks. The first encompassed many brain regions in the right temporal lobe and the bilateral frontal lobes. Interestingly, this network showed a very rapid increase (between 100 and 200 ms) in effective connectivity. It was characterized by effective predominant feedforward connectivity, consistent with the facts already known about the rapidity and flow of information from the visual ventral stream [299, 300]. The second encompassed brain regions in the left temporal lobes, as well as the parietal and frontal lobes. It is highly important to note that it encompassed both the left and the right hippocampi. The effective connectivity of this second network peaked later than the first, albeit rapidly after stimulus onset between 200 and 300 ms. It was characterized by effective predominant feedback connectivity. A third network comprised regions in the posterior frontal and anterior temporal lobes. Unlike the two previous networks, it did not have a clear information flow direction. The first network was characterized by high community stability (few nodes changed allegiance over the

periods). The second and third communities were less stable, with nodes interchanging allegiance throughout the period. Follow-up analyses showed that the first connectivity network pattern was very similar to the feedforward connectivity pattern observed in the right hemisphere. Likewise, the second network connectivity pattern was very similar to the feedback connectivity pattern observed in the left hemisphere. Overall, these analyses provide the picture of three functional networks that underlie visual recognition memory, each with specific topography, temporal dynamics, preferred direction of information flow, and stability. In other words, within 300 ms, the brain undergoes a massive dynamic functional reorganization phase that involves several networks.

6.4.2 A large-scale network account of recognition memory

The first functional network was partly expected since previous iEEG studies had already demonstrated a high early involvement of the right visual ventral pathway in visual recognition memory [275, 279]. Furthermore, it has already been established that frontal lobe regions are involved in recognition memory [279, 301, 302], as early as 110 ms after stimulus presentation [275, 303]. Identifying a second network was more unexpected, particularly a network that tended to be more left-sided and prominently characterized by feedback connectivity.

Although further studies will be required to clarify each network's role, they highly correspond with current knowledge of the neurocognitive architecture that underlies recognition memory. Familiarity and recollection are the two processes that underlie successful recognition memory [270]. Familiarity is a fast process that relies mainly on the perirhinal cortex as the core brain region, along with the ventral visual pathway. It does not include the hippocampus [271]. Therefore, the first network could be mainly involved in familiarity. In contrast, recollection is assumed to be a slower process that relies on the hippocampus as the core brain region and the extended hippocampal system in general, which involves relays in the mammillary bodies, anterior thalamus, cingulate cortex, and parietal lobes [304]. Therefore, the second network could be more involved in recollection, as suggested by the fact that it was delayed compared to the first network, but also by the fact that both right and hippocampi belonged to this network.

While familiarity depends mainly on processing the world surrounding the subject (i.e., bottom-up processes), recollection requires interactions with the internal world (i.e.,

memory) to retrieve the spatio-temporal context of occurrence of the stimuli. The notion that the first network is characterized mainly by feedforward connectivity while the second is characterized by feedback connectivity is consistent with these hypotheses. Moreover, Staresina *et al.* [305] found a recollection-related hippocampal response in iEEG data at 250ms - a similar timing to the present left-lateralized feedback response. Recently, Kar *et al.* [306] showed the advantage of recurrent computations for object recognition. Increased feedback connectivity could represent top-down modulation [307], the build-up of an internal representation of the stimulus [308], or access to a distributed semantic system [35]. This is supported by the notion that the second slower network could be related to language or the need for internal speech, which would explain why it is more left-lateralized.

Recently, Bastin *et al.* [276] proposed a large-scale functional architecture that supports familiarity and recollection. This Integrative Memory Model emphasizes the large number of brain regions involved in familiarity and recollection processes. Moreover, it proposed that an "attribution and attention" system, mainly dependent on frontal lobe regions, was involved in recognition memory. This system involves top-down attention, activity maintenance, metacognitive knowledge, and monitoring and decision-making, leading to subjective feelings and explicit judgments during recognition memory. The fact that the first and third networks encompassed many frontal lobe regions is consistent with this proposal. It may also explain why the second and third networks are less stable than the first and exchange node allegiances over time if monitoring and decision-making are underway.

A switch from a goal-oriented network (familiarity) to an introspective one (recollection) requires significant reorganization of the brain, which also involves the hippocampus [309]. Previous studies have independently identified network changes occurring after 240 ms during recognition memory tasks [275, 310], which lends support to the idea that this switch between networks occurs. Studies that focus on functional connectivity using fMRI have consistently revealed brain network reorganizations during cognitive tasks [207, 209, 311]. Note that the switch (between external and internal worlds) also involves the frontal lobes [312]. Westphal *et al.* [294] suggested that a cross-talk between two large-scale networks during episodic memory may push the brain into a globally more integrated state, enabling higher information transfer fluidity. This increase in global integration is driven

by an increase in cognitive load, whereby the brain can adopt a more global workspace configuration [206, 207]. Moreover, higher task demands were already noted to decrease modularity [208]. Overall, the network topology is tightly linked to information transmission [192]. These notions are consistent with our findings of a critical switch between different networks that precede a change in information flow and underscore the brain's ability to reconfigure dynamic networks in response to changing cognitive demands [200].

It is highly noteworthy that these findings indicate that large-scale functional networks can have several modes of relationships, for instance, critical moments of transition between networks (such as between the first and second network) or strong interactions (such as between the second and third network where node allegiance fluctuates between the two networks over time). Overall, this study provides a richer and more integrated picture of the brain networks that underlie recognition memory.

6.4.3 Recognizing stimuli: Hits vs. Correct rejection

It is of note that the pattern of predominantly feedforward and feedback information flow observed in the right and left hemispheres were identified only for Hits but not for Correct rejections. The visual recognition memory task used in this study was based on a go/no-go paradigm. The response (raising fingers from a response pad) was provided only for Hits, while CR did not require a response. This paradigm was chosen because it forces subjects to use their fastest strategy [313]. Consequently, Hits required the involvement of more brain regions than CR. There might be a concern if the memory task is confounded with a motoric task. However, we focused on interpreting only the first 300 ms, and the first responses occurred after 350 ms. Moreover, in our previous research, we found the motor activity related to activity in the supplementary motor area but not to the parahippocampal gyrus or hippocampus activity [279]. Finally, multivariate methods are able to account for group interactions.

Watrous *et al.* [314] suggested that functional connectivity related to correct versus incorrect context retrieval was rather global than regionally specific. We consistently found significant differences between Hits and CR in global FC from approximately 290 ms. These increased functional interactions are believed to be a signature of successful recollection [315, 316].

If findings are not related to behavioral performance, there is a risk that they may reflect non-psychological factors. Therefore, we tried to verify whether the right feedforward connectivity pattern, possibly underlying familiarity, drove fast behavioral responses. The left feedback pattern, possibly related to recollection, was associated with slower responses [317, 318]. We found that effective feedforward connectivity was negatively correlated with reaction times, while positive correlations were found for feedback connectivity. However, these correlations did not have high statistical power. The number of subjects or the variability of the implantations (impacting the typicality of the neural responses) may have decreased the statistical power. Even though Shine *et al.* [209] suggested a direct link between cognitive performance and dynamical brain network reorganization, we found no significant correlation between modularity or efficiency and performance, probably due to the factors just mentioned.

6.4.4 Challenges of iEEG connectivity analyses

Intracranial EEG has the tremendous advantage of providing an excellent spatial and temporal resolution not provided by other methods. However, it also has drawbacks that may have impeded the connectivity analyses. Very few studies focus on whole-brain, dynamic, effective connectivity using iEEG data because of the specific challenges posed by this approach, such as the relatively low number of subjects, short non-stationary time-series, and tailored electrode implantations, which may under-sample some brain regions. Moreover, the disproportion in brain region sampling requires synthesizing information across edges and nodes Thus, most of the previous studies predefined regions of interest *a priori* [305] and did not focus on large-scale networks or their temporal dynamics (see exceptions such as [287]). Finally, some patients also participated in more trials than others; however, we had to restrict our analyses to the same number of trials per patient because the number of trials directly influences the magnitude of connectivity estimates.

To overcome these issues, we pooled results from all 18 patients and mapped channel locations to the AAL atlas. We were thereby able to reconstruct signals from 68 out of 90 brain regions. Using vertical regression in all trials (limited to 64 per patient), we could estimate causality in short (250 ms) and stationary time windows. Dedicated statistical analyses had to be designed at each stage of the analyses to assess the value of the findings. In addition, we followed the definition by Gaillard *et al.* [287] of feedforward

and feedback processes, but this was only a rough simplification. In contrast, a hierarchical anatomically based model might be better to represent brain processes [319]. Furthermore, functional rather than anatomical parcellation could better associate network topology and behavioral responses [320]. Future studies could also benefit from frequency-resolved measures to detect networks that operate on specific frequencies [321]. As this next step would generate additional dimensions of data, using machine learning techniques is desirable.

It is worth mentioning that iEEG involved recordings from epileptic patients. Therefore, epilepsy could impact the generalization of the results. However, as in all similar studies, we removed the interictal activity periods recorded simultaneously with the task. Previous studies have also shown that similar ERPs, characterized by latency, morphology, and amplitudes, are found across independent studies and epilepsy centers (e.g., [275, 322]). Interestingly, a recent study combining iEEG and fMRI demonstrated only small functional neuroanatomical differences during an episodic memory task between a group of epileptic patients and a group of matched healthy subjects [323]. Overall, despite the limitations, iEEG studies appear to provide useful and reliable information.

6.5 Conclusion

In conclusion, this study reveals novel findings regarding the dynamics of the large-scale functional networks that underlie recognition memory. It could generate hypotheses that could be specifically tested in future work. For example, during a recognition memory task, neuronal activity should mainly reflect feedforward and early activity in the first right hemisphere network [324]. Such activity should also differ from the neuronal activity recorded in the second network. It would also be interesting to examine the physiological mechanisms that enable the transition between different networks. In general, this study shows that whole-brain dynamic connectivity analyses using intracranial EEG offer a promising avenue to study different classes of cognitive abilities.

Chapter 7

Factors influencing connectivity pathways of epileptogenesis: a single subject case

Here, we present preliminary results of a collaborative project between Centre de Recherche Cervau et Cognition and the Institute of Complex Systems of the Czech Academy of Sciences. This project is supported by the Barrande grant nb. 8J20FR037.

The proposed project aims to investigate the mechanisms leading up to epileptic seizures. We aim to identify brain connectivity changes that correspond to differences in brain states during the pre-ictal period, which can help seizure treatment and prediction. The unpredictability of seizures is one of the main health risks and psychological burdens in epilepsy. Hence, successful seizure prediction can significantly improve the health and quality of life of epilepsy patients, minimizing disabilities and injury risk. Furthermore, investigating pre-ictal connectivity changes helps to characterize the interaction between brain areas during epileptogenesis. The gained insight could thus contribute to the development of new and the optimization of already established treatment strategies for epilepsy. We already gathered high-quality iEEG data for 74 patients with drug-resistant epilepsy. These patients were under evaluation for neurosurgery at CHU Purpan hospital. After arrival at the hospital, patients underwent electrode implantation. Per patient, 9-15 standard DIXI electrodes with 8-15 contacts (diameter 0.8 mm, length of contact 2 mm) were used, leading to an average of 110 contacts per patient. The iEEG recording was then started and lasted for one to two weeks while the patient remained in the hospital.

The anti-epileptic medication was slowly decreased after implantation to facilitate seizure occurrence. In most patients, seizures started around day 4 to 6. Usually, several seizures were recorded before anti-epileptic medication was resumed, and the electrodes were removed. Out of the 74 patients, we will select those with the same type of epilepsy, i.e., temporal lobe epilepsy (the most common case). This unique data set will allow us to examine brain dynamics at timescales up to days before a seizure occurs. Understanding the temporal evolution of connectivity changes is of fundamental value in uncovering the mechanisms evolved in epileptogenesis, as well as in ictogenesis.

Since the project is currently ongoing, we present a single-subject case that will show fundamental aspects of all future analyses. Moreover, in the current retrospective study of already recorded subjects, we are limited by the number of segments that have been stored. However, we will conduct a prospective study on subjects that are being and will be recorded. There we will make use of full continuous recordings with very high sampling frequency.

Finally, the brilliant work of Schroeder *et al.* [325] has to be acknowledged as it inspired presented results. Furthermore, the collaborators on this project deserve special appreciation, namely, Isa Dallmer-Zerbe, who helped write the grant proposal, conducted a literature review, processed the data, and Anna Pidnebesna, who helped with data analysis.

7.1 Introduction

Epilepsy is a chronic neurological disorder that affects people of all ages. The disorder is characterized by repeated seizures, leading to various symptoms, including temporary loss of consciousness. According to the World Health Organization, around 50 million people worldwide are diagnosed with epilepsy. Epilepsy patients suffer physically, emotionally, and socially. The risk of premature death is up to three times higher than in the general population. It has been estimated that 70 % of people living with epilepsy could live seizure-free if properly diagnosed and treated [326]. In approximately 30 % of the patients, epilepsy is drug-resistant. In these cases, neurosurgery is evaluated as a second-line treatment in order to remove the brain tissue where the seizure originates. Thus, the success of surgery is conditioned on the correct determination of the seizure onset zone

(SOZ). When non-invasive methods (scalp EEG, MRI, PET) do not identify the SOZ, the standard clinical procedure involves the invasive implantation of iEEG electrodes for SOZ determination [327].

Our understanding of epilepsy mechanisms has shifted its focus towards a more dynamic, whole-brain network perspective in the last decades. In this epileptogenic network, we differ among several zones based on their characteristic involvement during ictal activity. These zones include the epileptogenic zone, propagation zone, irritative zone, and non-involved zone. The rapidly growing field of connectomics investigates the relationships between different zones and brain regions across various scales derived from respective neuroimaging techniques [328, 329]. Moreover, using functional and effective connectivity techniques, which form the basis of functional brain networks, recent studies showed the existence of altered brain states before seizures that are measurably different from a normal state [328]. Altered connectivity has also been found in the area of SOZ, suggesting a hyperexcitable state of the cortex of the epileptogenic zone [330, 331].

A specific type of network topology featuring a high number of outgoing connections from the SOZ to seizure propagation areas has been suggested as a network architecture promoting SOZ influence [331, 332]. The alterations in connectivity were already successfully used in diagnosing epilepsy, providing useful new biomarkers of the disorder and targets for its treatment. Moreover, these alterations were shown to be not only useful to differentiate between patients and controls but also between different brain states relevant in epilepsy pathology. Finally, resting-state connectivity disturbances in focal epilepsy have been related to neurocognitive problems like memory and language impairments [333]. Nevertheless, connectivity should not be studied only from a static perspective. Moraes *et al.* [334] convincingly stressed the importance of assessing temporal dynamics in the ictogenic networks. Given the dynamic nature of epilepsy, such an approach is necessary to understand the generative mechanisms underlying the disease.

Investigating epilepsy dynamics requires a definition of the time interval before a seizure. Current line of research differentiates between two types of epilepsy dynamics. Ictogenesis reflects the short-term changes in the scope of minutes to hours before the seizure. It is usually studied in the context of seizure prediction, where the connectivity changes were proven to be a valuable biomarker [155–157]. On the other hand, epileptogenesis focuses on long-term changes in the scope of days to years leading to the first seizure.

These long-term changes are reflected in a gradual increase of seizure susceptibility, i.e., the probability of seizure occurrence in the epileptogenic network, as opposed to ictogenesis, where seizure susceptibility fluctuates on much faster timescales. The mechanisms involved in both in ictogenesis and epileptogenesis remain insufficiently understood [335, 336]. Therefore, analyzing connectivity as a time-evolving parameter and its relationship to evolving seizure susceptibility can fill our gaps in understanding epilepsy generations.

Studying epileptogenesis is a very difficult task as it requires long-term recordings even before the occurrence of the first seizure. Current knowledge of epilepsy mechanisms does not allow predictions whether someone will develop epilepsy in the foreseeable future. Therefore, most of the existing research has been limited to studies on animal models [337] and computational modeling (for a review, see [338]). These studies highlighted the increasing connectivity asymmetry and the importance of nodes located outside of the region of initial insult during epileptogenesis. However, no study in humans so far systematically assessed the connectivity changes days prior to a seizure [157]. This time-course is characterized by increasing levels of seizure susceptibility. We propose investigating intracranial EEG recordings of epileptic patients admitted for identifying and possible subsequent resection of the epileptogenic zone. In current clinical routines, these patients are implanted with iEEG electrodes, and the anti-epileptic drugs are continuously decreased. First seizures typically arise between the fourth and sixth day, when drug dosage has decreased below a critical threshold. We believe that this time period of several days could serve as a valuable model of epileptogenesis.

Here we present a single subject case where the first seizure occurred 11 days after electrode implantation. We aim to identify changes in brain connectivity that correspond to differences in brain states. Our primary hypothesis is that we will observe connectivity changes that would be a hallmark of increasing seizure susceptibility. Moreover, we assume these changes to be related to daily cycles [325] and the number of high-frequency oscillations [36]. Understanding the temporal evolution and identifying critical changes of connectivity patterns is of fundamental value in uncovering the mechanisms evolved in epileptogenesis, as well as in ictogenesis. The unpredictability of seizures is one of the main health risks and psychological burdens in epilepsy. Hence, successful seizure prediction can significantly improve the health and quality of life of epilepsy patients.

7.2 Materials and methods

7.2.1 Patients

High-quality iEEG data was recorded for a single patient with drug-resistant epilepsy (male, 31 years old). The patient was admitted to the Epilepsy Monitoring Unit at Toulouse University Hospital to identify and possibly remove the epileptogenic zone. After arrival at the hospital, the patient underwent electrode implantation. Twelve standard intracranial electrodes (Microdeep depth electrode, DIXI medical, France) with 8-15 platinum/iridium contacts (diameter 0.8 mm, length of contact 2 mm) were used, leading to 130 contacts. The implantation was individually tailored to the seizure onset zone, and the placement of each depth electrode was based exclusively on clinical criteria independently of this study.

Intracranial EEG activity was recorded using two synchronized 64-channel acquisition systems (SystemPlus Evolution, SD LTM 64 EXPRESS, Micromed, France) with a sampling frequency of 256 Hz (high pass-filter: 0.15 Hz). The iEEG recording started after electrode implantation and lasted 13 days while the patient remained in the hospital. On the 11th day, a first unprovoked seizure occurred. Currently, we have 16 recording segments at our disposal scattered throughout the first ten days before the occurrence of the first seizure (Fig. 7.1).

Drug dosing

The anti-epileptic medication was slowly decreased from the first day of recordings to facilitate seizure occurrence. After the eighth day, the drug dose dropped to zero and remained there until the first seizure (Fig. 7.2). The patient took a combination of Lamotrigine and Carbamazepine. We normalized the dosage to a 0-1 scale to facilitate further computations. The maximal summed dosage corresponds to 1, and the minimal summed dosage is 0. We assume that the minimal relative dosage corresponds to the highest susceptibility to having a seizure.

7.2.2 iEEG recordings

Data processing was conducted with Matlab (Version 9.8.0, The Mathworks Inc, Natick, MA, USA) and the interactive Matlab toolbox EEGLAB [339]. One 15 minute segment

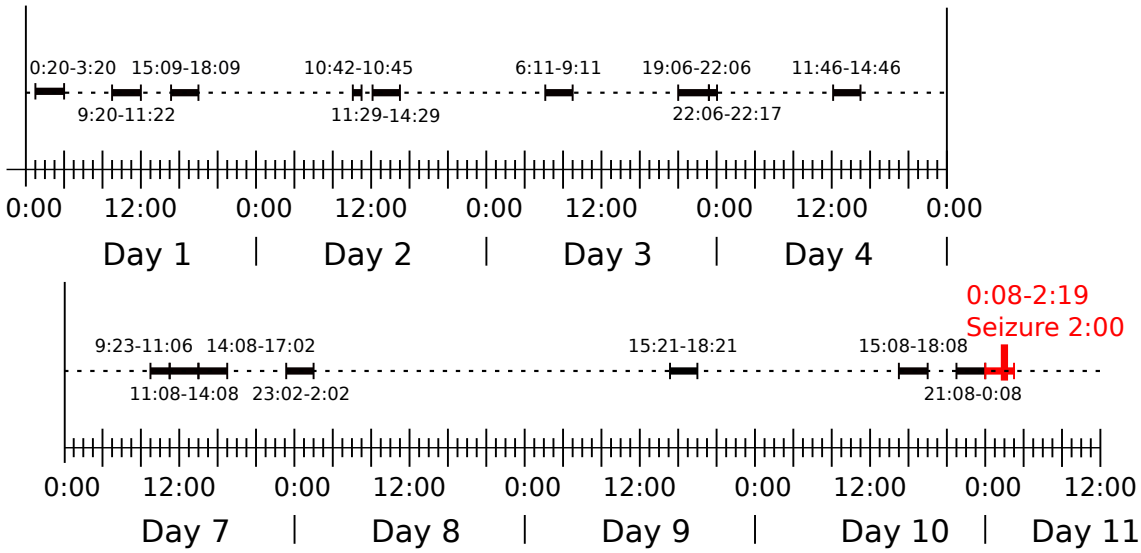

Figure 7.1: Schematic of recording times. For our single-subject case, we were able to gather 16 measurements of various lengths scattered throughout the first 10 days before the occurrence of the first seizure. On the 11th day, a first unprovoked seizure occurred.

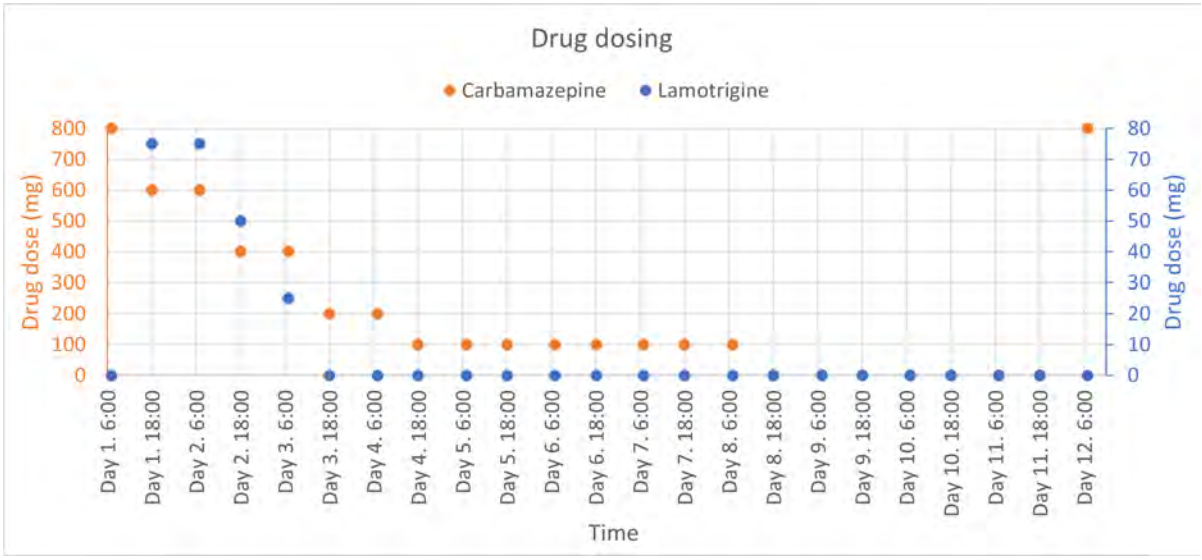

Figure 7.2: Drug dosing. Visualization of decreasing drug level across the first ten seizure-free days. The subject took a combination of Carbamazepine and Lamotrigine. After the eighth day, the drug dose dropped to zero and remained there until the first seizure.

was extracted for each available data file before a patient's first recorded seizure. It comprised the first 15 minutes of the recording. Processing steps then included downsampling to 256 Hz, high-pass filtering with a cut-off frequency of 0.5 Hz, removing non-EEG channels, re-referencing to bipolar montage, and finally, the exclusion of error channels from

the data. For re-referencing, the difference in activity between (only) directly neighboring contacts was calculated. Error channel rejection consisted of a two-step procedure using EEGLAB *pop_rejchan()* function with the *'spec'* rejection method. Firstly, channels with significantly high power in 48-52 Hz frequency range (>3 standard deviations from mean channel power in this range), and secondly, outlier channels with regards to the whole 1-128 Hz frequency range (>4 standard deviations from mean channel power) were identified. As channel exclusions needed to result in the same channels across files, the same error channels (accumulated error channels over all files) were excluded from all files. For the same reason, iEEG channels that were present in some but not all files were disregarded. This procedure yielded a total of 91 bipolar channels. A single bipolar montage (i.e., A 1-2) is referred to as a "channel" throughout this study.

7.2.3 Connectivity analyses

We aim to identify brain connectivity changes that correspond to differences in brain states during the pre-ictal period. Here, we adopted the methodology from Schroeder *et al.* [325]. However, unlike the authors who compared seizures, we evaluate connectivity in all recordings before the first seizure. More specifically, we calculated the mean coherence of 15 consecutive windows of 60 seconds lengths for each recording segment. The 15 minutes length of a window was selected based on exploratory results on 2 hours long segment. By correlating windows of various lengths, we found that 15 minutes long segments showed a very high similarity with the full 2 hours long segment (Fig. 7.3), proving 15 minutes segments to be sufficiently long to capture the main connectivity patterns.

Coherence is a mathematical method quantifying the similarity of frequency content recorded from two brain regions. For each 60s window, we calculated magnitude-squared coherence (MSC) between each pair of iEEG channels in six frequency bands: delta (1-4 Hz), theta (4-8 Hz), alpha (8-13 Hz), beta (13-30 Hz), gamma (30-80 Hz), and high gamma (80-126 Hz). For a given band, MSC between all pairs of channels is represented by a matrix of real-valued numbers between 0 and 1. Its magnitude between two channels is defined as:

$$Coh_{x.y} = \frac{|G_{x,y}|^2}{G_{x,x}G_{y,y}} \tag{7.1}$$

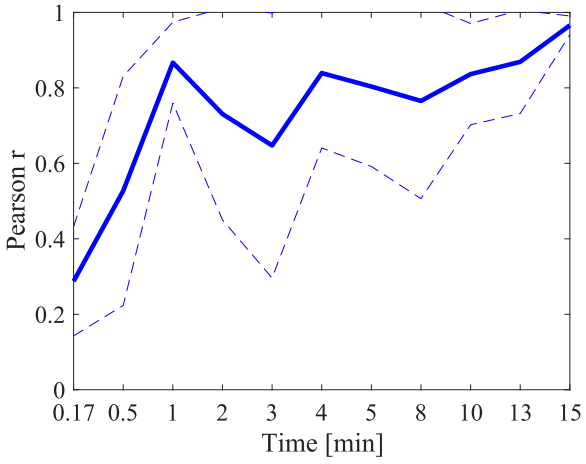

Figure 7.3: Selection of window length. We correlated gamma coherence matrix from 2 hours long window with other gamma coherence matrices from windows of various lengths. These short windows were chosen randomly from the original 2 hours. Mean ± standard deviation of Pearson correlation between two vectorized connectivity matrices across 10,000 runs is plotted. The results show that there is almost no difference between 15 minutes and 2 hours long widows. Therefore, we used 15 minutes long windows in the analysis.

where $G_{x,y}$ is a cross-spectral density between signals x and y, $G_{x,x}$ is auto-spectral density of signal x, respectively y. The auto-spectra and cross-spectra were calculated using Welch's method (2-s sliding window with 1-s overlap and Hamming tapering).

Connectivity pathway and dissimilarity

For each measurement of iEEG recordings, we obtained 15 connectivity matrices in each frequency band representing consecutive 60s segments. To be able to compare connectivity measurements at different times, the matrices of each measurement underwent a series of steps. For a single measurement and a single segment, we first vectorized connectivity matrices of all six frequency bands by taking the upper triangular form without the diagonal. Further, we vertically concatenated these six connectivity vectors. Since we aim to identify changes in connectivity patterns rather than changes in global connectivity levels, we normalized the connectivity vector so that the L^1 norm (i.e., the sum of all elements) was 1. Finally, we horizontally concatenated all the 15 vectors, each corresponding to all frequency bands of a given segment. Thus, each measurement was represented by a single connectivity matrix.

Small fluctuations in the functional connectivity due to noise would create a high baseline dissimilarity between seizures. Therefore according to [325], we applied nonnegative matrix factorization (NMF) to each connectivity matrix to reduce noise in the connectivity matrices. NMF decomposes a single connectivity matrix V into two nonnegative matrices, W and H, such that $V \approx W \times H$. The optimal number of basis vectors was determined using stability NMF [340]. After the factorization, the return to the original feature space was achieved by calculating $V^{\star} = W \times H$. This operation is not lossless, but it is primarily the small fluctuations and noise that are omitted. Finally, each vector was again normalized so that the L^1 norm was 1.

We hypothesize to observe gradual connectivity changes as the seizure susceptibility increases. In order to do so, we mapped the high-dimensional connectivity matrices to low-dimensional space. Multidimensional scaling allows visualizing the level of similarity of individual vectors. We used MDS in combination with L^1 distance. Note that using MDS with L^2 Euclidean distance is identical to the use of PCA. However, the L^1 distance was shown to be preferable in higher-dimensions, as it is less susceptible to outliers [341].

To find the driving effects of connectivity changes, we need to quantify how the connectivity changes. Therefore, we defined the connectivity dissimilarity as the mean L^1 distance between two FC matrices (Fig. 7.4).

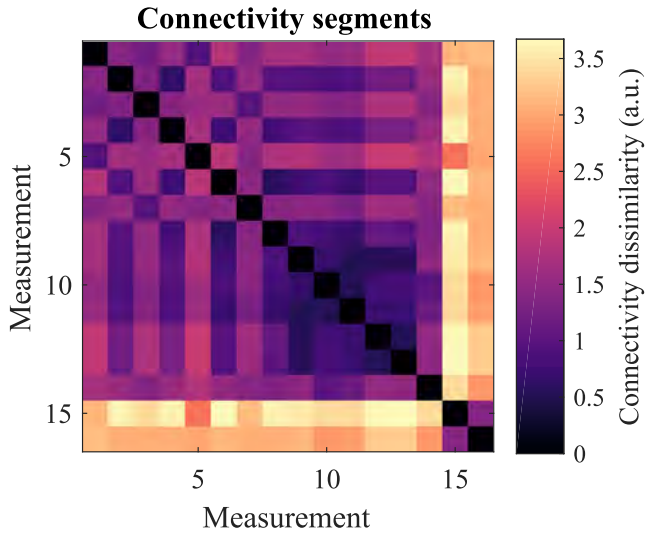

Figure 7.4: Connectivity dissimilarity. Each measurement was characterized by concatenated vectorized coherence matrices across all frequency bands representing connectivity in 15 consecutive time windows. The final connectivity dissimilarity between two of such matrices was defined as the mean L^1 distance between two FC matrices.

7.2.4 Statistical analyses

Our goal is to find factors driving the differences among connectivity profiles. Previous research shows that seizure susceptibility change on circadian and slower timescales [342]. Therefore, we calculated a linear temporal distance matrix containing the amount of time elapsed between the onset times of each pair of measurements (Fig. 7.5). A similar approach was used for circadian rhythms, but the actual time of each measurement was first recalculated to the distance to midday (i.e., 14:00). Thus, the final circadian temporal distance matrix was based on temporal distance from the midday. Hence it reflected day and night cycles.

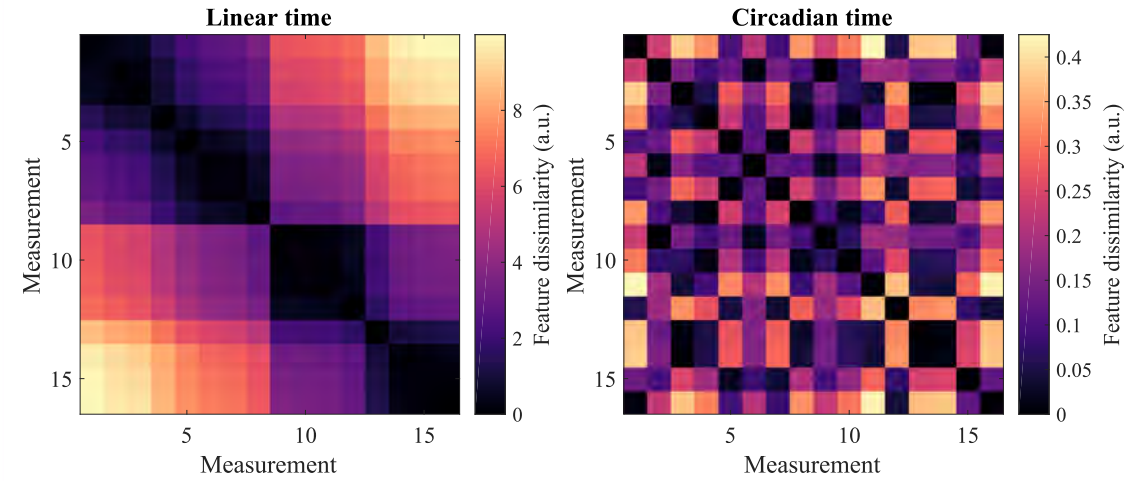

Figure 7.5: Linear and circadian time dissimilarity. Linear temporal distance matrix contains the amount of time elapsed between the onset times of each pair of measurements. A similar approach was used for circadian rhythms, but the actual time of each measurement was first recalculated to the distance to midday (i.e., 14:00). Thus, the final circadian temporal distance matrix reflects the day and night cycles.

We investigated two other driving factors. The first factor was the drug dosage that should correspond (with some time-lag) to seizure susceptibility. Since the patient usually took the medication twice per day, we calculated the actual drug dose corresponding to the measurement time as a linear interpolation between the previous and following dose if the dosage was decreasing and as the previous dose if it was increasing. Then, the drug dose dissimilarity was calculated as the absolute difference between two drug doses (Fig. 7.6). Finally, spikes and high-frequency oscillations (HFO) were proven to be valuable biomarkers of epileptogenic tissues [36]. We used the AnyWave software [343] to

detect spikes and HFO (80-126 Hz). Each channel was thus characterized by the cross-rate, i.e., the sum of HFOs and spike rates per minute. The dissimilarity between two measurements is based on a correlation between cross-rates (rates across channels), and it is defined as:

$$CR_{dissimilarity} = \frac{1 - r_{i,j}}{2} \tag{7.2}$$

where $r_{i,j}$ represents Pearson correlation between cross-rate of segment i and j.

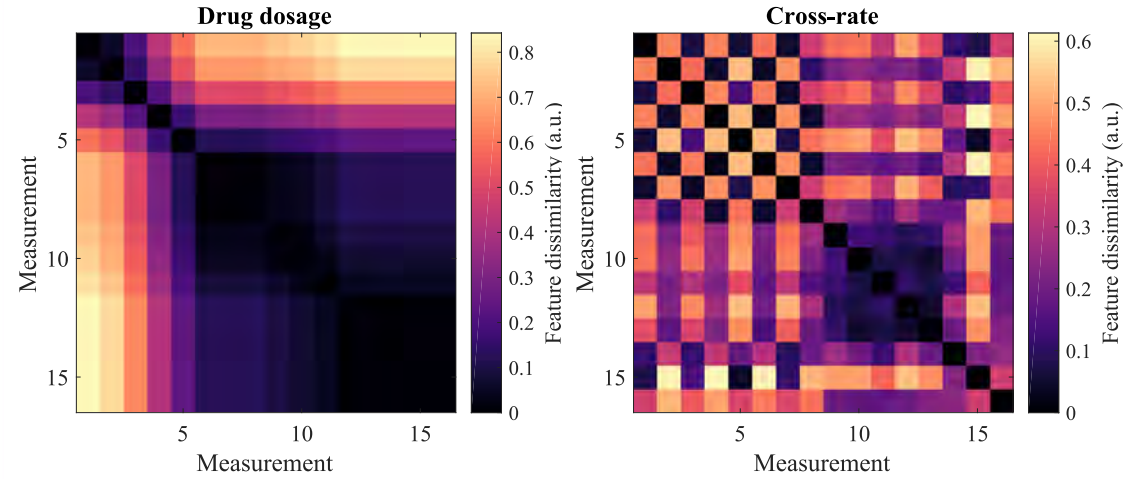

Figure 7.6: Cross-rate and drug dose dissimilarity. Each measurement is described by interpolated relative drug dosage and a cross-rate. The drug dose dissimilarity is calculated as the absolute difference between drug doses. The cross-rate dissimilarity between two measurements is based on correlation cross-rates among channels.

Finally, we compared the connectivity dissimilarities to temporal, dosage, and cross-rate dissimilarities. We computed Spearman's correlation between the upper triangular elements of the seizure dissimilarity matrix and each other matrix. Since the distances in each matrix are not independent observations, we performed the Mantel test [344] to determine each correlation's significance. We randomly permuted the rows and columns of one matrix 10,000 times. After each permutation, we computed the correlation between the two sets of upper triangular elements. Such procedure results in a distribution of correlation values to which the original correlation was compared, and thus appropriate p-value is derived.

7.3 Results

We investigate connectivity patterns changes in the scope of days as the susceptibility to seizure increases. First, we focused on analyzing whether there are any changes. Further, upon the identification, we try to find the driving effects of such changes. Using MDS (with Sammon mapping) and L^1 distance, we projected vectorized connectivity matrices across all frequency bands to a two-dimensional space. In Fig. 7.7, we can observe that most connectivity profiles occupy the same space. However, the last two measurements seem to be very different in terms of connectivity. These two correspond to connectivity six, respectively, two hours before the first seizure.

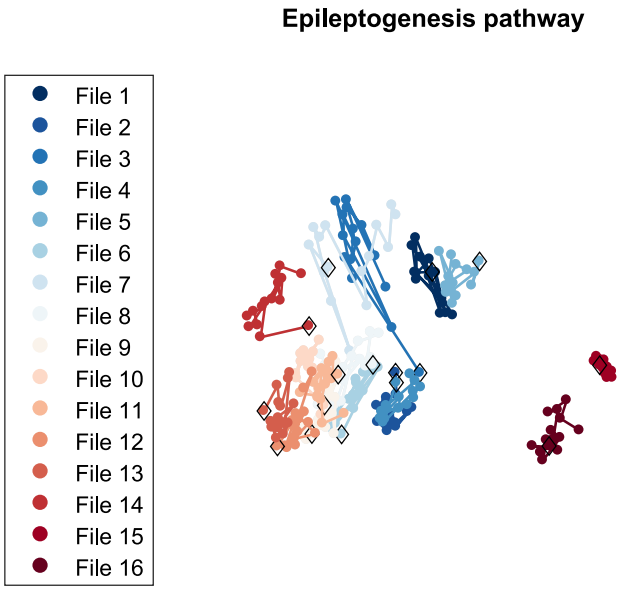

Figure 7.7: Connectivity pathway of epileptogenesis. All connectivity matrices are projected to two-dimensional space using Multidimensional scaling and L^1 distance. The last two measurements are visually very different than the rest of the measurements.

Therefore, we investigated which frequency bands drive such significant dissimilarity. We know that it is not the amount of synchrony as coherence matrices in each frequency band were normalized. Therefore, we calculated the Pearson correlation of mean upper triangular elements across the 16 measurements between each frequency band (Fig. 7.8). The first 14 measurements are very similar across all bands. However, the last two measurements show very different connectivity profiles, mainly in higher frequency bands, such as the gamma and high gamma band. In other bands, even these two measurements were highly similar to other measurements (Person $r > 0.7$).

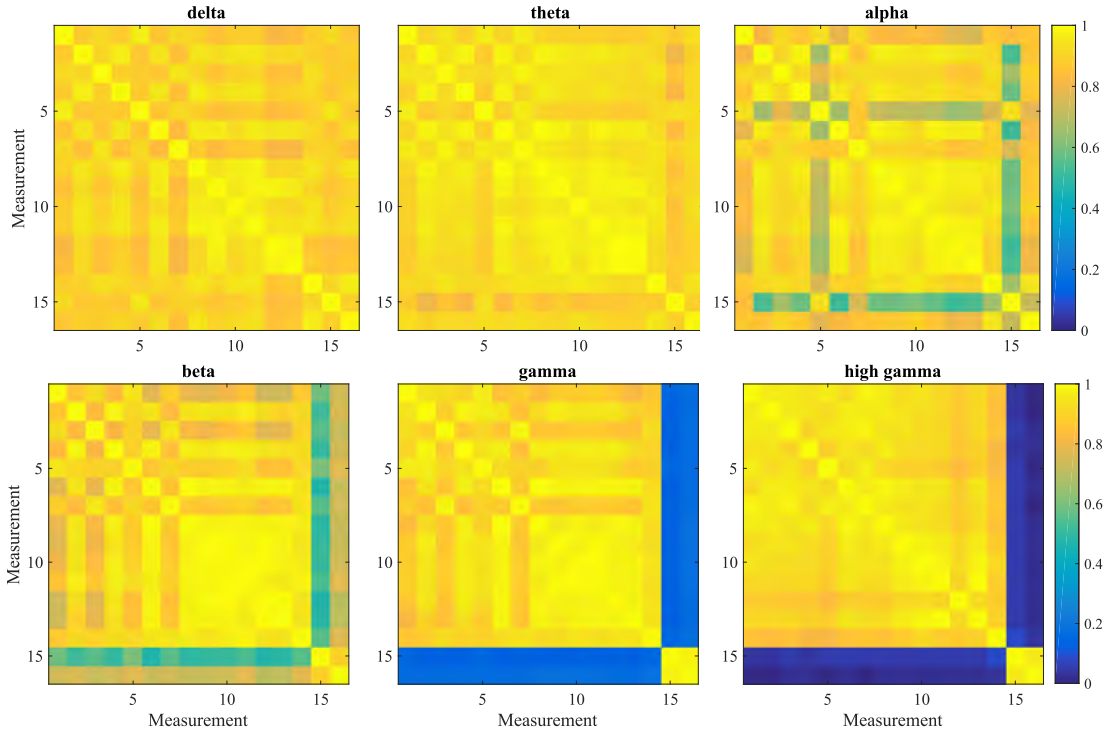

Figure 7.8: Correlation between connectivity matrices of different frequency bands. The two outlying points in connectivity pathways are driven by the differences in gamma and high gamma frequency bands. Here, the correlation between vectorized mean coherence matrices of all measurements is plotted for each frequency band. Only gamma and high gamma band show differences in connectivity profiles.

Indeed, if we visualize the high gamma band connectivity matrix from measurement 14 and 15, we easily observe significant differences (Fig. 7.9). Note that the first 14 matrices showed visually very similar high gamma band connectivity profiles as well as the last two measurements.

In order to find driving factors behind this change in pattern, we correlated connectivity dissimilarity with other types of dissimilarities. We observed a significant correlation with cross-rate, linear time, and circadian time dissimilarities (Fig. 7.10). Furthermore, to find the optimal combination of all factors that would best explain the driving effects, we first used a stepwise linear model that sequentially adds and removes features to identify the optimal model. All features, namely cross-rate, linear time, circadian time, and drug dosage dissimilarities, were identified as significant parameters in the multiple linear regression model (adjusted $R^2 = 0.40$, $p = 0.01$). However, we assessed each factor's significance again using a Mantel test, and we excluded circadian time ($p = 0.06$). The regression coefficients and their p-values are in Tab. 7.1.

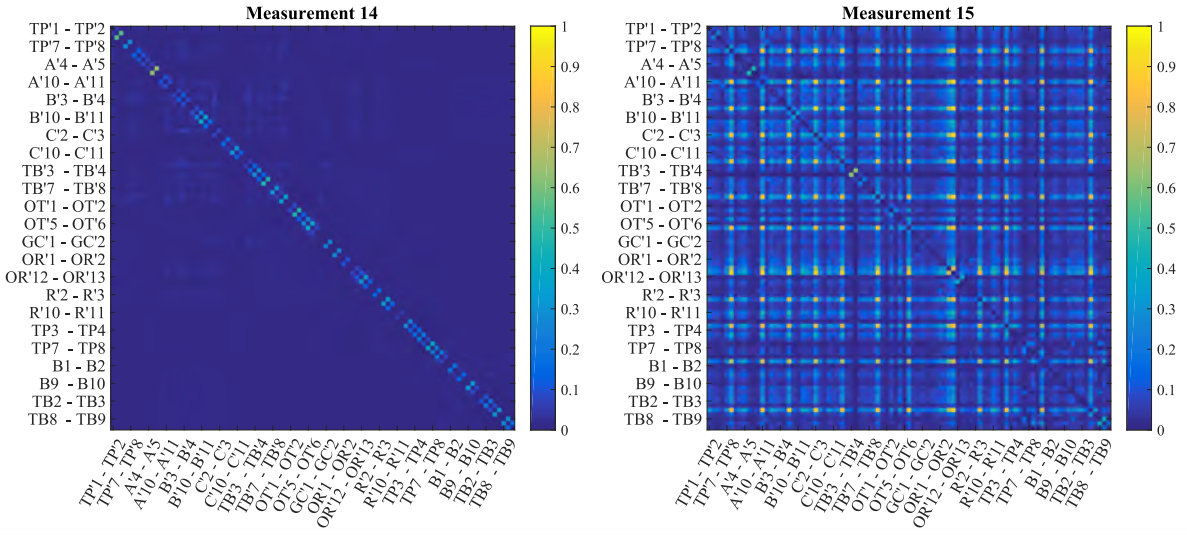

Figure 7.9: Examples of gamma connectivity matrices. Differences in the correlation between gamma coherence matrices between measurement 14 and 15 are visually detectable. Future analyses will investigate how these changes are localized with respect to zones of the epileptogenic network.

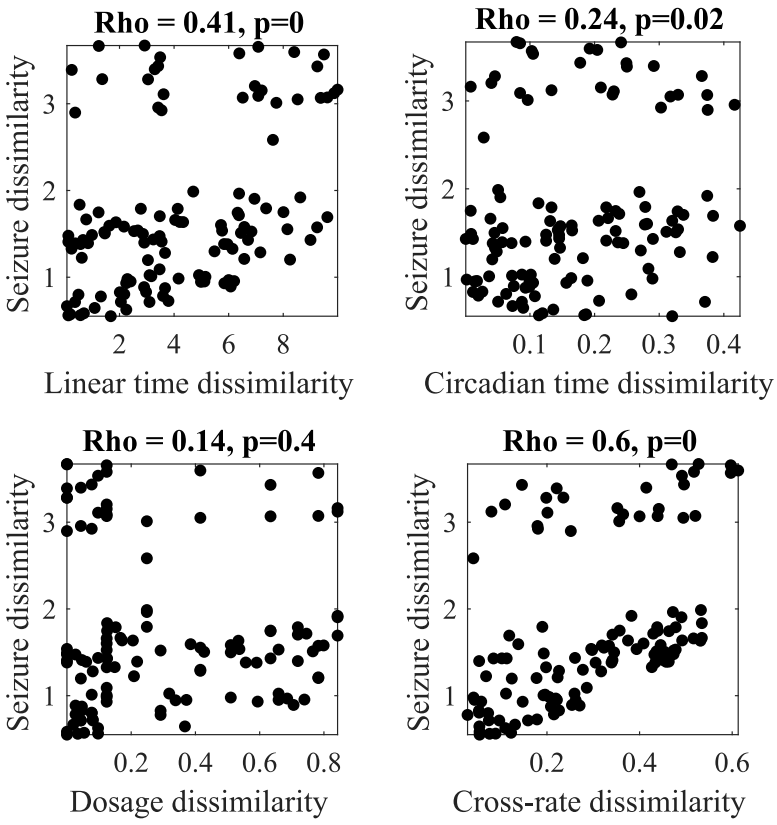

Figure 7.10: Correlation between connectivity dissimilarity and other factors. Connectivity dissimilarity is correlated with linear time, circadian time, drug dosage, and cross-rate dissimilarities. Only the correlation with drug dosage is not significant.

Correlation analysis			**Multiple linear regression analysis**		
	Spearman	Pearson	Adjusted R^2	**0.40** (0.01)	
Linear time	0.41 (10^{-5})	0.38 (10^{-5})		Estimate	p-value
Circadian time	0.24 (0.02)	0.20 (0.05)	Linear time	0.16	10^{-5}
Drug dosage	0.14 (0.40)	0.02 (0.95)	Drug dosage	-0.98	0.05
Cross-rate	0.60 (10^{-5})	0.48 (10^{-5})	Cross-rate	2.23	10^{-4}

Table 7.1: Correlation and multiple regression analysis. We found significant factors driving the connectivity dissimilarity. Cross-rate dissimilarity appears to be the most significant factor. In correlation analysis, p-values are in brackets. Moreover, the multiple linear regression model identified linear time, drug dosage, and cross-rate as important features behind connectivity changes.

7.4 Discussion

In these preliminary results, we present how we can model epileptogenesis using recordings from patients that are selected for possible resection of seizure onset zone. These patients typically spend several days in the hospital while the drug dosage is being decreased, and thus the susceptibility to having a seizure gradually increases. We calculated functional connectivity for this time period before the first seizure. Using modern machine learning tools, the temporal connectivity profile can be visualized in order to identify the critical times of epileptogenesis. Moreover, we investigated factors that are driving these connectivity changes. We identified linear time, drug dosage, and the cross-rate (defined as the sum of high-frequency oscillations and spikes) as the main driving factors. Even though this is only a single subject case, we believe that the methodology could be applied to other subjects as well. The reason for choosing this subject was that there are 11 days between the implantation and the first seizure. Moreover, we have our disposal 16 measurements that are scattered throughout the 11 days. Furthermore, these recordings are at different time-points of the day, including few night recordings.

Using MDS and subsequent investigations, we localized the main connectivity changes to gamma and high gamma band six hours before the first seizure. A similar specific state of brain synchronization was observed several hours before the actual seizure in other studies as well [345]. Moreover, different gamma connectivity patterns were already proven to distinguish the epileptogenic zone from other cortical regions not only during the ictal event but also during the inter- and pre-ictal periods [346]. These altered patterns

included increases in high-frequency energy in the ictal onset zone and its vicinity [347]. Therefore, in our future studies, we will localize the connectivity changes with respect to different zones of the epileptogenic network. Moreover, we will focus on finding alterations days prior to the seizure.

One of the main factors of connectivity changes was cross-rate. It is important to note that it was not the number of spikes and HFO that differ among measurements. The cross-rate did not show significant changes among measurements. However, where the spikes and oscillation occurred varied significantly. That is why we used the correlation between cross-rates of all channels instead of the difference in the amount of all cross-rates to compare two measurements. We confirm that using HFO and spikes could serve as a viable biomarker of epileptogenic tissues [36].

Previous studies highlighted the importance of circadian rhythms in seizure forecasting [325, 348]. Even though the circadian time dissimilarity was not finally selected into our multiple linear regression model, it does not necessarily downplay its importance. The main reason for the absence of a significant dependence is that only 4 out of 16 measurements were recorded between 22:00 and 6:00. Increasing the number of night recordings would increase the importance of this factor. Indeed, based on preliminary results in other subjects, where more night recording are at disposal, we observed a significant circadian trend in connectivity matrices. Therefore, we assume the circadian rhythm to be an important feature in all future models.

In the correlation analysis, we did not find a significant relationship between drug dosage and connectivity dissimilarity. However, the decrease in the antiepileptic drug was shown to increase excitability and modulate seizure likelihood [349]. In our current setup, the drug dosage closely resembles linear time. The linear component of the model may reflect gradual changes in pathways on slower timescales, ranging from days to weeks. It was already reported that very slow cycles (20–30 days) are an important biomarker for determining relative seizure risk [342]. Nevertheless, we believe that the decrease in drug dosage should be the most important factor [349]. This assumption can be supported by our observations of seizures occurring soon after dosage decrease. Typically, we observed the first seizure to occur 4-6 days after the anticonvulsant discontinuation. Therefore, a more biologically relevant drug dosage model will be needed in our future analyses. A model that takes into account the time-lag between drug administration and drug effect.

Moreover, the actual drug level in the blood could be assessed using the half-life of the molecules.

We acknowledge that in the future setup, the analysis of a large sample size might cause challenges as epilepsy is a heterogeneous disease, and electrode implantation setup varied across patients. Therefore, we assume a variability in seizure functional network evolutions and dynamics. Even though the factors modulating seizure likelihood are comparable across subjects, the comparison needs to be carried out carefully. It is significantly affected by the day of the first seizure, the number of day/night recordings, and the number of available measurements in general. However, overcoming these challenges is desirable as this is a general limitation to most studies of epilepsy samples.

In the single-subject case, we identified a critical change in brain connectivity six hours prior to the seizure. However, our aim is to investigate long-term changes days prior to a seizure as we are interested in the mechanisms of epileptogenesis rather than ictogenesis. It seems that the possible changes are subtle. In order to detect them, our preprocessing pipeline will need to improve as current data can still be contaminated by artifacts. Another limitation of the current study could be that we do not possess a good model of epileptogenesis because seizures caused by the decrease of anticonvulsant medication are different from those occurring spontaneously. However, the dosage decrease extremely rarely causes the appearance of seizures having an electrical onset or a clinical pattern different from those observed on full medication [350]. Finally, relating our findings to biophysical models of seizure dynamics will be of high importance [338].

7.5 Conclusion

Studying epileptogenesis is a very difficult task as it requires long-term recordings even before the occurrence of the first seizure. In these preliminary results, we investigated a model of epileptogenesis using recordings from a patient with drug-refractory epilepsy who was selected for possible resection of the epileptogenic zone. We analyzed connectivity changes and their driving factors ten days before the occurrence of a first seizure. This time-course is characterized by increasing levels of seizure susceptibility. Significant alterations driven by cross-rate, drug dosage, and slow timescale changes were found six hours before the first seizure. Given the dynamic nature of epilepsy, such an approach is

necessary to understand the mechanisms underlying the disease. Understanding the temporal evolution and identifying critical changes of connectivity patterns is of fundamental value in uncovering the mechanisms underlying epileptogenesis, as well as in ictogenesis. They could help solve the ultimate goal, i.e., successful seizure prediction, which can significantly improve the health and quality of life of epilepsy patients.

Part V

Discussion

Chapter 8

Leveraging the tools of connectivity

In this thesis, we focused on estimating and using connectivity in functional neuroimaging. We described the most common functional brain imaging modalities. As they are built upon different physical phenomena, their characteristics vary significantly. We tried to emphasize the strengths and weaknesses of each modality. We paid special attention to the currently most common techniques: fMRI and EEG (including intracerebral recordings). From the data point of view, maybe the most prominent difference among them is the spatial and temporal resolution. While fMRI is currently the state-of-the-art in macroscale brain networks, EEG still offers an unmatched temporal resolution. EEG and its invasive analogous iEEG are able to record neuronal activity with millisecond resolution. Such a feature appears to be critical, for example, in epilepsy, where high-frequency oscillations play an important role in the build-up towards a seizure. The knowledge of imaging technique properties is crucial for all subsequent analyses. It is important to know how the data were recorded, what they represent, and how they are influenced by artifacts in order to critically assess any obtained results. For example, the head movement artifacts can be falsely interpreted as markers of brain age as they inflate connectivity differences among groups of young and old subjects in fMRI.

In principle, any connectivity method can be applied to any imaging modality. It can be illustrated by the fact that most of the measures were not originally derived for neuroscientific approaches, but they found application across various fields, including weather forecasting or stock markets. Nevertheless, one cannot blindly apply these methods without considering their usability. A method has to be in concordance with the investigated hypothesis, and it should be suitable for the imaging modality. That is why the coherence

might be of special interest in EEG studies where distinct frequency bands (ranging from delta band of 1-4 Hz to high gamma bands with frequencies above 60 Hz) are commonly investigated. On the other hand, fMRI is usually filtered to a narrow frequency band, approximately 0.009-0.01 Hz, and thus the correlation coefficient might be sufficient. We tried to describe how to calculate each metric, where it is commonly applied, and what are its strengths and weaknesses. All in all, this description could provide instructions on how to choose an optimal metric.

Once estimated, the analysis does not finish there. There are various paths on how to study connectivity estimates. We witnessed the advent of resting-state studies along with the identification of large-scale canonical networks. These networks form the basis of our understanding of brain processes. Even though they are built on functional connectivity, structural connectivity shapes both functional and effective connectivity. Nevertheless, the question of how to estimate function from the structure is yet not resolved. There have been significant improvements as we shifted our focus from simple one-to-one mapping to investigations of different multiplexed communication strategies [162]. It seems that the relationship varies according to the gradient of unimodal to transmodal hierarchical representation of cortex [163]. Not only the structure-function mapping varies across this gradient, but also inter-individual differences were reported to be higher in multimodal areas compared to unimodal areas [147]. Indeed, all types of connectivities exhibit rich dynamics. We observe changing patterns in scales from milliseconds to years. Currently, the FC has been conceived as a multistable process wherein the patterns pass through multiple discrete states. Analyzing these states bring important features serving as biomarkers to disease conditions [173]. There are several factors behind fluctuations in connectivity, one of them being artifactual due to our estimation methods or the presence of noise. Discerning between true and false differences among subjects is of the highest importance to understand rich brain dynamics.

Our current methods investigate the brain with increasing complexity. Hand in hand with the complexity comes increasing dimensionality of results. Graph theory offers an elegant way of how to characterize the properties of brain networks. We reviewed the methods that identify critical regions, quantify communication efficacy, and examine functional segregation. We already knew that the segregated large-scale communities correspond to distinct functional systems and convey functional specialization [191, 196].

However, now we are able to track how the brain reconfigures to accommodate for task demands. Investigating graph dynamics brings new tools for quantifying how the brain balances the functional specialization via segregation and coordinates the activity of distributed regions via integration. This dynamic network reconfiguration is a fundamental neurophysiological process that supports the idea of a dynamic, adaptable brain network configuration underlying successful cognition [17, 206, 211].

We feel that at the beginning of big data neuroscience, it is of utmost importance to be able to critically assess all aspects of performed analyses. Firstly, it could help shape the research question. For example, in the context of epilepsy, the seizure onset zone was reported to display altered connectivity patterns, especially in higher frequency bands. Therefore, to solve the task of seizure prediction and localization, one could turn to intracranial EEG data and analyze coherence or partial directed coherence in the gamma band. This is an oversimplified example; however, it should illustrate that the question, data, and method are closely linked. Having an overview of different methods could save time and resources that would be spent in exhaustive testing of all possible algorithms and their complicated comparisons. Secondly, knowing the methods helps to prevent mistakes in their interpretation. Acknowledging that EEG could display spurious increases in connectivity due to volume conduction, one can also investigate the imaginary part of coherency to provide additional support to the conclusions. Therefore, the success of analysis lies in the ability to step back, overview the methodology, and assess the results and all potential risks, dangers, and confounds.

However, this thesis intended not only to review current methods, issues, and applications but mainly to present original research associated with some of the mentioned issues. More specifically, we addressed several specific questions:

- How to estimate the quality of connectivity estimates in fMRI?
- How does the quality depend on head motion, preprocessing, or applied parcellation?
- How to perform whole-brain network analysis in iEEG?
- Can we observe network reconfiguration also on a millisecond scale?
- What are the mechanisms of successful recognition of visual stimuli?
- How does the connectivity change as the brain approaches seizure?

These questions are highly relevant to the field of neuroscience, and their investigation needed the combination of state-of-the-art algorithms as well as deriving new approaches. Moreover, these questions investigate connectivity on different timescales. We began with characterizing static FC in rs-fMRI. Then, we moved towards mapping fast connectivity dynamics in iEEG on the scales of milliseconds. Finally, we searched for connectivity changes driving epileptogenesis on the scope of hours and days. Altogether, these studies demonstrate the various aspects and use that connectivity offers to current neuroscientific research. Moreover, the investigation itself brought new questions and hypotheses that could be tested in future studies. We now summarize the main contributions of each project.

Quality of rs-fMRI connectivity estimates

The first research was of methodological nature. Previous studies reported that functional connectivity estimates are known to be detrimentally affected by various artifacts, including those due to in-scanner head motion. Even though the degradative effect of head motion is theoretically acknowledged, it is prone to be neglected in practice. There is still a lack of a sufficiently sensitive and robust measure that would quantify the individual functional connectivity quality. We proposed that similarity with a group-mean FC matrix could serve as a reliable template to which subjects are compared. While minor or moderate deviations may represent effects of interest corresponding to inter-individual variation in brain function, larger anomalies are likely to arise due to artifactual sources of signal variation and should be subject to screening. Indeed, we extensively studied this index across atlas granularity, preprocessing options, and various datasets. The Typicality of Functional Connectivity allows extensive use in screening data quality, comparing high-movement groups or denoising strategies, and choosing optimal brain parcellation. We paid special attention to head motion, but in principle, the index is also sensitive to other types of artifacts, processing errors, and possibly also brain pathology. The estimation of connectivity quality is connected to many issues discussed in this thesis. Each examination of inter-subject variability needs to carefully consider all possible confounding effects. Moreover, it could serve as one of the tools measuring preprocessing pipeline efficacy. The current lack of consensus on optimal pipeline hampers all connectivity analyses.

Fast timescale connectivity dynamics in iEEG

The second, more experimental research combined several important aspects. Mainly, it is the first whole-brain data-driven analysis on recognition memory. Commonly, recognition memory is studied by analyzing the activity of *a priori* defined regions such as the hippocampus or perirhinal cortex. Even though they are critical for the task, there is a surprisingly large number of brain regions that are activated as well. Only their synchronized activity leads to successful recognition. However, how and when the regions are synchronized was unknown. It was due to the fact that current studies of whole-brain network dynamics are based either on fMRI or EEG. Thus, we investigated network dynamics using iEEG data. Of course, there are inherent disadvantages to iEEG, such as the fact that subjects suffer from epilepsy, their implantation varies significantly, and the sample size is small. Nevertheless, using various techniques, including mapping electrodes to fMRI atlases or using vertical regression to estimate causality, we tried to overcome these obstacles. We confirmed previous results that the task generates rich connectivity patterns and forces the brain to dynamically balance segregation and integration. Moreover, for the first time, we present how, in 300 ms, the brain undergoes a massive dynamic functional reorganization phase that involves several networks. Now we dispose of a robust working pipeline that can be further improved by acquiring more subjects or using frequency-resolved measures. Until now, we investigated only the broadband signal without paying attention to distinct frequencies. As this next step would generate additional dimensions of data, using machine learning techniques is desirable. Moreover, the study generated specific questions about the mechanisms of recognition memory, such as what physiological mechanisms enable the transition between different networks. Indeed, the whole-brain dynamic connectivity analyses using intracerebral EEG offer a promising avenue to study different classes of cognitive abilities.

Modeling epileptogenesis using connectivity

Finally, the third project was focused on brain dysfunction rather than brain function. More specifically, we presented preliminary results on tracking connectivity in a model of epileptogenesis. We illustrated how connectivity changes as the susceptibility to seizure increases. We found several driving factors of these connectivity alterations, namely

decreasing drug dosage, presence of spikes and high-frequency oscillations, and long-term fluctuations. The next step is to localize the changes with respect to epileptogenic zones. Furthermore, we found major changes hours before the first seizure, but future research will focus on more subtle fluctuations days prior to the seizure. Although we presented only a single subject case, such methodology will be applied to a cohort of already recorded subjects. Even though connectivity estimates are not comparable across subjects due to different electrode implantations, the driving factors of epileptogenesis are. Moreover, once collected enough data, modern machine learning tools could further help discover hidden patterns that could serve as biomarkers of brain state alterations. Ultimately, identifying critical aspects of epileptogenesis could serve as potential targets of deep brain stimulation and prevent seizure occurrence.

8.1 Other means of estimation or application

8.1.1 Computational neuroscience

There are many other ways where connectivity estimates can be applied or how they can be derived. One large field of neuroscience that we almost completely omitted here is computational modeling. Computational neuroscience is defined as

> *"The field of study in which mathematical tools and theories are used to investigate brain function. It can also incorporate diverse approaches from electrical engineering, computer science, and physics in order to understand how the nervous system processes information [351]."*

Computational neuroscience can accompany the data-driven approaches that we described here. These approaches provide essential information about structure and activity that can be incorporated into the mathematical dynamical models. They are represented by a set of differential equations that can be coupled together using SC coefficient obtained from diffusion-weighted imaging or FC estimates from fMRI studies.

Indeed the models were able to reflect and reproduce much of the dynamics and complexity of the real brain. Furthermore, by exploring possible dynamical repertoires that the models can support and their relation to the phenomena observed in the data, they can help formulate predictions and hypotheses serving as a basis for further experimental

investigation and data analyses [352]. We already pictured how computational modeling helped us understand the correspondence between structural and functional connectivity [151]. Moreover, models have been able to provide a mechanistic explanation of the origin of large-scale canonical networks [353]. Finally, recent studies modeled dynamic FC and showed that non-stationary connectivity dynamics could demonstrate a rich spatio-temporal structure and fast switching between a few discrete states as observed in empirical data [354]. All in all, computational neuroscience using the connectivity estimates can help to explain observed phenomena and thus contribute to our understanding of brain dynamics and treatment of diseases (for a review, see [352]).

Our original research can improve the derivation of functional connectivity estimates free of head motion and other artifacts. The estimates represent essential coupling parameters that bind together different nodes of the network. Moreover, these models could also help explain the observation of outliers in the distribution of typicality indices. What kind of change in network structure leads to significant degradation of FC quality? Such knowledge would help understand how different types of artifacts affect FC and how to remove them efficiently. However, coupling parameters do not necessarily have to be estimated from static rs-fMRI. Deriving coupling parameters from connectivity based on iEEG can bring further advantages as these estimates reflect fast dynamic conversely to fMRI measurements. On the other hand, computational models could shed new light on the generation of specific connectivity patterns that we observed during the first 300 ms of the recognition memory test. Furthermore, exploring and perturbing such a model could reveal mechanisms underlying unsuccessful recognition, i.e., how does a mismatch between stimulus and anticipated motor response arise. Finally, computational models play an invaluable role in understanding the mechanisms of seizure generation. Having a good representative model of epilepsy dynamics can identify critical transitions and thus a way how to prevent them.

8.1.2 Connectivity and stimulation

At the beginning of the connectivity chapter, we mentioned a powerful tool for connectivity estimation. Brain connectivity can also be estimated via the brain's response to perturbation and stimulation. Although we talked about invasive stimulation, several

methods are capable of non-invasive stimulation as well. These methods include transcranial magnetic stimulation (TMS), focused pulsed ultrasound, or transcranial direct current stimulation. Currently, TMS is the most commonly used method (see [355]). It utilizes short, rapidly changing magnetic field pulses to induce electrical currents in underlying cortical tissue. According to a large body of studies, TMS modulates neuronal activity not only at the site of stimulation, but the effects can propagate, impacting a distributed network of brain regions. There are multiple ways of how to estimate connectivity between separate cortical areas. One example is to perform a dual-coil experiment by pairing stimulations together with two TMS coils. This technique is powerful in probing the timing and directionality of the connectivity between cortical regions [355]. Moreover, TMS can be paired with imaging techniques, such as EEG, PET, and fMRI.

However, there are several limitations to these approaches. One of them that exogenously and artificially induced perturbations may create connectivity patterns that are different from those revealed under more physiological conditions [355]. Moreover, TMS selectively targets areas along the cortical surface, and even though techniques to target subcortical areas are being developed, selectivity remains an issue [356]. Nevertheless, TMS should not be viewed as an alternative to fMRI but rather as a complementary approach because it offers a good temporal resolution and, most importantly ability to exert causal perturbations. Therefore, combining these two methods holds great promises.

One of the applications could be the treatment of neurological disorders. Using FC and methods of graph theory, we are able to identify pathological network interactions or sources of pathological activity. TMS could target these sources and, with repeated stimulation, restore normal functioning. Precise identification and localization of pathological activity is a key parameter. The TFC could be used as a biomarker by highlighting which part of the network shows the highest atypicality and hence is subject to atypical functionality. Another potential use is the experimental modulation of FC patterns in order to change cognitive state or behavioral performance. Successful change in performance would provide causal evidence for the cognitive and behavioral relevance of connectivity dynamics [169]. Moreover, it would help us uncover the mechanisms by which the brain transition from one brain state to another.

Finally, iEEG has primarily been used for seizure onset zone identification in epilepsy

patients. As the cortex displays hyperexcitability when approaching seizure, graph metrics have been proven to successfully identify the epileptogenic network [357]. Moreover, the cortex could be modeled by means of computation modeling. By thorough examination of the model, stimulation frequency and exact stimulation target can be found within the network. The gained knowledge could be further used to precisely guide TMS stimulation. Successful stimulation can then prevent the brain from transitioning to the ictal state. There is a whole field of network control that offers an elegant and mathematically tractable framework that naturally links brain connectivity, dynamics, and activity [185].

8.2 Big data - challenges and future directions

We are entering an era of big data and open neuroscience. A continuously increasing number of available online neuroscience databases provide information regarding gene expression, neurons, macroscopic brain structure, and neurological or psychiatric disorders. Moreover, there are many new initiatives, such as the Human Connectome Project, the UK Biobank Imaging Study, or the Enhancing NeuroImaging Genetics through Meta-Analysis (ENIGMA), that aim to create a large dataset with thousands of subjects. That is a big shift compared to the early 1990s when the typical fMRI analysis included only several subjects [5]. However, these extreme amounts of data will require new statistical approaches in everyday data analysis.

We witness a large increase in not only sample size, i.e., the number of scanned subjects, but also in the number of observed parameters per subject. UK Biobank already has tens of thousands of recorded participants with different features available. When the number of participants largely exceeds the number of features, we talk about a "long-data" setting. On the other hand, in the context of neuroimaging, we scan the brain with increasing spatial and temporal resolution, which in fMRI can be regarded as measuring more voxels more often. Moreover, using connectivity measures, we study relationships between tens of thousands of voxels. These relationships further evolve in time and frequency, adding more dimensions to the analysis. Therefore, we talk about a high-dimensional "wide-data" setting (the number of variables is much higher than the number of participants) [358]. These miss-proportions can lead to the so-called curse of dimensionality [359]. Due to the dimensionality increase, the volume of the space increases

so fast that the available data becomes sparse. The sparsity then leads to the fact that increasingly subtle differences are deemed significant, which is very problematic for statistical inference. Therefore, the increase in data abundance and complexity will challenge many classical statistical methods.

As a consequence of increasing sample size, it possible to extract details and nuances from the data distribution that would be indistinguishable from random fluctuations in small studies. Moreover, more data points allow for a higher number of parameters to be reliably estimated, which in return can produce models with extremely complex statistical relationships. Bzdok & Yeo [360] predicts four new trends that we will encounter more and more often. Firstly, parametric methods will be complemented by flexible non-parametric methods. Non-parametric methods make weaker assumptions about the underlying structure of the acquired brain data. Moreover, they can capture higher-order non-linear interactions in the data and are able to represent more subtle aspects of the brain. Typical representatives of non-parametric models are k-means, decision trees, or kernel support vector machines.

Another important advantage of these methods is that the number of model parameters scales naturally with the number of participants. The second trend includes the applications of a generative model that will accompany discriminative methods. The generative methods aim to uncover the mechanisms for how the observed data arose. A typical representative is ICA. ICA separates a multivariate signal into additive subcomponents and finds hidden multivariate patterns that explain the variation in the data. In the context of epilepsy, we face the challenge of large variability, and we are unable to control for all factors. Being able to exploit the data-hungry approaches in data-driven analysis can help to generate exact research questions as the data are being analyzed. The third tendency is to utilize Bayesian approaches along with frequentist inference. Bayesian methods make the use of *a priori* assumptions placed on the model parameters. Finally, out-of-sample generalization will become an attractive alternative to classical null-hypothesis hypothesis testing.

In the wide-data scenario, it is more challenging to address the multiple comparisons problem [358]. As already stated, due to the large mismatch between the number of variables and subjects, it is increasingly difficult to distinguish between statistical and

practical significance. Classical statistics, such as t-tests or ANOVA, are based on pre-specified modeling assumptions and cannot make use of unseen or future data points. Therefore, they are referred to as retrospective models [360]. On the other hand, out-of-sample generalization focuses on accurate statements about new, previously unseen data (e.g., subjects or participants). The prediction success in new individuals is directly linked with clinical relevance because the diagnostic algorithm gathers information from all available patients to make inferences about a new subject. This is the important difference between inference and prediction. Instead of isolating important variables, the focus shifts to identifying variables that together enable accurate prediction of outcomes based on new data [361]. In other words, we are not looking for significant differences between connectivity before and during a seizure (in terms of low p-value), but we are interested in predicting transition to seizure state.

The out-of-sample estimates are typically employed in many machine learning approaches. Machine learning (ML) is defined as:

> *"The use and development of computer systems that are able to learn and adapt without following explicit instructions, by using algorithms and statistical models to analyse and draw inferences from patterns in data."*

Machine learning algorithms build models of the observed data (called training data) to make predictions or decisions about new unobserved data. They have the power to prospectively characterize and predict the development because they are able to capitalize on the high dimensionality and multivariate nature of data by pattern-learning algorithms. The algorithms make minimal assumptions about the data-generating systems and are driven by a single goal, and that is the maximal predictive power. They allow us to extract the dimensions that explain the most variance in our data. In a way, they let the brain data "speak for themselves". Interestingly, their functionality is not that different from the brain. The brain gathers multisensory information to make relevant inferences. Similarly, ML algorithms must learn the structure from large multidimensional data [362]. Moreover, they make use of data from multiple modalities. Allowing them to fully interact and inform each other leads to more powerful biomarkers. Therefore, multimodal neuroimaging features combined with machine learning classification algorithms have been widely applied to discriminate patients with various brain diseases from healthy controls

(for review, see [363]). Apart from classification, neuroimaging-based ML regression approaches have been used to predict continuous variables, such as behavioral or cognitive abilities [364]. However, a caveat in methods lacking an explicit model is the explainability and interpretability, i.e., how they relate to existing biological knowledge (Fig. 8.1). Furthermore, the classifier's discriminative power could be diminished by the overlapping or similar symptoms of various diseases [365].

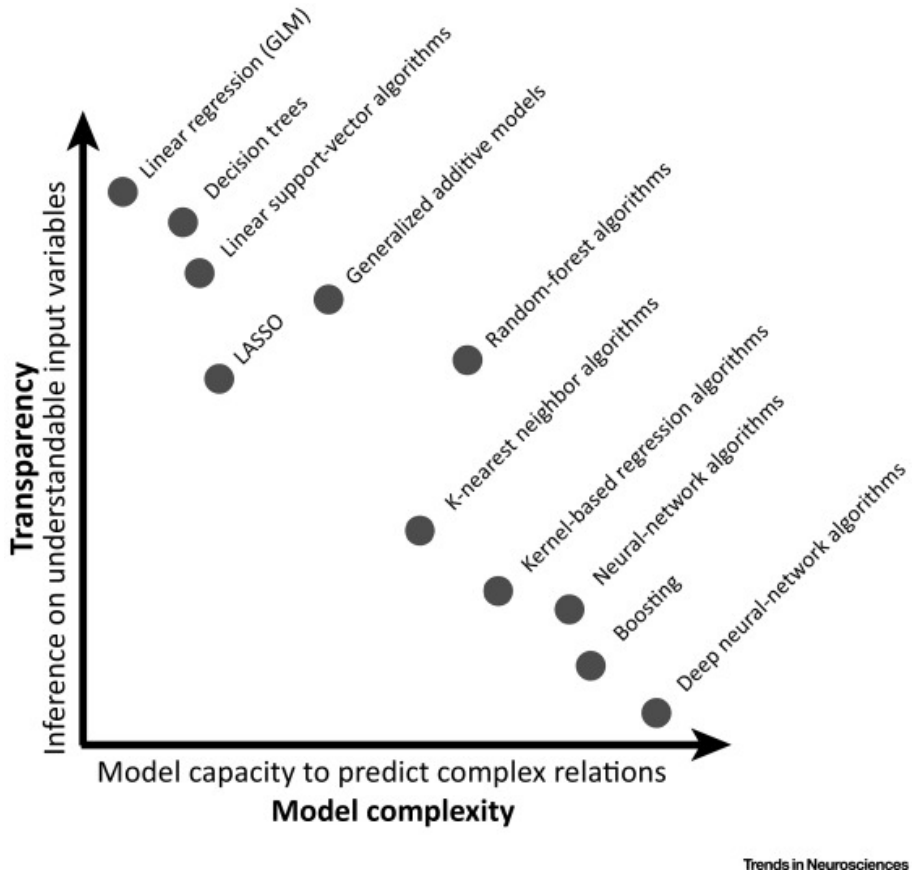

Figure 8.1: Machine learning methods and their characteristics. Machine learning methods represent a powerful tool in capturing underlying patterns. However, the ability to predict complex relations is compensated by explainability and interpretability. In the search for the maximum predictive power, the most complex algorithms have only low transparency and act as black-box models. Adopted from [361].

In conclusion, we already knew that brain-imaging has the potential to improve diagnosis, risk detection, and disease treatment in single patients. Now entering the "big-data" neuroimaging, we will need to adapt our tools to be more in line with current needs and more efficient in current goals. We gather data from more subjects with ever-increasing precision. In the high dimensional space, machine learning algorithms might help to

generate new, testable hypotheses by revealing hidden structures in the data. The algorithms benefit from the multimodal nature of the data enabling them to utilize both structural data (for example, in the form of fractal anisotropy) and functional data (in the form of connectivity estimates either from fMRI or EEG). By combining these different aspects, we can greatly improve our prediction of various neurological disorders. Moreover, TFC could represent another aspect providing additional information and performance enhancement. Furthermore, the ML tools have an invaluable role in seizure prediction in iEEG recordings since they are able to find hidden patterns in the data. As we saw, dimension reducing methods uncovered epileptogenesis pathways that help visualize connectivity progression towards a seizure. The number of studies using ML in clinical research significantly increased in recent years [366]. Thanks to the accumulation of relevant data and the development of increasingly effective algorithms, we advanced in the diagnosis, surgical treatment, intra-operative assistance, and postoperative predicting of outcomes in many clinical scenarios. We improved detection mechanisms for Alzheimer's disease and other cognitive impairments as well as the characterization of various brain tissues, including brain tumors [363]. Finally, the aim is not to replace our current methods but to accompany them with new tools in a converging fashion with a common goal - understanding complex brain mechanisms.

8.3 Novel advances in methodology

There are many paths for future neuroscientific research. The speed of progress is continually increasing as it has never been so easy to collaborate among teams from different parts of the world. Moreover, it became a standard to put emphasis on open data research. Therefore, a researcher could easily use data recorded by other teams or reproduce results from other analyses. Experimentally based teams could benefit from algorithms derived by more methodologically focused groups. Neuroscience is a multidisciplinary field, and that should be reflected in large collaborations among teams and in great diversity within a team. Even more, the big data era will significantly change our current work conditions. We got used to the fact that programming became a fundamental skill for each researcher; maybe, working knowledge of machine learning will be the next skills that we will soon take for granted. Hand in hand with the growth of our data repositories come

the advances in imaging techniques and methodology. There are several promising lines of research in terms of connectivity estimation and network exploration that we think will aid in investigating underlying phenomena.

We mentioned that one of the disadvantages of dynamic connectivity estimation is the arbitrary selection of window length. There are both concerns for a too long and too short window. A lower limit to safely avoid artifacts is set to the largest wavelength present in the preprocessed fMRI signal [172]. On the other hand, a short window increases the risks of introducing spurious fluctuations [165]. A future method could benefit from the use of Kalman filters combined with Granger causality. Kalman filter adaptively estimates the multivariate autoregressive model and thus provide a dynamic estimate of effective connectivity. Therefore, the use of the window is omitted. Moreover, it allows for avoiding the stationarity assumption in standard multivariate autoregressive modeling. Indeed, having a model for non-stationary network dynamics is one of the current theoretical challenges. However, Kalman filter-based models are very computationally expensive. Therefore, a future challenge is an effective implementation of these algorithms so that they are feasible even in very large datasets.

Another new emerging field is graph signal processing (GSP). Given how much structural connectivity mediates functional connectivity, GSP offers a new way to incorporate brain structure when studying brain activity. In this framework, signals recorded at the nodes of the graph are studied atop the underlying graph structure. Hence the important distinction is that we do not operate in the classical regular domains such as time or space but rather in irregular domains that can be conveniently represented by a graph. There is an increasing number of fundamental operations that have been generalized to the graph setting. Starting with the graph Fourier transform, we can define low graph frequency components representing signals that change slowly with respect to brain networks and high graph frequency components representing signals that change swiftly with respect to the connectivity networks. Having the notion of graph frequency components, we can apply graph filters. Finally, other operations, such as surrogate data generation or decompositions informed by cognitive systems, were derived as well. Moreover, this rapid development of theory is accompanied by new applications spanning many areas, including neuroscience (for a review, see [367]). In summary, GSP offers a novel framework for analyzing brain imaging data where both structural and functional brain data

are integrated by studying the interplay between graphs and signals on graphs.

In terms of network neuroscience, we already discussed dynamic and multilayer networks as modern tools of brain circuit investigations. Much research has already been done on the topic of dynamic networks in fMRI. There is a challenging question of how these dynamics relate to the network dynamics of iEEG networks. We presented a framework on how to derive such metrics. It will be interesting to investigate how these two relate to each other. Specifically, whether the dynamics revealed in iEEG correspond, after an aggregation, to dynamics observed in fMRI. We showed that the brain is able to undergo a massive reconfiguration, even in less than 300 ms. Compared to the increasing number of publications on fMRI network dynamics, multilayer network research is only beginning. Nevertheless, this approach holds great promise as it can integrate information from different modalities such as fMRI, MEG, or iEEG or different kinds of information, e.g., structural and functional connectivity. Finally, Sporns [183] predicts tools from algebraic topology and topological data analysis to contribute to future research. Currently, we assume pairwise (directed or undirected) connections. However, higher-order interactions can be highly informative for understanding the non-random attributes of brain networks. The study of complexes or simplices as well as investigating mesoscale structure present in complex network data could provide useful markers for clinical diagnosis and treatment as these methods capitalize on higher-order and high-dimensional features that have so far been inaccessible with simple graph methods. Future models of network mechanisms should indeed incorporate knowledge across different scales. It would be particularly interesting to relate the dynamics of the micro- (at the neuronal level), meso- and large-scales in the same model (e.g., [368]).

The shift from brain mapping to the connectomics perspective of the human brain put connectivity into the spotlight of current research. Network neuroscience witnessed a sharp increase in popularity as it is an elegant follow-up to connectivity estimation. Nevertheless, there are also other high-prolific branches of neuroscience, such as computational modeling. Both network neuroscience and computational modeling have their strengths and weaknesses. Our computational models are currently represented by individual brain circuits performing specific computational functions. However, future research will use models of many interconnected circuits to reflect the rich dynamics present at the level of whole-brain [5]. On the other hand, networks treat their nodes equivalently as if they are

homogeneous. However, we know that there is a large variation among them. Annotation of nodes and edges can address this issue. Annotated graphs allow for scalar values or categories to be associated with each node. This extra layer of information could help us understand the relationships between regional characteristics and inter-regional estimates of structural or functional connectivity [369]. Moreover, it can be useful for identifying biologically meaningful network communities. In the end, it will be necessary to bridge computational modeling and network neuroscience to develop a fuller understanding of how the brain gives rise to high-level cognitive functions [5].

Finally, a few other aspects relevant to the whole neuroscientific field should not be omitted. The first issue is connected to the ever-increasing number of data repositories. In order to facilitate collaboration, increase reproducibility, and improve comparability, a unified (or even just a general) consensus on an optimal preprocessing pipeline, mainly for fMRI, would greatly benefit the whole community. However, we acknowledge that there are still unresolved issues such as minimizing the influence of head motion. Furthermore, a unified terminology will simplify the understanding of already a vast field. Even upon discussing various challenges and future directions, there are still fundamental questions to be answered. For example, how does the brain switches between regional segregation and system-wide integration? Nowadays, we possess the perfect tools, namely the publicly shared data, analytic framework, and computational resources, to investigate such a question. However, answering it will require collaborative, multidisciplinary, and open work.

Chapter 9

Conclusion

In this thesis, we went from the beginnings of functional neuroimaging to state-of-the-art methods of analyzing network dynamics. In the vast field of imaging techniques and mathematical tools, I tried to introduce important concepts, stress differences, and show possible applications. Hopefully, even though sometimes very methodological, this work could serve as a short summary of modern functional neuroscience. Moreover, I applied the gained knowledge to three specific questions. The original research ranges from the methodological investigation of functional connectivity in fMRI to experimental analyses of effective connectivity in iEEG underlying brain function and dysfunction. The modest goal was that the obtained results at least partially answer some of the many challenges that current neuroscience is facing. Finally, as we entered a new era of open big data neuroscience, I tried to illustrate a few possible pathways for future research. No matter which path will be followed, the field will remain exciting, diverse, and multidisciplinary even more than it is now.

Bibliography

1. Azevedo, F. A. C. *et al.* Equal numbers of neuronal and nonneuronal cells make the human brain an isometrically scaled-up primate brain. *The Journal of Comparative Neurology* **513,** 532–541 (2009).
2. Ackerman, S. *The Development and Shaping of the Brain* (National Academies Press (US), 1992).
3. Milner, P. M. *The Autonomous Brain: A Neural Theory of Attention and Learning* ISBN: 978-1-135-67027-6 (Psychology Press, 1999).
4. Yeung, A. W. K., Goto, T. K. & Leung, W. K. The Changing Landscape of Neuroscience Research, 2006–2015: A Bibliometric Study. *Frontiers in Neuroscience* **11** (2017).
5. Bassett, D. S. *et al.* Reflections on the past two decades of neuroscience. *Nature Reviews Neuroscience* **21,** 524–534 (2020).
6. Bressler, S. L. & Menon, V. Large-scale brain networks in cognition: emerging methods and principles. *Trends in Cognitive Sciences* **14,** 277–290 (2010).
7. Fox, M. D. Mapping Symptoms to Brain Networks with the Human Connectome. *New England Journal of Medicine* **379,** 2237–2245 (2018).
8. Joutsa, J., Horn, A., Hsu, J. & Fox, M. D. Localizing parkinsonism based on focal brain lesions. *Brain: A Journal of Neurology* **141,** 2445–2456 (2018).
9. Burke, M. J. *et al.* Mapping migraine to a common brain network. *Brain* **143,** 541–553 (2020).
10. Fox, M. Brain Lesions Associated With Depression are Characterized by a Unique Pattern of Brain Connectivity. *Biological Psychiatry* **83,** S46–S47 (2018).
11. Mišić, B. *et al.* Network-Level Structure-Function Relationships in Human Neocortex. *Cerebral Cortex* **26,** 3285–3296 (2016).
12. Xu, J. *et al.* Large-Scale functional network overlap is a general property of brain functional organization: Reconciling inconsistent fMRI findings from general-linear-model-based analyses. *Neuroscience and biobehavioral reviews* **71,** 83–100 (2016).
13. Sejnowski, T. J. & Churchland, P. S. in *Foundations of cognitive science* 301–356 (The MIT Press, 1989).
14. Sporns, O. Network attributes for segregation and integration in the human brain. *Current Opinion in Neurobiology* **23,** 162–171 (2013).
15. Petersen, S. E. & Sporns, O. Brain Networks and Cognitive Architectures. *Neuron* **88,** 207–219 (2015).
16. Varela, F., Lachaux, J.-P., Rodriguez, E. & Martinerie, J. The brainweb: Phase synchronization and large-scale integration. *Nature Reviews Neuroscience* **2,** 229–239 (2001).
17. Fries, P. A mechanism for cognitive dynamics: neuronal communication through neuronal coherence. *Trends in Cognitive Sciences* **9,** 474–480 (2005).

18. Buzsáki, G. & Draguhn, A. Neuronal oscillations in cortical networks. *Science* **304,** 1926–1929 (2004).
19. Lisman, J. E. Bursts as a unit of neural information: making unreliable synapses reliable. *Trends in Neurosciences* **20,** 38–43 (1997).
20. Nunez, P. L. & Srinivasan, R. *Electric Fields of the Brain: The neurophysics of EEG* ISBN: 978-0-19-505038-7 (Oxford University Press, 2006).
21. Katzner, S. *et al.* Local origin of field potentials in visual cortex. *Neuron* **61,** 35–41 (2009).
22. *What is Brain Mapping?* `https://worldbrainmapping.org/Annual-Congress/` (2020).
23. Catani, M., Thiebaut de Schotten, M., Slater, D. & Dell'Acqua, F. Connectomic approaches before the connectome. *NeuroImage* **80,** 2–13 (2013).
24. Scoville, W. B. & Milner, B. Loss of Recent Memory after Bilateral Hippocampal Lesions. *Journal of Neurology, Neurosurgery & Psychiatry* **20,** 11–21 (1957).
25. Savoy, R. L. History and future directions of human brain mapping and functional neuroimaging. *Acta Psychologica* **107,** 9–42 (2001).
26. Duffau, H. Stimulation mapping of white matter tracts to study brain functional connectivity. *Nature Reviews. Neurology* **11,** 255–265 (2015).
27. Thiebaut de Schotten, M. *et al.* Direct evidence for a parietal-frontal pathway subserving spatial awareness in humans. *Science* **309,** 2226–2228 (2005).
28. Duffau, H. The anatomo-functional connectivity of language revisited. New insights provided by electrostimulation and tractography. *Neuropsychologia* **46,** 927–934 (2008).
29. Louis, E. K. S. *et al. Electroencephalography (EEG): An Introductory Text and Atlas of Normal and Abnormal Findings in Adults, Children, and Infants* (American Epilepsy Society, 2016).
30. Seeber, M. *et al.* Subcortical electrophysiological activity is detectable with high-density EEG source imaging. *Nature Communications* **10,** 753 (2019).
31. Robbins, K. A., Touryan, J., Mullen, T., Kothe, C. & Bigdely-Shamlo, N. How Sensitive Are EEG Results to Preprocessing Methods: A Benchmarkin Study. *IEEE transactions on neural systems and rehabilitation engineering* **28,** 1081–1090 (2020).
32. Bigdely-Shamlo, N., Mullen, T., Kothe, C., Su, K.-M. & Robbins, K. A. The PREP pipeline: standardized preprocessing for large-scale EEG analysis. *Frontiers in Neuroinformatics* **9,** 16 (2015).
33. Vanrullen, R. Four Common Conceptual Fallacies in Mapping the Time Course of Recognition. *Frontiers in Psychology* **2** (2011).
34. Crone, N. E., Sinai, A. & Korzeniewska, A. High-frequency gamma oscillations and human brain mapping with electrocorticography. *Progress in Brain Research* **159,** 275–295 (2006).
35. Burke, J. F. *et al.* Human intracranial high-frequency activity maps episodic memory formation in space and time. *NeuroImage. New horizons for neural oscillations* **85,** 834–843 (2014).
36. Roehri, N. *et al.* High-frequency oscillations are not better biomarkers of epileptogenic tissues than spikes. *Annals of Neurology* **83,** 84–97 (2018).
37. Zhang, H., Wang, C.-D., Lai, J.-H. & Yu, P. S. Modularity in complex multilayer networks with multiple aspects: a static perspective. *Applied Informatics* **4,** 7 (2017).
38. Michel, C. M. & Brunet, D. EEG Source Imaging: A Practical Review of the Analysis Steps. *Frontiers in Neurology* **10.** ISSN: 1664-2295 (2019).

39. Grech, R. *et al.* Review on solving the inverse problem in EEG source analysis. *Journal of NeuroEngineering and Rehabilitation* **5,** 25 (2008).
40. Parvizi, J. & Kastner, S. Promises and limitations of human intracranial electroencephalography. *Nature Neuroscience* **21,** 474 (2018).
41. Reif, P. S., Strzelczyk, A. & Rosenow, F. The history of invasive EEG evaluation in epilepsy patients. *Seizure* **41,** 191–195 (2016).
42. Enatrsu, R. & Mikuni, N. Invasive evaluations for Epilepsy Surgery: A Review of the Literature. *Neurologia medico-chirurgica* **56,** 221–227 (2016).
43. Catani, M. & Thiebaut de Schotten, M. A diffusion tensor imaging tractography atlas for virtual in vivo dissections. *Cortex; a Journal Devoted to the Study of the Nervous System and Behavior* **44,** 1105–1132 (2008).
44. Sutterer, M. J. & Tranel, D. Neuropsychology and cognitive neuroscience in the fMRI era: A recapitulation of localizationist and connectionist views. *Neuropsychology* **31,** 972–980 (2017).
45. Logothetis, N. K., Pauls, J., Augath, M., Trinath, T. & Oeltermann, A. Neurophysiological investigation of the basis of the fMRI signal. *Nature* **412,** 150–157 (2001).
46. Vazquez, A. L. & Noll, D. C. Nonlinear Aspects of the BOLD Response in Functional MRI. *NeuroImage* **7,** 108–118 (1998).
47. Bianciardi, M. *et al.* Sources of functional magnetic resonance imaging signal fluctuations in the human brain at rest: a 7 T study. *Magnetic Resonance Imaging* **27,** 1019–1029 (2009).
48. Chang, C. & Glover, G. H. Relationship between respiration, end-tidal CO2, and BOLD signals in resting-state fMRI. *NeuroImage* **47,** 1381–1393 (2009).
49. Poldrack, R. A., Mumford, J. A. & Nichols, T. E. *Handbook of Functional MRI Data Analysis* (Cambridge University Press, 2011).
50. Murphy, K., Birn, R. M. & Bandettini, P. A. Resting-state fMRI confounds and cleanup. *NeuroImage* **80,** 349–359 (2013).
51. Hlinka, J., Alexakis, C., Hardman, J. G., Siddiqui, Q. & Auer, D. P. Is sedation-induced BOLD fMRI low-frequency fluctuation increase mediated by increased motion? *Magnetic Resonance Materials in Physics, Biology and Medicine* **23,** 367–374 (2010).
52. Van Dijk, K. R. A., Sabuncu, M. R. & Buckner, R. L. The influence of head motion on intrinsic functional connectivity MRI. *NeuroImage* **59,** 431–438 (2012).
53. Power, J. D., Barnes, K. A., Snyder, A. Z., Schlaggar, B. L. & Petersen, S. E. Spurious but systematic correlations in functional connectivity MRI networks arise from subject motion. *NeuroImage* **59,** 2142–2154 (2012).
54. Satterthwaite, T. D. *et al.* Impact of in-scanner head motion on multiple measures of functional connectivity: Relevance for studies of neurodevelopment in youth. *NeuroImage* **60,** 623–632 (2012).
55. Bright, M. G. & Murphy, K. Removing motion and physiological artifacts from intrinsic BOLD fluctuations using short echo data. *NeuroImage* **64,** 526–537 (2013).
56. Mowinckel, A. M., Espeseth, T. & Westlye, L. T. Network-specific effects of age and in-scanner subject motion: A resting-state fMRI study of 238 healthy adults. *NeuroImage* **63,** 1364–1373 (2012).
57. Satterthwaite, T. D. *et al.* An improved framework for confound regression and filtering for control of motion artifact in the preprocessing of resting-state functional connectivity data. *NeuroImage* **64,** 240–256 (2013).

58. Tyszka, J. M., Kennedy, D. P., Paul, L. K. & Adolphs, R. Largely Typical Patterns of Resting-State Functional Connectivity in High-Functioning Adults with Autism. *Cerebral Cortex* **24,** 1894–1905 (2014).

59. Yan, C.-G. *et al.* A comprehensive assessment of regional variation in the impact of head micromovements on functional connectomics. *NeuroImage* **76,** 183–201 (2013).

60. Van Dijk, K. R. A. *et al.* Intrinsic Functional Connectivity As a Tool For Human Connectomics: Theory, Properties, and Optimization. *Journal of Neurophysiology* **103,** 297–321 (2009).

61. Pruim, R. H. R., Mennes, M., Buitelaar, J. K. & Beckmann, C. F. Evaluation of ICA-AROMA and alternative strategies for motion artifact removal in resting state fMRI. *NeuroImage* **112,** 278–287 (2015).

62. Ciric, R. *et al.* Benchmarking of participant-level confound regression strategies for the control of motion artifact in studies of functional connectivity. *NeuroImage* **154,** 174–187 (2017).

63. Aurich, N. K. *et al.* Evaluating the reliability of different preprocessing steps to estimate graph theoretical measures in resting state fMRI data. *Frontiers in Neuroscience* **9,** 48 (2015).

64. Esteban, O. *et al.* fMRIPrep: a robust preprocessing pipeline for functional MRI. *Nature Methods* **16,** 111–116 (2019).

65. Thirion, B., Varoquaux, G., Dohmatob, E. & Poline, J.-B. Which fMRI clustering gives good brain parcellations? *Frontiers in Neuroscience* **8,** 167 (2014).

66. Shen, X., Tokoglu, F., Papademetris, X. & Constable, R. T. Groupwise whole-brain parcellation from resting-state fMRI data for network node identification. *NeuroImage* **82,** 403–415 (2013).

67. Zalesky, A. *et al.* Whole-brain anatomical networks: does the choice of nodes matter? *NeuroImage* **50,** 970–983 (2010).

68. Arslan, S. *et al.* Human brain mapping: A systematic comparison of parcellation methods for the human cerebral cortex. *NeuroImage* **170,** 5–30 (2018).

69. Mesulam, M. The evolving landscape of human cortical connectivity: facts and inferences. *NeuroImage* **62,** 2182–2189 (2012).

70. Thiebaut de Schotten, M. *et al.* Visualization of disconnection syndromes in humans. *Cortex; a Journal Devoted to the Study of the Nervous System and Behavior* **44,** 1097–1103 (2008).

71. Sporns, O. The human connectome: origins and challenges. *NeuroImage* **80,** 53–61 (2013).

72. Hux, K. in *Encyclopedia of Clinical Neuropsychology* 2702–2703 (Springer, 2011).

73. Ramón y Cajal, S. *Estructura del asta de Ammon y fascia dentata* (tip. de Fortanet, Madrid, 1893).

74. Felleman, D. J. & Van Essen, D. C. Distributed hierarchical processing in the primate cerebral cortex. *Cerebral Cortex* **1,** 1–47 (1991).

75. Thiebaut de Schotten, M., Croxson, P. L. & Mars, R. B. Large-scale comparative neuroimaging: Where are we and what do we need? *Cortex* **118,** 188–202 (2019).

76. Horwitz, B. The elusive concept of brain connectivity. *NeuroImage* **19,** 466–470 (2003).

77. Brazier, M. A. B. & Barlow, J. S. Some applications of correlation analysis to clinical problems in electroencephalography. *Electroencephalography and Clinical Neurophysiology* **8,** 325–331 (1956).

78. Aertsen, A. & Preissl, H. Dynamics of activity and connectivity in physiological neuronal networks. *Nonlinear Dynamics and Neuronal Networks,* 281–301 (1991).

79. Sporns, O. Brain connectivity. *Scholarpedia* **2,** 4695 (2007).

80. Sporns, O. Contributions and challenges for network models in cognitive neuroscience. *Nature Neuroscience* **17,** 652–660 (2014).

81. Lord, L.-D., Stevner, A. B., Deco, G. & Kringelbach, M. L. Understanding principles of integration and segregation using whole-brain computational connectomics: implications for neuropsychiatric disorders. *Philosophical Transactions. Series A, Mathematical, Physical, and Engineering Sciences* **375** (2017).

82. Wager, T. D. & Lindquist, M. A. *Principles of fMRI* (Leanpub, 2015).

83. Bassett, D. S. & Sporns, O. Network neuroscience. *Nature Neuroscience* **20,** 353–364 (2017).

84. Aung, W. Y., Mar, S. & Benzinger, T. L. Diffusion tensor MRI as a biomarker in axonal and myelin damage. *Imaging in medicine* **5,** 427–440 (2013).

85. Jeurissen, B., Descoteaux, M., Mori, S. & Leemans, A. Diffusion MRI fiber tractography of the brain. *NMR in biomedicine* **32,** e3785 (2019).

86. Chen, Z. J., He, Y., Rosa-Neto, P., Germann, J. & Evans, A. C. Revealing Modular Architecture of Human Brain Structural Networks by Using Cortical Thickness from MRI. *Cerebral Cortex* **18,** 2374–2381 (2008).

87. Hagmann, P. *et al.* Mapping human Whole-Brain Structural Networks with Diffusion MRI. *PLOS ONE* **2,** e597 (2007).

88. Yeh, C.-H., Jones, D. K., Liang, X., Descoteaux, M. & Connelly, A. Mapping Structural Connectivity Using Diffusion MRI: Challenges and Opportunities. *Journal of Magnetic Resonance Imaging* (2020).

89. Jones, D. K. *Diffusion MRI: Theory, Methods, and Applications* ISBN: 978-0-19-536977-9 (Oxford University Press, 2011).

90. Osher, D. E. *et al.* Structural Connectivity Fingerprints Predict Cortical Selectivity for Multiple Visual Categories across Cortex. *Cerebral Cortex* **26,** 1668–1683 (2016).

91. Aertsen, A., Erb, M. & Palm, G. Dynamics of functional coupling in the cerebral cortex: an attempt at a model-based interpretation. *Physica D: Nonlinear Phenomena* **75,** 103–128 (1994).

92. Biswal, B., Yetkin, F. Z., Haughton, V. M. & Hyde, J. S. Functional connectivity in the motor cortex of resting human brain using echo-planar MRI. *Magnetic Resonance in Medicine* **34,** 537–541 (1995).

93. Greicius, M. D., Krasnow, B., Reiss, A. L. & Menon, V. Functional connectivity in the resting brain: A network analysis of the default mode hypothesis. *Proceedings of the National Academy of Sciences* **100,** 253–258 (2003).

94. Friston, K., Frith, C., Liddle, P. & Frackowiak, R. Functional Connectivity: The Principal-Component Analysis of Large (PET) Data Sets. *Journal of cerebral blood flow and metabolism* **13,** 5–14 (1993).

95. Farahani, F. V., Karwowski, W. & Lighthall, N. R. Application of Graph Theory for Identifying Connectivity Patterns in Human Brain Networks: A Systematic Review. *Frontiers in Neuroscience* **13** (2019).

96. Calhoun, V. D., Adali, T., Pearlson, G. D. & Pekar, J. J. A method for making group inferences from functional MRI data using independent component analysis. *Human Brain Mapping* **14,** 140–151 (2001).

97. Smith, S. M. *et al.* Network modelling methods for FMRI. *NeuroImage* **54,** 875–891 (2011).

98. Bastos, A. M. & Schoffelen, J.-M. A Tutorial Review of Functional Connectivity Analysis Methods and Their Interpretational Pitfalls. *Frontiers in Systems Neuroscience* **9** (2016).

99. Blinowska, K., Kus, R. & Kaminski, M. Granger causality and information flow in multivariate processes. *Physical review. E, Statistical, Nonlinear, and Soft Matter Physics* **70,** 050902–050902 (2004).

100. Meszlényi, R. J., Hermann, P., Buza, K., Gál, V. & Vidnyánszky, Z. Resting State fMRI Functional Connectivity Analysis Using Dynamic Time Warping. *Frontiers in Neuroscience* **11** (2017).

101. Stam, C. J., Pijn, J. P., Suffczynski, P. & Lopes da Silva, F. H. Dynamics of the human alpha rhythm: evidence for non-linearity? *Clinical Neurophysiology* **110,** 1801–1813 (1999).

102. Hlinka, J., Palus, M., Vejmelka, M., Mantini, D. & Corbetta, M. Functional connectivity in resting-state fMRI: Is linear correlation sufficient? *NeuroImage* **54,** 2218–2225 (2011).

103. Pereda, E., Quian, R. & Bhattacharya, J. Nonlinear multivariate analysis of Neurophysiological Signals. *Progress in neurobiology* **77,** 1–37 (2005).

104. Fornito, A., Zalesky, A. & Bullmore, E. *Fundamentals of Brain Network Analysis* in (2016).

105. Marrelec, G. *et al.* Partial correlation for functional brain interactivity investigation in functional MRI. *NeuroImage* **32,** 228–237 (2006).

106. Engel, A. K., Fries, P. & Singer, W. Dynamic predictions: Oscillations and synchrony in top–down processing. *Nature Reviews Neuroscience* **2,** 704–716 (2001).

107. Nolte, G. *et al.* Identifying true brain interaction from EEG data using the imaginary part of coherency. *Clinical Neurophysiology* **115,** 2292–2307 (2004).

108. Bowyer, S. M. Coherence a measure of the brain networks: past and present. *Neuropsychiatric Electrophysiology* **2,** 1 (2016).

109. Fries, P. Rhythms for Cognition: Communication through Coherence. *Neuron* **88,** 220–235 (2015).

110. Jensen, O. & Lisman, J. E. Hippocampal sequence-encoding driven by a cortical multi-item working memory buffer. *Trends in Neurosciences* **28,** 67–72 (2005).

111. Mormann, F., Lehnertz, K., David, P. & E. Elger, C. Mean phase coherence as a measure for phase synchronization and its application to the EEG of epilepsy patients. *Physica D Nonlinear Phenomena* **144,** 358–369 (2000).

112. Axmacher, N. *et al.* Cross-frequency coupling supports multi-item working memory in the human hippocampus. *Proceedings of the National Academy of Sciences* **107,** 3228–3233 (2010).

113. González, J. *et al.* Communication Through Coherence by Means of Cross-frequency Coupling. *Neuroscience* **449,** 157–164 (2020).

114. McLelland, D. & VanRullen, R. Theta-Gamma Coding Meets Communication-through-Coherence: Neuronal Oscillatory Multiplexing Theories Reconciled. *PLOS Computational Biology* **12,** e1005162 (2016).

115. Bonnefond, M., Kastner, S. & Jensen, O. Communication between Brain Areas Based on Nested Oscillations. *eNeuro* **4** (2017).

116. Kopal, J. *et al.* Complex continuous wavelet coherence for EEG microstates detection in insight and calm meditation. *Consciousness and Cognition* **30,** 13–23 (2014).

117. Kopal, J. *et al.* EEG Synchronizations Length During Meditation. *Journal of Medical and Biological Engineering* **37,** 220–229 (2017).

118. Chang, C. & Glover, G. H. Time–frequency dynamics of resting-state brain connectivity measured with fMRI. *NeuroImage* **50,** 81–98 (2010).

119. Lachaux, J.-P., Rodriguez, E., Martinerie, J. & Varela, F. J. Measuring phase synchrony in brain signals. *Human Brain Mapping* **8,** 194–208 (1999).

120. Bruña, R., Maestú, F. & Pereda, E. Phase locking value revisited: teaching new tricks to an old dog. *Journal of Neural Engineering* **15,** 056011 (2018).

121. Friston, K. J. Functional and effective connectivity: a review. *Brain Connectivity* **1,** 13–36 (2011).

122. Barnett, L., Barrett, A. B. & Seth, A. K. Misunderstandings regarding the application of Granger causality in neuroscience. *Proceedings of the National Academy of Sciences* **115,** E6676–E6677 (2018).

123. Fairhall, S. L. & Ishai, A. Effective Connectivity within the Distributed Cortical Network for Face Perception. *Cerebral Cortex* **17,** 2400–2406 (2007).

124. Massimini, M. *et al.* Breakdown of Cortical Effective Connectivity During Sleep. *Science* **309,** 2228–2232 (2005).

125. Geweke, J. Measurement of Linear Dependence and Feedback Between Multiple Time Series. *Journal of the American Statistical Association* **77,** 304–313 (1982).

126. Barnett, L. & Seth, A. K. The MVGC multivariate Granger causality toolbox: a new approach to Granger-causal inference. *Journal of Neuroscience Methods* **223,** 50–68 (2014).

127. Seth, A. K., Barrett, A. B. & Barnett, L. Granger Causality Analysis in Neuroscience and Neuroimaging. *Journal of Neuroscience* **35,** 3293–3297 (2015).

128. Astolfi, L. *et al.* Tracking the Time-Varying Cortical Connectivity Patterns by Adaptive Multivariate Estimators. *IEEE Transactions on Biomedical Engineering* **55,** 902–913 (2008).

129. Baccalá, L. A. & Sameshima, K. Partial directed coherence: a new concept in neural structure determination. *Biological Cybernetics* **84,** 463–474 (2001).

130. Sato, J. R. *et al.* Frequency domain connectivity identification: An application of partial directed coherence in fMRI. *Human Brain Mapping* **30,** 452–461 (2009).

131. Kaminski, M. J. & Blinowska, K. J. A new method of the description of the information flow in the brain structures. *Biological Cybernetics* **65,** 203–210 (1991).

132. Blinowska, K. J. Review of the methods of determination of directed connectivity from multichannel data. *Medical & Biological Engineering & Computing* **49,** 521–529 (2011).

133. Friston, K. J., Harrison, L. & Penny, W. Dynamic causal modelling. *NeuroImage* **19,** 1273–1302 (2003).

134. David, O. *et al.* Dynamic causal modeling of evoked responses in EEG and MEG. *NeuroImage* **30,** 1255–1272 (2006).

135. Lee, M. H., Smyser, C. D. & Shimony, J. S. Resting-State fMRI: A Review of Methods and Clinical Applications. *American Journal of Neuroradiology* **34,** 1866–1872 (2013).

136. Biswal, B. B. *et al.* Toward discovery science of human brain function. *Proceedings of the National Academy of Sciences* **107,** 4734–4739 (2010).

137. Damoiseaux, J. S. *et al.* Consistent resting-state networks across healthy subjects. *Proceedings of the National Academy of Sciences* **103,** 13848–13853 (2006).

138. Van Dijk, K. R. A. *et al.* Intrinsic functional connectivity as a tool for human connectomics: theory, properties, and optimization. *Journal of Neurophysiology* **103,** 297–321 (2010).

139. Fan, Y. *et al.* Lifespan Development of the Human Brain Revealed by Large-Scale Network Eigen. *Entropy* **19,** 471 (2017).

140. Raichle, M. E. *et al.* A default mode of brain function. *Proceedings of the National Academy of Sciences* **98,** 676–682 (2001).

141. Fransson, P. How default is the default mode of brain function? Further evidence from intrinsic BOLD signal fluctuations. *Neuropsychologia* **44,** 2836–2845 (2006).

142. Spreng, R. N. The Fallacy of a "Task-Negative" Network. *Frontiers in Psychology* **3** (2012).

143. Broyd, S. J. *et al.* Default-mode brain dysfunction in mental disorders: a systematic review. *Neuroscience and Biobehavioral Reviews* **33,** 279–296 (2009).

144. Seghier, M. L. & Price, C. J. Interpreting and Utilising Intersubject Variability in Brain Function. *Trends in Cognitive Sciences* **22,** 517–530 (2018).

145. Elton, A. & Gao, W. Task-related modulation of functional connectivity variability and its behavioral correlations. *Human Brain Mapping* **36,** 3260–3272 (2015).

146. Zilles, K. & Amunts, K. Individual variability is not noise. *Trends in Cognitive Sciences* **17,** 153–155 (2013).

147. Mueller, S. *et al. Individual variability in functional connectivity architecture of the human brain* 2013.

148. Van den Heuvel, M. P. & Sporns, O. An anatomical substrate for integration among functional networks in human cortex. *Journal of Neuroscience* **33,** 14489–14500 (2013).

149. Finn, E. S. *et al.* Functional connectome fingerprinting: identifying individuals using patterns of brain connectivity. *Nature Neuroscience* **18,** 1664–1671 (2015).

150. Oliver, I., Hlinka, J., Kopal, J. & Davidsen, J. Quantifying the Variability in Resting-State Networks. *Entropy* **21,** 882 (2019).

151. Honey, C. J. *et al.* Predicting human resting-state functional connectivity from structural connectivity. *Proceedings of the National Academy of Sciences* **106,** 2035–2040 (2009).

152. Muschelli, J. *et al.* Reduction of motion-related artifacts in resting state fMRI using aCompCor. *NeuroImage* **96,** 22–35 (2014).

153. Hohenfeld, C., Werner, C. J. & Reetz, K. Resting-state connectivity in neurodegenerative disorders: Is there potential for an imaging biomarker? *NeuroImage: Clinical* **18,** 849–870 (2018).

154. Filippi, M., Spinelli, E. G., Cividini, C. & Agosta, F. Resting State Dynamic Functional Connectivity in Neurodegenerative Conditions: A Review of Magnetic Resonance Imaging Findings. *Frontiers in Neuroscience* **13** (2019).

155. Su, J. *et al.* fMRI functional connectivity as an indicator of interictal epileptic discharges. *NeuroImage: Clinical* **24,** 102038 (2019).

156. Kuhlmann, L., Lehnertz, K., Richardson, M. P., Schelter, B. & Zaveri, H. P. Seizure prediction - ready for a new era. *Nature Reviews. Neurology* **14,** 618–630 (2018).

157. Freestone, D. R. *et al.* Seizure Prediction: Science Fiction or Soon to Become Reality? *Current Neurology and Neuroscience Reports* **15,** 73 (2015).

158. Greicius, M. Resting-state functional connectivity in neuropsychiatric disorders. *Current Opinion in Neurology* **21,** 424–430 (2008).

159. Stephan, K. E., Tittgemeyer, M., Knösche, T. R., Moran, R. J. & Friston, K. J. Tractography-based priors for dynamic causal models. *NeuroImage* **47,** 1628–1638 (2009).

160. Honey, C. J., Thivierge, J.-P. & Sporns, O. Can structure predict function in the human brain? *NeuroImage* **52,** 766–776 (2010).

161. Koch, M. A., Norris, D. G. & Hund-Georgiadis, M. An Investigation of Functional and Anatomical Connectivity Using Magnetic Resonance Imaging. *NeuroImage* **16,** 241–250 (2002).

162. Vázquez-Rodríguez, B. *et al.* Gradients of structure–function tethering across neocortex. *Proceedings of the National Academy of Sciences* **116,** 21219–21227 (2019).

163. Margulies, D. S. *et al.* Situating the default-mode network along a principal gradient of macroscale cortical organization. *Proceedings of the National Academy of Sciences* **113** (2016).

164. Suárez, L. E., Markello, R. D., Betzel, R. F. & Misic, B. Linking Structure and Function in Macroscale Brain Networks. *Trends in Cognitive Sciences* **24,** 302–315 (2020).

165. Preti, M. G., Bolton, T. A. & Van De Ville, D. The dynamic functional connectome: State-of-the-art and perspectives. *NeuroImage. Functional architecture of the brain* **160,** 41–54 (2017).

166. Ringach, D. L. Spontaneous and driven cortical activity: implications for computation. *Current Opinion in Neurobiology. Sensory systems* **19,** 439–444 (2009).

167. Calhoun, V. D., Miller, R., Pearlson, G. & Adalı, T. The Chronnectome: Time-Varying connectivity Networks as the Next Frontier in fMRI Data Discovery. *Neuron* **84,** 262–274 (2014).

168. Hutchison, R. M. *et al.* Dynamic functional connectivity: Promise, issues, and interpretations. *NeuroImage. Mapping the Connectome* **80,** 360–378 (2013).

169. Lurie, D. J. *et al.* Questions and controversies in the study of time-varying functional connectivity in resting fMRI. *Network Neuroscience* **4,** 30–69 (2019).

170. Kiviniemi, V. *et al.* A sliding time-window ICA reveals spatial variability of the default mode network in time. *Brain Connectivity* **1,** 339–347 (2011).

171. Hansen, E. C. A., Battaglia, D., Spiegler, A., Deco, G. & Jirsa, V. K. Functional connectivity dynamics: Modeling the switching behavior of the resting state. *NeuroImage* **105,** 525–535 (2015).

172. Leonardi, N. & Van De Ville, D. On spurious and real fluctuations of dynamic functional connectivity during rest. *NeuroImage* **104,** 430–436 (2015).

173. Allen, E. A. *et al.* Tracking whole-brain connectivity dynamics in the resting state. *Cerebral Cortex* **24,** 663–676 (2014).

174. Gonzalez-Castillo, J. & Bandettini, P. A. Task-based dynamic functional connectivity: Recent findings and open questions. *NeuroImage* **180,** 526–533 (2018).

175. Bassett, D. S. *et al.* Dynamic reconfiguration of human brain networks during learning. *Proceedings of the National Academy of Sciences* **108,** 7641–7646 (2011).

176. Hlinka, J. & Hadrava, M. On the danger of detecting network states in white noise. *Frontiers in Computational Neuroscience* **9,** 11 (2015).

177. Hindriks, R. *et al.* Can sliding-window correlations reveal dynamic functional connectivity in resting-state fMRI? *NeuroImage* **127,** 242–256 (2016).

178. Efron, B. & Tibshirani, R. J. *An Introduction to the Bootstrap* 456 pp. ISBN: 978-0-412-04231-7 (CRC Press, 1994).

179. Prichard, D. & Theiler, J. Generating surrogate data for time series with several simultaneously measured variables. *Physical Review Letters* **73,** 951–954 (1994).

180. Tagliazucchi, E., von Wegner, F., Morzelewski, A., Brodbeck, V. & Laufs, H. Dynamic BOLD functional connectivity in humans and its electrophysiological correlates. *Frontiers in Human Neuroscience* **6** (2012).

181. Kopell, N. J., Gritton, H. J., Whittington, M. A. & Kramer, M. A. Beyond the connectome: the dynome. *Neuron* **83,** 1319–1328 (2014).

182. Bullmore, E. & Sporns, O. Complex brain networks: graph theoretical analysis of structural and functional systems. *Nature Reviews Neuroscience* **10,** 186–198 (2009).

183. Sporns, O. Graph theory methods: applications in brain networks. *Dialogues in Clinical Neuroscience* **20,** 111–121 (2018).

184. Muldoon, S. F. & Bassett, D. S. Network and Multilayer Network Approaches to Understanding human Brain Dynamics. *Philosophy of Science* **83,** 710–720 (2016).

185. Betzel, R. Network neuroscience and the connectomics revolution. *arXiv:2010.01591 [q-bio]* (2020).

186. Rubinov, M. & Sporns, O. Weight-conserving characterization of complex functional brain networks. *NeuroImage* **56,** 2068–2079 (2011).

187. Garrison, K. A., Scheinost, D., Finn, E. S., Shen, X. & Constable, R. T. The (in)stability of functional brain network measures across thresholds. *NeuroImage* **118,** 651–661 (2015).

188. Ran, Q. *et al.* Reproducibility of graph measures at the subject level using resting-state fMRI. *Brain and Behavior* **10,** e01705 (2020).

189. Rubinov, M. & Sporns, O. Complex network measures of brain connectivity: uses and interpretations. *NeuroImage* **52,** 1059–1069 (2010).

190. Newman, M. E. J. Modularity and community structure in networks. *Proceedings of the National Academy of Sciences of the United States of America* **103,** 8577–8582 (2006).

191. Sporns, O. & Betzel, R. F. Modular Brain Networks. *Annual Review of Psychology* **67,** 613–640 (2016).

192. Lynn, C. W., Papadopoulos, L., Kahn, A. E. & Bassett, D. S. Human information processing in complex networks. *Nature Physics* **16,** 965–973 (2020).

193. Bassett, D. S. & Bullmore, E. T. Small-World Brain Networks Revisited. *The Neuroscientist: A Review Journal Bringing Neurobiology, Neurology and Psychiatry* **23,** 499–516 (2017).

194. Hlinka, J., Hartman, D. & Paluš, M. Small-world topology of functional connectivity in randomly connected dynamical systems. *Chaos: An Interdisciplinary Journal of Nonlinear Science* **22,** 033107 (2012).

195. Cohen, J. D. & Tong, F. The Face of Controversy. *Science* **293,** 2405–2407 (2001).

196. Fox, P. T. & Friston, K. J. Distributed processing; distributed functions? *NeuroImage* **61,** 407–426 (2012).

197. Wig, G. S. Segregated Systems of Human Brain Networks. *Trends in Cognitive Sciences* **21,** 981–996 (2017).

198. Bassett, D. S. *et al.* Cognitive fitness of cost-efficient brain functional networks. *Proceedings of the National Academy of Sciences* **106,** 11747–11752 (2009).

199. Achard, S. & Bullmore, E. Efficiency and Cost of Economical Brain Functional Networks. *PLOS Computational Biology* **3,** e17 (2007).

200. Cohen, J. R. & D'Esposito, M. The Segregation and Integration of Distinct Brain Networks and Their Relationship to Cognition. *The Journal of Neuroscience* **36,** 12083–12094 (2016).

201. Meunier, D., Lambiotte, R., Fornito, A., Ersche, K. D. & Bullmore, E. T. Hierarchical Modularity in Human Brain Functional Networks. *Frontiers in Neuroinformatics* **3** (2009).

202. Bassett, D. S. *et al.* Robust detection of dynamic community structure in networks. *Chaos* **23,** 013142 (2013).

203. Deco, G., Tononi, G., Boly, M. & Kringelbach, M. L. Rethinking segregation and integration: contributions of whole-brain modelling. *Nature Reviews Neuroscience* **16,** 430–439 (2015).

204. Raichle, M. E. The restless brain: how intrinsic activity organizes brain function. *Philosophical Transactions of the Royal Society of London. Series B, Biological Sciences* **370** (2015).

205. Fransson, P., Schiffler, B. C. & Thompson, W. H. Brain network segregation and integration during an epoch-related working memory fMRI experiment. *NeuroImage* **178,** 147–161 (2018).

206. Kitzbichler, M. G., Henson, R. N. A., Smith, M. L., Nathan, P. J. & Bullmore, E. T. Cognitive Effort Drives Workspace Configuration of Human Brain Functional Networks. *Journal of Neuroscience* **31,** 8259–8270 (2011).

207. Ekman, M., Derrfuss, J., Tittgemeyer, M. & Fiebach, C. J. Predicting errors from reconfiguration patterns in human brain networks. *Proceedings of the National Academy of Sciences* **109,** 16714–16719 (2012).

208. Vatansever, D., Menon, D. K., Manktelow, A. E., Sahakian, B. J. & Stamatakis, E. A. Default mode Dynamics for Global Functional Integration. *Journal of Neuroscience* **35,** 15254–15262 (2015).

209. Shine, J. M. *et al.* The Dynamics of Functional Brain Networks: Integrated Network States during Cognitive Task Performance. *Neuron* **92,** 544–554 (2016).

210. Zalesky, A., Fornito, A., Cocchi, L., Gollo, L. L. & Breakspear, M. Time-resolved resting-state brain networks. *Proceedings of the National Academy of Sciences* **111,** 10341–10346 (2014).

211. Braun, U. *et al.* Dynamic reconfiguration of frontal brain networks during executive cognition in humans. *Proceedings of the National Academy of Sciences* **112,** 11678–11683 (2015).

212. Stevens, A. A., Tappon, S. C., Garg, A. & Fair, D. A. Functional brain network modularity captures inter- and intra-individual variation in working memory capacity. *PlOS One* **7,** e30468 (2012).

213. Meunier, D. *et al.* Modular structure of functional networks in olfactory memory. *NeuroImage* **95,** 264–275 (2014).

214. Stanley, M. L., Dagenbach, D., Lyday, R. G., Burdette, J. H. & Laurienti, P. J. Changes in global and regional modularity associated with increasing working memory load. *Frontiers in Human Neuroscience* **8,** 954 (2014).

215. Holme, P. & Saramäki, J. Temporal networks. *Physics Reports* **519,** 97–125 (2012).

216. Kivelä, M. *et al.* Multilayer networks. *Journal of Complex Networks* **2,** 203–271 (2014).

217. Mucha, P. J., Richardson, T., Macon, K., Porter, M. A. & Onnela, J.-P. Community Structure in Time-Dependent, Multiscale, and Multiplex Networks. *Science* **328,** 876–878 (2010).

218. Kopal, J., Pidnebesna, A., Tomeček, D., Tintěra, J. & Hlinka, J. Typicality of functional connectivity robustly captures motion artifacts in rs-fMRI across datasets, atlases, and preprocessing pipelines. *Human Brain Mapping* **41,** 5325–5340 (2020).

219. Nir, Y., Hasson, U., Levy, I., Yeshurun, Y. & Malach, R. Widespread functional connectivity and fMRI fluctuations in human visual cortex in the absence of visual stimulation. *NeuroImage* **30,** 1313–1324 (2006).

220. Scholvinck, M. L., Maier, A., Ye, F. Q., Duyn, J. H. & Leopold, D. A. Neural basis of global resting-state fMRI activity. *Proceedings of the National Academy of Sciences* **107,** 10238–10243 (2010).

221. Eickhoff, S. B., Yeo, B. T. T. & Genon, S. Imaging-based parcellations of the human brain. *Nature Reviews Neuroscience* **19,** 672–686 (2018).

222. Buckner, R. L., Krienen, F. M. & Yeo, B. T. T. Opportunities and limitations of intrinsic functional connectivity MRI. *Nature Neuroscience* **16,** 832–837 (2013).

223. Friston, K. J., Williams, S., Howard, R., Frackowiak, R. S. J. & Turner, R. Movement-Related effects in fMRI time-series. *Magnetic Resonance in Medicine* **35,** 346–355 (1996).

224. Hajnal, J. V. *et al.* Artifacts due to stimulus correlated motion in functional imaging of the brain. *Magnetic Resonance in Medicine* **31,** 283–291 (1994).

225. Patel, A. X. *et al.* A wavelet method for modeling and despiking motion artifacts from resting-state fMRI time series. *NeuroImage* **95,** 287–304 (2014).

226. Spisak, T. *et al.* Voxel-Wise Motion Artifacts in Population-Level Whole-Brain Connectivity Analysis of Resting-State fMRI. *PLOS ONE* **9,** 1–19 (2014).

227. Power, J. D. *et al.* Methods to detect, characterize, and remove motion artifact in resting state fMRI. *NeuroImage* **84,** 320–341 (2014).

228. Power, J. D., Schlaggar, B. L. & Petersen, S. E. Recent progress and outstanding issues in motion correction in resting state fMRI. *NeuroImage* **105,** 536–551 (2015).

229. Satterthwaite, T. D. *et al.* Motion artifact in studies of functional connectivity: Characteristics and mitigation strategies. *Human Brain Mapping* **40,** 2033–2051 (2019).

230. Yan, C.-G., Craddock, R. C., He, Y. & Milham, M. P. Addressing head motion dependencies for small-world topologies in functional connectomics. *Frontiers in Human Neuroscience* **7,** 910 (2013).

231. Carbonell, F., Bellec, P. & Shmuel, A. Global and System-Specific Resting-State fMRI Fluctuations Are Uncorrelated: Principal Component Analysis Reveals Anti-Correlated Networks. *Brain Connectivity* **1,** 496–510 (2011).

232. Shmueli, K. *et al.* Low-frequency fluctuations in the cardiac rate as a source of variance in the resting-state fMRI BOLD signal. *NeuroImage* **38,** 306–320 (2007).

233. Fair, D. A. *et al.* Distinct neural signatures detected for ADHD subtypes after controlling for micro-movements in resting state functional connectivity MRI data. *Frontiers in Systems Neuroscience* **6,** 80 (2013).

234. Maclaren, J., Herbst, M., Speck, O. & Zaitsev, M. Prospective motion correction in brain imaging: A review. *Magnetic Resonance in Medicine* **69,** 621–636 (2013).

235. Caballero-Gaudes, C. & Reynolds, R. C. Methods for cleaning the BOLD fMRI signal. *NeuroImage. Cleaning up the fMRI time series: Mitigating noise with advanced acquisition and correction strategies* **154,** 128–149 (2017).

236. Siegel, J. S. *et al.* Data Quality Influences Observed Links Between Functional Connectivity and Behavior. *Cerebral Cortex* **27,** 4492–4502 (2017).

237. Tomeček, D. *et al.* Personality reflection in the brain's intrinsic functional architecture remains elusive. *PLOS ONE* **15,** e0232570 (2020).

238. Ugurbil, K. *et al.* Pushing spatial and temporal resolution for functional and diffusion MRI in the Human Connectome Project. *NeuroImage* **80,** 80–104 (2013).

239. Van Essen, D. C. *et al.* The WU-Minn Human Connectome Project: an overview. *NeuroImage* **80,** 62–79 (2013).

240. Burgess, G. C. *et al.* Evaluation of denoising strategies to Address motion-Correlated Artifacts in Resting-State Functional Magnetic Resonance Imaging Data from the Human Connectome Project. *Brain Connectivity* **6,** 669–680 (2016).

241. Parkes, L., Fulcher, B., Yücel, M. & Fornito, A. An evaluation of the efficacy, reliability, and sensitivity of motion correction strategies for resting-state functional MRI. *NeuroImage* **171,** 415–436 (2018).

242. Bartoň, M. *et al.* Evaluation of different cerebrospinal fluid and white matter fMRI filtering strategies—Quantifying noise removal and neural signal preservation. *Human Brain Mapping* **40,** 1114–1138 (2019).

243. Hartman, D., Hlinka, J., Palus, M., Mantini, D. & Corbetta, M. The role of nonlinearity in computing graph-theoretical properties of resting-state functional magnetic resonance imaging brain networks. *Chaos* **21,** 013119 (2011).

244. Zar, J. H. *Biostatistical Analysis* ISBN: 978-0-13-081542-2 (Prentice Hall, 1999).

245. Craddock, R. C., James, G. A., Holtzheimer, P. E., Hu, X. P. & Mayberg, H. S. A whole brain fMRI atlas generated via spatially constrained spectral clustering. *Human brain mapping* **33,** 1914–1928 (2012).

246. Tzourio-Mazoyer, N. *et al.* Automated Anatomical Labeling of Activations in SPM Using a Macroscopic Anatomical Parcellation of the MNI MRI Single-Subject Brain. *NeuroImage* **15,** 273–289 (2002).

247. Waheed, S. H. *et al.* Reporting of Resting-State Functional Magnetic Resonance Imaging Preprocessing Methodologies. *Brain Connectivity* **6,** 663–668 (2016).

248. Smyser, C. D. *et al.* Longitudinal analysis of neural network development in preterm infants. *Cerebral Cortex* **20,** 2852–2862 (2010).

249. Venkatesh, M., Jaja, J. & Pessoa, L. Comparing functional connectivity matrices: A geometry-aware approach applied to participant identification. *NeuroImage* **207,** 116398 (2020).

250. Bodurka, J., Ye, F., Petridou, N., Murphy, K. & Bandettini, P. A. Mapping the MRI voxel volume in which thermal noise matches physiological noise — Implications for fMRI. *NeuroImage* **34,** 542–549 (2007).

251. De Winter, J. C. F., Gosling, S. D. & Potter, J. Comparing the Pearson and Spearman correlation coefficients across distributions and sample sizes: A tutorial using simulations and empirical data. *Psychological Methods* **21,** 273–290 (2016).

252. Power, J. D., Plitt, M., Kundu, P., Bandettini, P. A. & Martin, A. Temporal interpolation alters motion in fMRI scans: Magnitudes and consequences for artifact detection. *PLOS ONE* **12,** 1–20 (2017).

253. Power, J. D., Plitt, M., Laumann, T. O. & Martin, A. Sources and implications of whole-brain fMRI signals in humans. *NeuroImage* **146,** 609–625.

254. Williams, J. C. & Snellenberg, J. X. V. Motion denoising of multiband resting state functional connectivity MRI data: An improved volume censoring method. *bioRxiv,* 860635 (2019).

255. Hallquist, M. N., Hwang, K. & Luna, B. The nuisance of nuisance regression: spectral misspecification in a common approach to resting-state fMRI preprocessing reintroduces noise and obscures functional connectivity. *NeuroImage* **82,** 208–225 (2013).

256. Saad, Z. S. *et al.* Correcting brain-wide correlation differences in resting-state fMRI. *Brain Connectivity* **3,** 339–352 (2013).

257. Engelhardt, L. E. *et al.* Children's head motion during fMRI tasks is heritable and stable over time. *Developmental Cognitive Neuroscience* **25,** 58–68 (2017).

258. Power, J. D., Barnes, K. A., Snyder, A. Z., Schlaggar, B. L. & Petersen, S. E. Steps toward optimizing motion artifact removal in functional connectivity MRI; a reply to Carp. *NeuroImage* **76,** 439–441 (2013).

259. Power, J. D. *et al.* Customized head molds reduce motion during resting state fMRI scans. *NeuroImage* **189,** 141–149 (2019).

260. Fair, D. A. *et al.* Correction of respiratory artifacts in MRI head motion estimates. *NeuroImage* **208,** 116400 (2020).

261. Beall, E. B. & Lowe, M. J. SimPACE: generating simulated motion corrupted BOLD data with synthetic-navigated acquisition for the development and evaluation of SLOMOCO: a new, highly effective slicewise motion correction. *NeuroImage* **101,** 21–34 (2014).

262. Power, J. D. *et al.* Distinctions among real and apparent respiratory motions in human fMRI data. *NeuroImage* **201,** 116041 (2019).

263. Gratton, C. *et al.* Removal of high frequency contamination from motion estimates in single-band fMRI saves data without biasing functional connectivity. *NeuroImage* **217,** 116866 (2020).

264. Power, J. D. *et al.* Ridding fMRI data of motion-related influences: Removal of signals with distinct spatial and physical bases in multiecho data. *Proceedings of the National Academy of Sciences of the United States of America* **115,** E2105–E2114 (2018).

265. Kopal, J. *et al.* Dynamic connectivity analyses of intracranial EEG during recognition memory reveal various large-scale functional networks. *bioRxiv,* 2020.10.30.360529 (2020).

266. Milner, B. Disorders of learning and memory after temporal lobe lesions in man. *Neurosurgery* **19,** 421–446 (1972).

267. Brady, T. F., Konkle, T., Alvarez, G. A. & Oliva, A. Visual long-term memory has a massive storage capacity for object details. *Proceedings of the National Academy of Sciences* **105,** 14325–14329 (2008).

268. Besson, G., Ceccaldi, M., Didic, M. & Barbeau, E. J. The speed of visual recognition memory. *Visual Cognition* **20,** 1131–1152 (2012).

269. Larzabal, C., Tramoni, E., Muratot, S., Thorpe, S. J. & Barbeau, E. J. Extremely long-term memory and familiarity after 12 years. *Cognition* **170,** 254–262 (2018).

270. Brown, M. W. & Aggleton, J. P. Recognition memory: What are the roles of the perirhinal cortex and hippocampus? *Nature Reviews Neuroscience* **2,** 51 (2001).

271. Eichenbaum, H., Yonelinas, A. P. & Ranganath, C. The medial temporal lobe and recognition memory. *Annual Review of Neuroscience* **30,** 123–152 (2007).

272. Milner, B. & Taylor, L. Right-hemisphere superiority in tactile pattern-recognition after cerebral commissurotomy: Evidence for nonverbal memory. *Neuropsychologia* **10,** 1–15 (1972).

273. Patterson, K. & Bradshaw, J. L. Diffrential hemispheric mediation of nonverbal visual stimuli. *Journal of Experimental Psychology: Human Perception and Performance* **1,** 246–252 (1975).

274. Elger, C. E. *et al.* Human temporal lobe potentials in verbal learning and memory processes. *Neuropsychologia* **35,** 657–667 (1997).

275. Barbeau, E. J. *et al.* Spatio temporal Dynamics of Face Recognition. *Cerebral Cortex* **18,** 997–1009 (2008).

276. Bastin, C. *et al.* An Integrative Memory model of recollection and familiarity to understand memory deficits. *Behavioral and Brain Sciences* **42,** e281 (2019).

277. Caharel, S., Ramon, M. & Rossion, B. Face familiarity decisions take 200 msec in the human brain: Electrophysiological evidence from a go/no-go speeded task. *Journal of Cognitive Neuroscience* **26,** 81–95 (2014).

278. Barragan-Jason, G., Cauchoix, M. & Barbeau, E. The neural speed of familiar face recognition. *Neuropsychologia* **75,** 390–401 (2015).

279. Despouy, E. *et al.* A Fast Visual Recognition Memory System in Humans Identified Using Intracerebral ERP. *Cerebral Cortex* **30,** 2961–2971 (2020).

280. Betzel, R. F. *et al.* The community structure of functional brain networks exhibits scale-specific patterns of inter- and intra-subject variability. *NeuroImage* **202,** 115990 (2019).

281. Bressler, S. L. & Menon, V. Large-scale brain networks in cognition: emerging methods and principles. *Trends in Cognitive Sciences* **14,** 277–290 (2010).

282. De Luca, M., Beckmann, C. F., De Stefano, N., Matthews, P. M. & Smith, S. M. fMRI resting state networks define distinct modes of long-distance interactions in the human brain. *NeuroImage* **29,** 1359–1367 (2006).

283. Kaplan, A. Y., Fingelkurts, A. A., Fingelkurts, A. A., Borisov, S. V. & Darkhovsky, B. S. Nonstationary nature of the brain activity as revealed by EEG/MEG: Methodological, practical and conceptual challenges. *Signal Processing* **85,** 2190–2212 (2005).

284. Fedorenko, E. & Thompson-Schill, S. L. Reworking the language network. *Trends in Cognitive Sciences* **18,** 120–126 (2014).

285. Lachaux, J. P., Rudrauf, D. & Kahane, P. Intracranial EEG and human brain mapping. *Journal of Physiology, Paris* **97,** 613–628 (2003).

286. MATLAB. *version 9.1.0 (R2016b)* (The MathWorks Inc., Natick, Massachusetts, 2016).

287. Gaillard, R. *et al.* Converging intracranial markers of conscious access. *PLOS biology* **7,** e61 (2009).

288. Penn, A. *iboot: Iterated Bootstrap for Small Samples and Samples with Complex Dependence Structures* 2020. `https://github.com/acp29/iboot`.

289. Lahiri, S. N. *Resampling Methods for Dependent Data* (Springer-Verlag, 2003).

290. Politis, D. N. & White, H. Automatic Block-Length Selection for the Dependent Bootstrap. *Econometric Reviews* **23,** 53–70 (2004).

291. Eickhoff, S. B. *et al.* A new SPM toolbox for combining probabilistic cytoarchitectonic maps and functional imaging data. *NeuroImage* **25,** 1325–1335 (2005).

292. Latora, V. & Marchiori, M. Efficient behavior of small-world networks. *Physical Review Letters* **87,** 198701 (2001).

293. Schreiber, T. & Schmitz, A. Surrogate time series. *Physica D: Nonlinear Phenomena* **142,** 346–382 (2000).

294. Westphal, A. J., Wang, S. & Rissman, J. Episodic Memory Retrieval Benefits from a Less Modular Brain Network Organization. *Journal of Neuroscience* **37,** 3523–3531 (2017).

295. Krzywinski, M. *et al.* Circos: An information aesthetic for comparative genomics. *Genome Research* **19,** 1639–1645 (2009).

296. Gonzalez, A. *et al.* Electrocorticography reveals the temporal dynamics of posterior parietal cortical activity during recognition memory decisions. *Proceedings of the National Academy of Sciences* **112,** 11066–11071 (2015).

297. Hoppstädter, M., Baeuchl, C., Diener, C., Flor, H. & Meyer, P. Simultaneous EEG–fMRI reveals brain networks underlying recognition memory ERP old/new effects. *NeuroImage* **116,** 112–122 (2015).

298. Rutishauser, U., Aflalo, T., Rosario, E. R., Pouratian, N. & Andersen, R. A. Single-neuron representation of memory strength and recognition confidence in left human posterior parietal cortex. *Neuron* **97,** 209–220 (2018).

299. VanRullen, R. & Thorpe, S. J. Is it a bird? Is it a plane? Ultra-rapid visual categorisation of natural and artifactual objects. *Perception* **30,** 655–668 (2001).

300. DiCarlo, J. J., Zoccolan, D. & Rust, N. C. How does the brain solve visual object recognition? *Neuron* **73,** 415–434 (2012).

301. Swick, D. & Knight, R. T. Contributions of prefrontal cortex to recognition memory: electrophysiological and behavioral evidence. *Neuropsychology* **13,** 155–170 (1999).

302. Bastin, C., Van der Linden, M., Lekeu, F., Andrés, P. & Salmon, E. Variability in the Impairment of Recognition Memory in Patients with Frontal Lobe Lesions. *Cortex* **42,** 983–994 (2006).

303. Bar, M. *et al.* Top-down facilitation of visual recognition. *Proceedings of the National Academy of Sciences* **103,** 449–454 (2006).

304. Yonelinas, A. P., Otten, L. J., Shaw, K. N. & Rugg, M. D. Separating the brain regions involved in recollection and familiarity in recognition memory. *The Journal of Neuroscience* **25,** 3002–3008 (2005).

305. Staresina, B. P., Fell, J., Do Lam, A. T. A., Axmacher, N. & Henson, R. N. Memory signals are temporally dissociated in and across human hippocampus and perirhinal cortex. *Nature Neuroscience* **15,** 1167–1173 (2012).

306. Kar, K., Kubilius, J., Schmidt, K., Issa, E. B. & DiCarlo, J. J. Evidence that recurrent circuits are critical to the ventral stream's execution of core object recognition behavior. *Nature Neuroscience* **22,** 974–983 (2019).

307. Ishai, A., Bikle, P. C. & Ungerleider, L. G. Temporal dynamics of face repetition suppression. *Brain Research Bulletin* **70,** 289–295 (2006).

308. Rijsbergen, N. J. V. & Schyns, P. G. Dynamics of trimming the content of face representations for categorization in the brain. *PLoS Computational Biology* **5,** e1000561 (2009).

309. Barbeau, E. J., Chauvel, P., Moulin, C. J. A., Regis, J. & Liégeois-Chauvel, C. Hippocampus duality: Memory and novelty detection are subserved by distinct mechanisms. *Hippocampus* **27,** 405–416 (2017).

310. Maillard, L. *et al.* From perception to recognition memory: Time course and lateralization of neural substrates of word and abstract picture processing. *Journal of Cognitive Neuroscience* **23,** 782–800 (2011).

311. Bola, M. & Borchardt, V. Cognitive processing involves dynamic reorganization of the whole-brain network's functional community structure. *The Journal of Neuroscience* **36,** 3633–3635 (2016).

312. Brincat, S. L. & Miller, E. K. Prefrontal cortex networks shift from external to internal modes during learning. *Journal of Neuroscience* **36,** 9739–9754 (2016).

313. Barragan-Jason, G., Besson, G., Ceccaldi, M. & Barbeau, E. J. Fast and famous: looking for the fastest speed at which a face can be recognized. *Frontiers in psychology* **4,** 100 (2013).

314. Watrous, A. J., Tandon, N., Conner, C. R., Pieters, T. & Ekstrom, A. D. Frequency-specific network connectivity increases underlie accurate spatiotemporal memory retrieval. *Nature Neuroscience* **16,** 349–356 (2013).

315. Schedlbauer, A. M., Copara, M. S., Watrous, A. J. & Ekstrom, A. D. Multiple interacting brain areas underlie successful spatiotemporal memory retrieval in humans. *Scientific Reports* **4,** 6431 (2014).

316. King, D. R., Chastelaine, M. d., Elward, R. L., Wang, T. H. & Rugg, M. D. Recollection-Related Increases in Functional Connectivity Predict Individual Differences in Memory Accuracy. *Journal of Neuroscience* **35,** 1763–1772 (2015).

317. Serre, T., Oliva, A. & Poggio, T. A feedforward architecture accounts for rapid categorization. *Proceedings of the National Academy of Sciences* **104,** 6424–6429 (2007).

318. Yoo, S.-A., Tsotsos, J. K. & Fallah, M. Feed-forward visual processing suffices for coarse localization but fine-grained localization in an attention-demanding context needs feedback processing. *PLOS ONE* **14,** e0223166 (2019).

319. Markov, N. T. *et al.* Anatomy of hierarchy: Feedforward and feedback pathways in macaque visual cortex. *Journal of Comparative Neurology* **522,** 225–259 (2014).

320. Salehi, M. *et al.* There is no single functional atlas even for a single individual: Functional parcel definitions change with task. *NeuroImage* **208,** 116366 (2020).

321. Mao, J.-W. *et al.* Dynamic network connectivity analysis to identify epileptogenic zones based on stereo-electroencephalography. *Frontiers in Computational Neuroscience* **10** (2016).

322. Trautner, P. *et al.* Recognition of famous faces in the medial temporal lobe: an invasive ERP study. *Neurology* **63,** 1203–1208 (2004).

323. Hill, P. F., King, D. R., Lega, B. C. & Rugg, M. D. Comparison of fMRI correlates of successful episodic memory encoding in temporal lobe epilepsy patients and healthy controls. *NeuroImage* **207,** 116397 (2020).

324. Sugase, Y., Yamane, S., Ueno, S. & Kawano, K. Global and fine information coded by single neurons in the temporal visual cortex. *Nature* **400,** 869–873 (1999).

325. Schroeder, G. M. *et al.* Seizure pathways change on circadian and slower timescales in individual patients with focal epilepsy. *Proceedings of the National Academy of Sciences* **117,** 11048–11058 (2020).

326. WHO. *Epilepsy: a public health imperative* (World Health Organization, 2019).

327. Bartolomei, F. *et al.* Defining epileptogenic networks: Contribution of SEEG and signal analysis. *Epilepsia* **58,** 1131–1147 (2017).

328. Gleichgerrcht, E., Kocher, M. & Bonilha, L. Connectomics and graph theory analyses: Novel insights into network abnormalities in epilepsy. *Epilepsia* **56,** 1660–1668 (2015).

329. Engel, J. *et al.* Connectomics and epilepsy. *Current opinion in neurology* **26,** 186–194 (2013).

330. Goldberg, E. M. & Coulter, D. A. Mechanisms of epileptogenesis: a convergence on neural circuit dysfunction. *Nature Reviews. Neuroscience* **14,** 337–349 (2013).

331. Parker, C. S. *et al.* Structural and effective connectivity in focal epilepsy. *NeuroImage: Clinical* **17,** 943–952 (2018).

332. Burns, S. P. *et al.* Network dynamics of the brain and influence of the epileptic seizure onset zone. *Proceedings of the National Academy of Sciences* **111,** E5321–E5330 (2014).

333. Englot, D. J., Konrad, P. E. & Morgan, V. L. Regional and global connectivity disturbances in focal epilepsy, related neurocognitive sequelae, and potential mechanistic underpinnings. *Epilepsia* **57,** 1546–1557 (2016).

334. Moraes, M. F. D., de Castro Medeiros, D., Mourao, F. A. G., Cancado, S. A. V. & Cota, V. R. Epilepsy as a dynamical system, a most needed paradigm shift in epileptology. *Epilepsy & Behavior,* 106838 (2019).

335. Blauwblomme, T., Jiruska, P. & Huberfeld, G. Mechanisms of ictogenesis. *International Review of Neurobiology* **114,** 155–185 (2014).

336. Pitkänen, A., Lukasiuk, K., Dudek, F. E. & Staley, K. J. Epileptogenesis. *Cold Spring Harbor Perspectives in Medicine* **5** (2015).

337. Słowiński, P. *et al.* Background EEG Connectivity Captures the Time-Course of Epileptogenesis in a Mouse Model of Epilepsy. *eNeuro* **6** (2019).

338. Kini, L. G., Gee, J. C. & Litt, B. Computational analysis in epilepsy neuroimaging: A survey of features and methods. *NeuroImage: Clinical* **11,** 515–529 (2016).

339. Delorme, A. & Makeig, S. EEGLAB: an open source toolbox for analysis of single-trial EEG dynamics including independent component analysis. *Journal of Neuroscience Methods* **134,** 9–21 (2004).

340. Wu, S. *et al.* Stability-driven nonnegative matrix factorization to interpret spatial gene expression and build local gene networks. *Proceedings of the National Academy of Sciences* **113,** 4290–4295 (2016).

341. Aggarwal, C. C., Hinneburg, A. & Keim, D. A. *On the Surprising Behavior of Distance Metrics in High Dimensional Space* in *Database Theory — ICDT 2001* (Springer, 2001), 420–434.

342. Baud, M. O. *et al.* Multi-day rhythms modulate seizure risk in epilepsy. *Nature Communications* **9,** 88 (2018).

343. Colombet, B., Woodman, M., Badier, J. M. & Bénar, C. G. AnyWave: A cross-platform and modular software for visualizing and processing electrophysiological signals. *Journal of Neuroscience Methods* **242,** 118–126 (2015).

344. Mantel, N. The Detection of Disease Clustering and a Generalized Regression Approach. *Cancer Research* **27,** 209–220 (1967).

345. Le Van Quyen, M. *et al.* Preictal state identification by synchronization changes in long-term intracranial EEG recordings. *Clinical Neurophysiology* **116,** 559–568 (2005).

346. Varotto, G., Tassi, L., Franceschetti, S., Spreafico, R. & Panzica, F. Epileptogenic networks of type II focal cortical dysplasia: a stereo-EEG study. *NeuroImage* **61,** 591–598 (2012).

347. Korzeniewska, A. *et al.* Ictal propagation of high frequency activity is recapitulated in interictal recordings: effective connectivity of epileptogenic networks recorded with intracranial EEG. *NeuroImage* **101,** 96–113 (2014).

348. Karoly, P. J. *et al.* The circadian profile of epilepsy improves seizure forecasting. *Brain: A Journal of Neurology* **140,** 2169–2182 (2017).

349. Meisel, C., Plenz, D., Schulze-Bonhage, A. & Reichmann, H. Quantifying antiepileptic drug effects using intrinsic excitability measures. *Epilepsia* **57,** e210–e215 (2016).

350. Marciani, M. G. & Gotman, J. Effects of drug withdrawal on location of seizure onset. *Epilepsia* **27,** 423–431 (1986).

351. *Computational neuroscience - Latest research and news — Nature* `https://www.nature.com/subjects/computational-neuroscience` (2020).

352. Popovych, O. V., Manos, T., Hoffstaedter, F. & Eickhoff, S. B. What Can Computational Models Contribute to Neuroimaging Data Analytics? *Frontiers in Systems Neuroscience* **12** (2019).

353. Deco, G. & Jirsa, V. K. Ongoing cortical activity at rest: criticality, multistability, and ghost attractors. *The Journal of Neuroscience* **32,** 3366–3375 (2012).

354. Deco, G., Kringelbach, M. L., Jirsa, V. K. & Ritter, P. The dynamics of resting fluctuations in the brain: metastability and its dynamical cortical core. *Scientific Reports* **7,** 3095 (2017).

355. Fox, M. D., Halko, M. A., Eldaief, M. C. & Pascual-Leone, A. Measuring and manipulating brain connectivity with resting state functional connectivity magnetic resonance imaging (fcMRI) and transcranial magnetic stimulation (TMS). *NeuroImage. Connectivity* **62,** 2232–2243 (2012).

356. Kedzior, K. K., Gerkensmeier, I. & Schuchinsky, M. Can deep transcranial magnetic stimulation (DTMS) be used to treat substance use disorders (SUD)? A systematic review. *BMC Psychiatry* **18,** 137 (2018).

357. Wilke, C., Worrell, G. & He, B. Graph analysis of epileptogenic networks in human partial epilepsy. *Epilepsia* **52,** 84–93 (2011).

358. Efron, B. *Large-Scale Inference: Empirical Bayes Methods for Estimation, Testing, and Prediction* (Cambridge University Press, 2012).

359. Hastie, T., Tibshirani, R. & Friedman, J. *The Elements of Statistical Learning: Data Mining, Inference, and Prediction, Second Edition* ISBN: 978-0-387-84857-0 (Springer-Verlag, 2009).

360. Bzdok, D. & Yeo, B. T. T. Inference in the age of big data: Future perspectives on neuroscience. *NeuroImage* **155,** 549–564 (2017).

361. Bzdok, D. & Ioannidis, J. P. A. Exploration, Inference, and Prediction in Neuroscience and Biomedicine. *Trends in Neurosciences* **42,** 251–262 (2019).

362. Vu, M.-A. T. *et al.* A Shared Vision for Machine Learning in Neuroscience. *The Journal of Neuroscience* **38,** 1601–1607 (2018).

363. Segato, A., Marzullo, A., Calimeri, F. & De Momi, E. Artificial intelligence for brain diseases: A systematic review. *APL Bioengineering* **4** (2020).

364. Gabrieli, J. D., Ghosh, S. S. & Whitfield-Gabrieli, S. Prediction as a Humanitarian and Pragmatic Contribution from Human Cognitive Neuroscience. *Neuron* **85,** 11–26 (2015).

365. Du, Y., Hao, H., Wang, S., Pearlson, G. D. & Calhoun, V. D. Identifying commonality and specificity across psychosis sub-groups via classification based on features from dynamic connectivity analysis. *NeuroImage: Clinical* **27,** 102284 (2020).

366. Woo, C.-W., Chang, L. J., Lindquist, M. A. & Wager, T. D. Building better biomarkers: brain models in translational neuroimaging. *Nature Neuroscience* **20,** 365–377 (2017).

367. Huang, W. *et al.* A Graph Signal Processing Perspective on Functional Brain Imaging. *Proceedings of the IEEE* **106,** 868–885 (2018).

368. Rutishauser, U., Ross, I. B., Mamelak, A. N. & Schuman, E. M. Human memory strength is predicted by theta-frequency phase-locking of single neurons. *Nature* **464,** 903–907 (2010).

369. Khambhati, A. N., Sizemore, A. E., Betzel, R. F. & Bassett, D. S. Modeling and interpreting mesoscale network dynamics. *NeuroImage. Brain Connectivity Dynamics* **180,** 337–349 (2018).